Project Report
NOAA-5

GOES SN03 Imager Final Thermal Vacuum IR Calibration Results

D. Cousins
E.C. Wack
R.M. Heinrichs

1 September 1993

Lincoln Laboratory

MASSACHUSETTS INSTITUTE OF TECHNOLOGY

LEXINGTON, MASSACHUSETTS

Prepared for the National Oceanographic and Atmospheric Administration under Air Force Contract F19628-90-C-0002.

Unclassified

The work reported in this document was performed at Lincoln Laboratory, a center for research operated by Massachusetts Institute of Technology. This work was sponsored by the National Oceanographic and Atmospheric Administration under Air Force Contract F19628-90-C-0002.

MASSACHUSETTS INSTITUTE OF TECHNOLOGY
LINCOLN LABORATORY

GOES SNO3 IMAGER FINAL THERMAL VACUUM IR CALIBRATION RESULTS

D. COUSINS
E.C. WACK
Group 96
R.M. HEINRICHS
Group 54

PROJECT REPORT NOAA-5

1 SEPTEMBER 1993

LEXINGTON MASSACHUSETTS

ABSTRACT

Data analysis of the thermal vacuum IR calibration testing of the GOES SN03 imager is presented. Responsivity versus time data indicate that the instrument is stable and uncontaminated. Data on responsivity versus various instrument temperatures are presented to assess expected diurnal on orbit thermal effects. A complete set of calibration coefficients, including offset, slope and quadratic terms along with corresponding statistical errors, is presented. A possible target related systematic quadratic calibration error source is discussed. On orbit radiance temperature errors are estimated to be about 0.1 K to 0.4 K, depending on instrument operating conditions. The effect on temperature error due to frequency of onboard blackbody calibrations is presented. Finally, the effect on drift related noise due to frequency of space clamps is shown to be smaller than previously anticipated.

ACKNOWLEDGMENTS

The authors would like to acknowledge the cooperation of the ITT engineering staff, particularly E. Jack and D. Leber, in providing access to the test data and helpful suggestions for processing methods. Members of the GOES calibration task force, particularly M. Weinreb of NOAA, W. Bryant of NASA and H. Farthing of Swales Associates, have been the source of many interesting calibration ideas. W. Brown and J. Lifsitz of MIT Lincoln Lab have provided important guidance and technical feedback for this work.

For the preparation of this document, I am also very much thankful for the help of Karen Bauer who prepared the document for publication.

TABLE OF CONTENTS

TABLE OF CONTENTS (Continued)

LIST OF ILLUSTRATIONS

LIST OF ILLUSTRATIONS (Continued)

LIST OF ILLUSTRATIONS (Continued)

LIST OF ILLUSTRATIONS (Continued)

LIST OF ILLUSTRATIONS (Continued)

LIST OF ILLUSTRATIONS (Continued)

LIST OF ILLUSTRATIONS (Continued)

LIST OF TABLES

LIST OF TABLES (Continued)

1. INTRODUCTION AND SUMMARY

The Imager and Sounder instruments, designed and built by ITT Aerospace/ Communications Division, are the first U.S. generation of geostationary 3-axis stabilized meteorological sensors. Serial number SN03 instruments are the first production units to be flight qualified and are scheduled for a mid 1994 launch. The instrument and satellite design are described in detail in Reference 1. The purpose of this report is to describe an independent analysis of the instrument level IR radiometric calibration testing of the SN03 Imager. Table 1 lists important Imager operating parameters for reference with the calibration results described in this report. The full ITT post processing calibration results are to be reported in Reference 2.

TABLE 1

Important Imager Parameters

Ch.	Band µm	FOV (µrad)	MAX SCENE TEMP (K)	MAX SCENE RADIANCE $\frac{mW}{m^2 sr cm^{-1}}$	NOM SCENE TEMP (K)	NEDT SPEC (@ NOM SCENE) (K)	RADIANCE THERMAL DERIV (@ NOM SCENE) $\frac{mW}{m^2 sr cm^{-1} K}$
2	3.78-4.02	102	320	2	300	1.4	0.037
3	6.5-7.0	196	320	50	230	1.0	0.146
4	10.2-11.2	98	320	160	300	0.35	1.678
5	11.5-12.5	98	320	120	300	0.35	1.751

The primary objective of the instrument level IR calibration testing is to measure response and noise while viewing a temperature controlled external calibration target (ECT) for all IR channel/detector/electronic side combinations. Tests are conducted at various instrument operating conditions characterized by different regulated patch (detector) and mission (baseplate) temperatures. Calibration equations relating instrument output counts (relative to space) to target radiance are determined. Calibration tests are conducted in test phases before and after vibration which are referred to as preliminary thermal vacuum (PTV) and final thermal vacuum (FTV), respectively. Table 2 lists the number of ECT temperatures used for IR calibration at the various instrument operating conditions for both PTV and FTV. Generally 7 or more ECT temperatures are necessary to satisfactorily determine calibration and coefficients; a single ECT temperature is used to check response and noise. The resulting full set of calibration coefficients is used in conjunction with on orbit instrument conditions and predefined algorithms in the operations ground equipment (OGE) during satellite operations (Reference 3).

TABLE 2

Number of ECT Temperatures In IR Calibration Testing (Pre T/V - Fin T/V)

	Patch Low (94 K)	Patch Mid (101 K)	Patch High (104 K)
Mission Low (baseplate 282 K)	10 - 7	1 - 7	0 - 0
Mission Nominal (baseplate 293 K)	1 - 7	1 - 7	1 - 7
Mission High (baseplate 300 K)	1 - 7	1 - 7	0 - 0

Other objectives of the IR calibration testing are to track instrument response through thermal transitions, to check for the presence of contaminants on cold instrument optical surfaces, and to assess the radiometric impact of the frequency of space clamp and onboard calibration intervals using the internal calibration target (ICT).

This report presents several IR calibration data analysis topics pursued independently of the standard ITT data post processing. In chapter 2, an analysis of ICT data is presented, including responsivity versus time during calibration runs, radiance temperature errors of the ICT and an estimate of the temperature errors of the ECT using an "on-orbit" data analysis scenario. In chapter 3, responsivity data for the various IR channels is shown as a function of the patch temperature and aft optics temperature. Results from PTV are compared with those from FTV. In chapter 4, estimates of the scene radiance temperature on-orbit due to detector responsivity changes as the aft optics temperatures vary diurnally are calculated. The temperature errors accumulate in between ICT looks and estimates of temperature errors versus frequency of ICT looks are presented. In chapter 5, the various calibration coefficients, including slope and quadratic coefficients, are trended over FTV testing for the various mission and patch temperature conditions. Chapter 6 presents a discussion of the temperature errors resulting from the assumption that the measured nonlinearity in channel 2 response is solely an artifact of the ECT. Finally, in chapter 7 an analysis of the imager drift data is presented which shows that only a slight increase in noise results from 36.6 second compared to 9.6 second space clamp intervals.

2. BB-ECAL RESULTS AND ON ORBIT TEMPERATURE ERRORS

2.1 INTRODUCTION

During imager thermal-vacuum testing at ITT, radiance measurements are collected from three separate targets: a cold space target, a variable-temperature external calibration target (ECT), and an instrument internal calibration target (ICT). The difference in radiance counts from the space target to the ECT versus ECT temperature is used to calibrate the instrument. The relative radiance counts between the space target and ICT (collected at approximately the same time as ECT measurements) can then be used to check for any systematic variations in instrument responsivity versus time and to check the accuracy of the ECT calibration as well as verify the efficacy of the ICT. In the first section, the responsivity versus time during final-thermal-vacuum testing is analyzed for the various mission and patch conditions. The second section then calculates the radiance temperature of the ICT, using the calibration parameters determined from ECT measurements, and compares these with the measured temperatures. The final section then used the ECT and ICT data to calculate an "on-orbit" temperature error, using an algorithm related to that used on-orbit for calculating the ECT radiance temperature.

2.2 RESPONSIVITY VERSUS TIME DURING FTV

Figures 1 through 7 show plots of the normalized two-point responsivity versus time for the various mission and patch conditions from FTV testing at ITT. As can be seen from the plots, most of the deviations appear to be random and typically less than 0.5%. Below this value, changes in responsivity have a negligible effect on the calculated target radiance. The one exception to this is the calibration run corresponding to mission normal / patch mid / side 1 data, which shows a decrease of about 5% for a few channels at one time point which corresponds to the 308-K ECT temperature. Plots of the residues show no anomalous behavior in the vicinity of this point. So, whatever the cause of this anomaly, it does not appear to have affected the calibration.

2.3 ICT RADIANCE TEMPERATURE ERROR

One calibration check of the ICT, performed by ITT and repeated here, is to calculate the radiance temperature of the ICT based on the measured counts using the quadratic fit parameters from that testing condition. Thus, for each testing condition the relative counts from the ICT measurements are converted into the corresponding radiance using the quadratic fit parameters and then converted to scene temperature by inverting the spectral radiance relationship for each channel. The results of these calculations are shown in Figures 8 through 11. The ordinate in the figures is the temperature difference between the calculated temperature, as described above, and the measured temperature of the ICT which is an equal weight average of the 8 sensors in the target over all 10 USI's. As can be seen from the figures, the temperature errors rarely exceed 0.5 K and are typically in the range of 0.1 - 0.4 K. The one anomalous point for the mission nominal / patch mid / side 1 conditions corresponds to the same anomalous responsivity described earlier. The temperature errors also appear to be uniformly positive, which implies that the measured radiance off the ICT is greater than that for the ECT at a given temperature. This may be due to reflected light off the ICT, which is not expected to have as high an emissivity as the ECT.

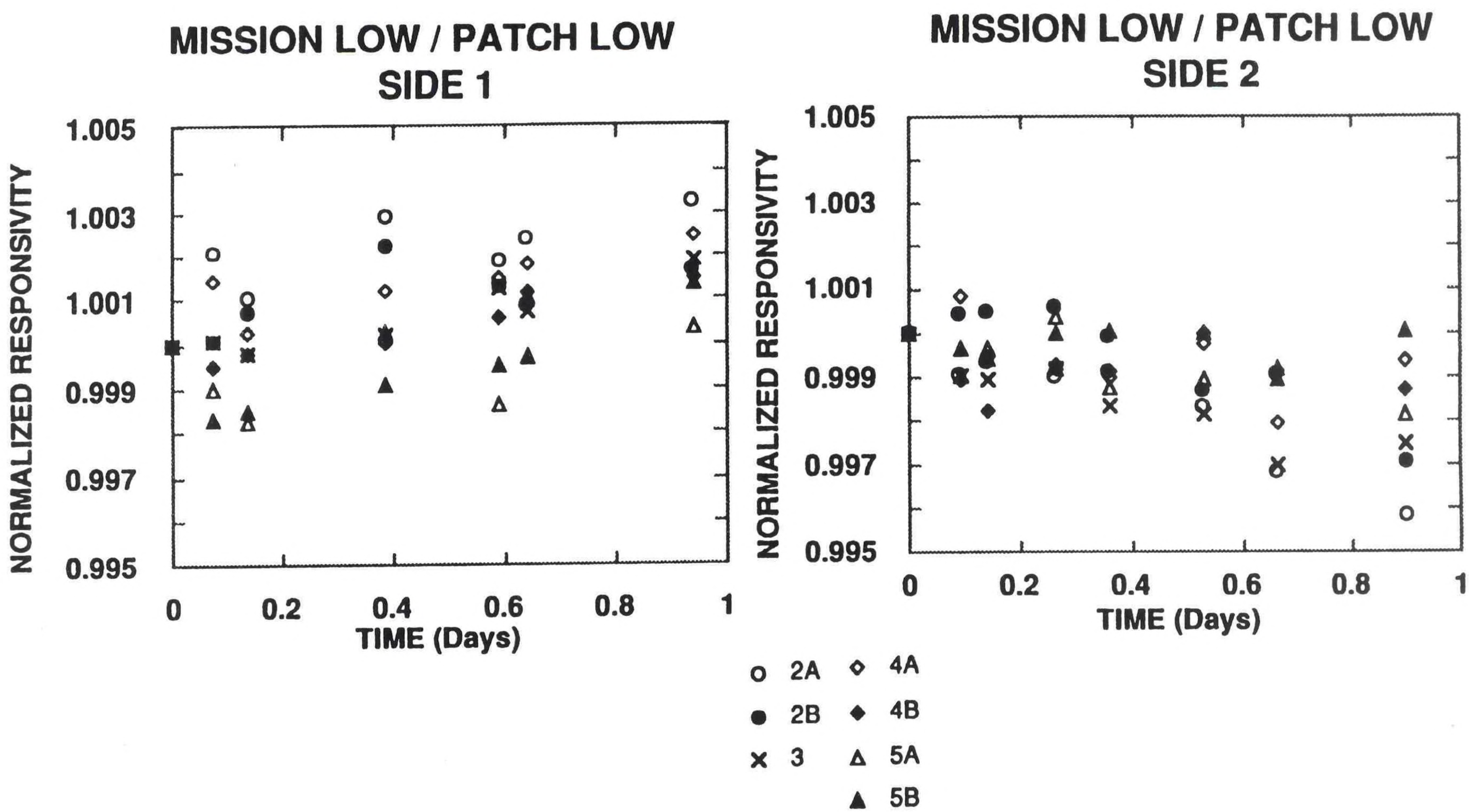

Figure 1. Normalized responsivity versus time during mission low / patch low calibration runs, determined from ICT measurements.

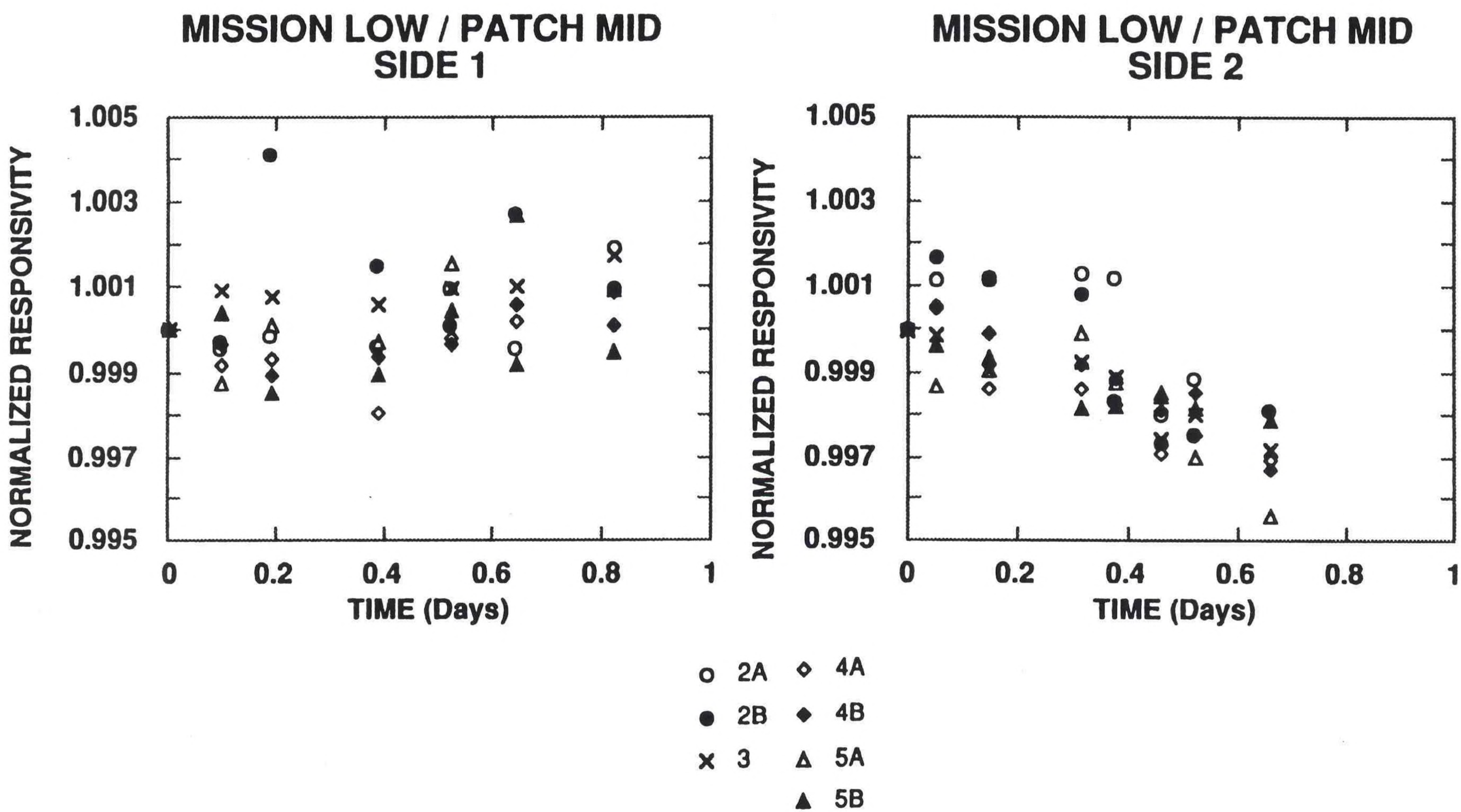

Figure 2. Normalized responsivity versus time for mission low / patch mid calibration runs, determined from ICT measurements.

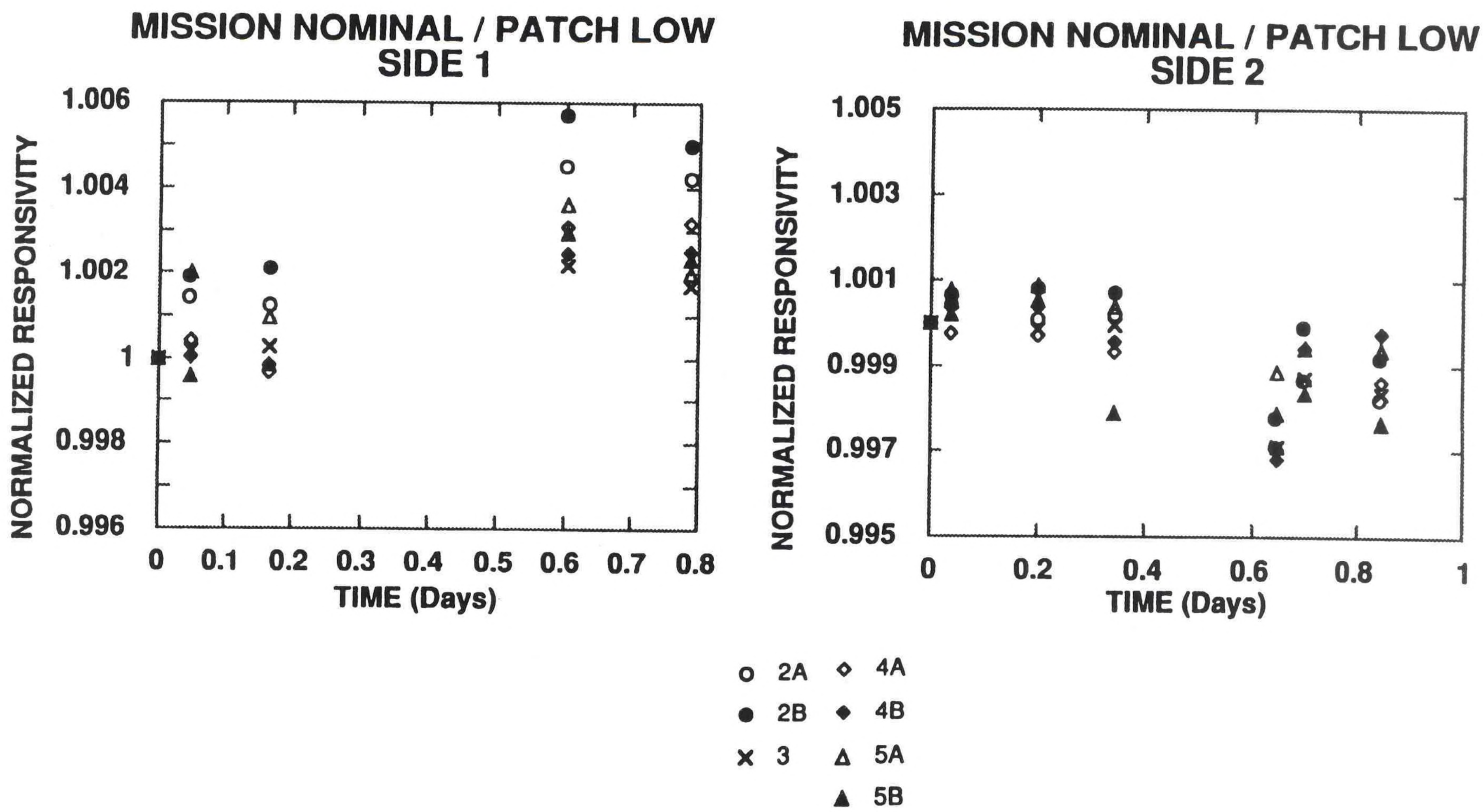

Figure 3. Normalized responsivity versus time for mission nominal / patch low calibration runs, determined from ICT measurements.

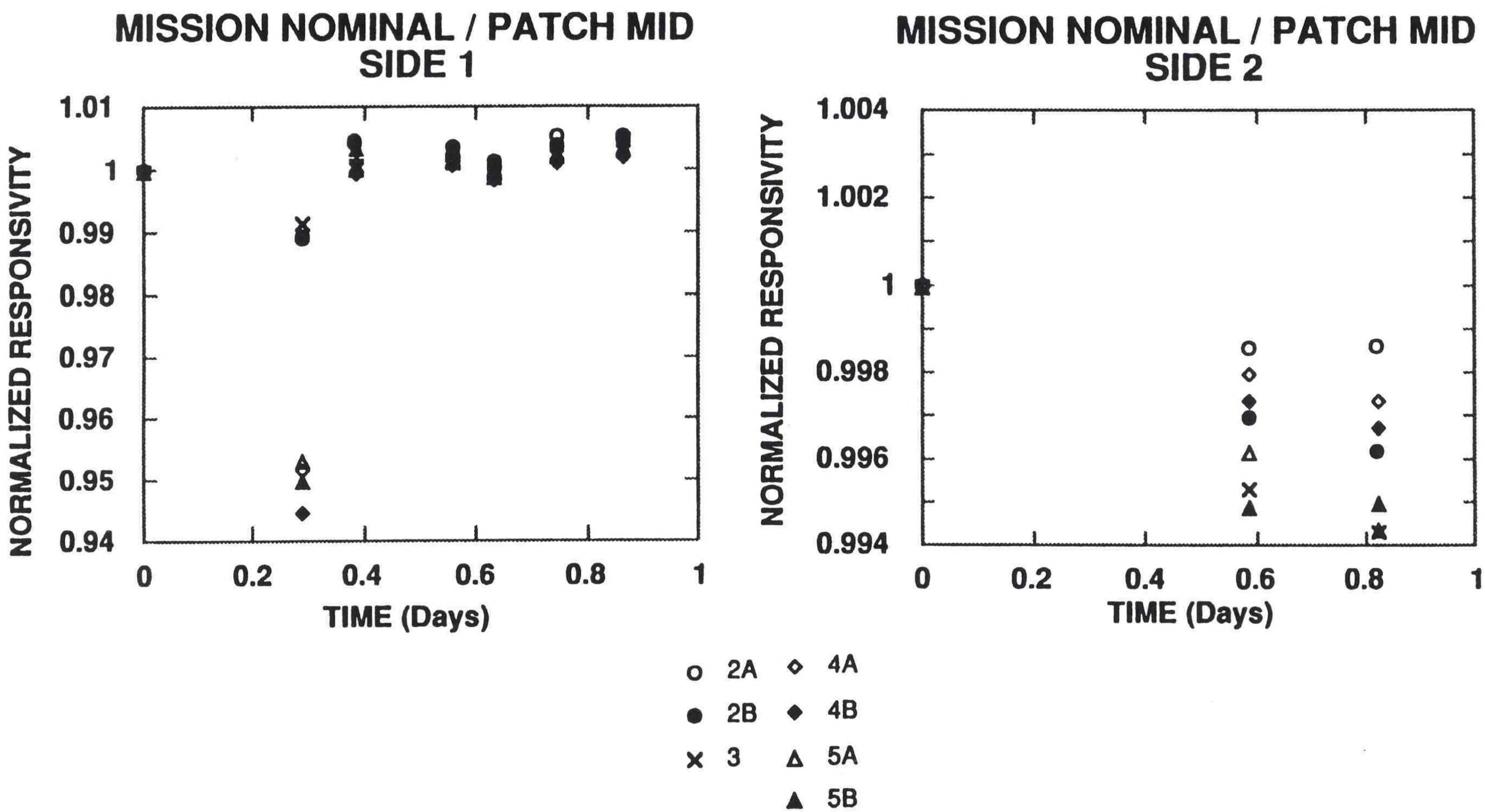

Figure 4. Normalized responsivity versus time for mission nominal / patch mid calibration runs, determined from ICT measurements.

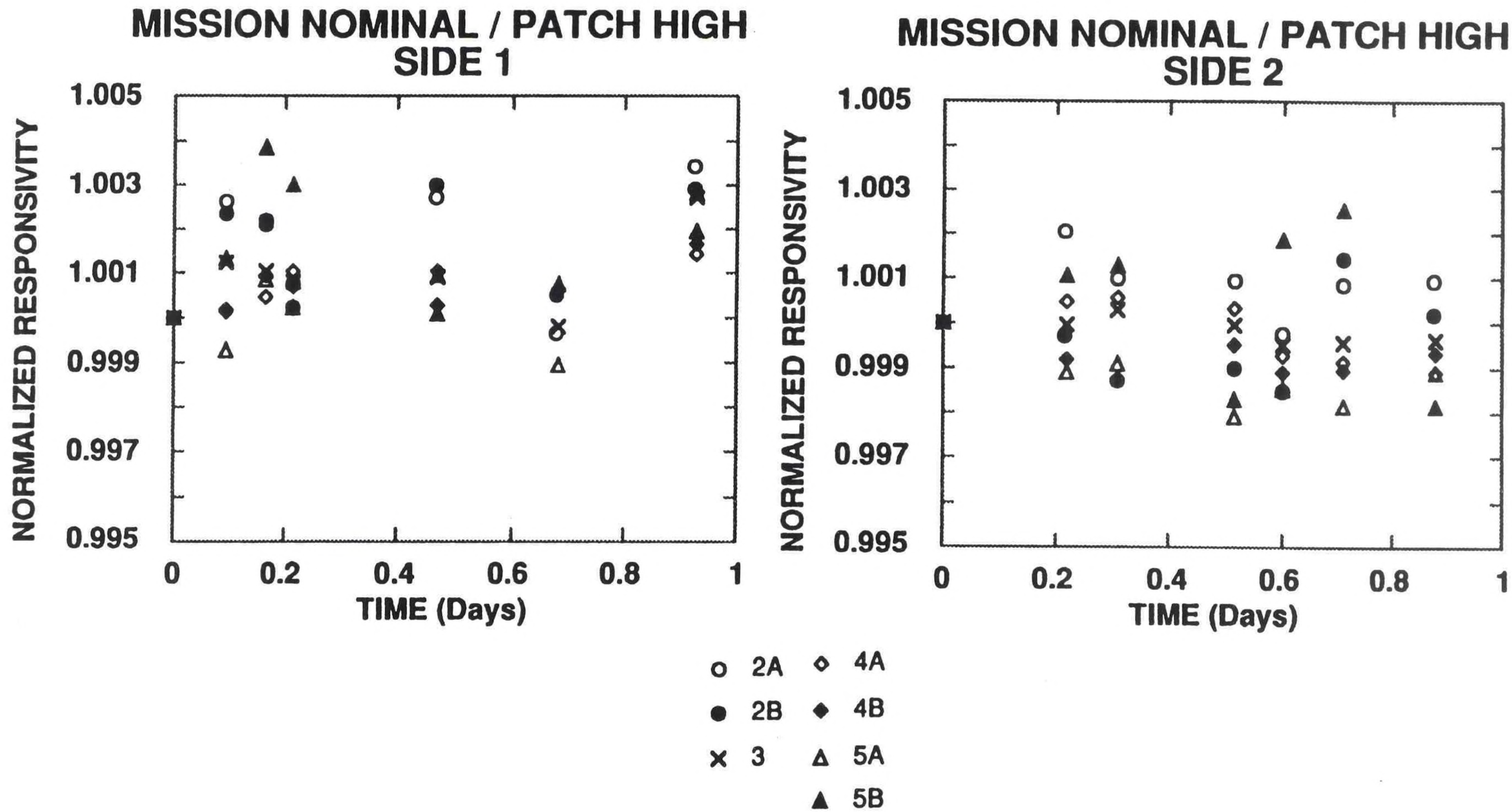

Figure 5. Normalized responsivity versus time for mission nominal / patch high calibration runs, determined from ICT measurements.

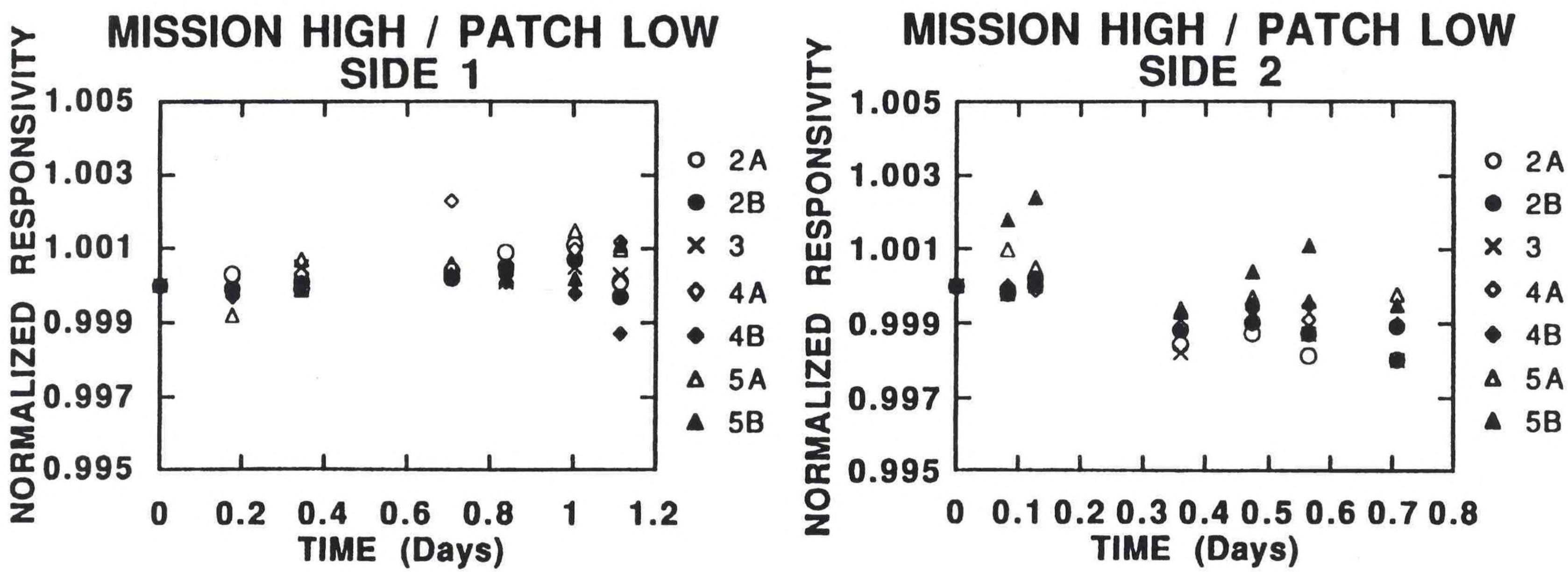

Figure 6. Normalized responsivity versus time during mission high / patch low calibration runs, determined from ICT measurements.

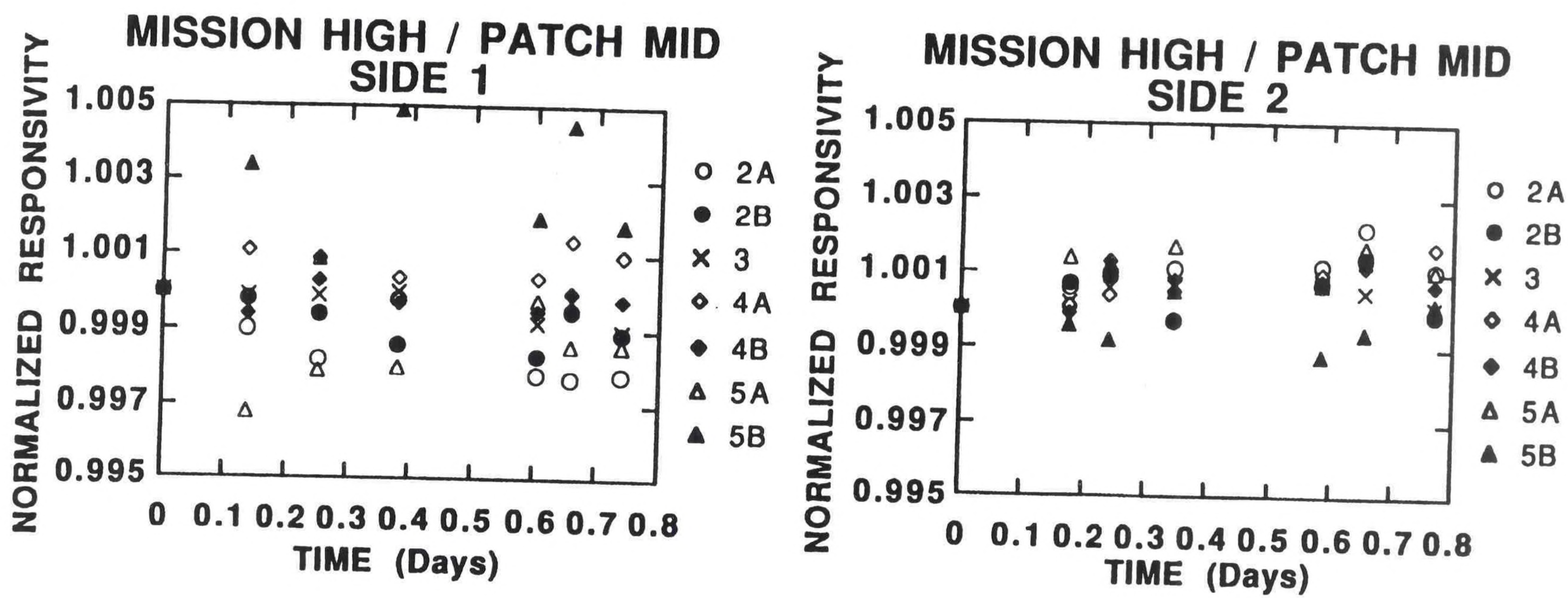

Figure 7. Normalized responsivity versus time during mission high / patch mid calibration runs, determined from ICT measurements.

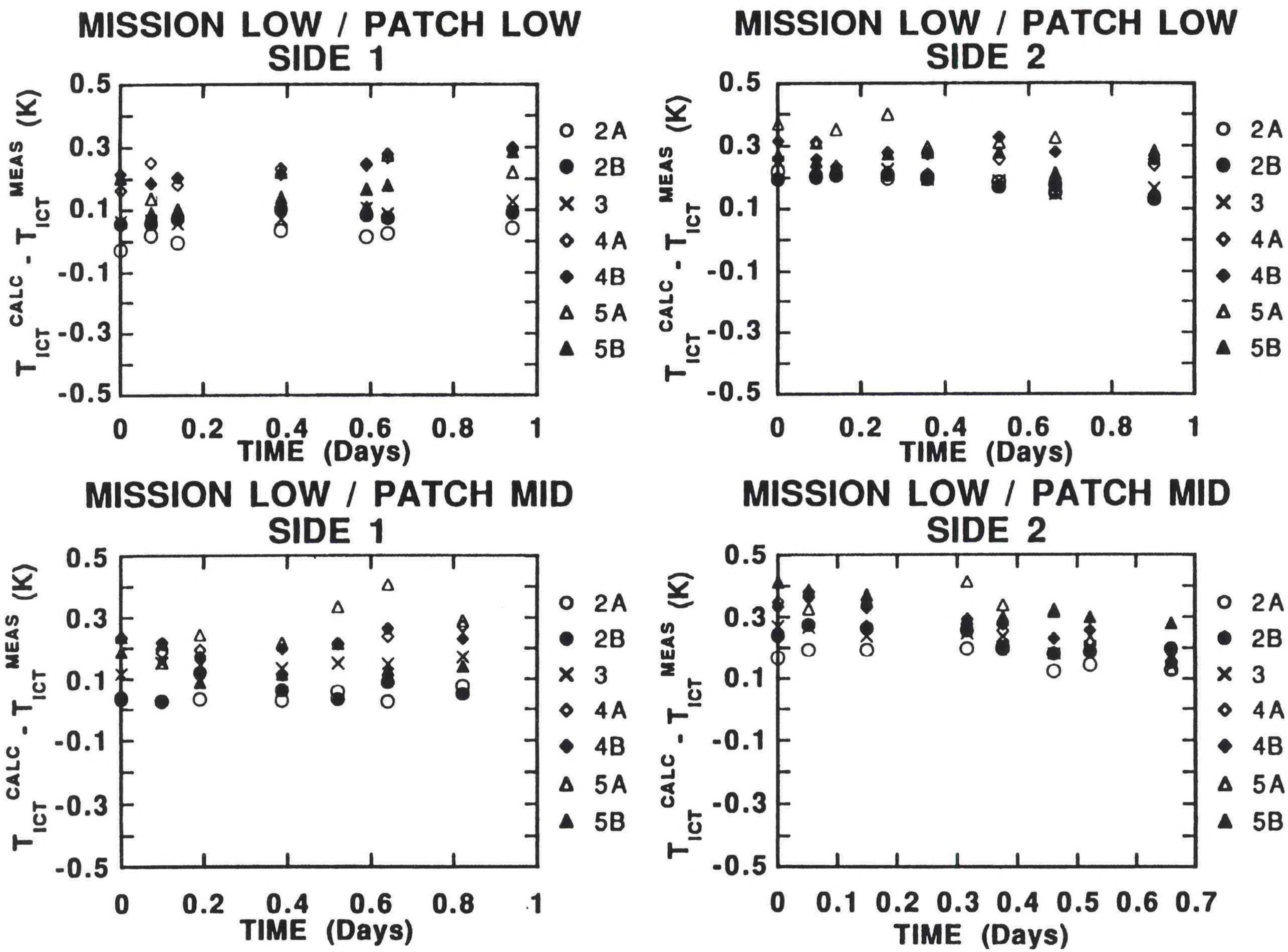

Figure 8. ICT temperature calculated from quadratic fit parameters minus measured ICT temperature for mission low calibration runs.

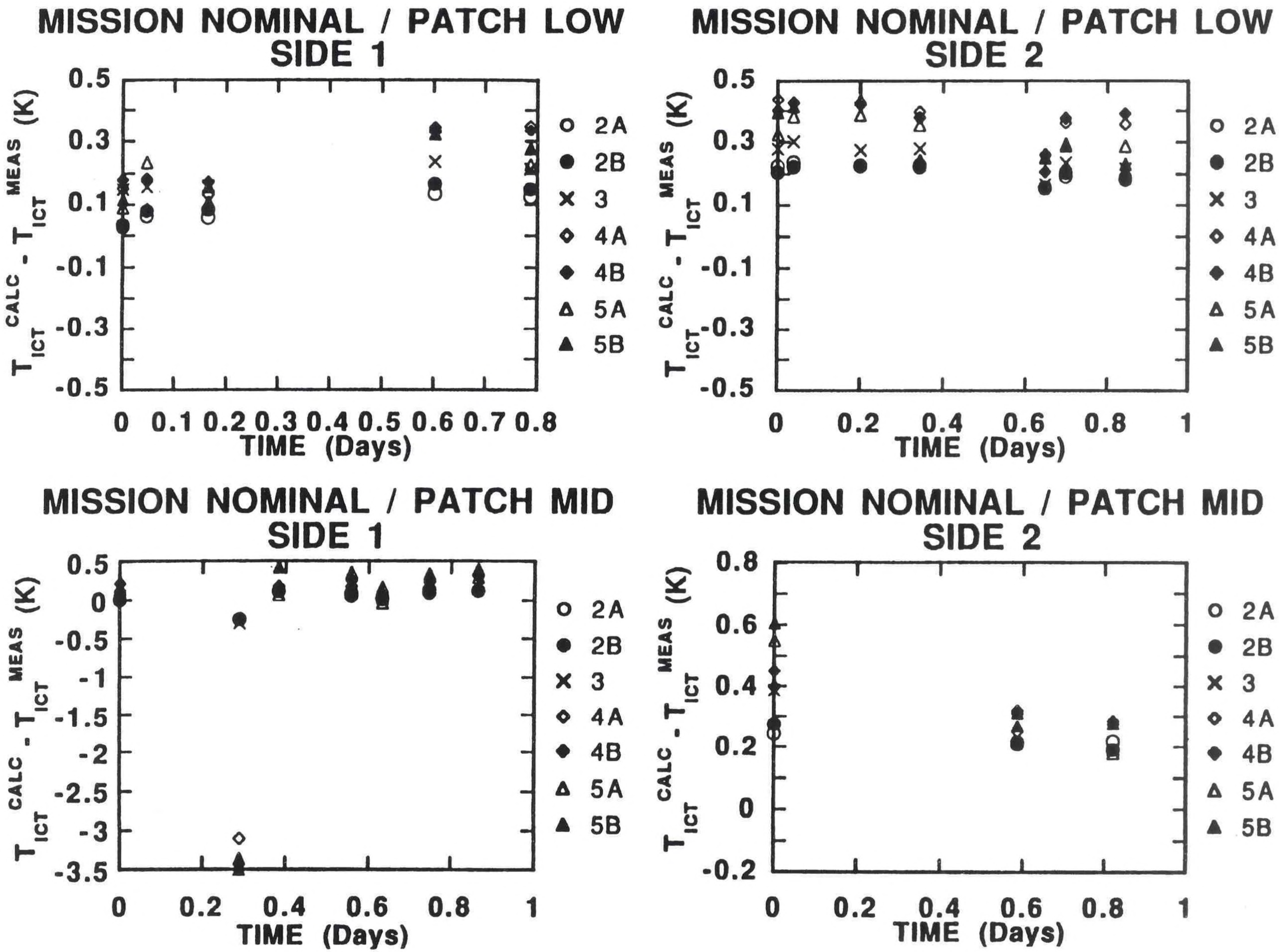

Figure 9. ICT temperature calculated from quadratic fit parameters minus measured ICT temperature for mission nominal, patch low and patch mid, calibration runs.

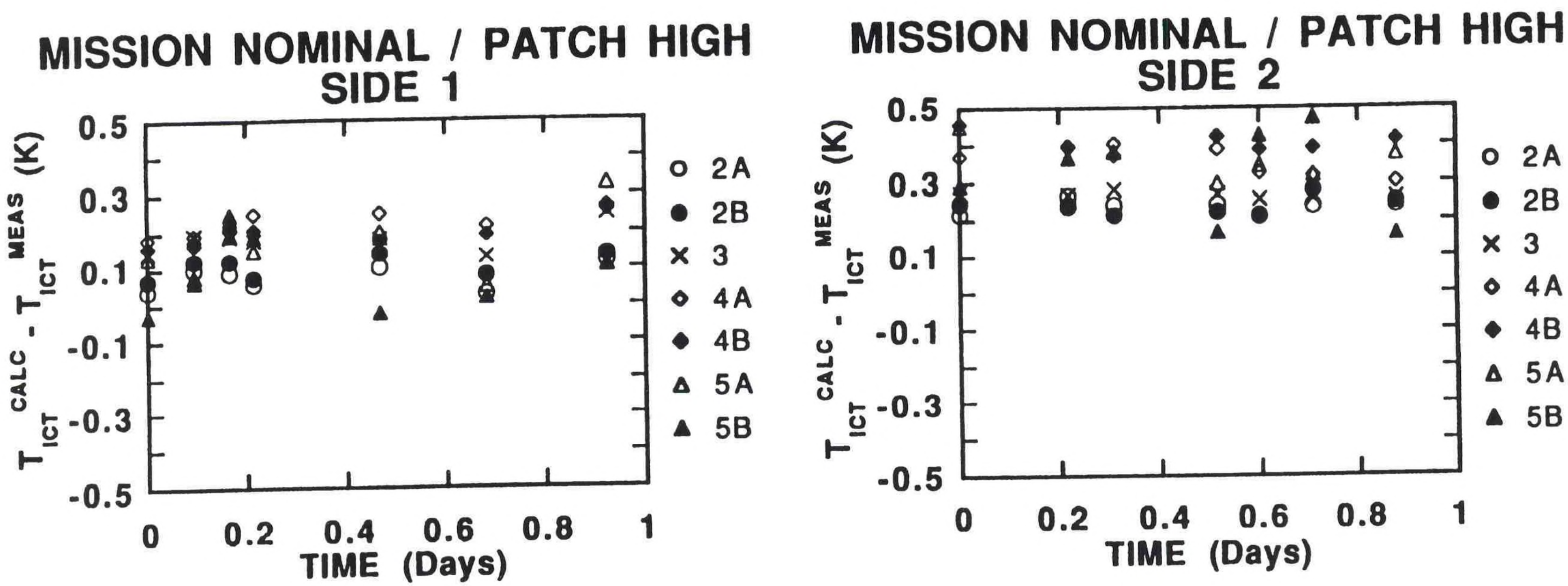

Figure 10. ICT temperature calculated from quadratic fit parameters minus measured ICT temperature for mission nominal, patch high, calibration runs.

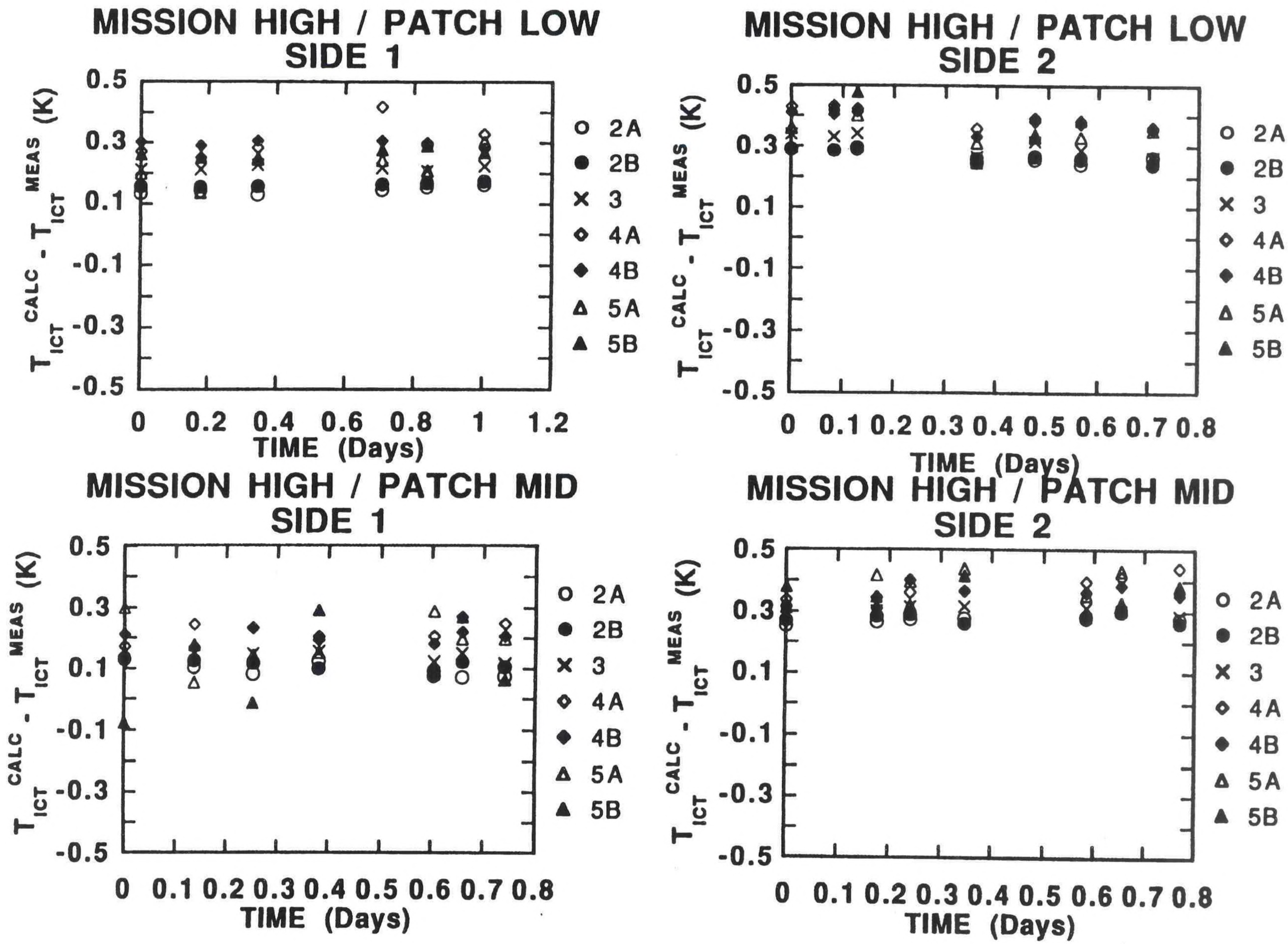

Figure 11. ICT temperature calculated from quadratic fit parameters minus measured ICT temperature for mission nominal calibration runs.

Any differences between the temperature errors presented here and those calculated and presented by ITT are due to differences between the way ITT calculates scene radiance temperatures and the way they are calculated for this analysis. ITT calculates the radiance of a target, either the ICT or the ECT, by taking the measured temperature and uses a previously calculated look-up table for the corresponding in-band radiance for each channel. These tables include the measured, except for imager channel 3, spectral transmissions for each of the detector channels convolved with the Planck function. When going from radiance to temperature, as in the present analysis, the ITT processing uses a polynomial approximation to the Planck function which has in-band transmission coefficients for each of the detector channels. The analysis performed for this memo, however, uses the same spectral radiance look-up tables to go from radiance back to temperature.

2.4 ON-ORBIT TEMPERATURE ERROR ANALYSIS

This analysis calculates a radiance temperature error for the ECT, using ICT measurements to set the linear part of the system calibration and ECT measurements for the quadratic part. These are then compared with the measured ECT temperatures. This is similar to the manner in which the instrument is calibrated on-orbit where ICT measurements define the linear calibration term and the quadratic term is derived from the FTV tests. The resulting temperature errors are seen to have a systematic dependence on ECT temperature. This is accounted for by including an offset term in the relative counts between ETC and space and ICT and space. The physical origin of this offset is unknown but may be related to emissivity differences between the three targets.

The standard on-orbit calibration of the GOES imager involves first fitting final thermal-vacuum data of ECT relative counts versus temperature to a quadratic function of the form:

$$N_{ECT} = \gamma + m_1(\Delta C_{ECT}) + R(\Delta C_{ECT})^2 \tag{1}$$

where N_{ECT} is the in-band target radiance of the ECT on the detector, ΔC_{ECT} is the difference in averaged counts of the ECT above the space target, and γ, m_1, and R are fit parameters. N_{ECT} is determined from temperature measurements of the ECT target along with previously generated spectral radiance look-up tables calculated from measured and inferred optical efficiencies convolved with the Planck function. When the instrument is on-orbit the quadratic part of the calibration is assumed to be maintained, while the offset term is assumed to be negligible and set to zero, and the linear term is calculated from measurements of the ICT. Thus, the linear m_1 term on-orbit, m_{ICT}, is calculated from

$$m_{ICT} = \frac{N_{ICT} - R(\Delta C_{ICT})^2}{(\Delta C_{ICT})} \tag{2}$$

where N_{ICT} is calculated from ICT temperature measurements and ΔC_{ICT} is the counts of the ICT relative to space. The radiance of the earth is then calculated, using these parameters, as

$$N_{earth} = m_{ICT}(\Delta C_{earth}) + R(\Delta C_{earth})^2 \quad . \tag{3}$$

The goal of the present analysis is to develop an estimate of the radiance-temperature error associated with N_{earth} from thermal-vac measurements. To this end an analysis is performed whereby N_{ECT} is calculated from equation (3) instead of N_{earth}. Thus, for each ECT measurement the value N_{ECT} is calculated from

$$N_{ECT} = \left[\frac{N_{ICT} - R(\Delta C_{ICT})^2}{(\Delta C_{ICT})}\right](\Delta C_{ECT}) + R(\Delta_{ECT})^2 \ . \tag{4}$$

The radiance temperature associated with N_{ECT}, T_{ECT}^{calc}, is then calculated by inverting the spectral radiance relation. This is then compared with the measured ECT temperature, T_{ECT}^{meas}, for various ECT temperatures. This analysis is somewhat circuitous since results of ECT measurements are used to calculate the quadratic parameter, R, which then goes into an equation to estimate the radiance temperature of the ECT. Nevertheless, some insight into the quality of the calibration can still be gleaned.

Plots of the "on-orbit" temperature error, $T_{ECT}^{calc} - T_{ECT}^{meas}$, versus T_{ECT} are shown in Figures 12 through 15 for each mission and patch condition tested. As can be seen from the figures, the general trend of the temperature error is to go from positive to negative values with increasing ECT temperature, crossing through zero at a point near the ICT temperature. This behavior is primarily observed in channels 4 and 5 and, to a lesser extent, in channels 2 and 3. The trend can be qualitatively understood if one assumes the existence of an offset, or non-zero value, of the relative counts as the ECT temperature is extrapolated to the temperature of the space target. Figure 16 shows diagrammatically the effect of such an offset in calculating "on-orbit" radiance errors. The solid line represents the actual relationship between the relative counts and the target radiance, which does no extrapolate to zero relative counts at zero radiance (the size of the offset has been greatly exaggerated and the nonlinearity has been neglected). On-orbit the system response is defined by a line which goes through zero relative counts at zero radiance as well as through the one calibration point, ΔC_{ICT}, at N_{ICT}. Neglect of the offset, then, will produce an overestimate of the actual scene radiance at low scene temperatures, relative to the ICT temperature, and an underestimate of the scene radiance at high scene temperatures. The effect on the calculated temperature errors will be a positive value of the calculated minus measured temperatures for $T < T_{ICT}$, negative values for the temperature errors for $T > T_{ICT}$, and zero temperature error for $T = T_{ICT}$.

In order to verify the above hypothesis, the count offset, δC, is estimated from the offset fit parameter, γ, from fits of N_{ECT} to ΔC_{ECT}. This is given by (neglecting the quadratic term)

$$\delta C \approx \frac{-\gamma}{m_1} \ . \tag{5}$$

It should be noted that the sign of δC is such that a signal is still measured when the hot target radiance goes to zero. Thus, this effect cannot be simply explained in terms of reflected energy off

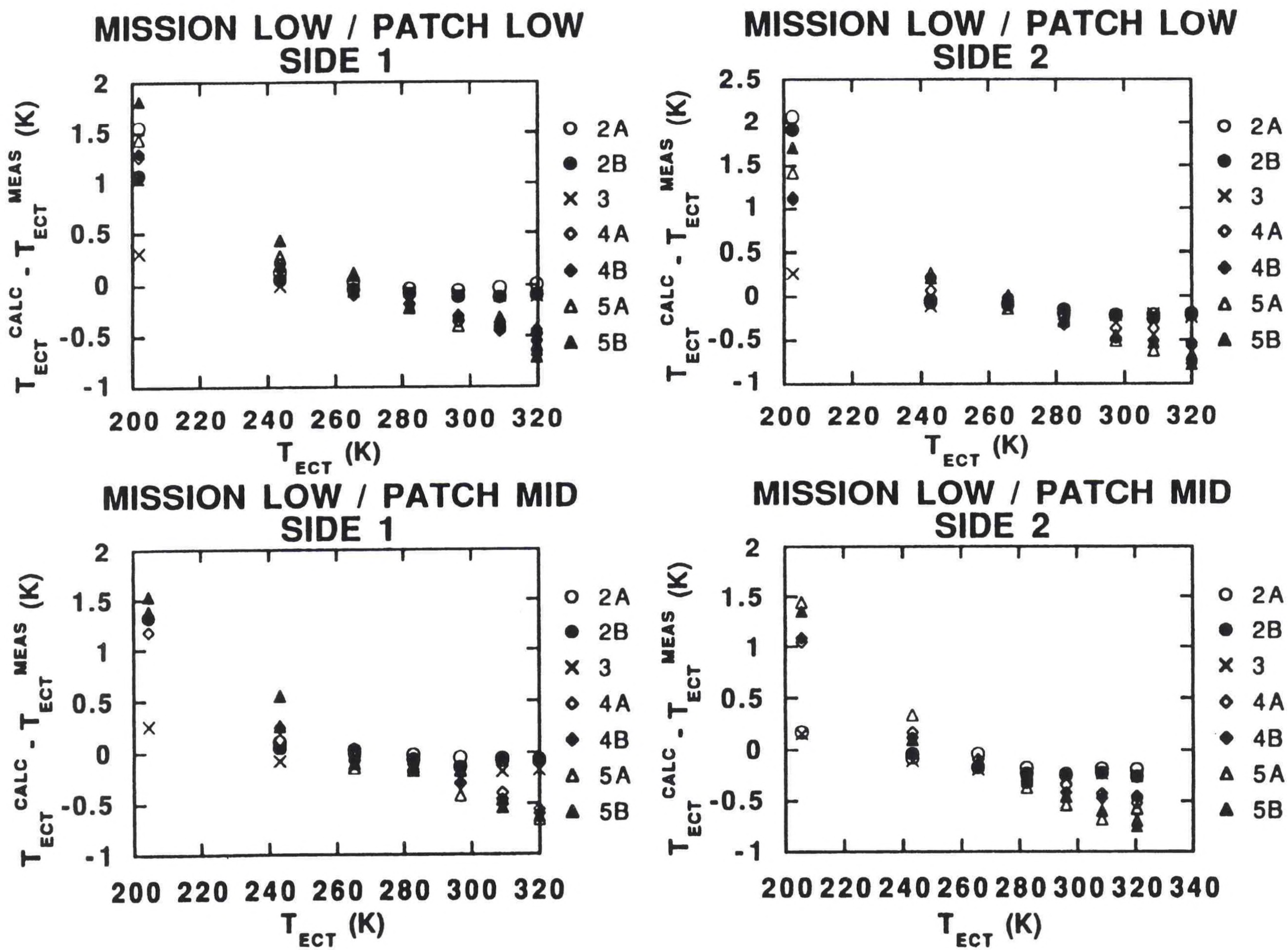

Figure 12. "On-orbit" temperature errors for mission low calibration runs with no offset correction.

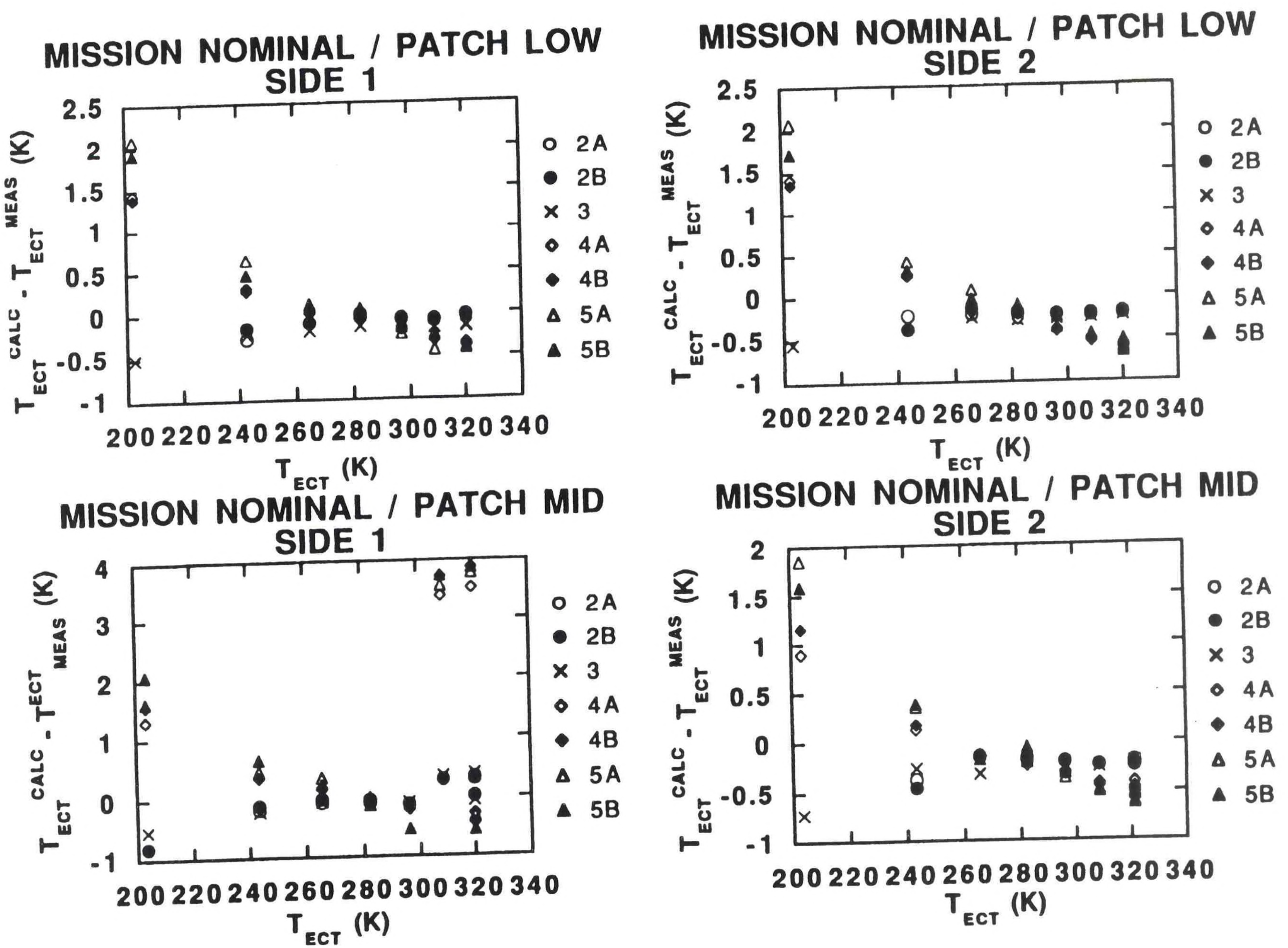

Figure 13. "On orbit" temperature errors for mission nominal, patch low and mid, calibration runs with no offset correction.

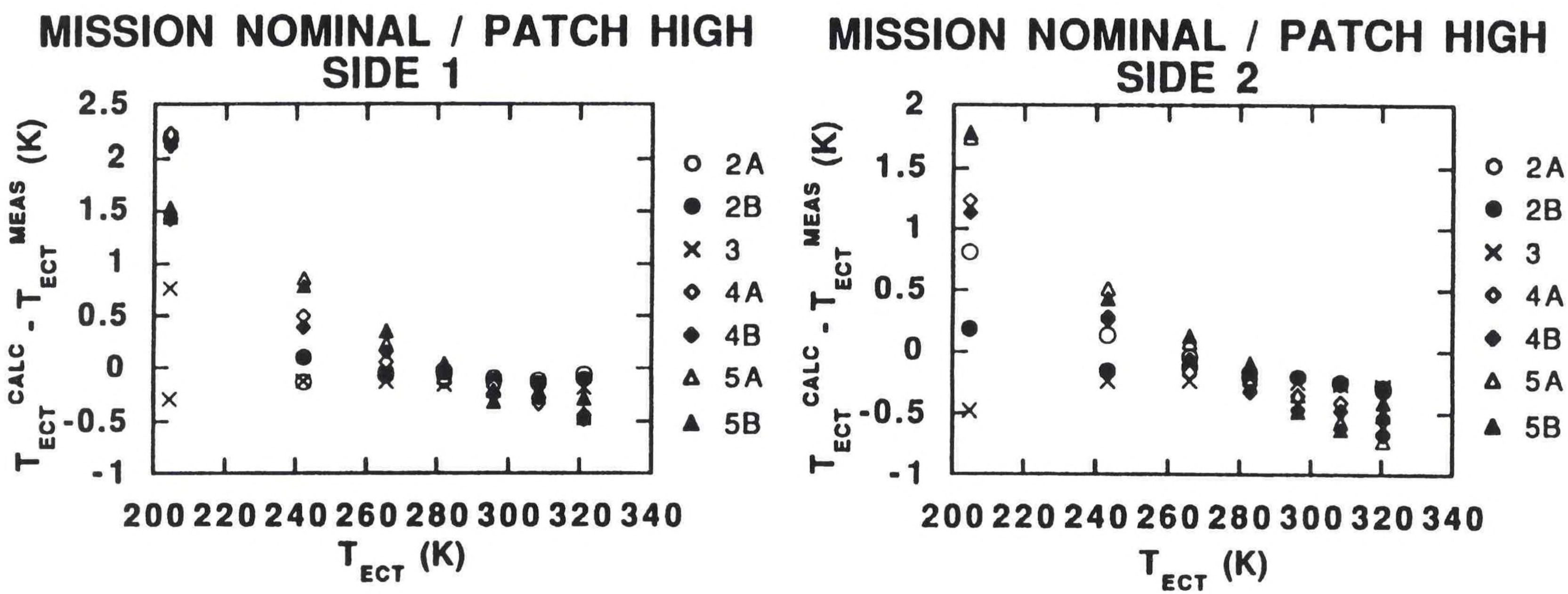

Figure 14. "On-orbit" temperature errors for mission nominal, patch high, calibration runs with no offset correction.

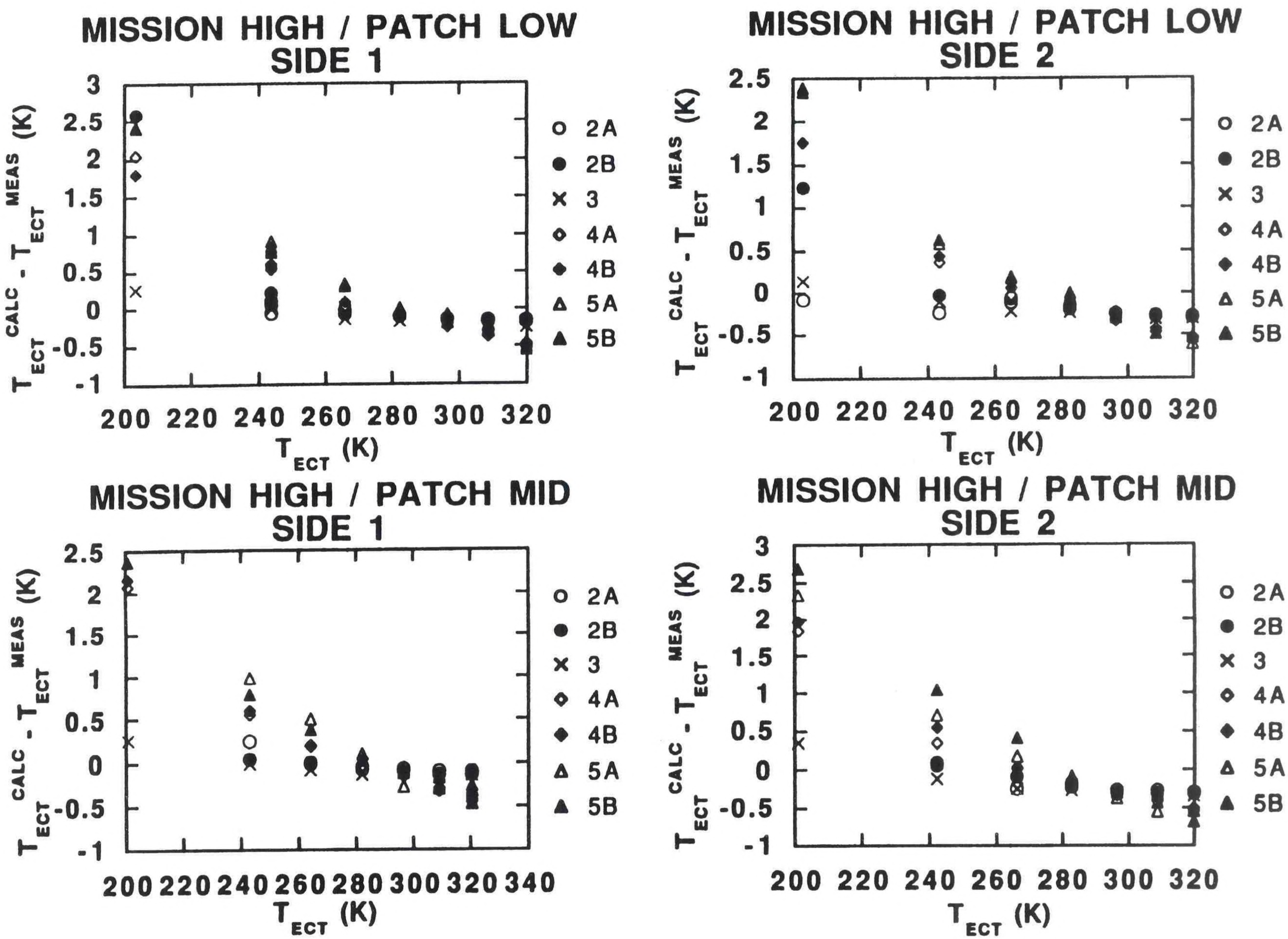

Figure 15. "On-orbit" temperature errors for mission high calibration runs with no offset correction.

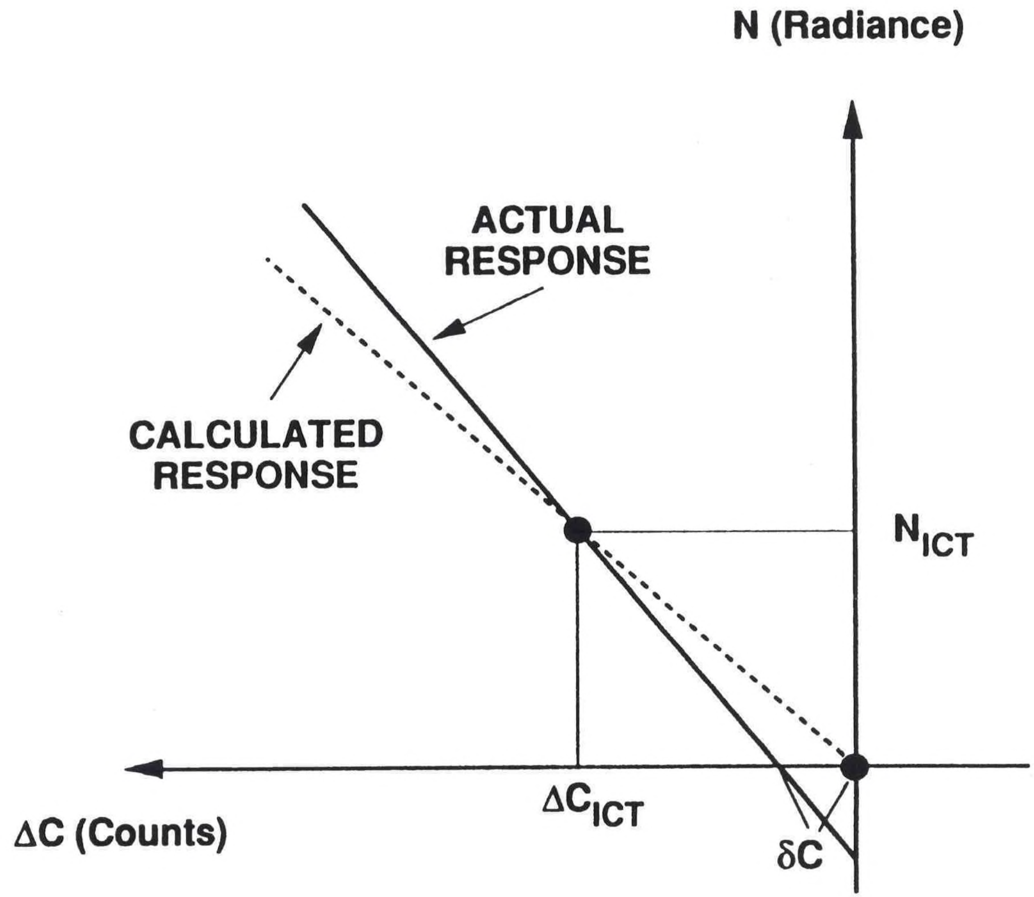

Figure 16. Diagram showing the effect of the offset in the two-point ICT calibration. If the actual response has an offset, shown by the solid line, then the two-point ICT calibration, shown by the dashed line, will tend to overestimate the target radiance at low target temperatures and underestimate the target radiance at higher temperatures, with the best estimation occuring at the temperature of the internal target (ICT).

the space target which would produce errors of the opposite sign. One possibility previously discussed[4] is a difference in emissivities between the space target and ECT target. Unfortunately, this has not been verified due to lack of proper instrumentation.

The offset from equation (5) must then be incorporated into the analysis in two places. The first corresponds to when the slope is estimated from the ICT measurement:

$$m'_{ICT} = \frac{N_{ICT} - R\left(\Delta C'_{ICT}\right)^2}{\Delta C'_{ICT}} \tag{6}$$

where $\Delta C'_{ICT} = \Delta C_{ICT} - \delta C$. This assumes that the mechanism which resulted in the offset between the ECT and space target is also active between the ICT and space target. The offset is again incorporated when the ECT radiance is calculated after equation (4):

$$N'_{ECT} = \left[\frac{N_{ICT} - R\left(\Delta C'_{ICT}\right)^2}{\left(\Delta C'_{ICT}\right)}\right]\left(\Delta C'_{ECT}\right) + R\left(\Delta C'_{ECT}\right)^2 \tag{7}$$

where $\Delta C'_{ECT} = \Delta C_{ECT} - \delta C$. Plots of the temperature error calculated from the results of equation (7) are shown in Figures 17 through 20. As can be seen, the incorporation of the offset brings the temperature errors much closer to zero and makes them for the most part independent of ECT temperature. If the assumption that the offset is an artifact of the experimental setup is valid, then these reduced temperature errors may be more indicative of on-orbit performance. Nevertheless, since δC is determined from the intercept fit parameter, γ, which itself is determined from fits to the ECT data and there is some uncertainty as to the physical origin of this parameter, then the analysis results may be more representative of an internal consistency check of the calibration.

A closer examination of the intercept, γ, which can be thought of as representing a stray radiance which is left over if the radiance versus counts is extrapolated to zero relative counts, shows little correlation with patch temperature, but some correlation with mission temperature, especially in channels 4 and 5. If γ is characteristic of the targets alone then it should not be affected by either mission or patch temperature unless it is influenced by emitted radiation from the instrument. When γ values for each of the channels is plotted versus wavelength and fit to a Planck function then the best-fit temperature is near 200 K for most of the mission / patch temperature conditions (Figure 21 shows one example). Thus, the equivalent temperature of the blackbody spectrum defined by these stray radiance values does not directly correspond to temperatures for likely sources of reflected radiation, including the instrument.

2.5 SUMMARY

Analysis of imager FTV ICT data has shown that, except for one wild point, the responsivity of the imager during calibration runs remained constant to within 0.5%. When the calibration fit parameters are used to determine the radiance temperature of the ICT, the results are uniformly higher. Calculated ICT temperatures are typically about 0.1 K higher for side 1, 0.3 K higher for side 2 and, in all cases, less than 0.5 K higher than the measured temperature for all channels. An

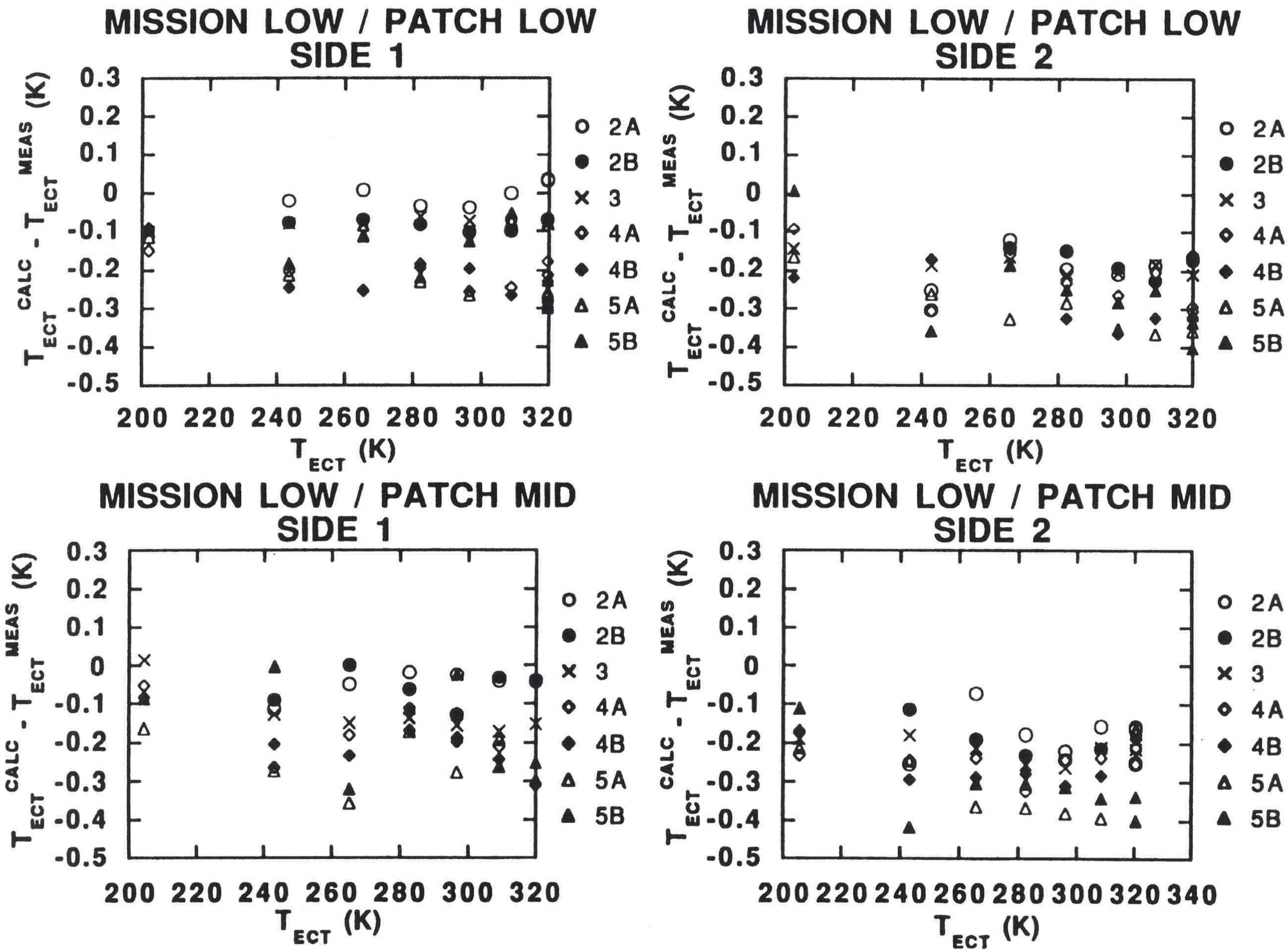

Figure 17. "On-orbit temperature errors for mission low calibration runs with offset correction.

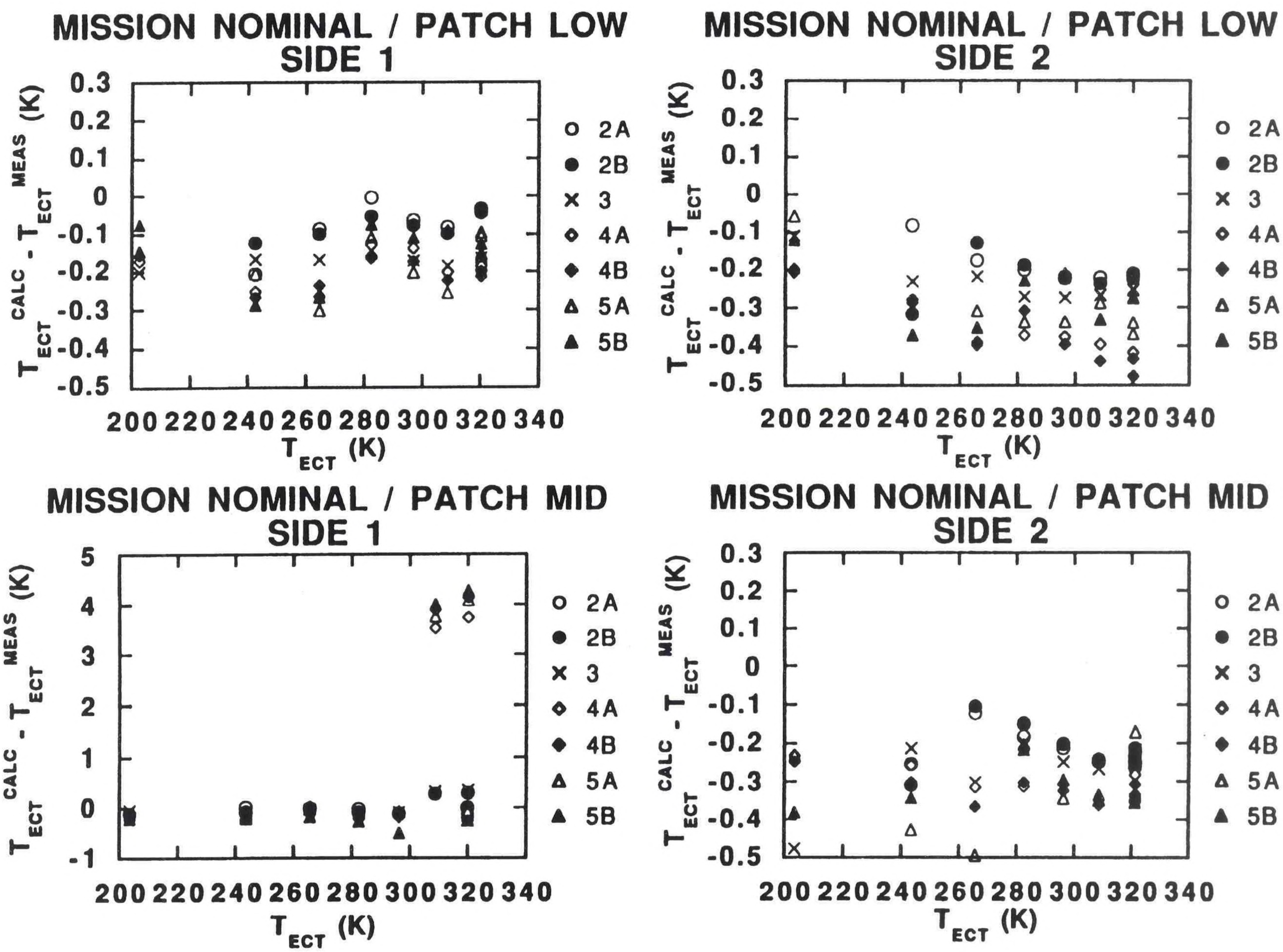

Figure 18. "On-orbit" temperature errors for mission nominal, patch low and mid, calibration runs with offset correction.

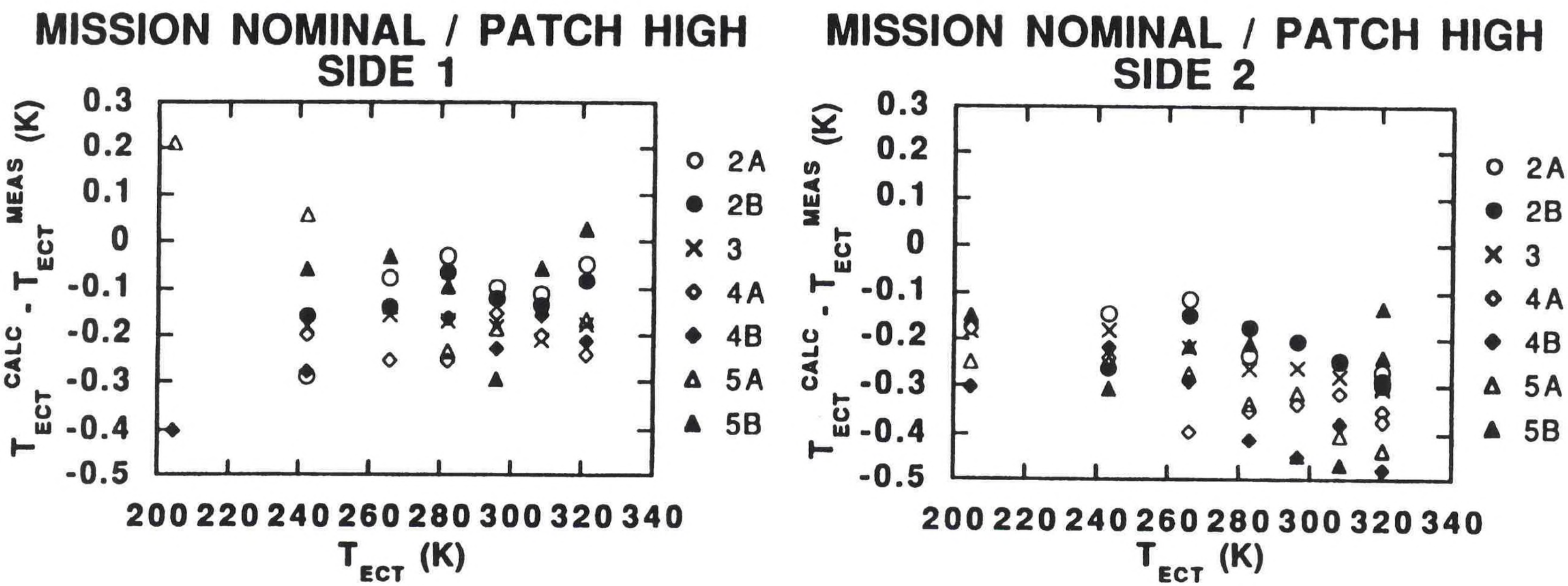

Figure 19. "On-orbit" temperature errors for mission nominal, patch high, calibration runs with offset correction.

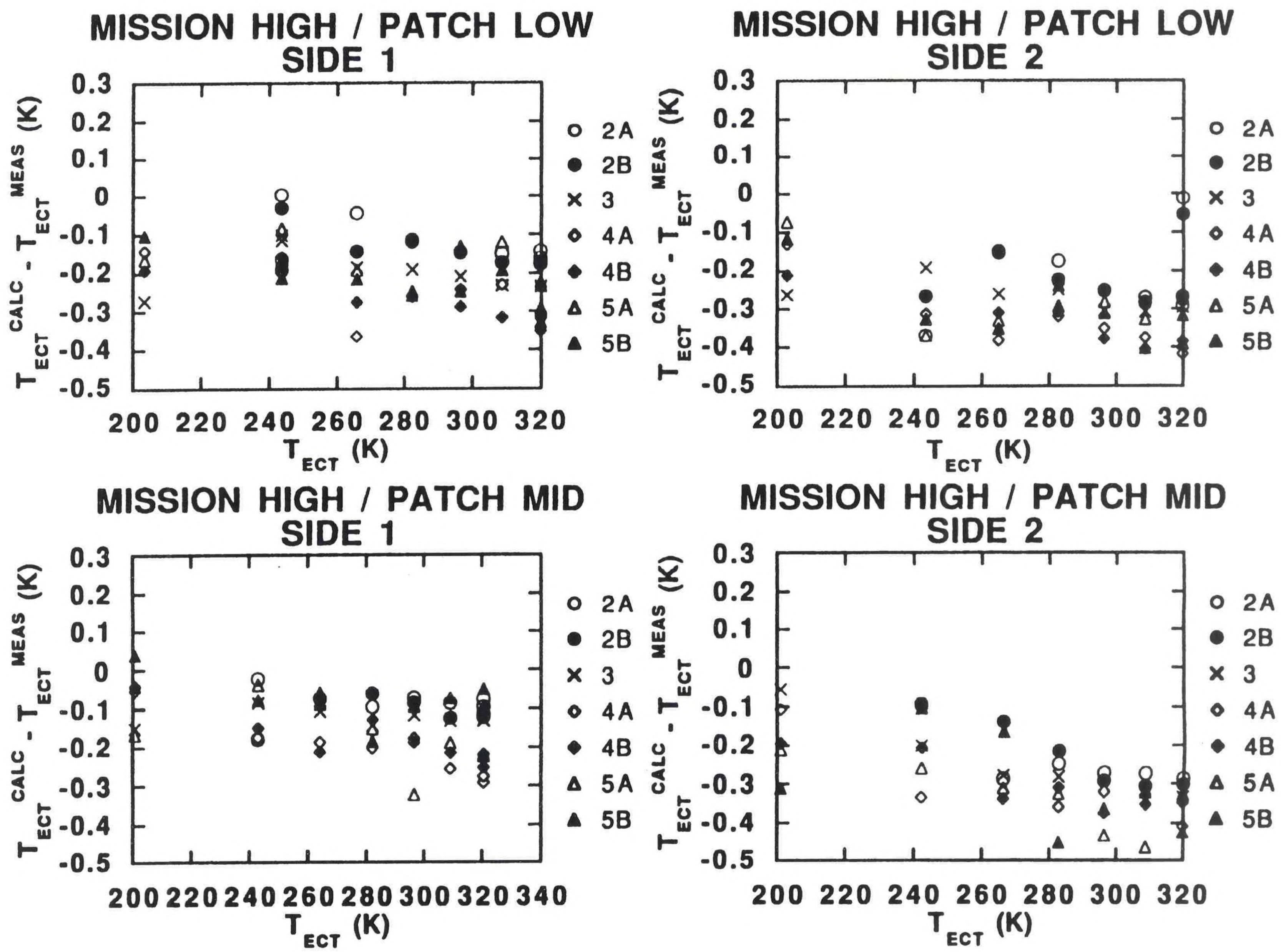

Figure 20. "On-orbit" temperature errors for mission high calibration runs with offset correction.

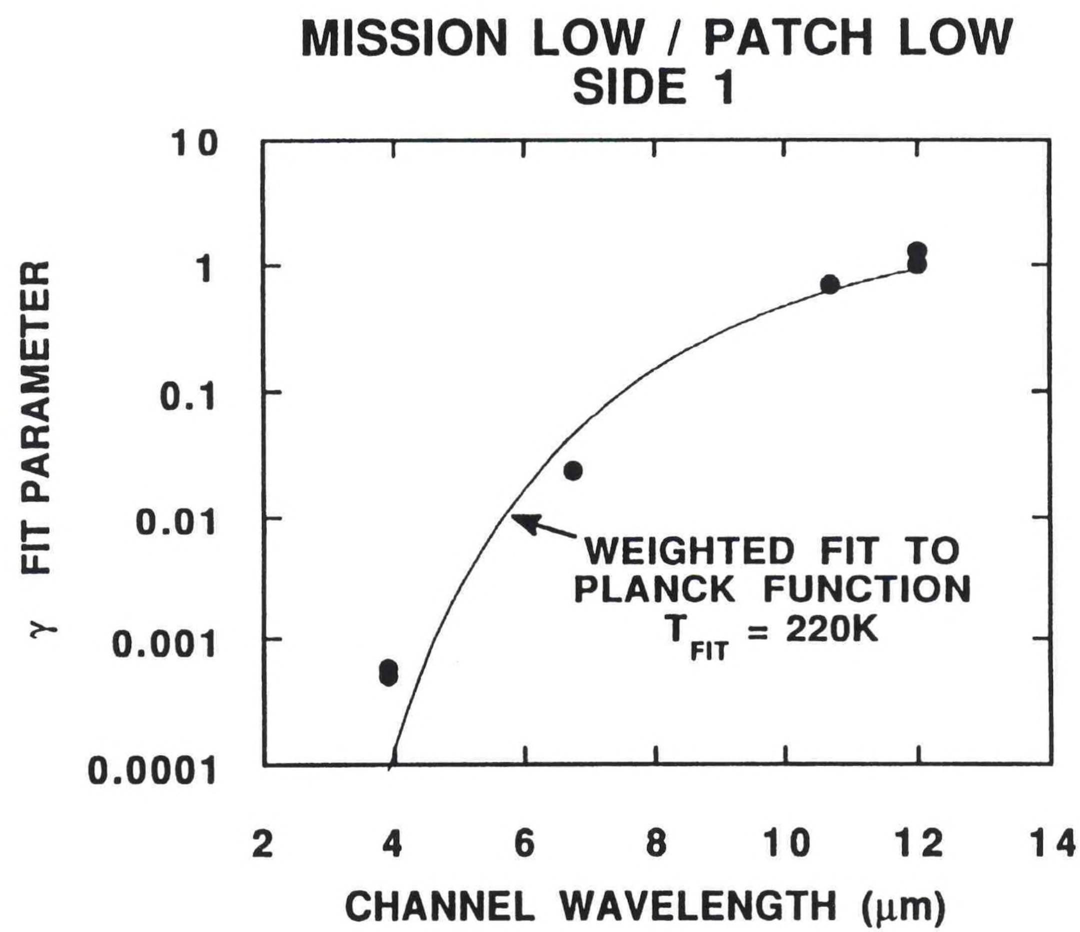

Figure 21. γ fit parameter (intercept) versus channel wavelength for the mission low / patch low calibration runs (solid circles). Included is a fit to the Planck function (solid line) which yielded a best fit temperature of 220K for this case.

analysis has also been performed which mimics the on-orbit determination of the calibration coefficients and uses these to determine the radiance temperature of the ECT. These temperatures show a systematic variation when compared with the measured ECT temperature which can be traced to the ignored intercept term of the calibration. The physical origin of this term is uncertain, although it is most likely due to an artifact of the calibration test configuration. The measured "on orbit" temperature error is small compared to the absolute radiometric accuracy requirement of +/- 1.0 K.

3. RESPONSIVITY DEPENDENCE ON OPTICS AND PATCH TEMPERATURES

The following presents ITT generated thermal-vacuum data of the normalized imager two-point responsivity versus patch and relay optics temperature. A comparison is made of the measured responsivity from PTV tests with that measured in FTV tests.

Figures 22 and 23 show plots of the normalized two-point responsivity versus patch temperature for the various imager IR channels corresponding to sides 1 and 2, respectively. In Figure 22, unregulated patch measurements, taken during PTV, are compared with regulated patch conditions in both PTV and FTV. In Figure 23, data from regulated patch measurements from PTV are compared with corresponding measurements from FTV. The data indicate a consistent drop in the responsivity between PTV and FTV of about 1% for all detectors. This could be due to a change in the target conditions, such as an aging of the external calibration target, or it could indicate a drop in the throughput of the imager system, as would be caused by dust buildup on the scanning mirror, for example. The fact that the responsivity decrease is uniform for all channels suggests that the problem is not due to any change in individual detector performance. The agreement of the regulated and unregulated patch data for PTV (Figure 22) suggests that the patch thermometer gives a good indication of the detector temperature. This information is valuable if the patch goes out of regulation on-orbit and responsivity changes in between blackbody looks have to be adjusted according to measurements of the patch temperature.

The total variation of the responsivity with patch temperature is on the order of 1% (from patch low to patch high) for channel 2, almost 3% for channel 3, and 20% and 25% for channels 25 and 26, respectively. The tendency of channel 3 detectors to increase their responsivity with patch temperature is due to a different bias point for these detectors.

Figures 24 through 26 contain plots of the normalized responsivity versus relay optics temperature for side 1 (Figure 24) and side 2 (Figures 25 and 26) IR detectors. Again, a generally uniform decrease in the responsivity from PTV to FTV measurements is observed. The decrease in responsivity with increased relay optics temperature is presumably due to an increase in the background radiation which causes the detector to operate closer to the nonlinear regime. The responsivity drop with mission conditions from mission low to mission high temperatures varies from about 2% for channel 2 to about 5% for channel 4 and 5 detectors. The agreement of the responsivity for side 2, FTV, data taken during thermal transition conditions with that taken during thermal regulated conditions suggests that the relay optics temperature can be used as an input for estimating the effect of temperature variations on responsivity on-orbit (see Section 4.0).

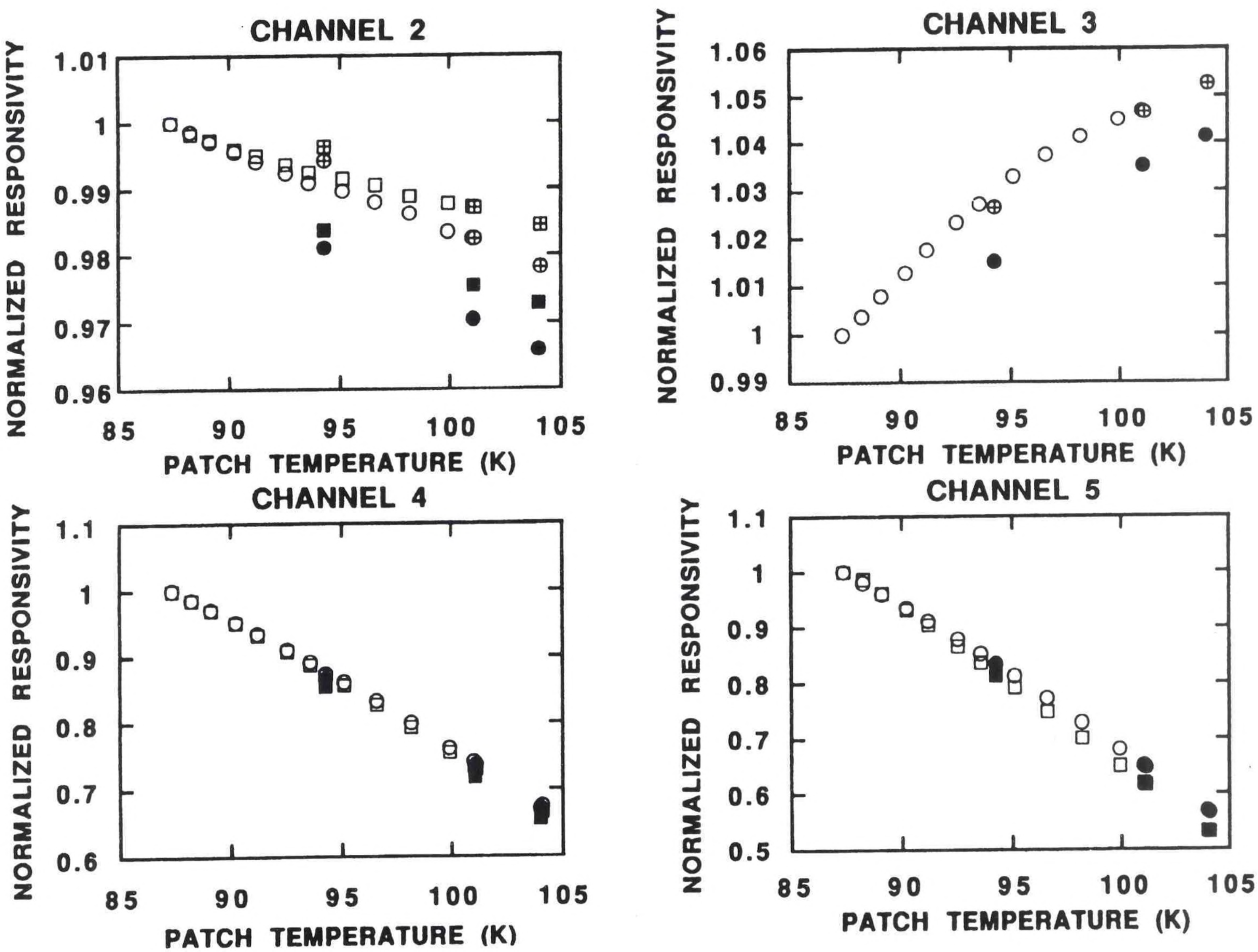

Figure 22. Normalized responsivity versus patch temperature for side 1 detectors, mission nominal conditions. The open symbols correspond to uncontrolled patch / preliminary thermal vacuum data, the crossed symbols correspond to regulated patch / pre. TV, and the solid symbols correspond to regulated patch / final TVdata. The circles and squares correspond to detectors A and B, respectively. All the responsivities are normalized to the lowest temperaturevalues for that detector.

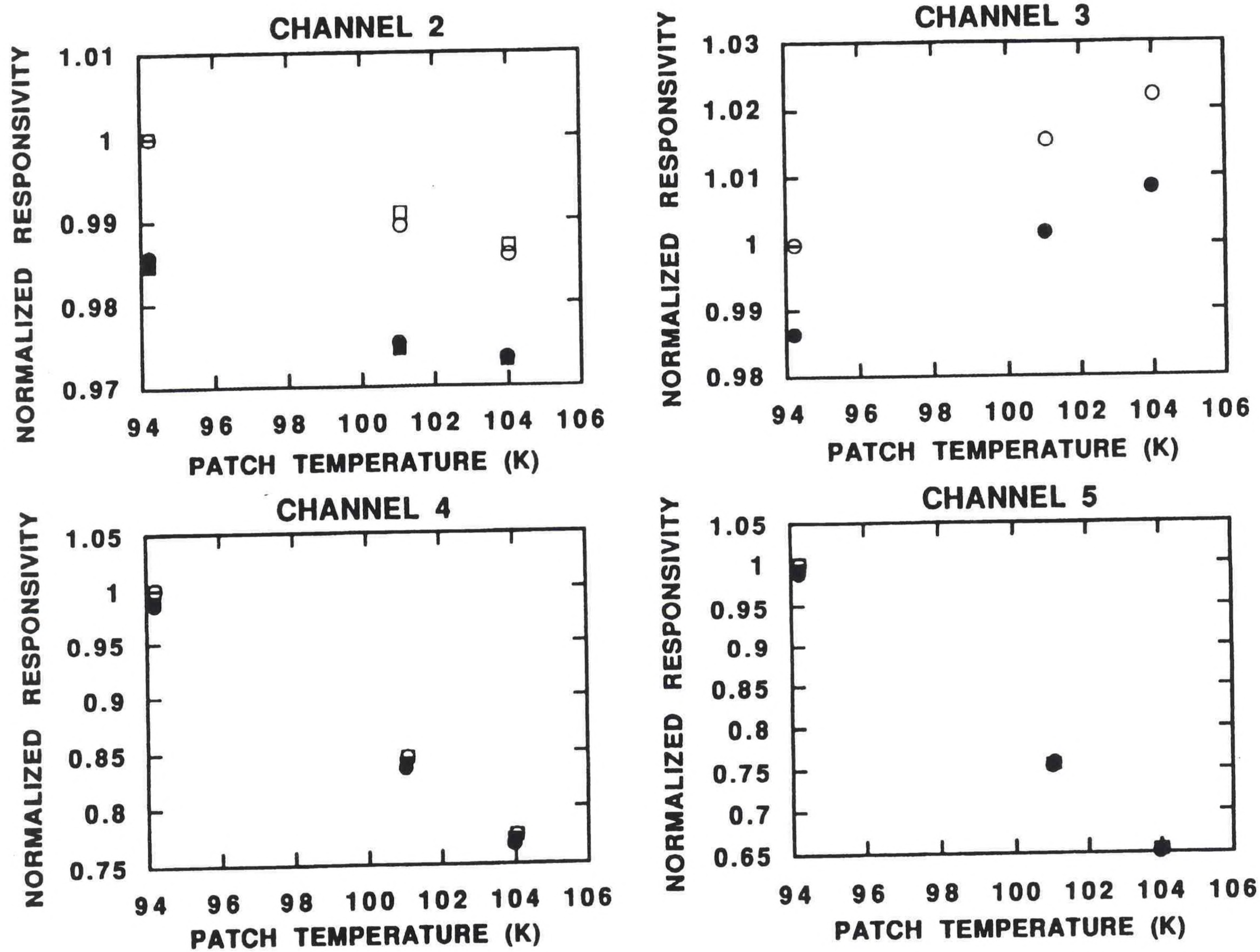

Figure 23. Normalized responsivity versus patch temperature for side 2 detectors, mission nominal conditions. The open and closed symbols correspond to preliminary and final thermal vacuum data, respectively. The circles and squares correspond to sides A and B, respectively. All responsivities correspond to regulated patch conditions and are normalized to the lowest temperature, preliminary thermal vacuum, values for that detector.

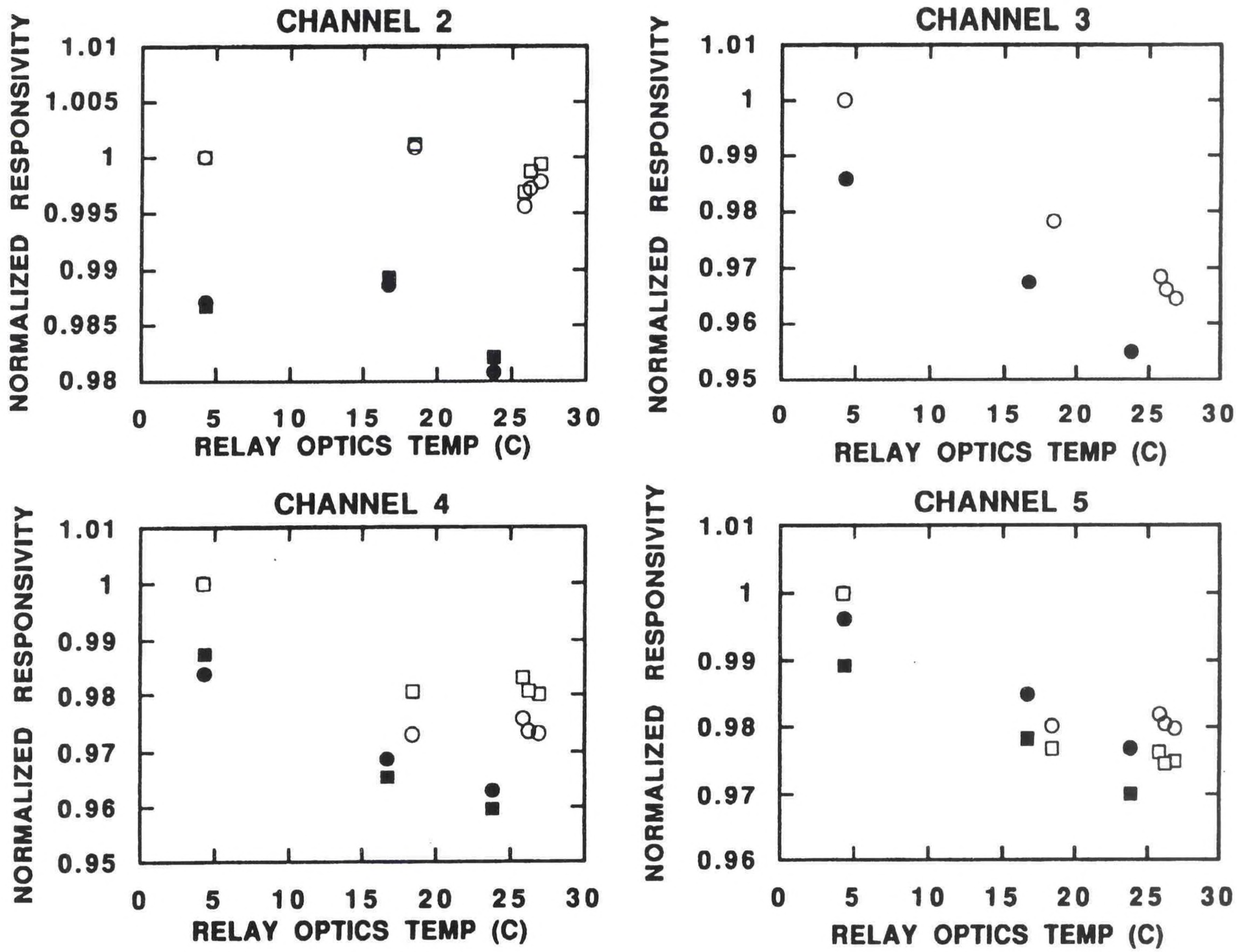

Figure 24. Normalized responsivity versus relay optics temperature for side 1 detectors, patch-mid. The open and closed symbols correspond to preliminary and final thermal vacuum data, respectively. The circles and squares correspond to sides A and B, respectively. All values are normalized to the lowest temperature responsivity for that detector.

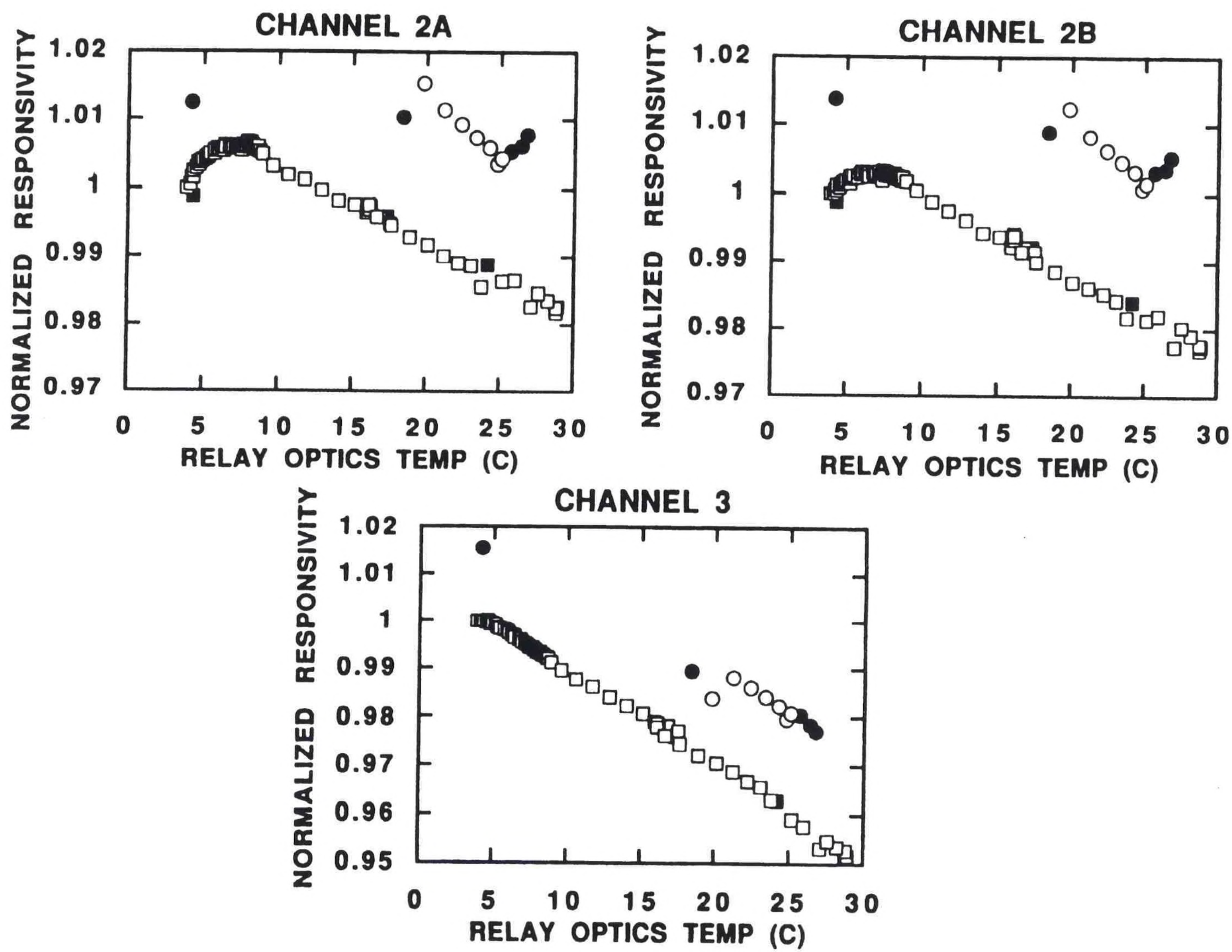

Figure 25. Normalized responsivity versus relay optics temperature for side 2 detectors, patch-mid. The circles and squares represent preliminary and final thermal vacuum data, respectively. The solid symbols correspond to regulated mission temperatures and the open symbols correspond to temperature transition conditions. All values are normalized to the lowest temperature responsivity for that detector.

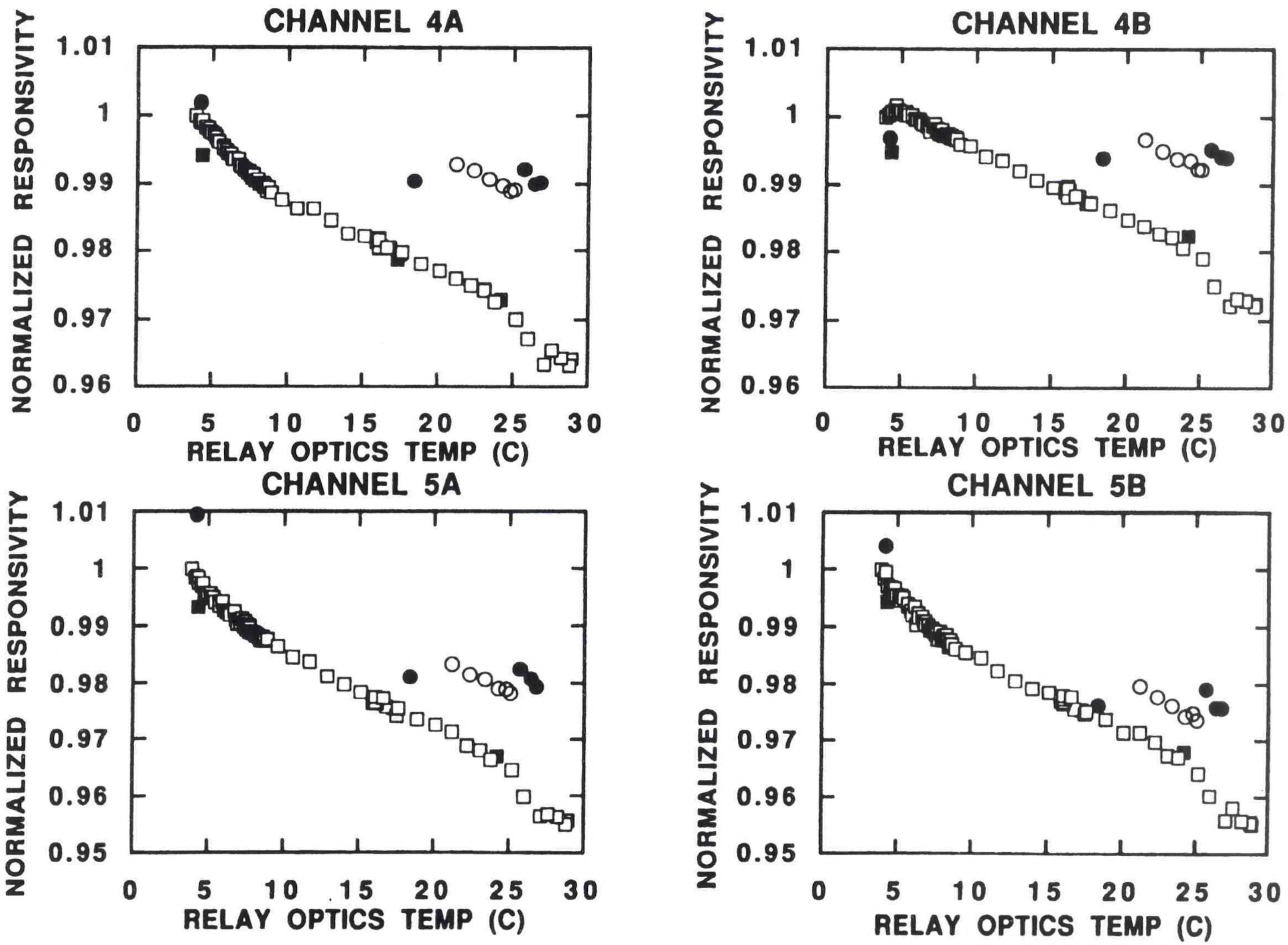

Figure 26. Normalized responsivity versus relay optics temperature for side 2 detectors, patch-mid. The circles and squares represent preliminary and final thermal vacuum data, respectively. The solid symbols correspond to regulated mission temperatures and the open symbols correspond to temperature transition conditions. All values are normalized to the lowest temperature responsivity for that detector.

4. DIURNAL RESPONSIVITY CHANGES AND ON-ORBIT TEMPERATURE ERRORS

4.1 INTRODUCTION

Thermal vacuum tests of the SN03 imager indicate that the responsivity of the IR channels varies in a systematic way with various instrument temperatures. The best correlation has been observed to be with the relay optics temperature. Figure 27 shows plots of the normalized responsivity versus relay optics temperature for patch-mid/side-2 in final thermal-vac testing. The open symbols are a compendium of data from two transition tests, taken about two weeks apart, one from mission low to mission nominal and one from mission nominal to mission high. The solid points on the figure are the normalized responsivities from the 320K ECT temperature points of the IR calibration runs for the three mission temperatures. All the data points are normalized to the lowest temperature responsivity from the mission low to mission nominal transition data. The decrease in responsivity with relay optics temperature is presumably due to the increased background flux from the optics causing the dynamic operating range of the detector to move further into the nonlinear range. The non-monotonic behavior for the lower temperature responsivities of channel 2 has also been observed in SN03 preliminary thermal-vac data. As can be seen from the plot, the total variation of responsivity with instrument temperature is about 2-5% and the agreement of the various responsivity data collected weeks apart and under steady-state versus thermal transition conditions attests to the validity of the correlation with relay optics temperature. One would, therefore, expect this correlation to remain valid on orbit.

Solar beam testing carried out at Space Systems/LORAL has generated various predictions of the on-orbit temperature variation of the imager during a diurnal cycle. Figure 28 shows the results of Phase 1 testing of the SN02 Imager (without the additional sun shield) depicting various instrument temperatures versus diurnal time for the 10 degrees north of equinox case with the scan mirror fixed and pointing at nadir. These data can be used in conjunction with the responsivity versus temperature data from Figure 27 to estimate the temperature error caused by changes in the responsivity between BB looks due to the diurnal variation of the optics temperatures. Since relay optics temperatures were unavailable at the time of the writing of this memo, the vis-optics temperature will be used from the Phase 1 tests. The instrument modifications for the Phase 2 tests (for which the vis optics temperature were not available) resulted in a diurnal variation of the baseplate temperature of 12C - 30C, compared with 12C - 34 C for Phase 1. Therefore, the inclusion of the sunshield should reduce the calculated temperature errors, though the difference is not expected to be significant.

4.2 PROCEDURE

The first step in the calculation was to parameterize the responsivity as a function of vis optics temperature. This was done by fitting the responsivity versus vis optics temperature to a second order polynomial (Figure 29) and vis optics temperature versus diurnal time to an eighth order polynomial (Figure 30). The order of the polynomial fits was chosen high enough to adequately represent the data but not so high as to be sensitive to noise irregularities. The fits served the purpose of averaging over noise and providing a uniform interpolation of the data. As can be seen from Figure 29, the responsivity is not as well correlated with vis optics temperature as with relay optics temperature. This reduction in correlation necessitated the use of only second

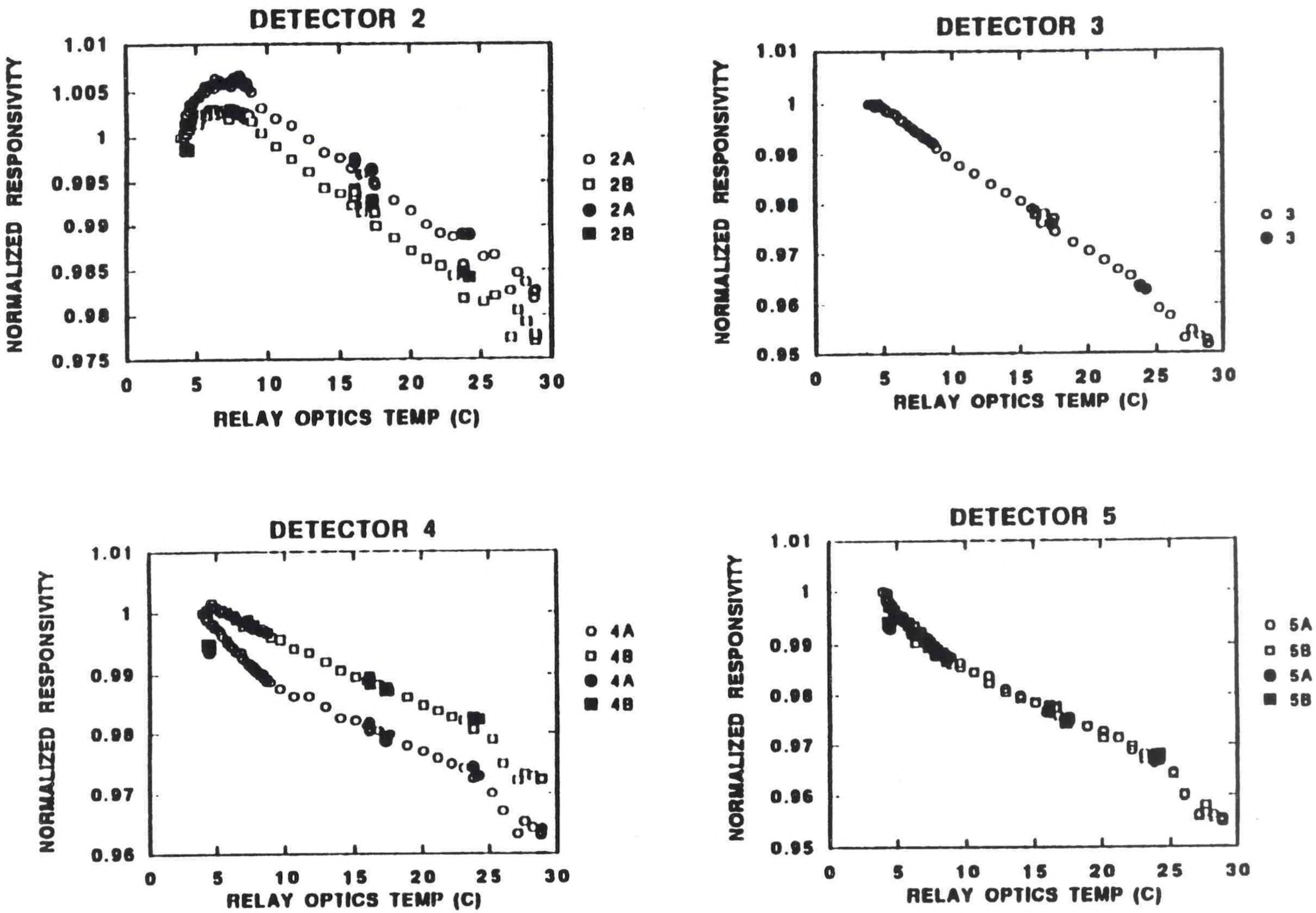

Figure 27. Normalized responsivity versus relay optics temperature for each of the Imager detectors. The open symbols are from measurements performed while the instrument was transitioning in temperature; the closed symbols correspond to measurements taken during IR calibration runs. All the responsivities are normalized to the lowest temperature value of the transition data.

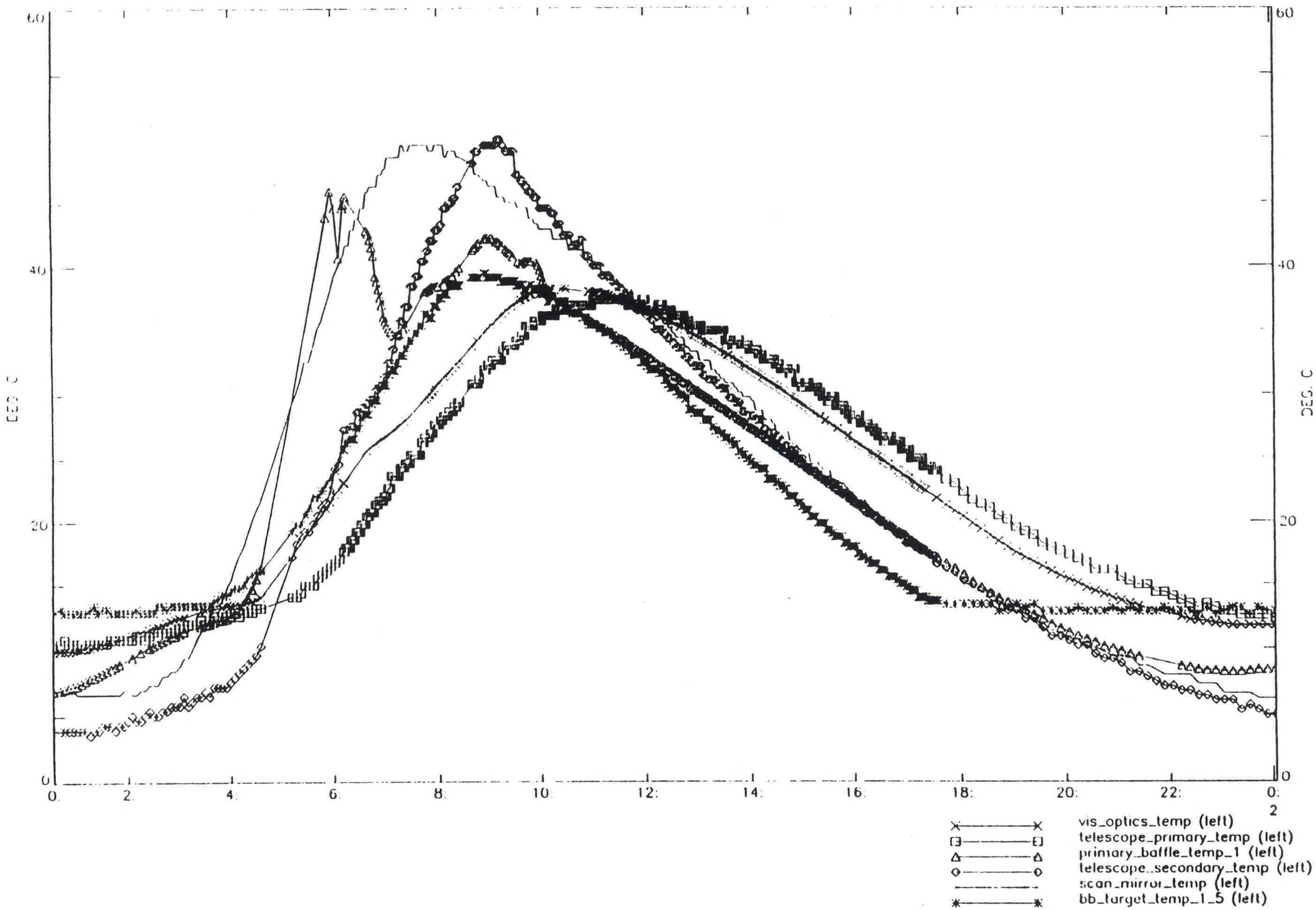

Figure 28. Various telemetry temperatures versus time from Phase 1 solar beam tests of the SN02 Imager. The units of the abcissa is hours with 6 corresponding to midnight. The test configuration was for a solar angle 10 degrees North of equinox with the scan mirror fixed at nadir.

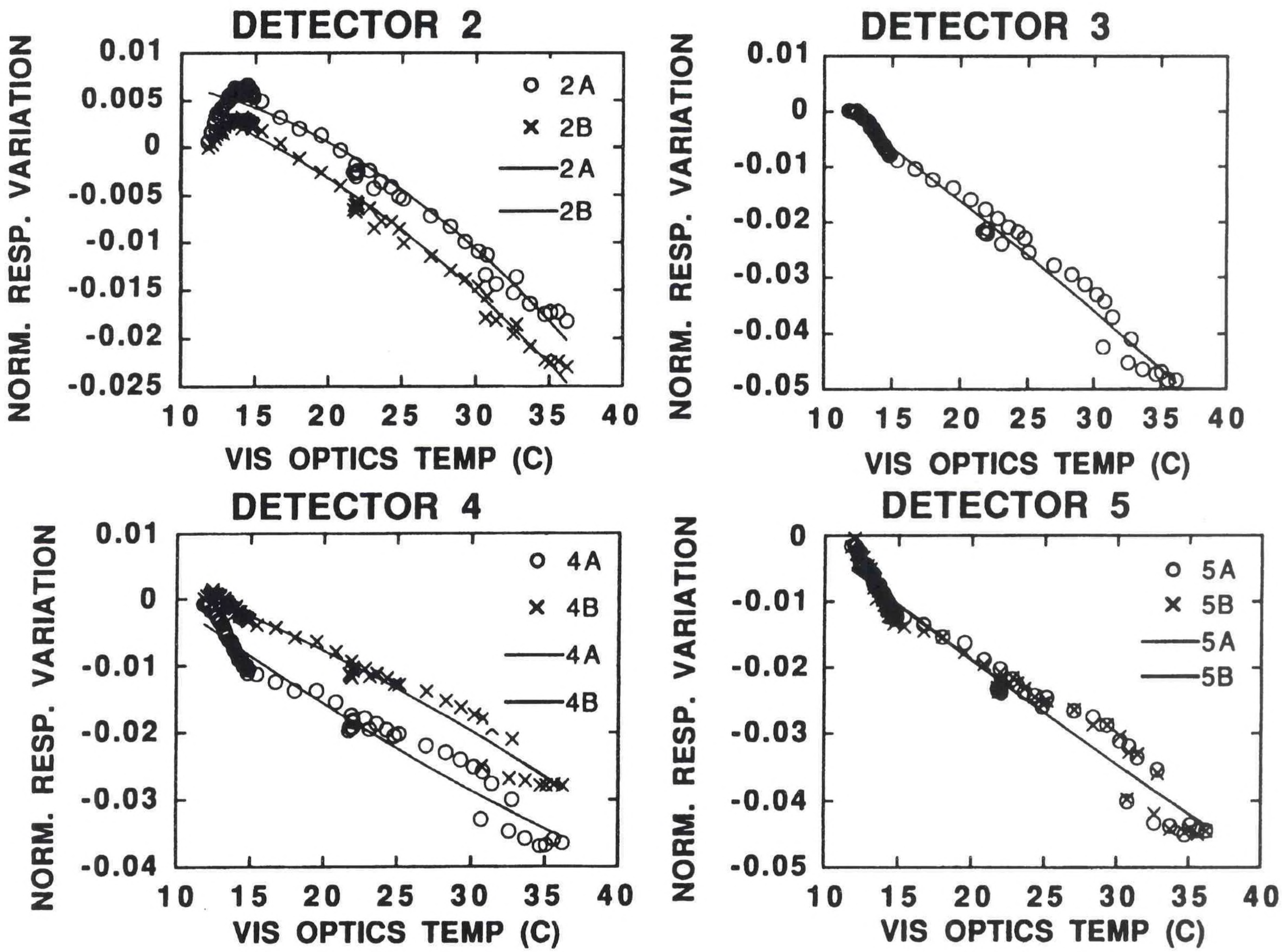

Figure 29. Same data as Figure 1 plotted against Vis Optics temperature along with results of fits to second order polynomials. The ordinate scale is equal to one minus the scale from Figure 1.

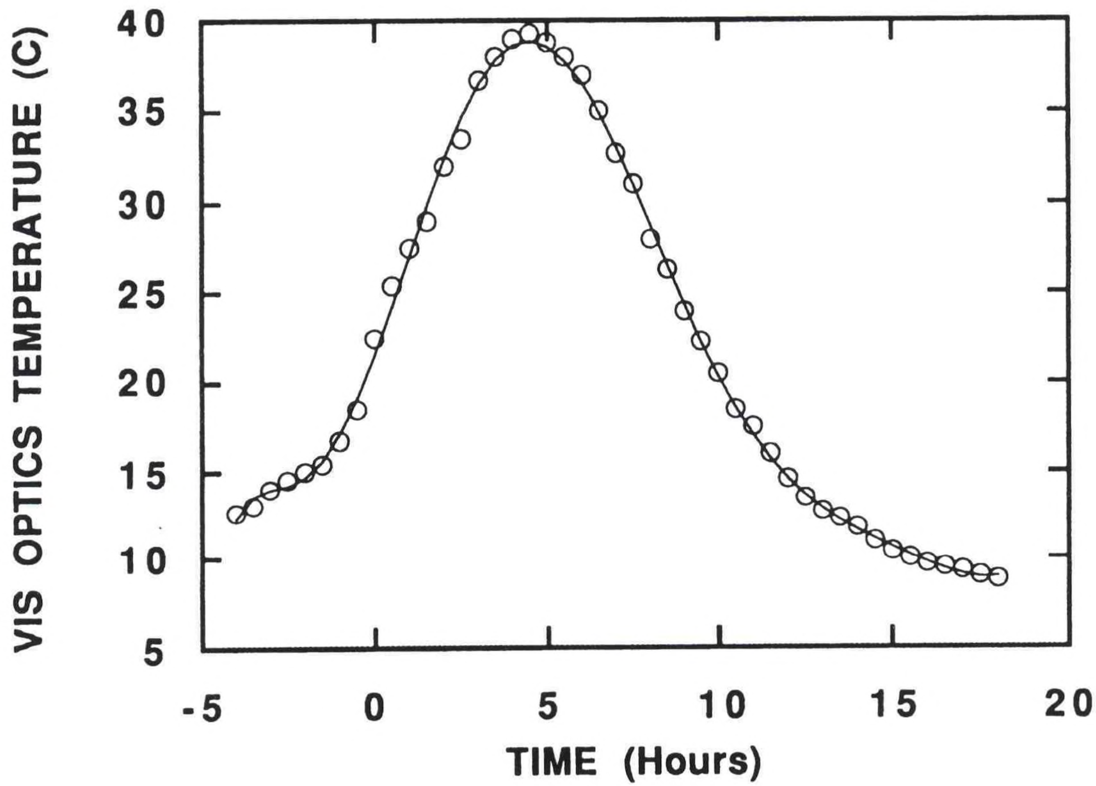

Figure 30. Vis Optics temperature versus diurnal time taken from Figure 2 (open symbols) along with results of fit to 8th order polynomial (solid line).

order polynomials for the fits. Higher order functions, while being able to represent the non-monotonic behavior in channel 2, became too sensitive to the noise in the data.

The temperature error was calculated as:

$$\delta T(t,\tau_{bb}) = \frac{dT}{dN}\delta N\left[T_{vo}(t),\tau_{bb}\right]$$

where δ is the maximum scene temperature error, which occurs just before the next blackbody look, τ_{bb} is the time between blackbody looks, dT/dN is the derivative of the function relating scene temperature (assumed to be 300K for this calculation) to the radiance on detector, δN is the perceived radiance change due to a responsivity change over a period between blackbody looks, and T_{vo} is the vis optics temperature which is a function of the diurnal time, t. For the sake of simplicity, the detector response is assumed to be linear, so the change in radiance can be linearly related to a change in responsivity as:

$$\delta N(t,\tau_{bb}) = (\Delta C)\delta m_1$$

$$= (\Delta C)\left[\frac{1}{R\left[T_{vo}(t+\tau_{bb})\right]} - \frac{1}{R\left[T_{vo}(t)\right]}\right]$$

where ΔC is the relative-mean counts above space, and $m_1 \approx 1/R$, where m_1 is the slope term from the instrument calibration equation and R is the responsivity in units of counts per radiance of (counts)(cm)(m^2)(Sr)/mw. The quantity $R[T_{vo}(t)]$ was calculated from the polynomial fits and ΔC is a constant and approximated by:

$$\Delta C \approx \frac{N_{300} - \gamma_0}{m_1},$$

where N_{300} is the radiance for each channel corresponding to a scene temperature of 300K and γ_0 and m_1 are the offset and slope fit parameters corresponding to the Imager mission-nominal/patch-mid/side-2 case. Both N_{300} and dT/dN are calculated from the ITT supplied spectral-radiance files. With the above formulation the temperature error, δT, can be considered the measured temperature minus the actual temperature at a time just before a blackbody look.

4.3 RESULTS AND CONCLUSIONS

δT as a function of the time of day has been calculated for times between blackbody looks, τ_{bb}, of 30 minutes, 20 minutes, and 5 minutes, which is shown on Figures 31, 32, and 33, respectively. As can be seen from the figures, the maximum temperature errors occur around 1:00 a.m. and 8:00 a.m. which correspond to the times when the rate of change of the vis optics temperature is a maximum. The times of the maximum temperature errors are shifted slightly from channel to channel which is presumably due to the small differences in nonlinearity of the responsivity versus temperature for each of the channels. The temperature errors also appear to generally be the greatest for the long wavelength channels and the least for the shorter wavelength

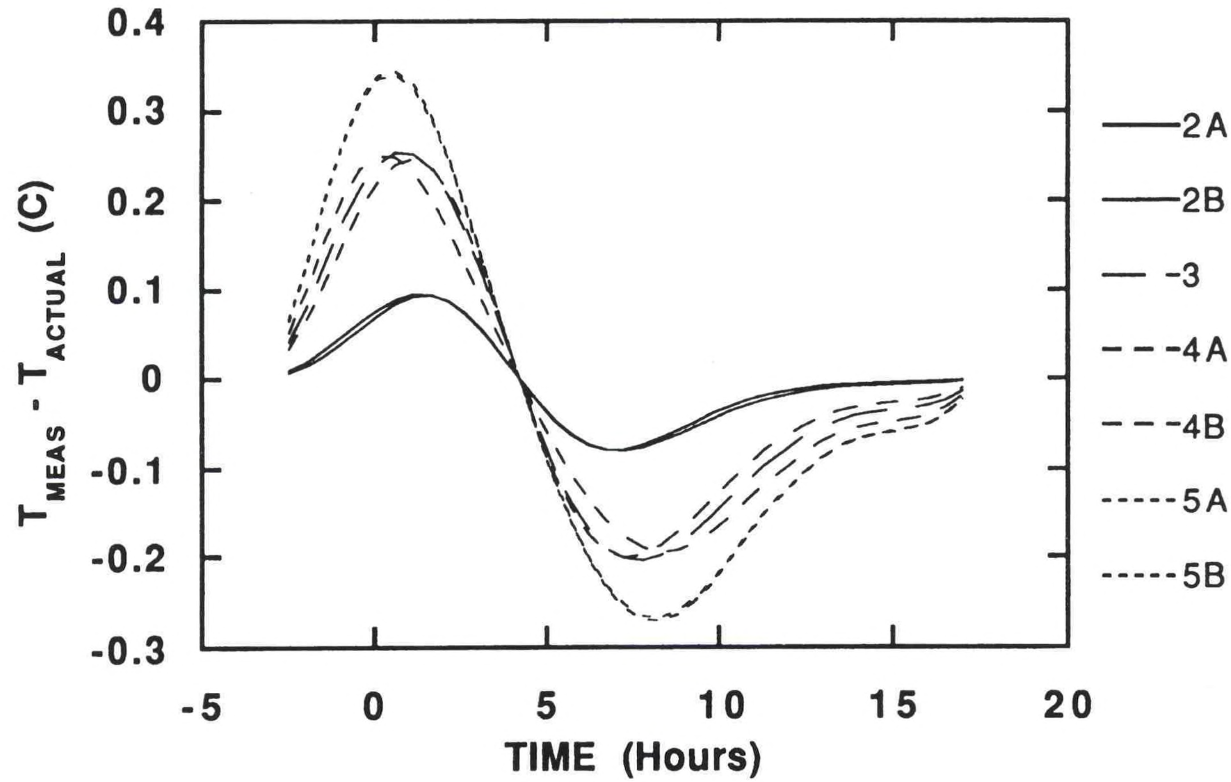

Figure 31. Temperature error versus diurnal time for 30 minute responsivity correction intervals (blackbody looks).

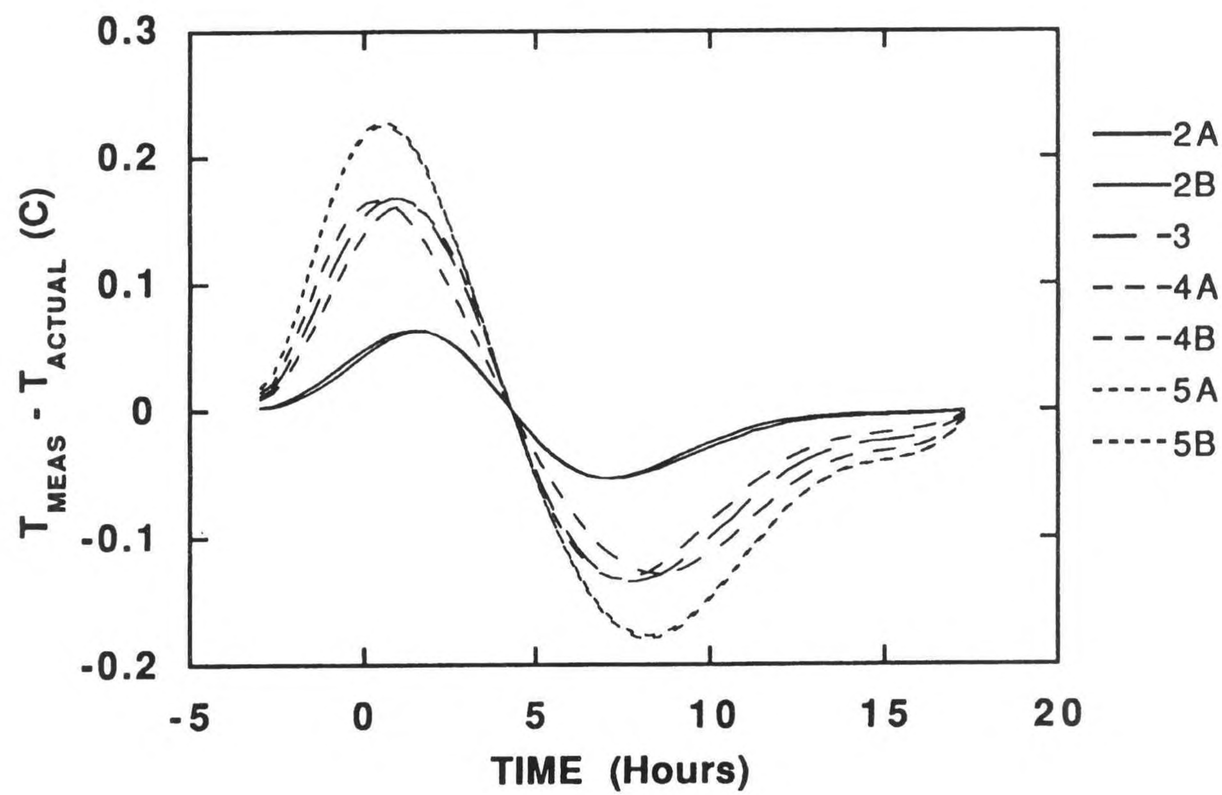

Figure 32. Temperature error versus diurnal time for 20 minute responsivity correction intervals.

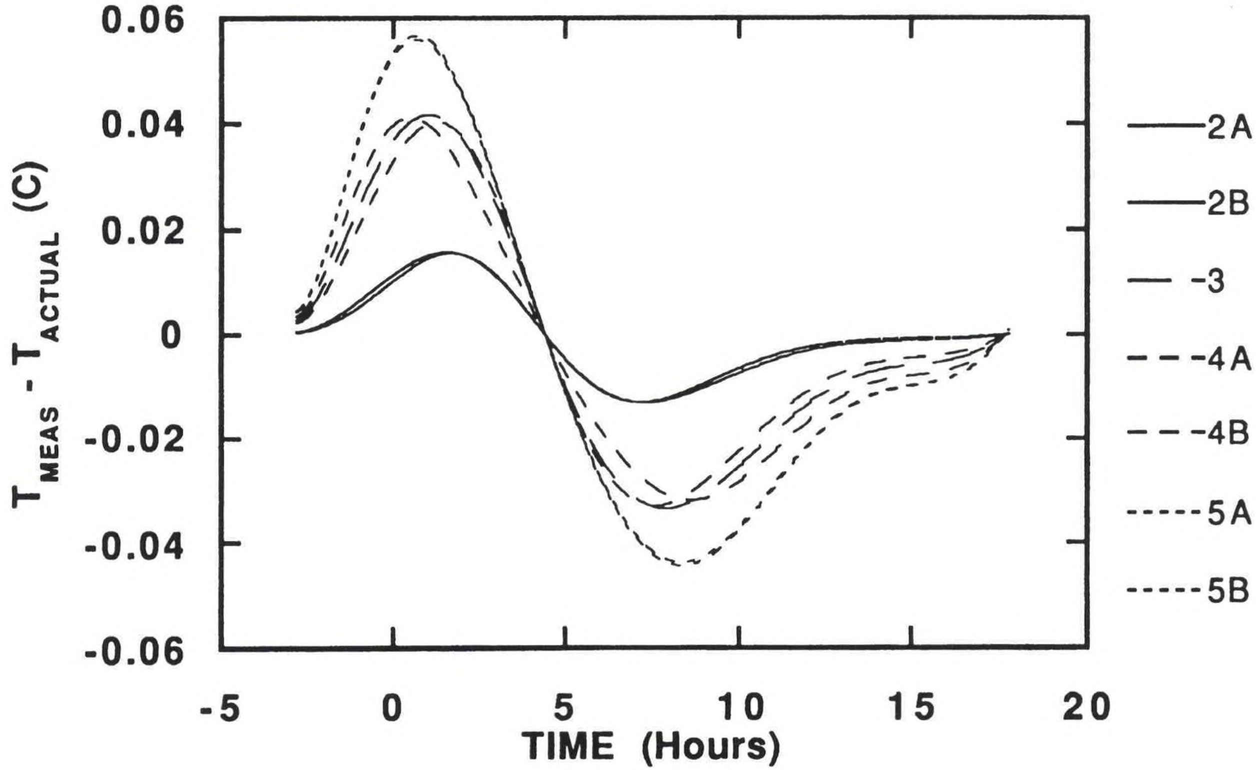

Figure 33. Temperature error versus diurnal time for 5 minute responsivity correction intervals.

channels, except for channel 3 whose temperature error splits the levels calculated for channels 4A and 4B. This interchannel variation is the results of the competition between the wavelength dependence of dT/dN, which is larger for the short wavelength channels, and the overall responsivity change, which is generally larger for the longer wavelength channels.

Over the range of periods for responsivity updates, or blackbody times, the character of the diurnal variation of the temperature error appears to remain fairly constant with the magnitude of the error scaling linearly with update period. This is demonstrated in Figure 34, which is a plot of the maximum temperature error over the diurnal cycle (which always occurs near 1:00 a.m.) as a function of the responsivity update period. The maximum temperature errors show a very linear dependence with update time. This linear dependence should eventually roll over for responsivity update periods of 2-3 hours, over which the vis optics temperature near midnight is no longer monotonically increasing.

It should be kept in mind that the temperature errors calculated here are the maximum errors which occur just before a new blackbody look, or some other form of responsivity correction, is performed. Just after each blackbody look the temperature error would be reset to zero and would then rise as the temperature changes in the instrument cause the responsivity to change. On orbit the period between blackbody looks will be 20 to 30 minutes and, while it is unrealistic to significantly shorten this time, there are several OGE processing scenarios which would allow the responsivity to be adjusted based on measurements of instrument temperatures which have known correlations with the response.[5] In this case the blackbody look interval would be replaced with the interval over which the responsivity was adjusted and these calculations should serve as a guide as to the relationship between the adjustment time and the temperature errors. Adjustment times as short as 2 minutes have been considered for OGE processing, which would result in temperature errors less than 0.03C.

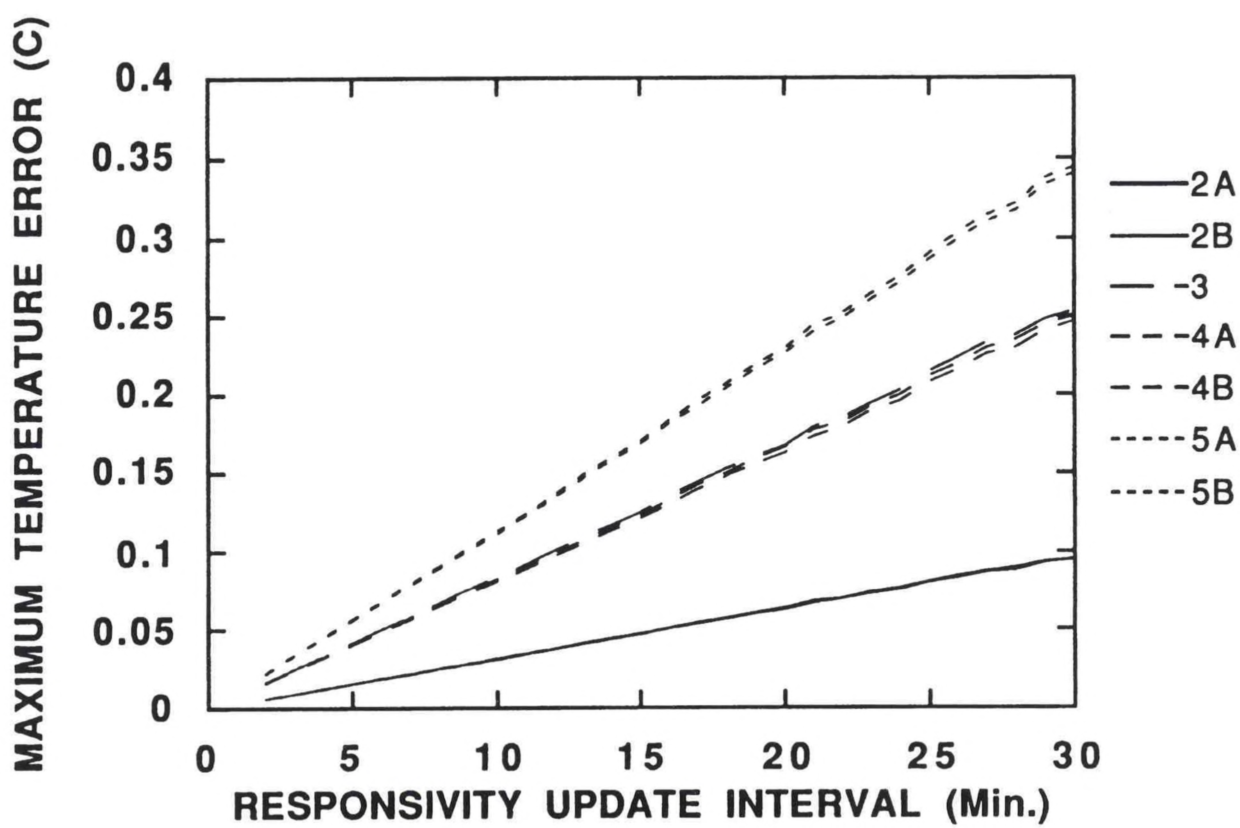

Figure 34. Absolute value of the maximum temperature error over a diurnal cycle versus blackbody look period.

5. MISSION TRENDS OF CALIBRATION COEFFICIENTS

Imager FTV calibration testing determined linear and quadratic calibration coefficients for 7 instrument operating conditions as shown in Table 2. Mission (baseplate) and patch 2 temperatures are regulated on orbit at fixed levels depending on season. An understanding of the variation of calibration coefficients as a function of these temperatures is useful in understanding seasonal limitations to instrument performance. While the complete listing of coefficients can be found in the Appendix, Figures 35 through 50 present characteristic trends of the slope and quadratic coefficients for each channel/detector/electronic side combination.

Figures 35 through 38 show slope variations with patch temperature (at mission nominal). Channel 2 shows very little change and channel 3 shows a slight decrease with increasing patch temperature. Channels 4 and 5 show large slope increases with increasing patch temperature. These effects are consistent with standard detector models.[6]

Figures 39 through 42 show quadratic coefficient variations with patch temperature (at mission nominal). Error bars indicate the standard statistical error obtained in the curve fitting process. It is clear that channels 4 and 5 show an increase with patch temperature. Since there is no reason to expect anything other than a constant or a monotonic variation with temperature, it is reasonable to interpret channels 2 and 3 as constant.

Figures 43 through 46 show slope variations with mission (baseplate) temperature (at patch low). Variations are generally smaller over the full range of mission temperatures than over the full range of patch temperatures. Again channel 2 shows very little change. The increase in channels 3, 4 and 5 slope is probably due to a change in detector response at increased background flux levels that accompany increased optics temperatures.

Figures 47 through 50 show quadratic variations with mission (baseplate) temperature (at patch low). Assuming that variations should be monotonic with temperature, it is difficult to attach significance to these variations. The relatively large size of the error bars also supports the interpretation that the quadratic coefficient is unaffected by mission temperature.

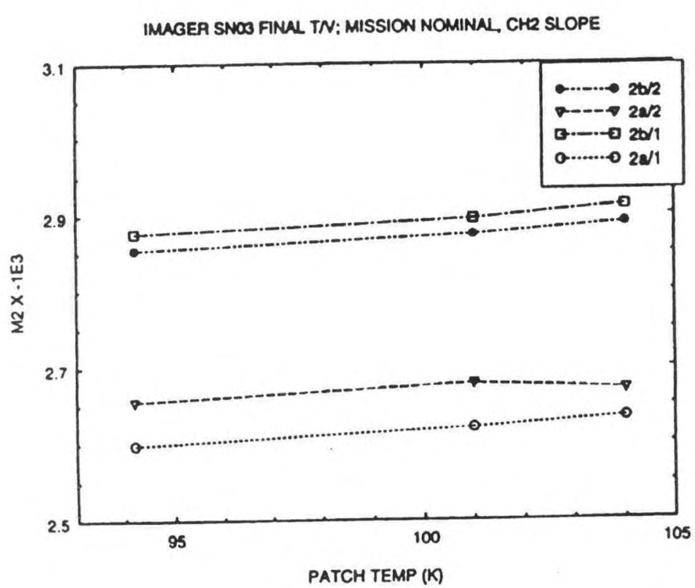

Fig 35. Slope versus patch temperature, channel 2.

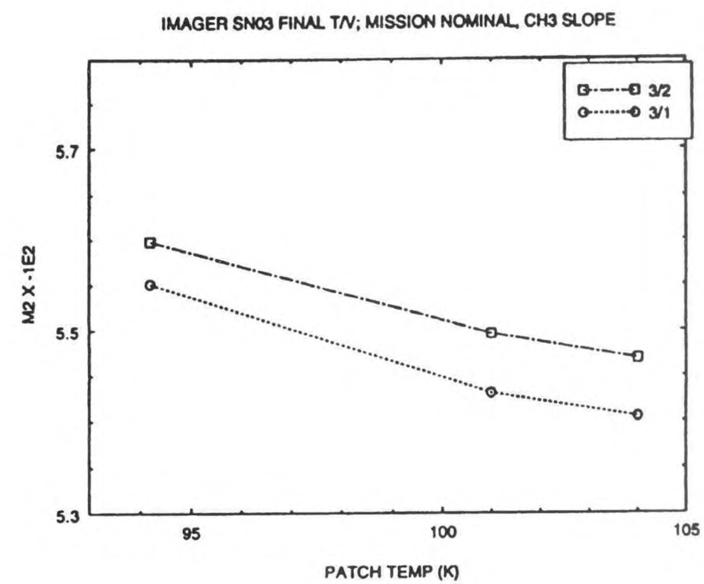

Fig 36. Slope versus patch temperature, channel 3.

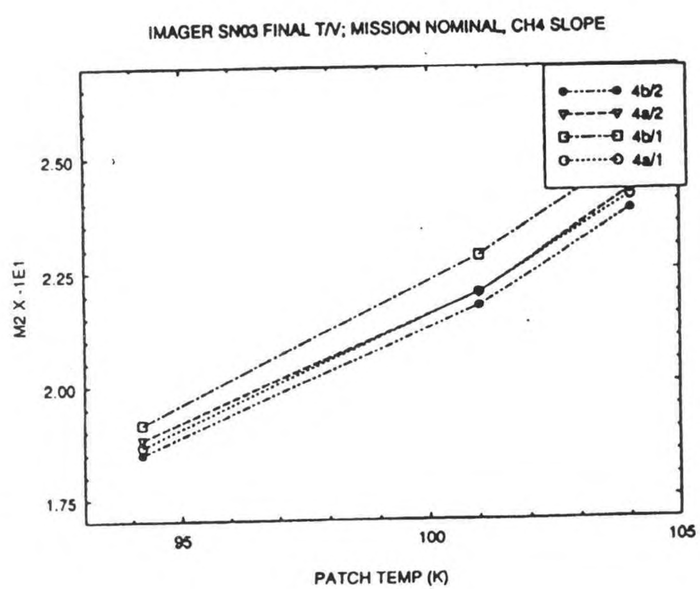

Fig 37. Slope versus patch temperature, channel 4.

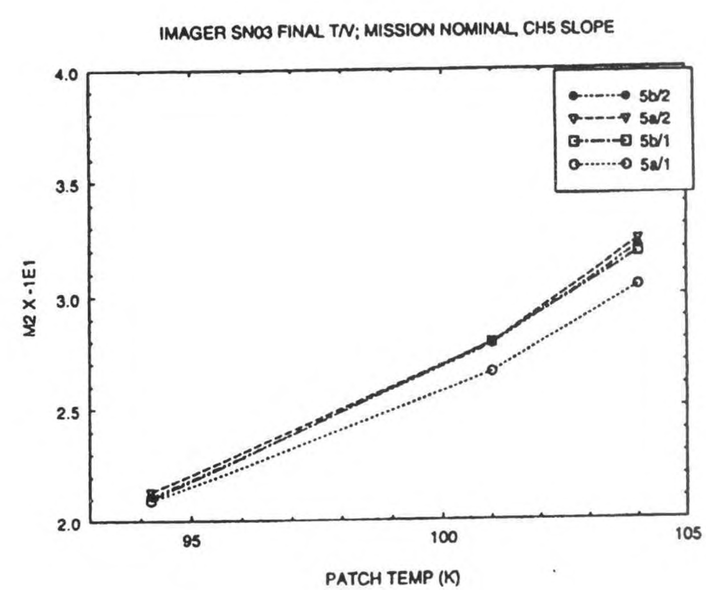

Fig 38. Slope versus patch temperature, channel 5.

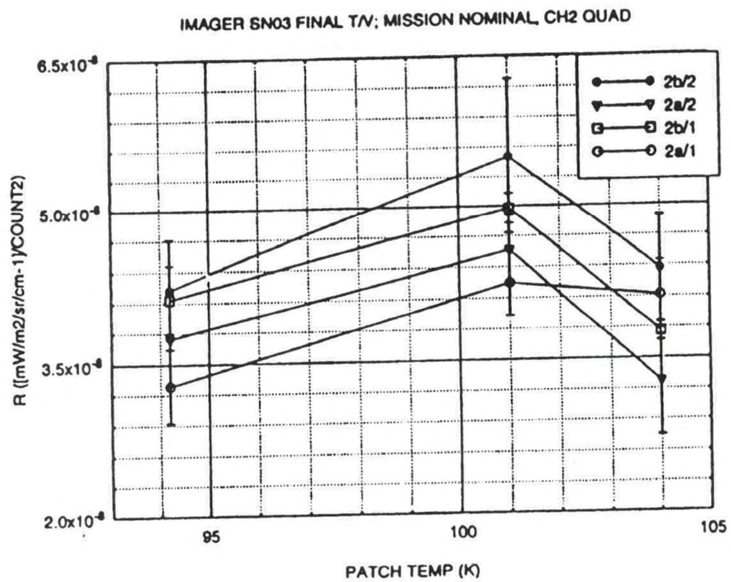

Fig 39. Quadratic versus patch temperature, channel 2.

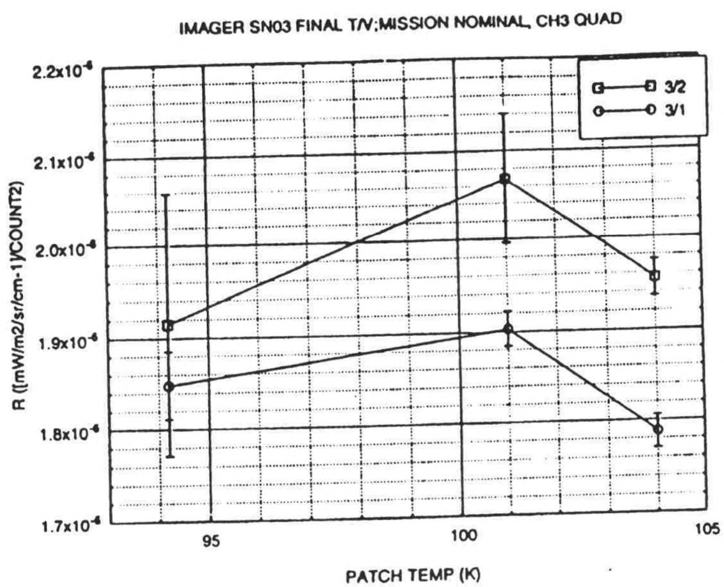

Fig 40. Quadratic versus patch temperature, channel 3.

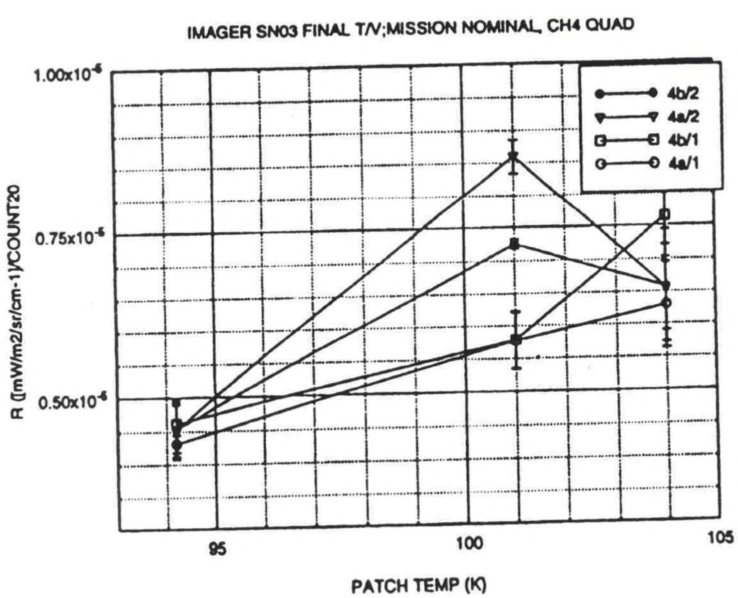

Fig 41. Quadratic versus patch temperature, channel 4.

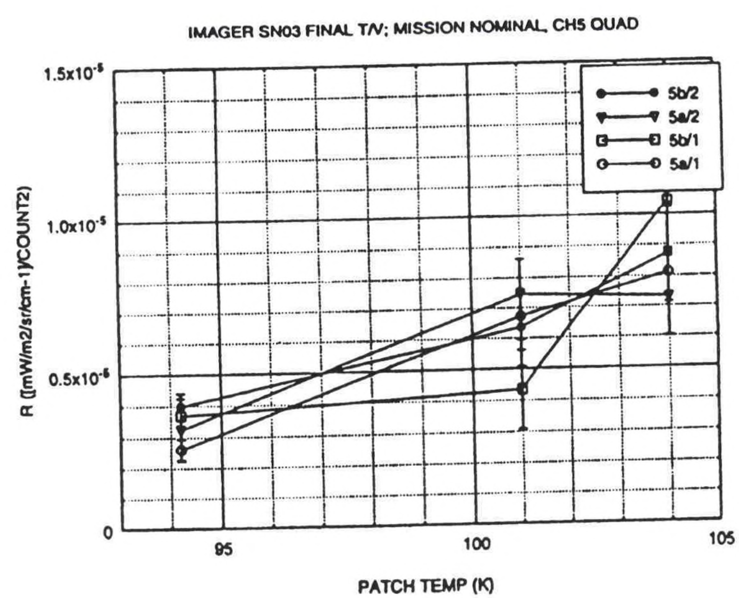

Fig 42. Quadratic versus patch temperature, channel 5.

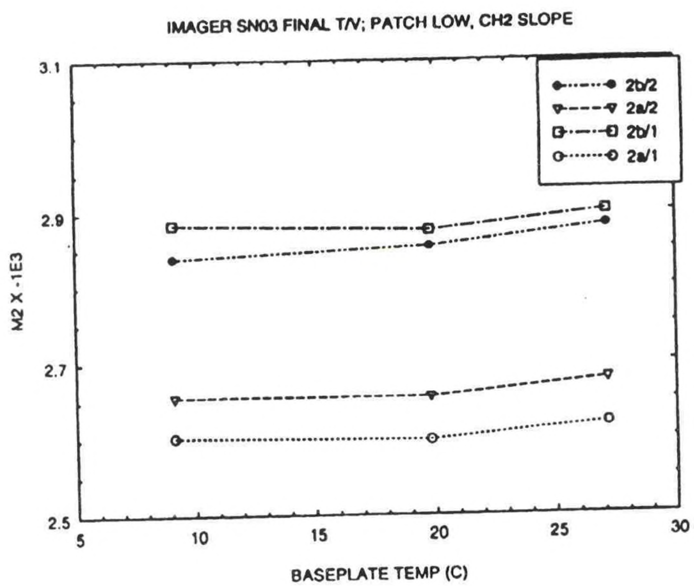

Fig 43. Slope versus baseplate temperature, channel 2.

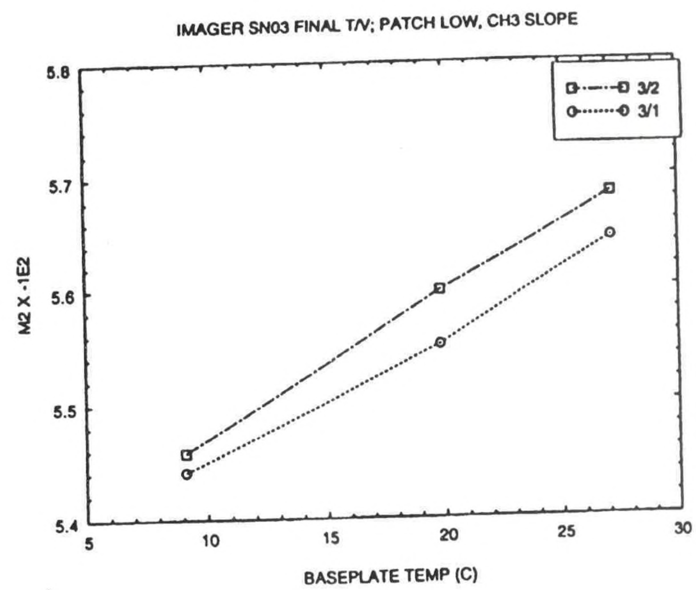

Fig 44. Slope versus baseplate temperature, channel 3.

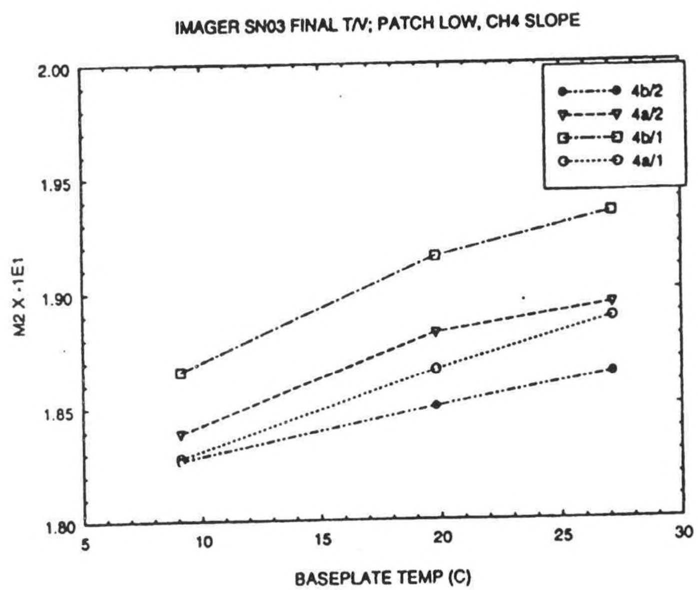

Fig 45. Slope versus baseplate temperature, channel 4.

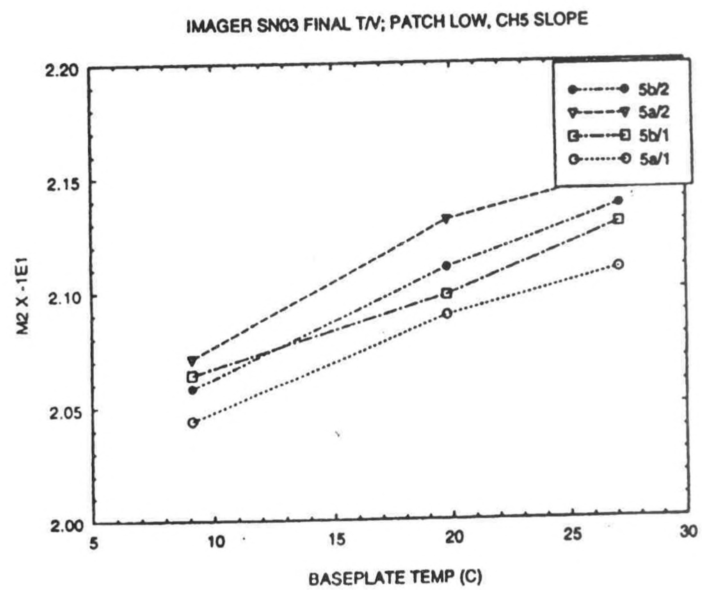

Fig 46. Slope versus baseplate temperature, channel 5.

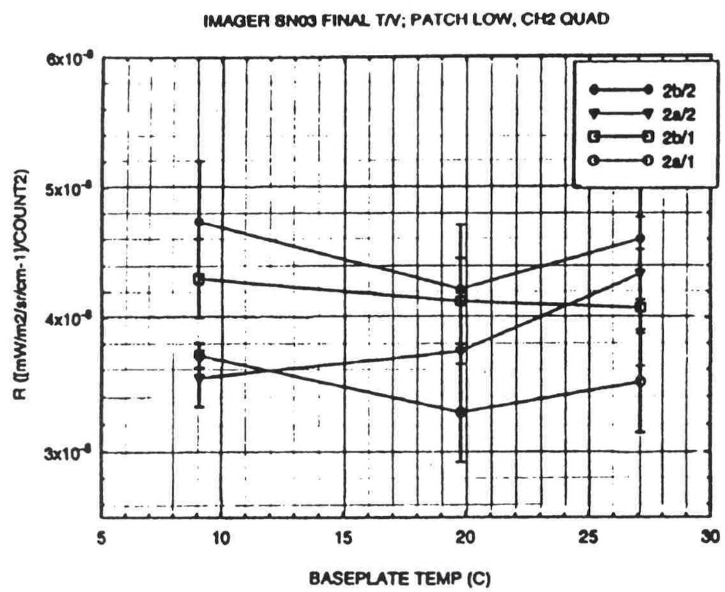

Fig 47. Quadratic versus baseplate temperature, channel 2.

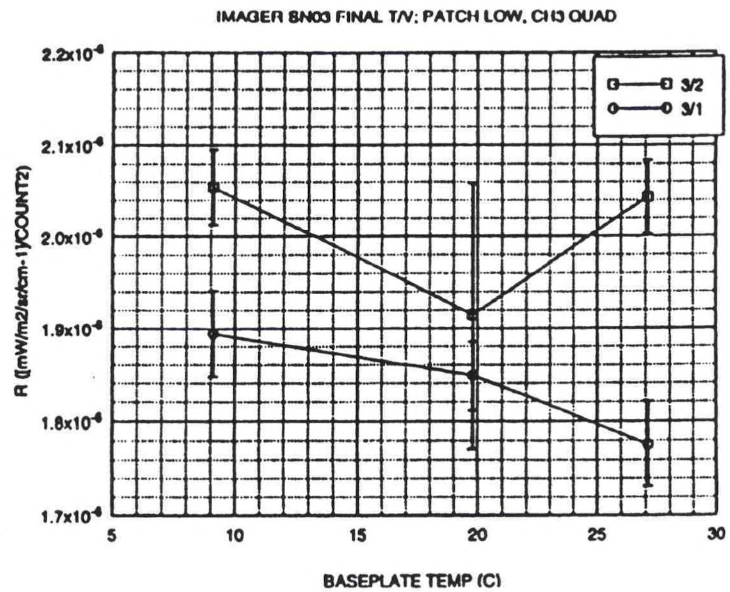

Fig 48. Quadratic versus baseplate temperature, channel 3.

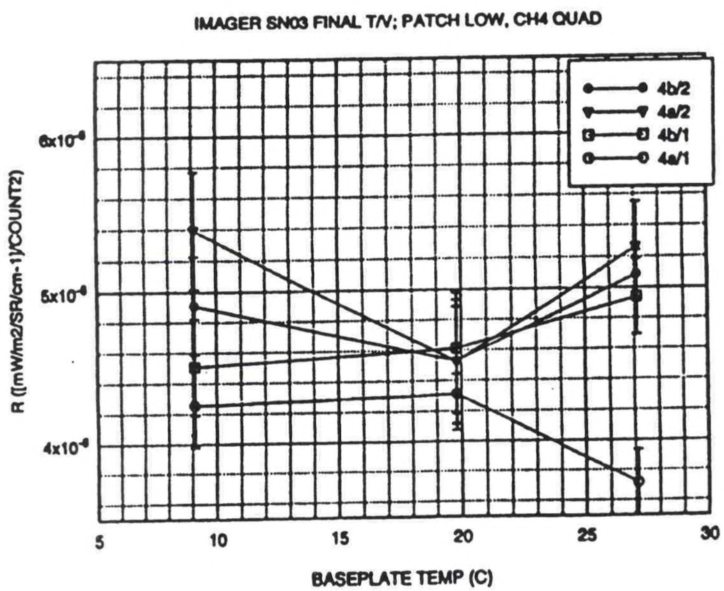

Fig 49. Quadratic versus baseplate temperature, channel 4.

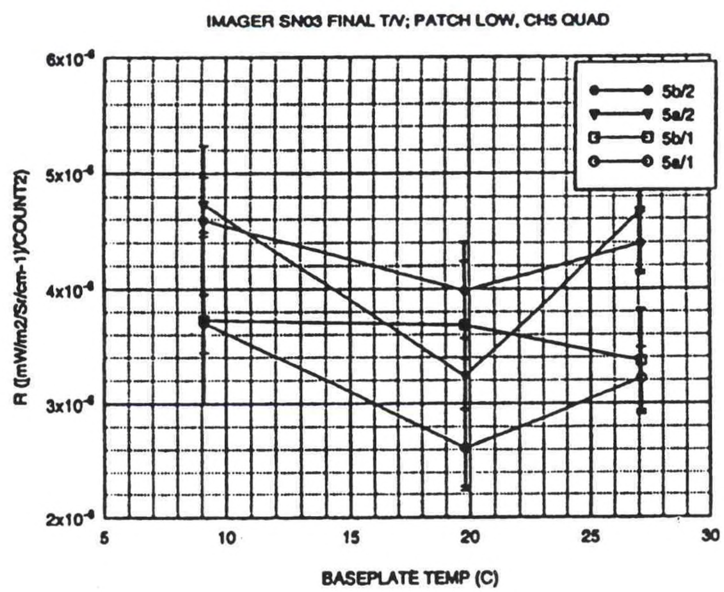

Fig 50. Quadratic versus baseplate temperature, channel 5.

6. SIGNIFICANCE OF THE QUADRATIC COEFFICIENT

For HgCdTe photoconductive channels 3, 4 and 5, a slight detector saturation mechanism called Auger recombination leads to a quadratic response at high detector photon flux loadings.[7] Based on maximum flux levels of up to 10^{16} photons/sec/cm^2, up to a 0.3% nonlinearity can be expected. This is approximately what is measured in FTV. However for InSb photovoltaic channel 2, no such physical detector mechanism is known to explain the observed nonlinearity. Also, no quadratic effect has been observed in prior development of AVHRR instruments which also use InSb detectors. Hypotheses for the channel 2 nonlinearity include: a nonlinear preamp feedback resistor; and inaccurate relative spectral response; large amplitude high frequency noise; a calibration error in target temperature sensors; and a thermal gradient into the surface of the calibration target.[8]

The thermal gradient hypothesis is based on the idea that a finite thermal conductance between the embedded target temperature sensors and the target radiating surface, as shown in Figure 51, leads to a temperature difference between the directly sensed temperature and the radiation emission temperature due to radiation exchange with the ambient surroundings. In Figure 51, Q indicates the thermal conductance and R(T) indicates radiance from a surface at temperature T. The temperatures of the target sensor, the emitting surface and the ambient surroundings are indicated by T_t, T_e and T_a, respectively. The general characteristics of target temperature error as a function of target radiance as shown in Figure 52 are suitable to generate the observed quadratic calibration coefficient. In addition, the target gradient hypothesis has attracted interest because there is reason to believe that the SN03 calibration targets were constructed without adequate thermal conduction between the temperature sensors and the emitting surface. Imager SN02 calibration using a different target did not show this channel 2 nonlinearity, although these results are somewhat difficult to interpret due to higher levels of instrument noise.

Such a target thermal gradient would result in a systematic error in the quadratic coefficients which are determined for all channels. A correction for this error could be made by assuming that channel 2 response is exactly linear between zero signal at zero target radiance and the measured signal at a target radiance corresponding to the temperature of the ambient surroundings. The adjusted linear radiance is less than the original quadratic radiance fit for hot targets, while it is greater for cold targets. Figure 53 shows the adjustment to target channel 2 radiance (for the case of 2a/1 mission high patch low) required to make channel 2 exactly linear as previously described, along with the radiance difference per K for this channel. Figure 54 shows the resulting target temperature error (adjusted - original) as a function of target temperature. In addition to results for the typical case of mission high patch low, results for test conditions corresponding to the maximum and minimum quadratics are also shown. The target temperature error is very similar for each case. The maximum error is about -0.25K for a 320K target. Note that by construction, there is essentially zero error at an ambient target temperature of about 290 K.

Table 3 shows the resulting adjustment to the measured quadratic coefficients for mission high patch low. Channels 4 and 5 are most affected, with the channel 5 quadratic becoming essentially zero. The overall desirability of this adjustment is still uncertain, and possibly can only be resolved by an independent radiometric measurement of the ECT.

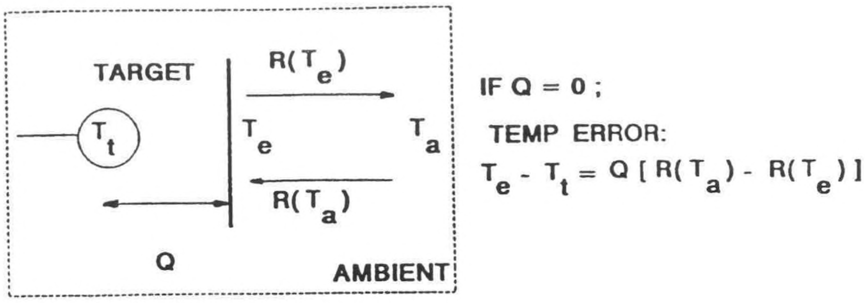

Figure 51. Target thermal gradient schematic.

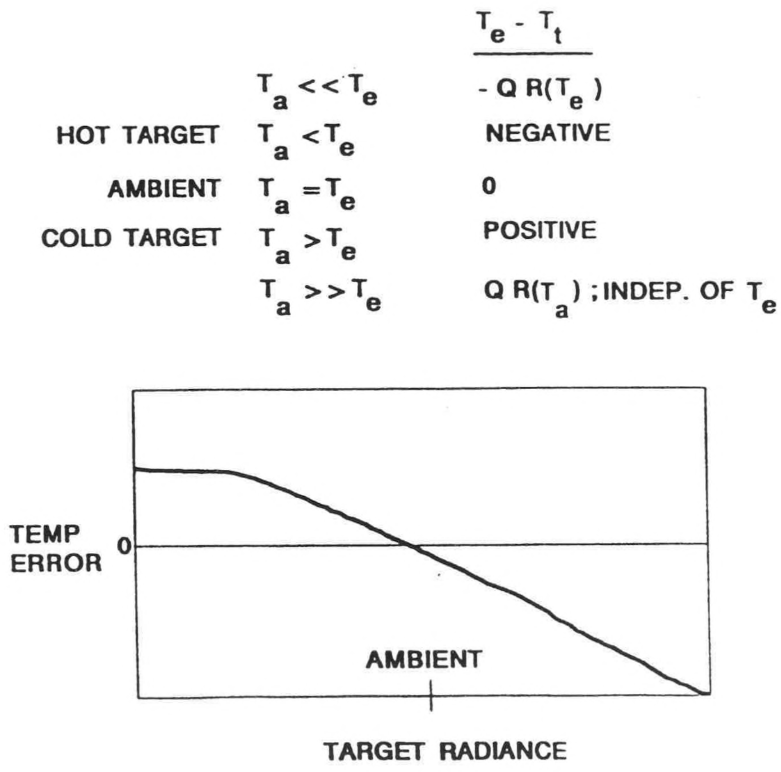

Figure 52. Target thermal gradient temperature error characteristics.

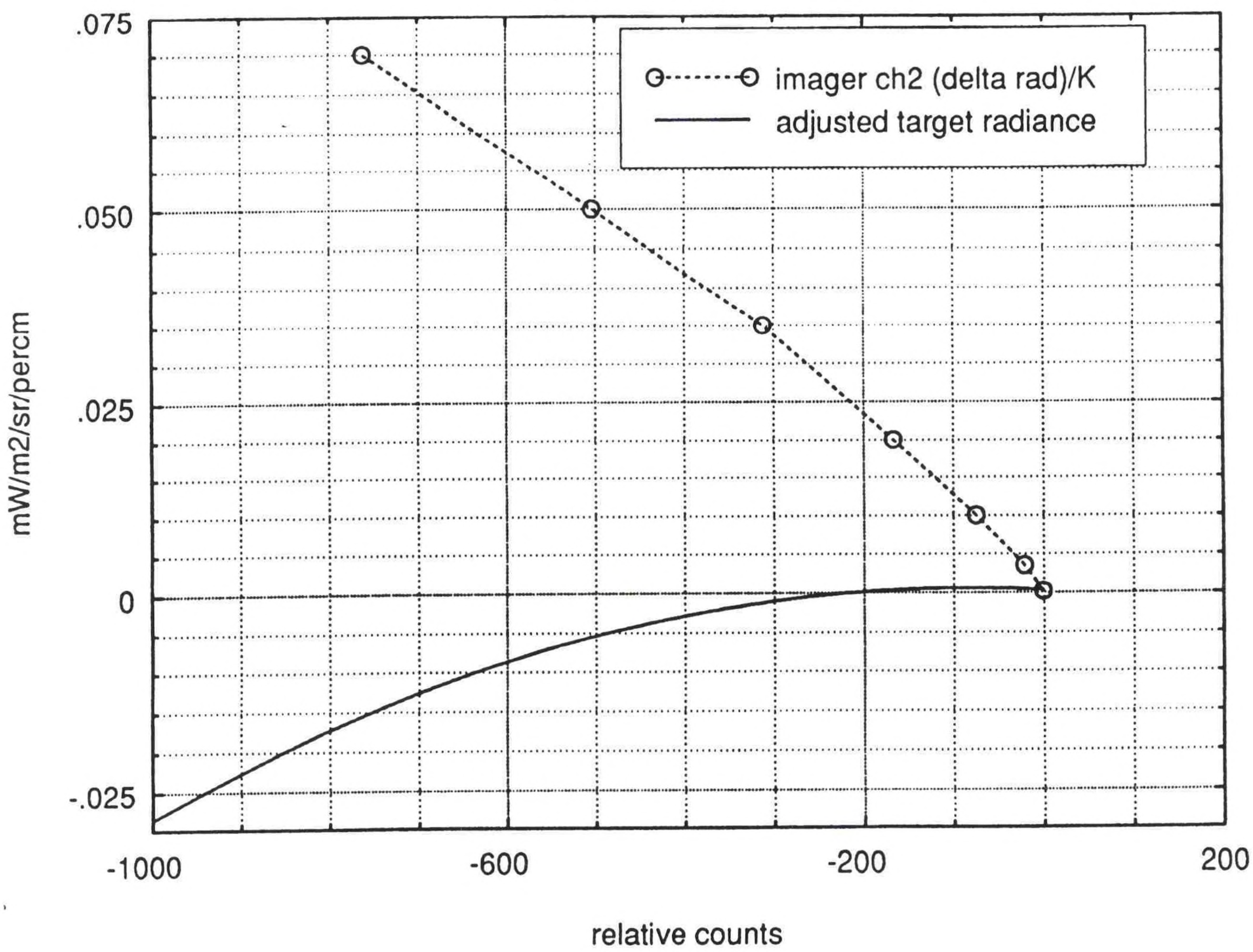

Figure 53. Adjusted target channel 2 radiance.

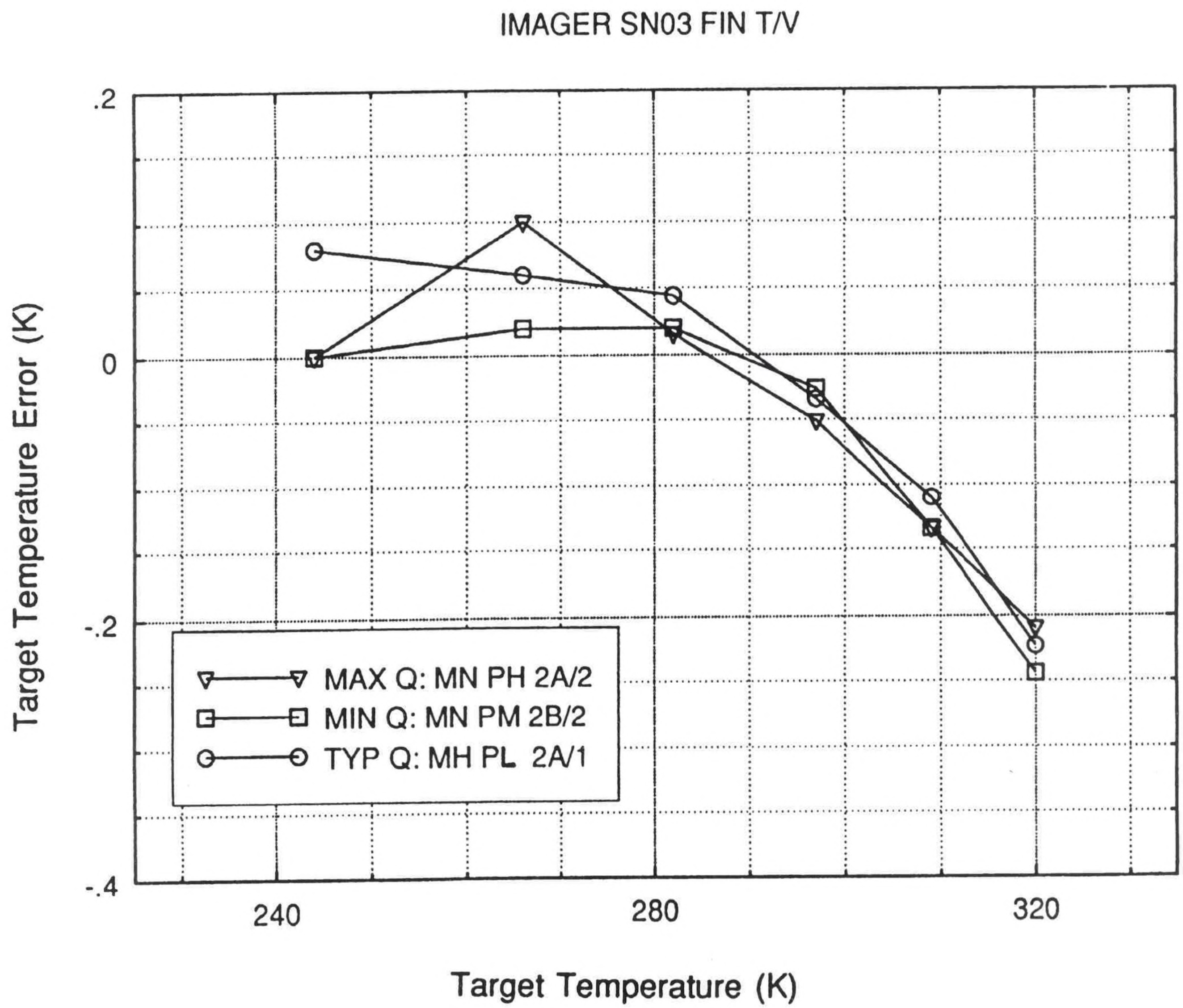

Figure 54. Target temperature error.

TABLE 3

Mission High, Patch Low, Adjusted Quadratic Coefficients

Channel #	Measured Q	Adjusted Q
3a/1	3.5 E-8	0
3/1	1.8 E-6	1.2 E-6
4a/1	3.7 E-6	1.2 E-6
5a/1	3.2 E-6	0.4 E-7

7. DRIFT NOISE AND FREQUENCY OF SPACE CLAMPS

7.1 BACKGROUND

The Imager performs space look and clamp operations to reduce the effects of low frequency drift on channel noise. In the full disk imaging mode, space clamps are made at the end of each 2.2 sec EW scan line. In the small area imaging mode, space clamps periodically interrupt imaging to scan to space. The more frequently space clamps are performed, the lower the resulting noise. However, more frequent space clamps also result in increased time needed to scan a given area. The actual frequency of space clamps should be determined by a tradeoff between the desired scan times and the allowable levels of channel noise.

Table 4 summarizes the Imager measured scan NEDT and low frequency drift characteristics. Drift characteristics have been obtained according to the method described below. Using approximately 96 seconds (2^{19} samples) of detector noise data, power density at nineteen frequencies is computed with a computationally efficient wavelet algorithm.[9] We used the Haar wavelet basis. Using an iterative maximum likelihood method, a $1/f$ function is fitted to the 19 wavelet coefficients. The $1/f$ function is described by three parameters: knee frequency, slope and white noise.

TABLE 4

Imager NEDT and Low Frequency Noise Status

CHANNEL	2a	2b	3	4a	4b	5a	5b
SPEC NEDT (K)	1.4	1.4	1.0	0.35	0.35	0.50	0.50
Scan NEDT (K) SN02 Mission N, Patch L, Side 1	0.23	0.19	0.35	0.22	0.20	0.47	0.48
Scan NEDT (K) SN03 Mission N, Patch L, Side 1	0.16	0.17	0.12	0.09	0.09	0.15	0.16
1/f KNEE FREQUENCY (Hz)	2.3	8.5	329.	249.	185.	101.	83.

The standard ITT IR drift post processing is intended to simulate the OGE data processing. Predictions of the NEDT levels corresponding to 2.2, 9.6 and 36.6 second space clamp intervals. Unfortunately, errors in the ITT computer code make the predicted SN03 NEDT levels larger than they actually should be.

7.2 SCAN TIMES FOR VARIOUS SPACE CLAMPS

The time required to scan a small area frame consists of time required to image and time required to perform space clamps. The following time allocation for scanning a 3000 km x 3000 km centered frame performing space clamps at 9.6 s intervals has been developed by E. Koenig, ITT.

In reading this list, it is helpful to know that 3000 km occupies 4.81 deg from geostationary altitude and requires 375 NS lines; the Imager scans 20 deg/s EW and 10 deg/s NS; and 8 deg is required to slew to space. In the list, I indicates time allocated for imaging functions and S for space clamp functions.

Initial space look and clamp:

S:	over and back	(10.4-2.4)x2/20	0.80 s
S:	turnaround at space		0.20 s
S:	settle at start location		0.50 s
I:	3 turnarounds	(3x0.2)	0.60 s
I:	375 scan lines	(365x4.81/20)	90.19 s
I:	375 turnarounds	(375x0.2)	75.00 s

Number of space looks (N=25):

S:	over and back	(2Nx8/20)	20.00 s
S:	invalid lines	(4Nx4.81/20)	24.05 s
S:	turnarounds	(5Nx0.20)	25.00 s
I:	retrace to start	(4.81/20+4.81/10)	0.72 s
I:	settle after slews	(0.5+2.)	2.60 s
	time required for space clamps		70.6 s
	time required for imaging		169.1 s
	total frame scan time		240.4 s

This time allocation can be generalized for different space clamp intervals, with the results shown in Figure 55. If space clamps were performed at 36.6 s rather than 9.6 s intervals, time required for imaging would remain constant at 169.1 s, time required for space clamps would reduce to 15.9 s and total frame scan time would reduce to 185 s, an overall time savings of about 25%.

7.3 PERFORMANCE IMPACT OF SPACE CLAMP FREQUENCY

The change in noise counts resulting from moving from 9.6 s to other space clamp intervals can be estimated by analytically passing 1/f noise of various knee frequencies through a filter equivalent to the space clamp timing. The results are shown in Figure 56, with T indicating the space clamp interval. Channel 3 has the highest knee frequency (about 300 Hz) and thus is most affected by the space clamp frequency. The noise penalty for channel 3 for moving from 9.6 sec to 36.6 sec is about 5%. The noise penalty for channels 2, 4 and 5 would be slightly smaller.

7.4 SUMMARY

The small amount of low frequency noise present in SN03 Imager makes the option of 36.6 sec space clamps during small frame imaging attractive. Compared to 9.6 sec space clamps, noise would increase by generally less than 5% while scan times would decrease by approximately 25%.

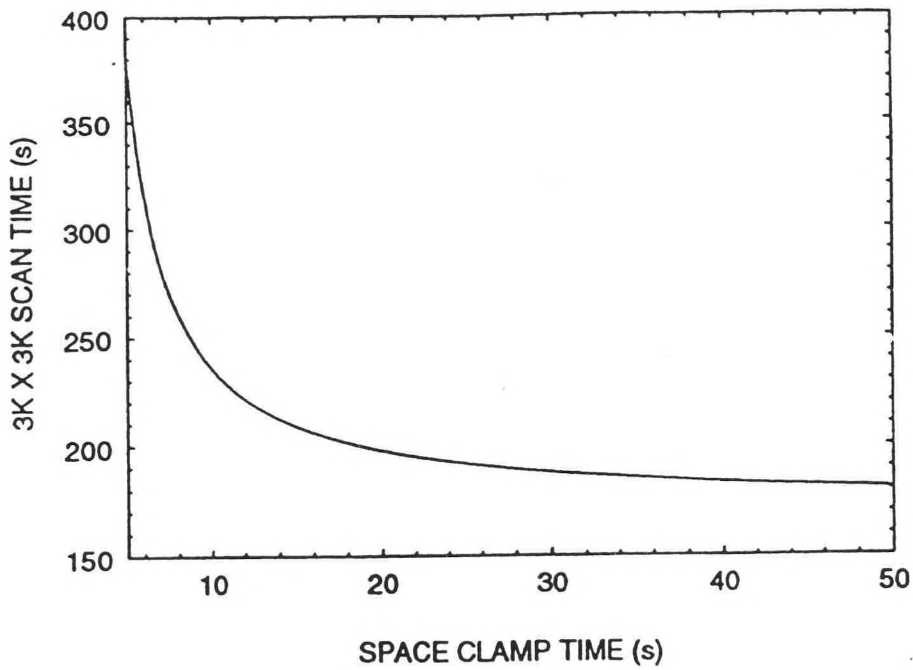

Figure 55. Small area scan time as a function of space clamp interval.

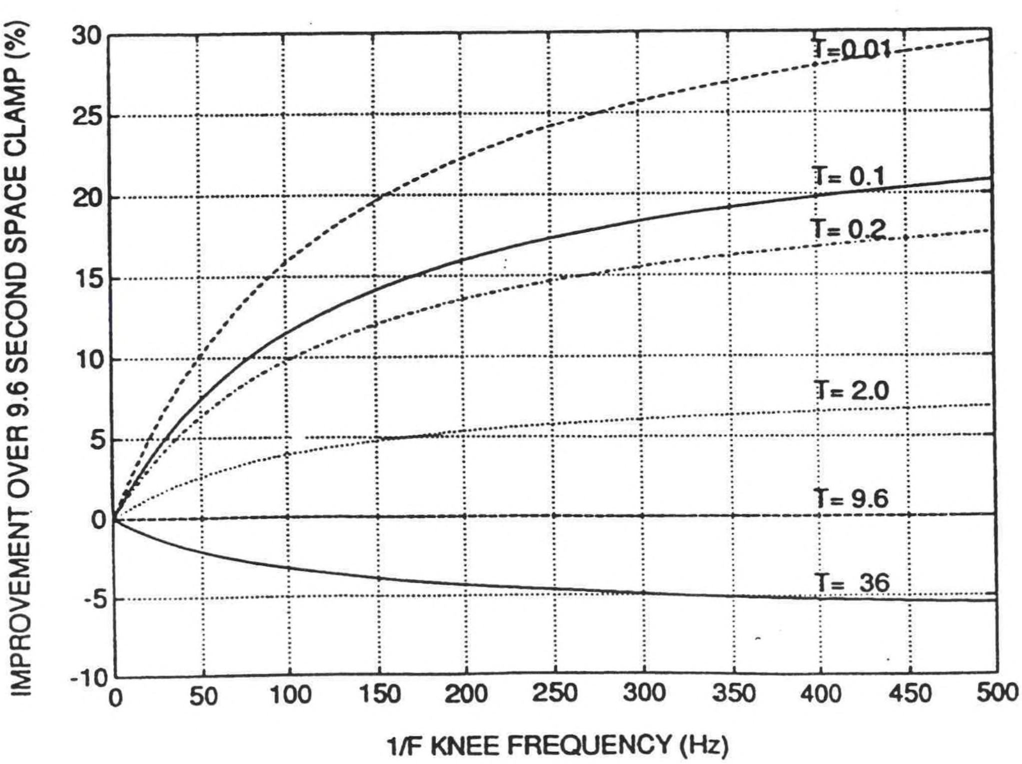

Figure 56. Noise penalty of various space clamp intervals compared to 9.6 s.

REFERENCES

1. *"GOES I-M System Description,"* J. Savides, Space Systems/LORAL, December 1992.

2. *"SN03 Alignment and Calibration Handbook,"* ITT/ACD, in preparation.

3. *"More GOES I-M OGE Modifications for Noise and Drift,"* M. Weinreb, NOAA, 16 October 1992.

4. *"Effects of emissivity and field of view differences on ground calibration of GOES imager,"* W.H. Farthing, 15 December 1992.

5. *"OGE Modifications Under CCR 385,"* M.P. Weinreb, 2 February 1993.

6. *"HgCdTe Detector Responsivity and GOES Instrument Calibration,"* W.E. Bicknell, MIT Lincoln Laboratory Project Report NOAA-3, 12 March 1993.

7. *"Nonlinear Response of 8-12 μm (HgCd)Te Photoconductor to Large Signal Photon Flux Levels,"* M.B. Reine, Honeywell, 5 May 1979.

8. *"Imager S/N 03 Channel 2 Nonlinearity,"* W.H Farthing, Swales Associates, 8 February 1993.

9. *"Estimation of Fractal Signals From Noisy Measurements Using Wavelets,"* G. Wornell and A. Oppenheim, Proc. IEEE, vol. 40, pp. 611-623, Mar. 1992.

APPENDIX A

IMAGER IR SCAN STANDARD REPORT FORMAT DESCRIPTION

The Imager IR scan Report (IIRR) software generates a summary of the Imager calibration from the IR scan test. The format of the IIRR output is concise and provides all of the relevant results of the test in both graphical and tabular form. All seven of the IIRR reports are in the data package (Appendix A1 - A7). The plots and tables are labeled for the first mission and patch temperature. The following is a brief explanation of the format of the report. The format described below for the first section is repeated in each of the seven sections.

Figures A1-1 through A1-4 are the linear fits and the measured data plotted on a radiance versus relative mean counts axis. These plots quickly verify the proper data was processed and that there were no gross anomalies in the data. They also show how much of the dynamic range is being used for each detector at a given sensor condition.

Figures A1-5 through A1-8 are the residues of the linear and quadratic fits. The y-axis is the residue as a percentage of the peak scene radiance and the x-axis is radiance. In smaller print at the bottom and top of the plot are the truncated ECT temperature and the truncated relative mean counts for each data point. At the far right of the plot, centered around zero, is the NEDN of the 320K point plotted as a percentage of peak radiance. This gives a sense of the single sample noise.

Table A1-1 summarizes the noise and residue statistics. The first column is the detector number and side. The second column is the measured NEDT at the ECT temperature tested closest to the specification temperature. The next column is the specification NEDT and temperature. The fourth column is the peak linear residue as a percentage of the maximum scene radiance with the next column being the specification. On the residue plot, this would correspond to the black circle furthest from zero. The sixth column is the root mean squared (RMS) of the linear residues as a percentage of the maximum scene radiance. The next column is the peak linear residue in radiance units. The eighth column is the peak quadratic residue as a percentage of the maximum scene radiance. The ninth column is the RMS of the quadratic residues as a percentage, and the last column in the peak quadratic residue in radiance units.

Table A1-2 lists the linear and quadratic fit coefficients with their standard errors. The units for the parameters are; radiance for gamma1 and gamma2; radiance/count for m1 and m2; and radiance count^2 for R.

Table A1-3 lists the run numbers that were processed in the report, the dates and times of the test runs, and a subset of the telemetry. The temperatures listed in the table identify the sensor state and can be correlated with sensor performance.

APPENDIX A1. IMAGER IR SCAN REPORT

GOES SN03 IMAGER

MISSION TEMPERATURE – LOW

PATCH TEMPERATURE – LOW

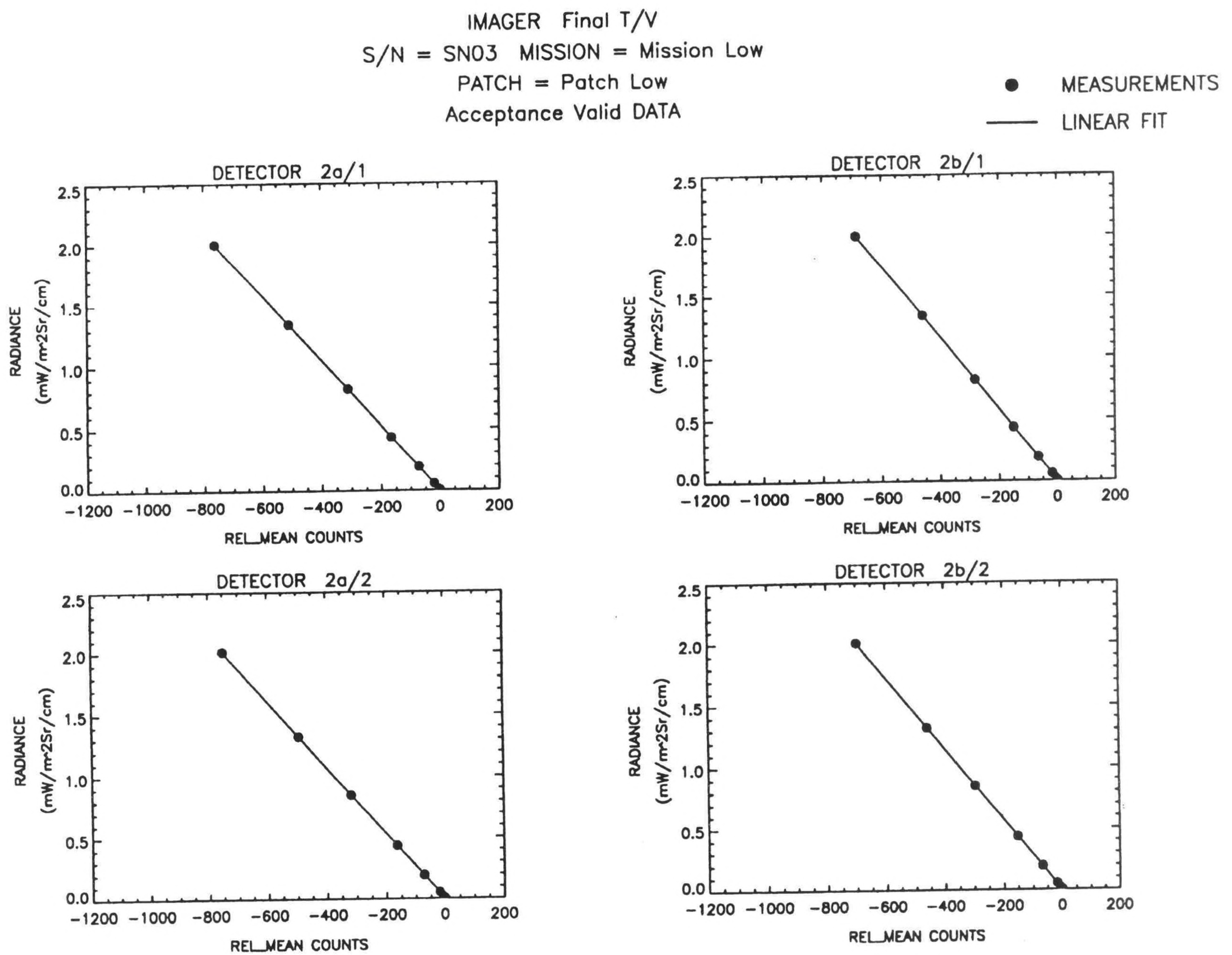

Figure A1-1. Radiance versus relative mean counts, channel 2.

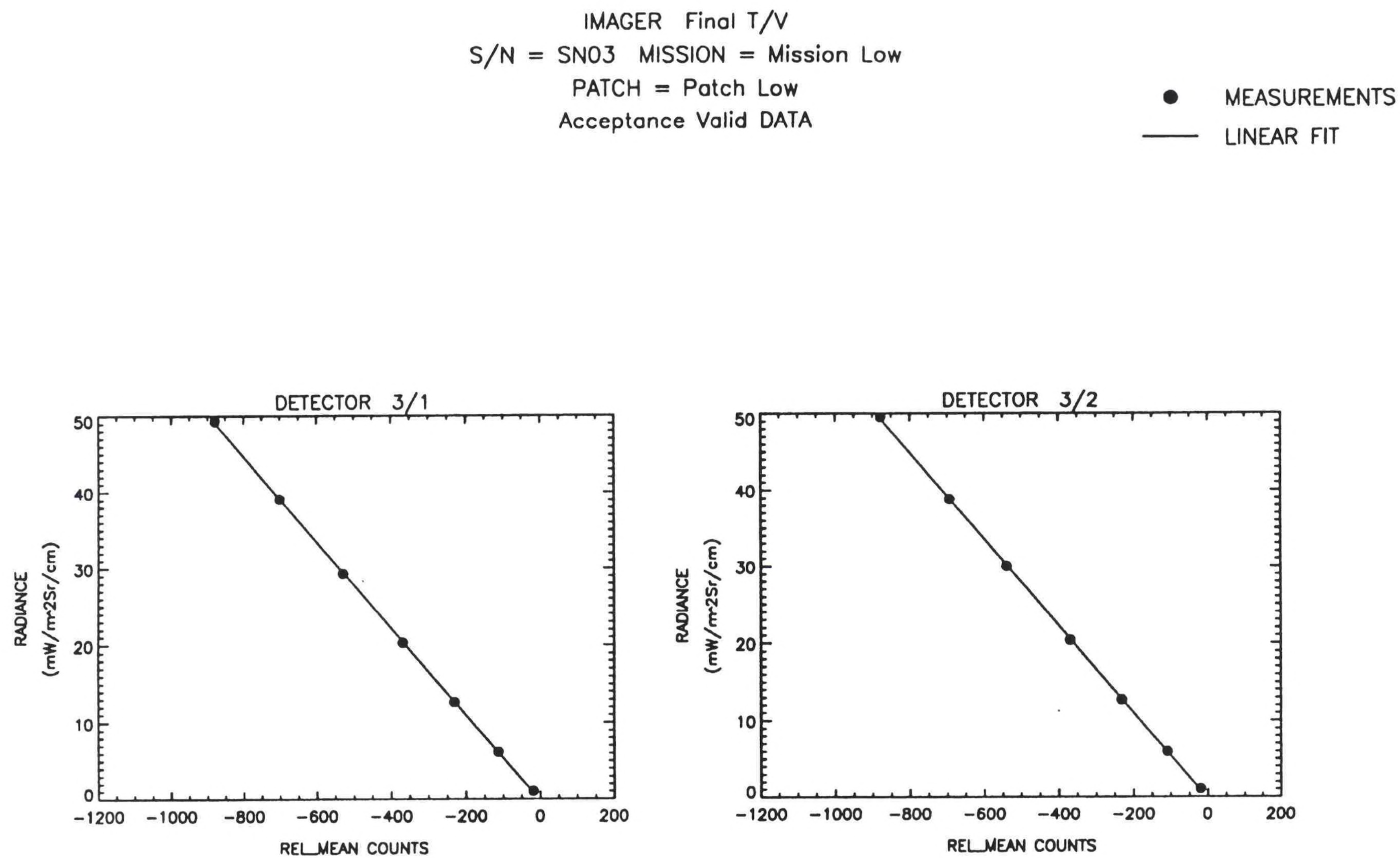

Figure A1-2. Radiance versus relative mean counts, channel 3.

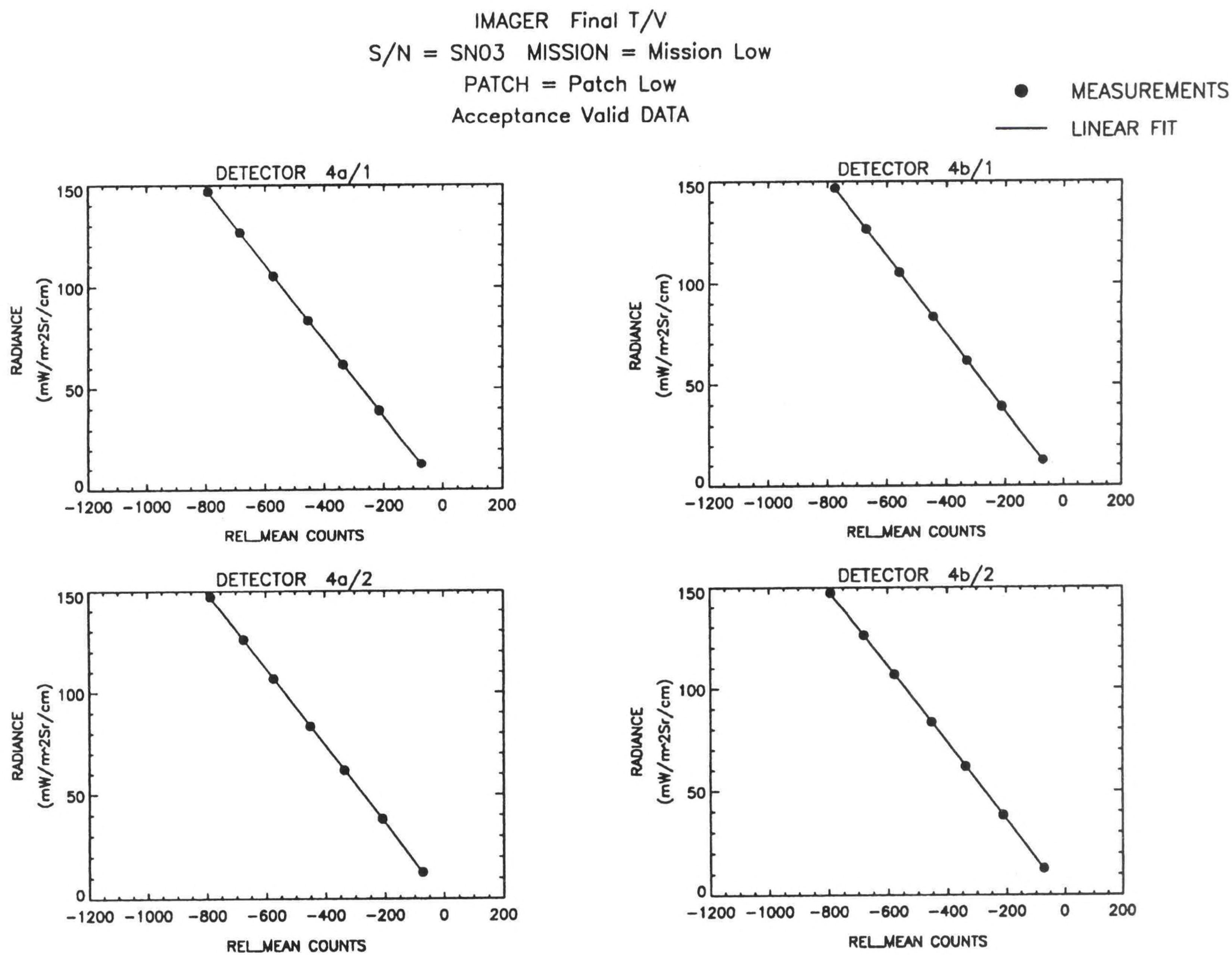

Figure A1-3. Radiance versus relative mean counts, channel 4.

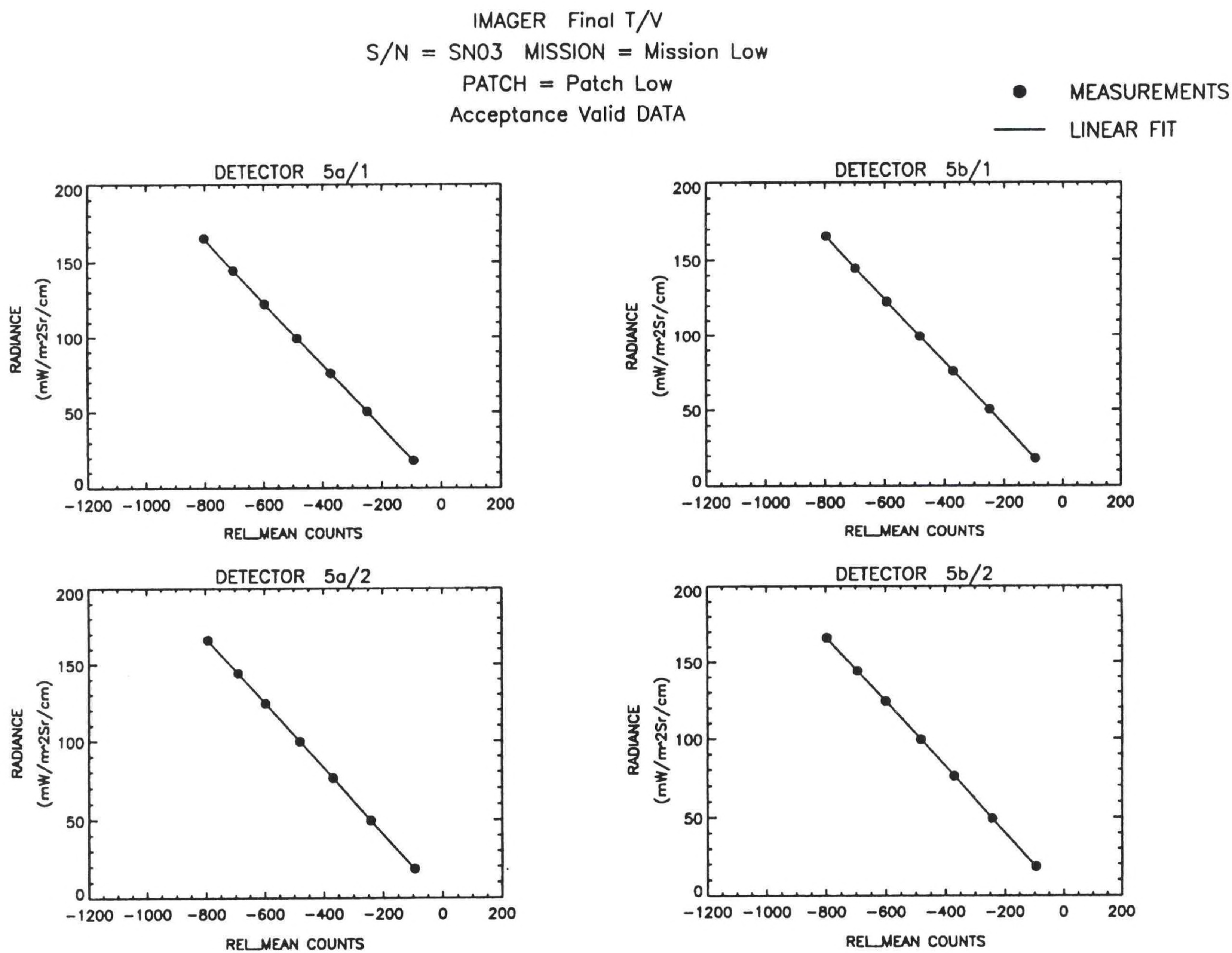

Figure A1-4. Radiance versus relative mean counts, channel 5.

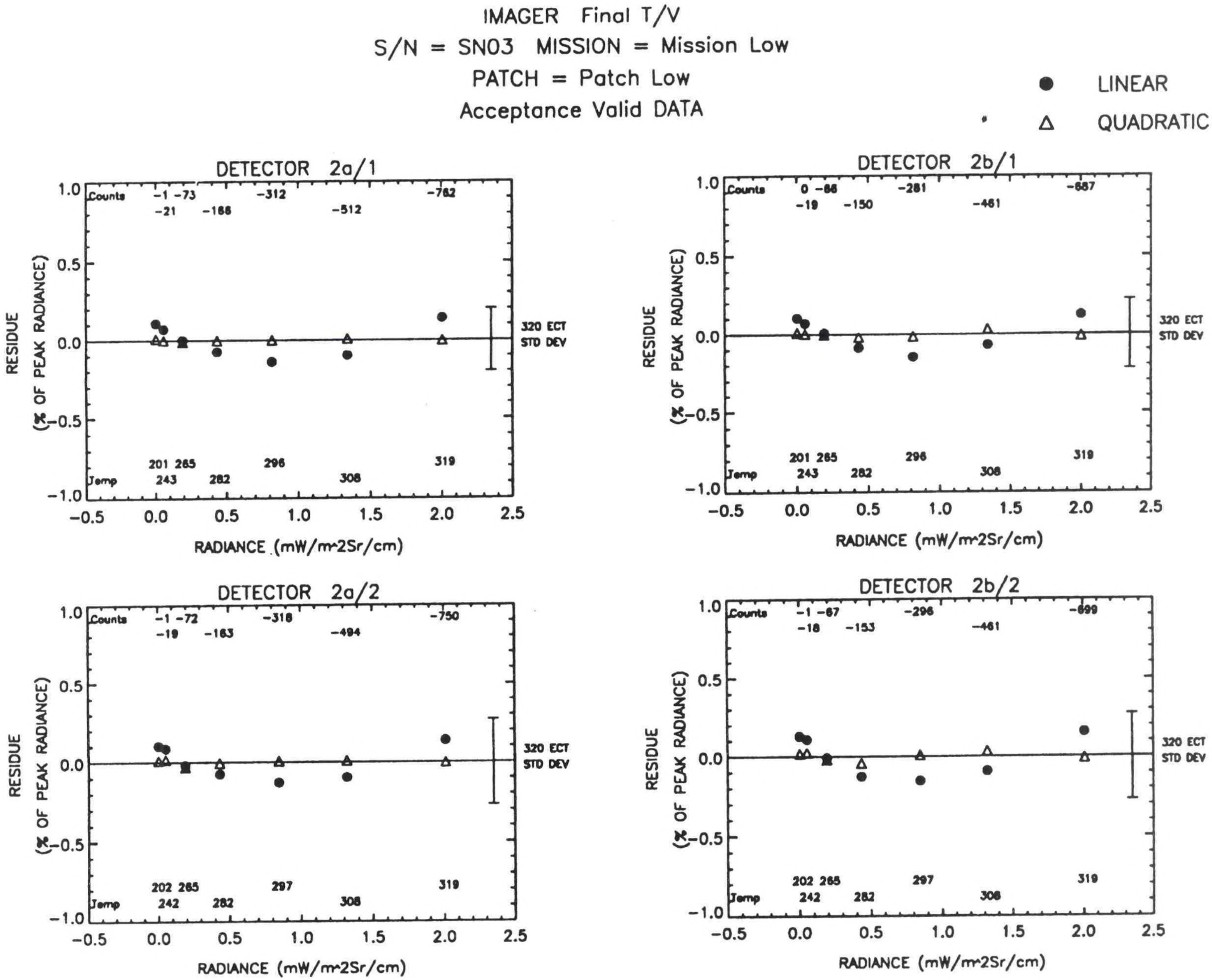

Figure A1-5. Residues of linear and quadratic fits versus radiance, channel 2.

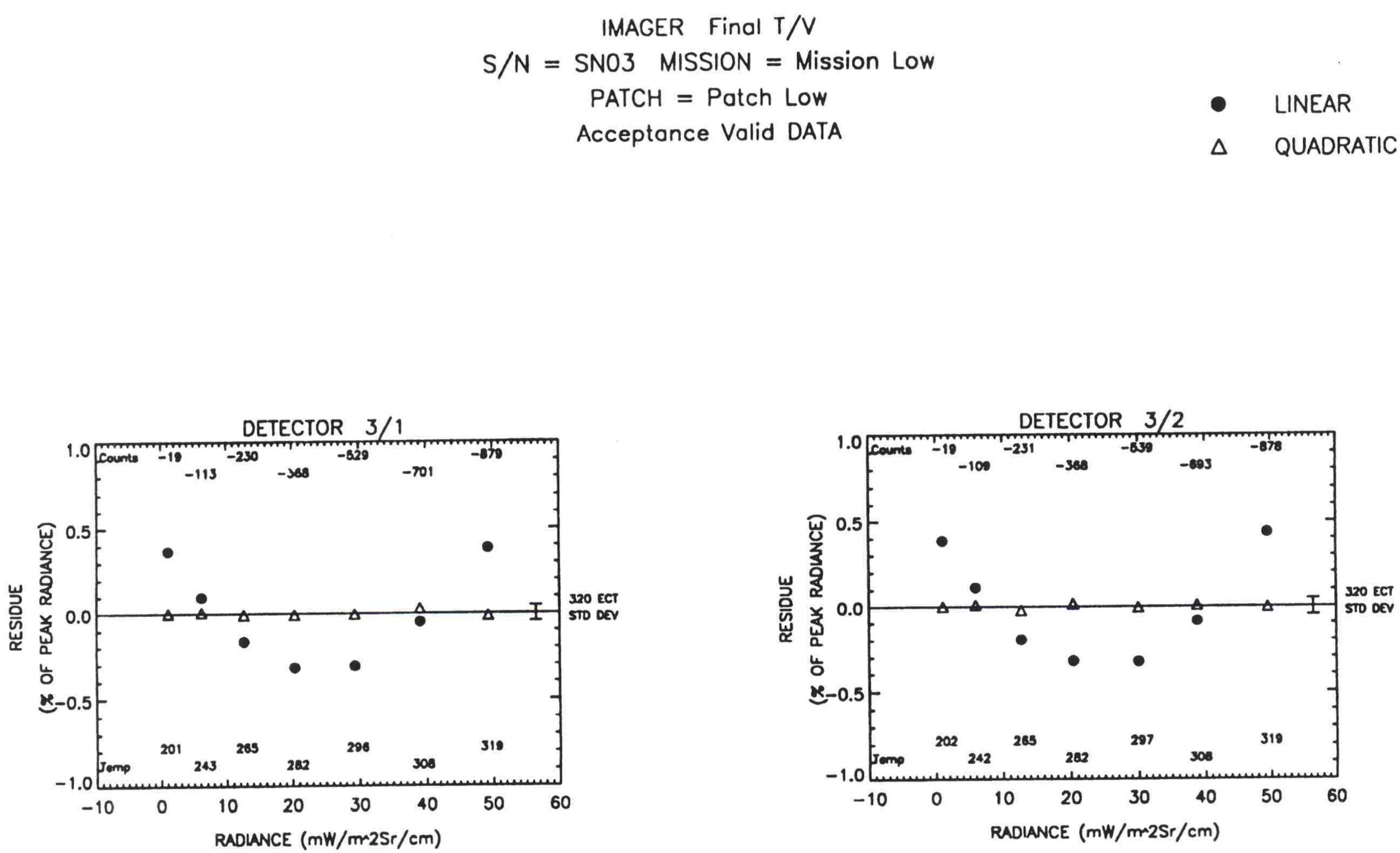

Figure A1-6. Residues of linear and quadratic fits versus radiance, channel 3.

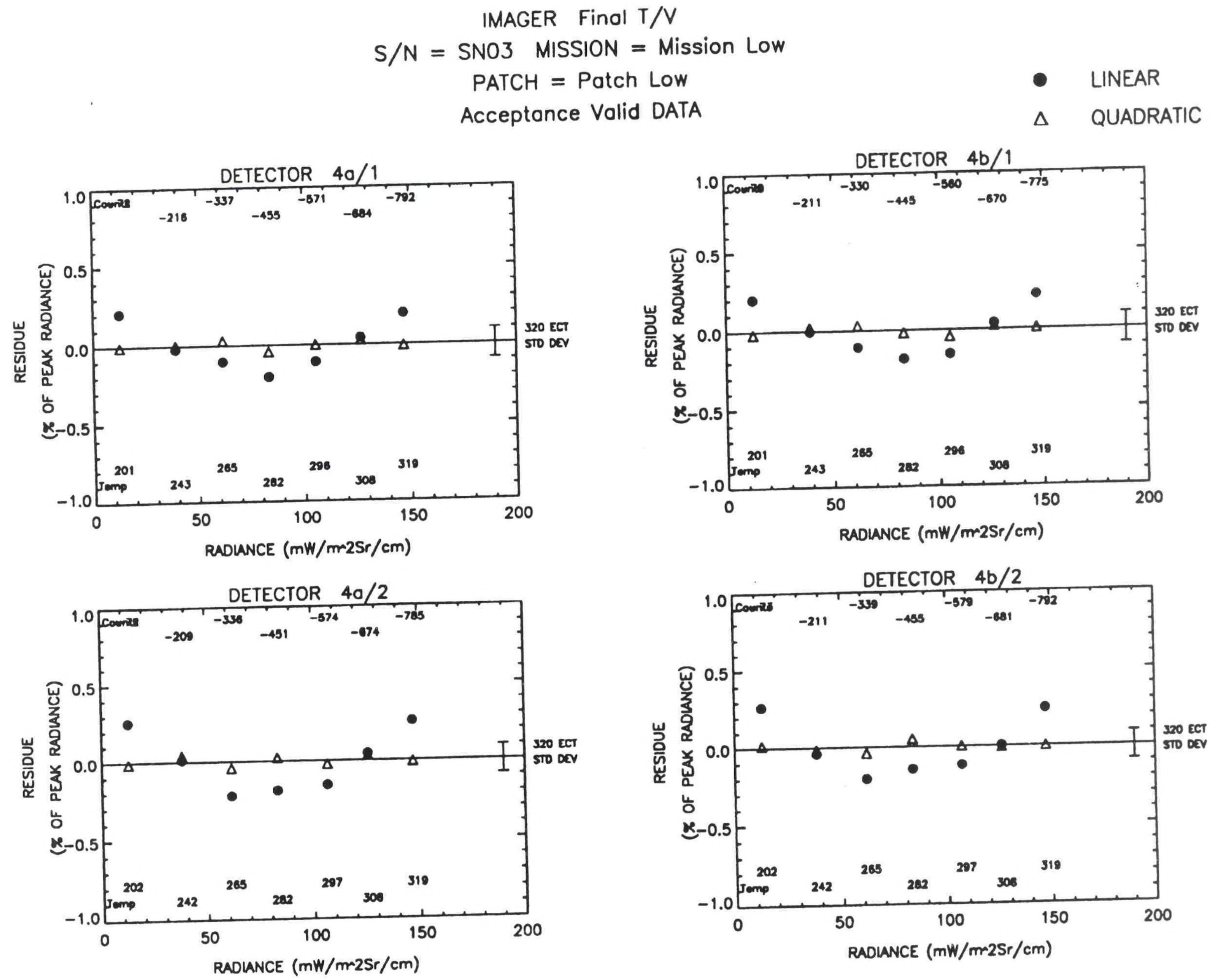

Figure A1-7. Residues of linear and quadratic fits versus radiance, channel 4.

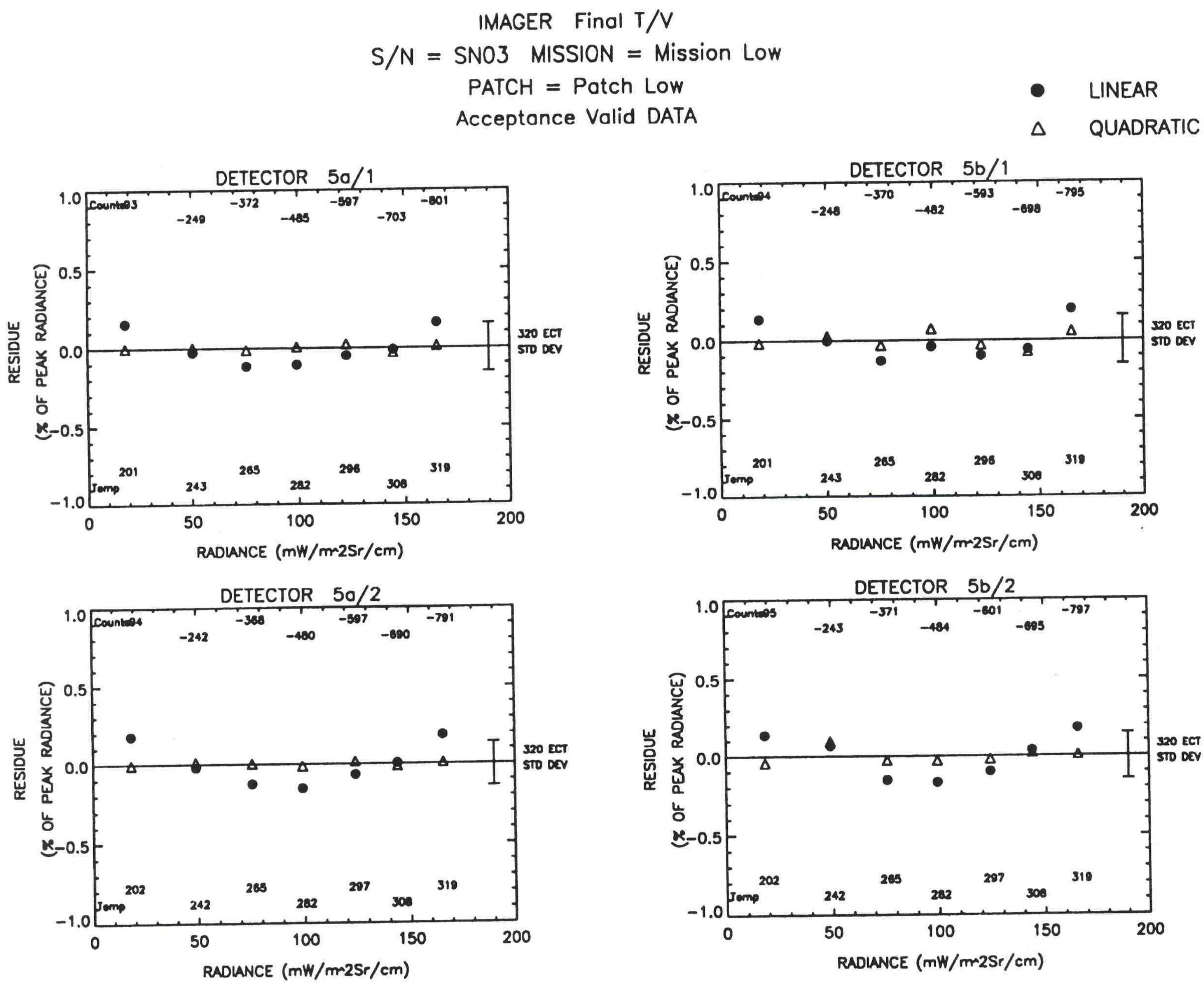

Figure A1-8. Residues of linear and quadratic fits versus radiance, channel 5.

TABLE A1-1

Noise and Residue Statistics

IMAGER
S/N = SN03

Final T/V
MISSION = Mission Low
PATCH = Patch Low

Acceptance Valid Data

CH/SIDE	NEDT(K) MEAS/TEMP	NEDT(K) SPEC/TSPEC	PEAK LIN RES %	SPEC %	RMS LIN RES %	PEAK LIN RES N (mW/m^2Sr/cm)	PEAK QUAD RES %	RMS QUAD RES %	PEAK QUAD RES N (mW/m^2Sr/cm)
2a/1	0.1350/296.4	1.40/300.0	0.1409	1.7	0.1007	0.0029	0.0097	0.0061	0.0002
2b/1	0.1503/296.4	1.40/300.0	0.1469	1.7	0.0959	0.0030	0.0313	0.0161	0.0006
3/1	0.1080/243.6	1.00/230.0	0.3843	1.7	0.2725	0.1911	0.0282	0.0133	0.0140
4a/1	0.0851/296.4	0.35/300.0	0.2072	1.7	0.1449	0.3058	0.0310	0.0231	0.0457
4b/1	0.0847/296.4	0.35/300.0	0.2147	1.7	0.1499	0.3168	0.0314	0.0256	0.0464
5a/1	0.1501/296.4	0.50/300.0	0.1568	1.7	0.1049	0.2604	0.0217	0.0159	0.0360
5b/1	0.1459/296.4	0.50/300.0	0.1930	1.7	0.1113	0.3206	0.0709	0.0484	0.1177
2a/2	0.1361/297.5	1.40/300.0	0.1356	1.7	0.0992	0.0027	0.0160	0.0141	0.0003
2b/2	0.1485/297.5	1.40/300.0	0.1563	1.7	0.1204	0.0032	0.0318	0.0250	0.0006
3/2	0.1083/242.6	1.00/230.0	0.4349	1.7	0.2953	0.2160	0.0148	0.0117	0.0073
4a/2	0.0878/297.5	0.35/300.0	0.2572	1.7	0.1856	0.3793	0.0402	0.0282	0.0593
4b/2	0.0823/297.5	0.35/300.0	0.2644	1.7	0.1720	0.3900	0.0498	0.0255	0.0735
5a/2	0.1362/297.5	0.50/300.0	0.1863	1.7	0.1267	0.3094	0.0126	0.0107	0.0210
5b/2	0.1582/297.5	0.50/300.0	0.1811	1.7	0.1306	0.3007	0.0976	0.0447	0.1621

TABLE A1-2

Linear and Quadratic Fit Coefficients

IMAGER
S/N = SN03

Final T/V
MISSION = Mission Low
PATCH = Patch Low

Acceptance Valid Data

RAD = GAMM1 + M1 * C

CH/SIDE	GAMMA1			M1		
2a/1	-2.5807e-03	+/-	1.2972e-03	-2.6286e-03	+/-	3.4767e-06
2b/1	-2.3863e-03	+/-	1.2328e-03	-2.9118e-03	+/-	3.6666e-06
3/1	-2.3556e-01	+/-	1.0397e-01	-5.6099e-02	+/-	2.0806e-04
4a/1	-1.2507e+00	+/-	2.0360e-01	-1.8652e-01	+/-	4.0187e-04
4b/1	-1.2640e+00	+/-	2.1063e-01	-1.9043e-01	+/-	4.2450e-04
5a/1	-1.5735e+00	+/-	1.7587e-01	-2.0768e-01	+/-	3.3408e-04
5b/1	-1.8159e+00	+/-	1.8710e-01	-2.0964e-01	+/-	3.5781e-04
2a/2	-2.6702e-03	+/-	1.2709e-03	-2.6805e-03	+/-	3.4658e-06
2b/2	-3.1180e-03	+/-	1.5400e-03	-2.8704e-03	+/-	4.5035e-06
3/2	-2.5109e-01	+/-	1.1250e-01	-5.6402e-02	+/-	2.2523e-04
4a/2	-1.3359e+00	+/-	2.6009e-01	-1.8855e-01	+/-	5.1731e-04
4b/2	-1.3316e+00	+/-	2.4118e-01	-1.8699e-01	+/-	4.7548e-04
5a/2	-1.7551e+00	+/-	2.1241e-01	-2.1122e-01	+/-	4.0825e-04
5b/2	-1.8346e+00	+/-	2.1913e-01	-2.0981e-01	+/-	4.1810e-04

RAD = GAMMA2 + M2 * C + R * C^2

CH/SIDE	GAMMA2			M2			R		
2a/1	-5.7798e-04	+/-	1.0747e-04	-2.6015e-03	+/-	8.6065e-07	3.7071e-08	+/-	1.1316e-09
2b/1	-5.0830e-04	+/-	2.8121e-04	-2.8836e-03	+/-	2.4982e-06	4.2813e-08	+/-	3.6443e-09
3/1	-2.2716e-02	+/-	7.6685e-03	-5.4397e-02	+/-	4.2955e-05	1.9155e-06	+/-	4.6632e-08
4a/1	-6.9387e-01	+/-	5.7804e-02	-1.8286e-01	+/-	3.0440e-04	4.2112e-06	+/-	3.4021e-07

TABLE A1-2 (Continued)

Linear and Quadratic Fit Coefficients

4b/1	-6.8850e-01	+/-	6.4154e-02	-1.8657e-01	+/-	3.4509e-04	4.5382e-06	+/-	3.9386e-07
5a/1	-1.0484e+00	+/-	5.0081e-02	-2.0449e-01	+/-	2.5079e-04	3.5332e-06	+/-	2.7083e-07
5b/1	-1.3030e+00	+/-	1.5372e-01	-2.0652e-01	+/-	7.7453e-04	3.4848e-06	+/-	8.4172e-07
2a/2	-7.6130e-04	+/-	2.4386e-04	-2.6542e-03	+/-	1.9645e-06	3.6649e-08	+/-	2.6290e-09
2b/2	-8.3323e-04	+/-	4.3245e-04	-2.8367e-03	+/-	3.7343e-06	5.0450e-08	+/-	5.3607e-09
3/2	-2.3646e-02	+/-	6.7176e-03	-5.4563e-02	+/-	3.7779e-05	2.0796e-06	+/-	4.1210e-08
4a/2	-6.2223e-01	+/-	7.0509e-02	-1.8379e-01	+/-	3.7665e-04	5.5300e-06	+/-	4.2553e-07
4b/2	-6.6912e-01	+/-	6.3848e-02	-1.8261e-01	+/-	3.3788e-04	5.0384e-06	+/-	3.7825e-07
5a/2	-1.1095e+00	+/-	3.4066e-02	-2.0724e-01	+/-	1.7356e-04	4.4652e-06	+/-	1.9005e-07
5b/2	-1.2044e+00	+/-	1.4208e-01	-2.0596e-01	+/-	7.1864e-04	4.2904e-06	+/-	7.8103e-07

TABLE A1-3

IR Scan Run Numbers and Telemetry

IMAGER
S/N = SN03

Final T/V
MISSION = Mission Low
PATCH = Patch Low

Acceptance Valid Data

RUN NO.	DATE:TIME	ELEC SIDE	ECT(K)	BASEPLATE(C)	NARROW PATCH(K)	SPACE TARGET(K)	COOLER RADIATOR(K)	COOLER HOUSING(K)	AFT OPTICS(C)	PATCH CONTROL(V)
501	10-MAR-1993 : 20:31:52.00	1	319.596	9.428	94.296	81.550	152.424	171.719	11.900	8.509
502	10-MAR-1993 : 23:54:22.00	1	308.806	9.461	94.308	81.400	152.260	171.675	12.000	8.686
504	11-MAR-1993 : 03:11:15.00	1	296.419	9.428	94.302	81.550	152.260	171.675	12.000	8.707
505	11-MAR-1993 : 05:20:37.00	1	282.027	9.370	94.308	81.850	152.260	171.653	12.000	8.843
506	11-MAR-1993 : 10:24:22.00	1	265.324	9.226	94.308	81.500	152.321	171.609	11.800	8.665
507	11-MAR-1993 : 14:26:15.00	1	243.568	9.137	94.290	81.300	152.260	171.631	11.700	8.759
508	11-MAR-1993 : 21:00:00.00	1	201.986	8.811	94.308	81.550	152.218	171.345	11.300	8.717
509	12-MAR-1993 : 00:00:00.00	2	202.557	8.555	94.248	81.350	152.280	171.367	11.300	9.010
511	12-MAR-1993 : 03:39:22.00	2	242.630	8.591	94.248	81.800	152.383	171.279	11.300	8.916
512	12-MAR-1993 : 06:16:52.00	2	265.566	8.653	94.248	81.900	152.548	171.301	11.300	8.863
513	12-MAR-1993 : 09:33:45.00	2	282.228	8.784	94.248	81.750	152.465	171.235	11.400	9.041
514	12-MAR-1993 : 14:03:45.00	2	297.491	8.881	94.248	81.550	152.260	171.301	11.600	10.335
515	12-MAR-1993 : 17:15:00.00	2	308.587	9.017	94.248	81.550	152.465	171.367	11.700	9.824
516	13-MAR-1993 : 00:22:30.00	2	319.882	9.127	94.248	81.550	152.363	171.631	11.900	9.333

APPENDIX A2. IMAGER IR SCAN REPORT

GOES SN03 IMAGER

MISSION TEMPERATURE — LOW

PATCH TEMPERATURE — MID

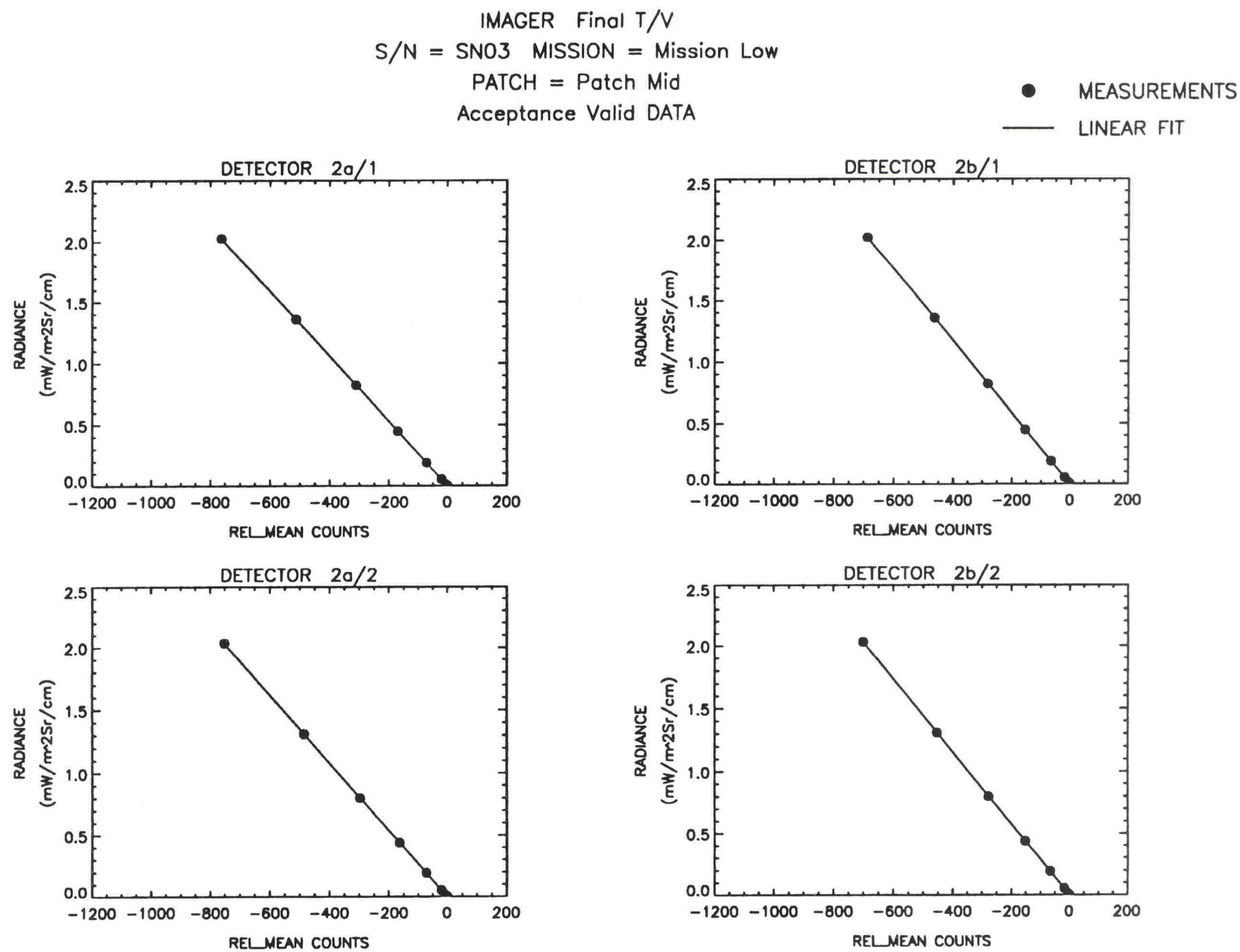

Figure A2-1. Radiance versus relative mean counts, channel 2.

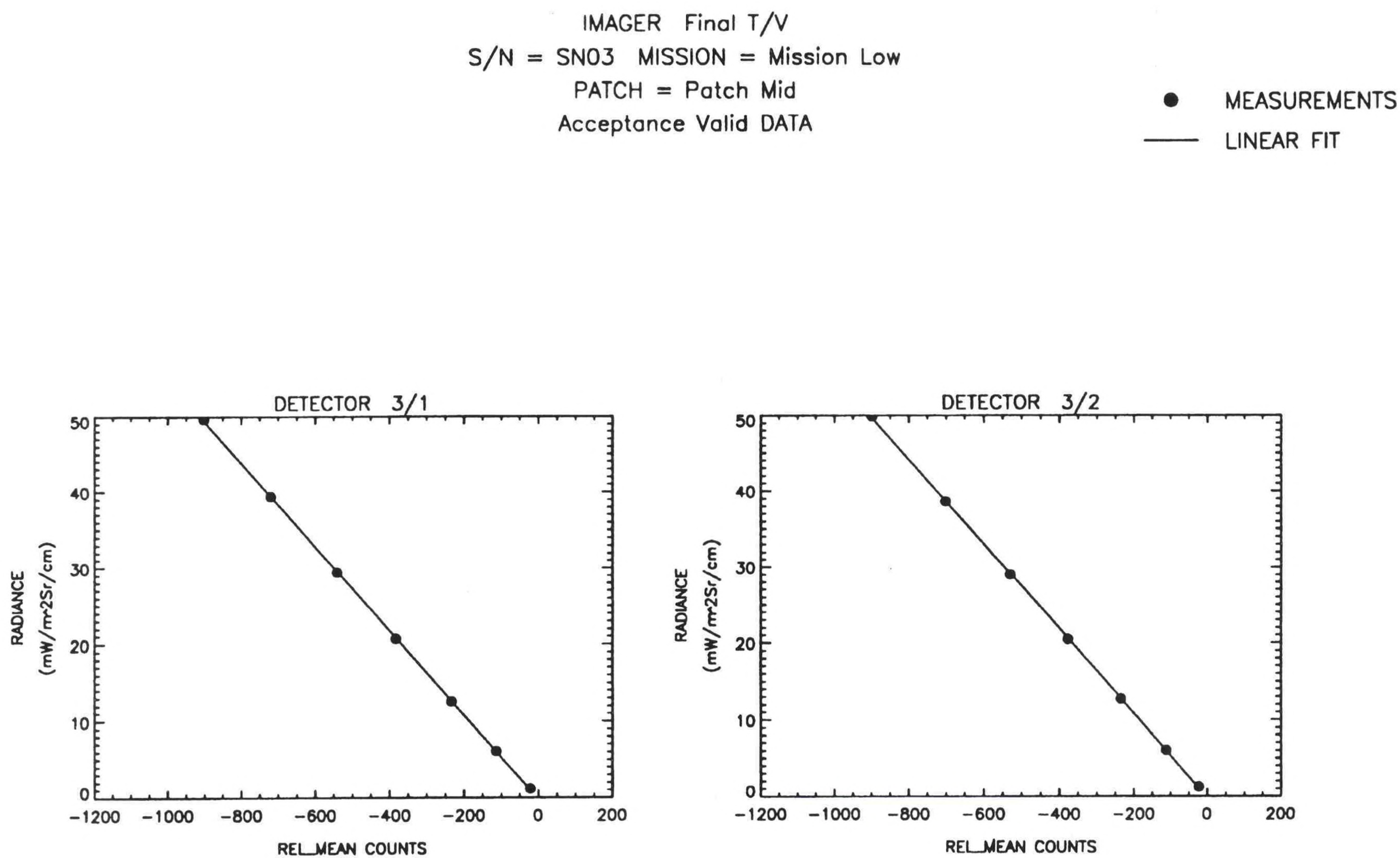

Figure A2-2. Radiance versus relative mean counts, channel 3.

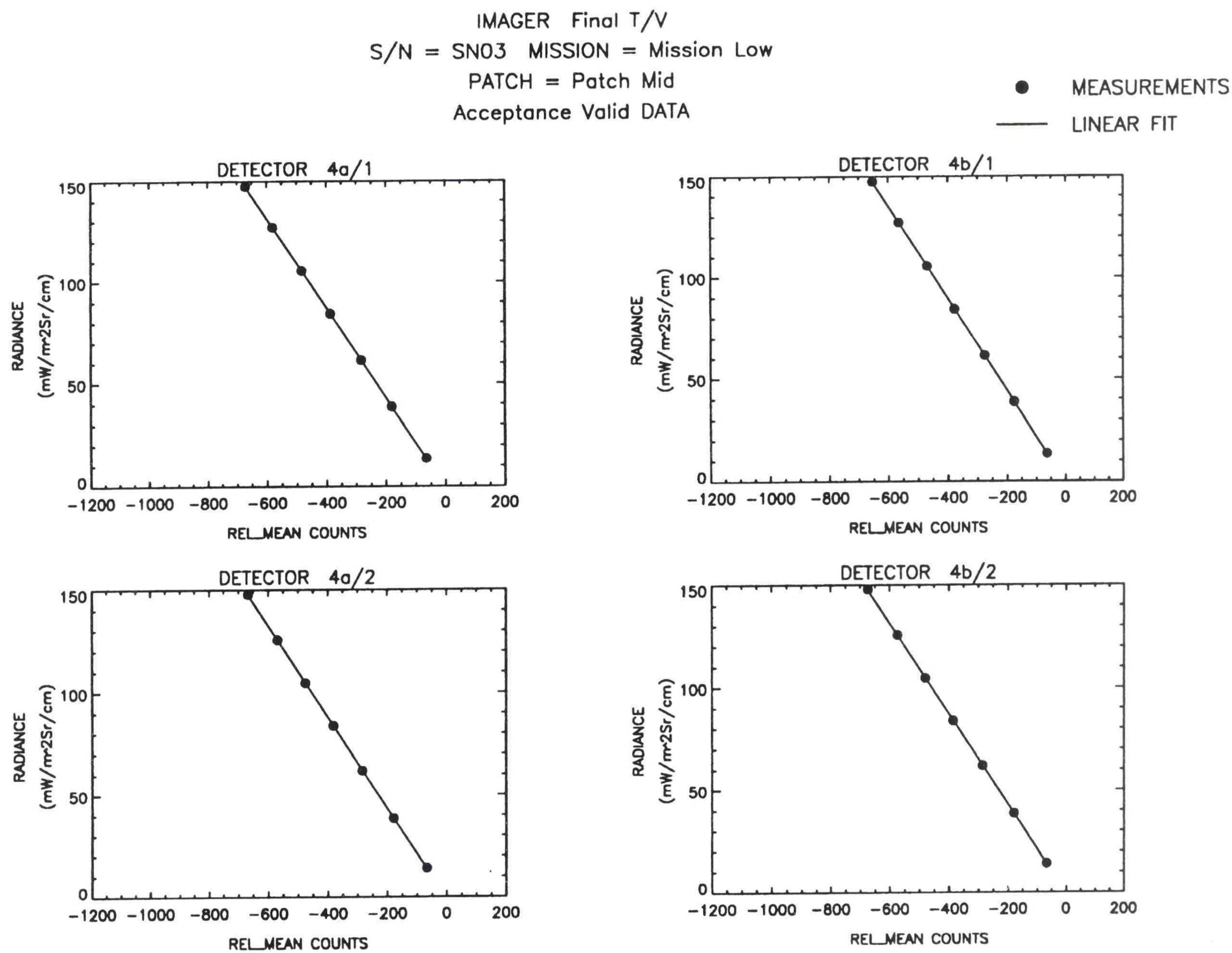

Figure A2-3. Radiance versus relative mean counts, channel 4.

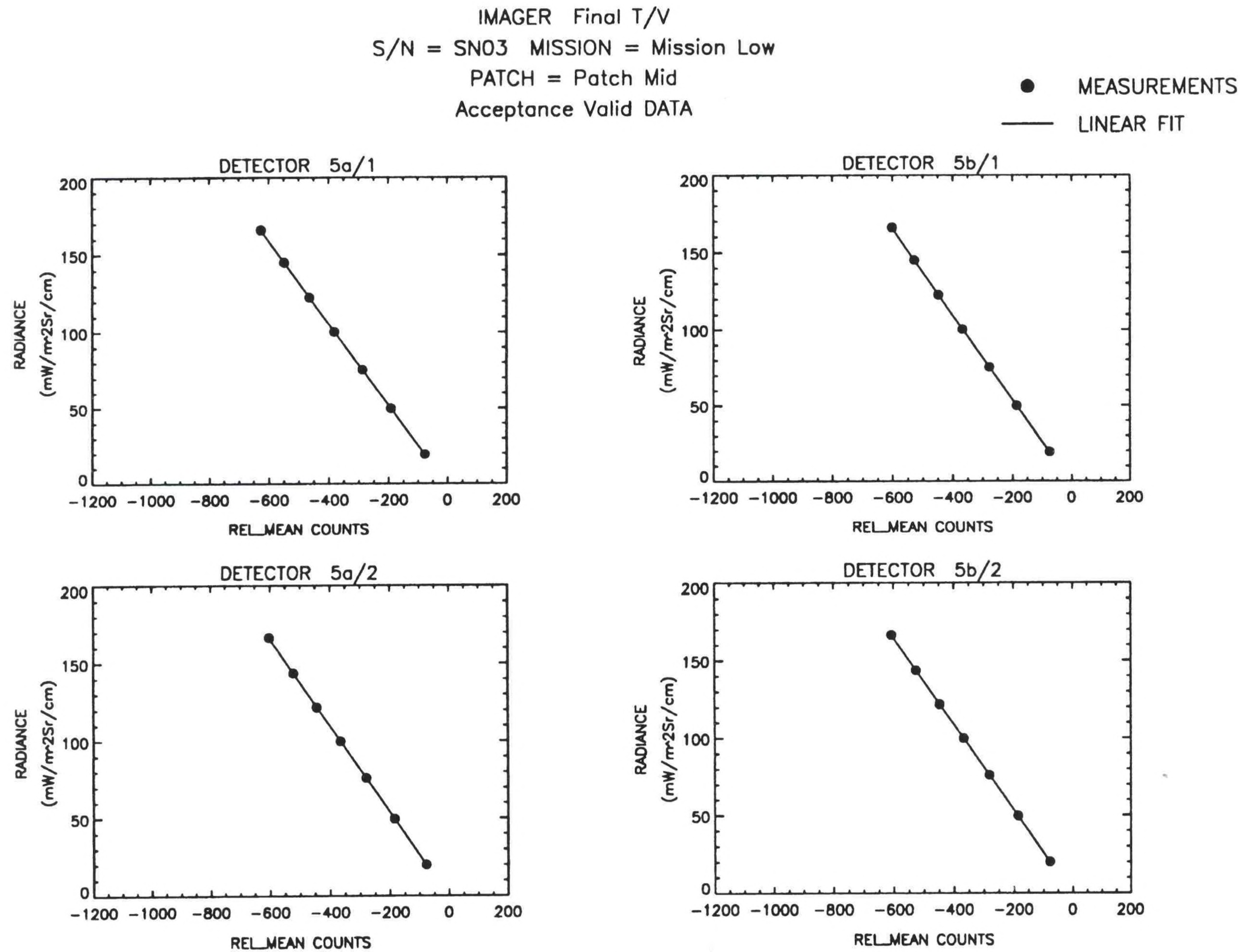

Figure A2-4. Radiance versus relative mean counts, channel 5.

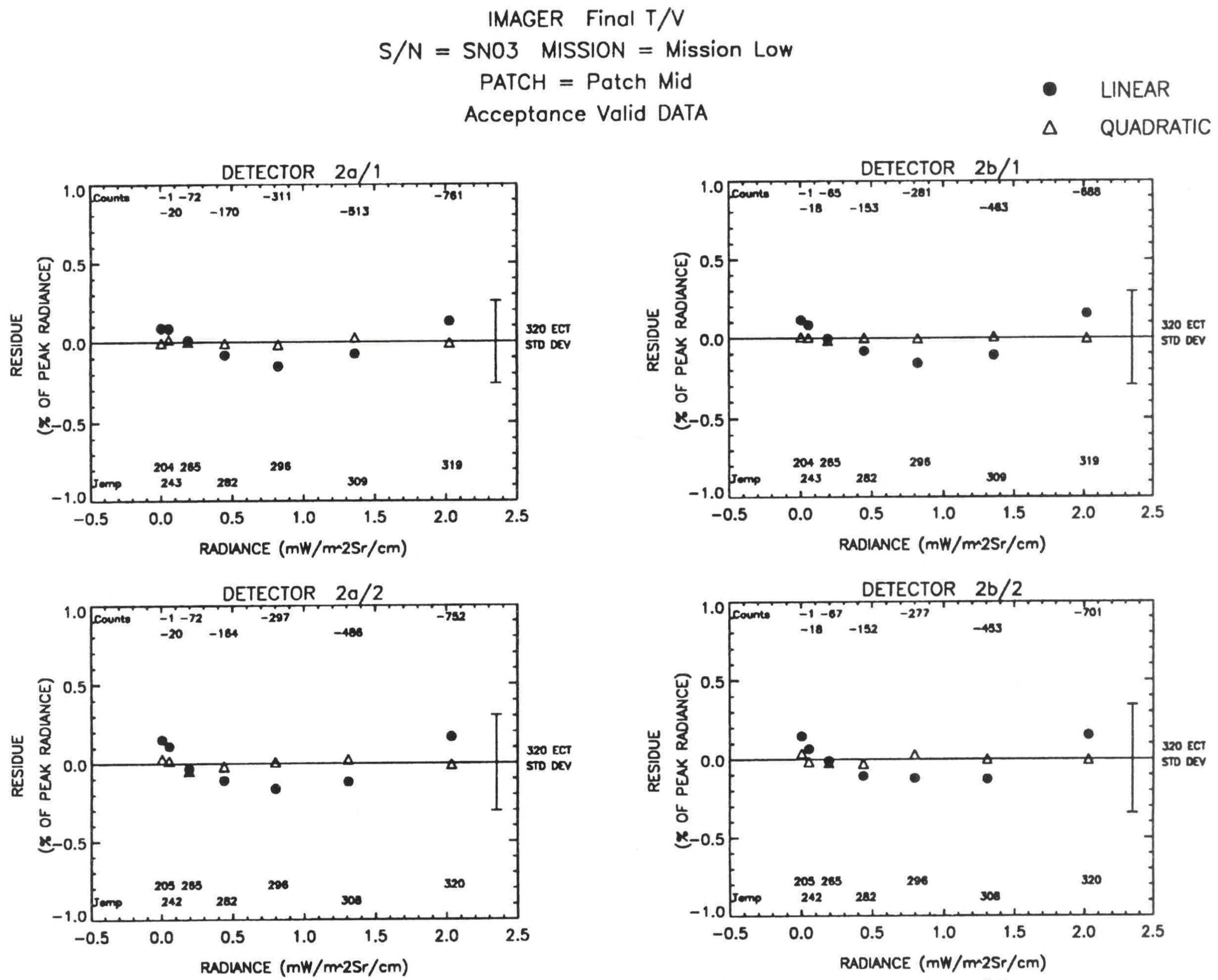

Figure A2-5. Residues of linear and quadratic fits versus radiance, channel 2.

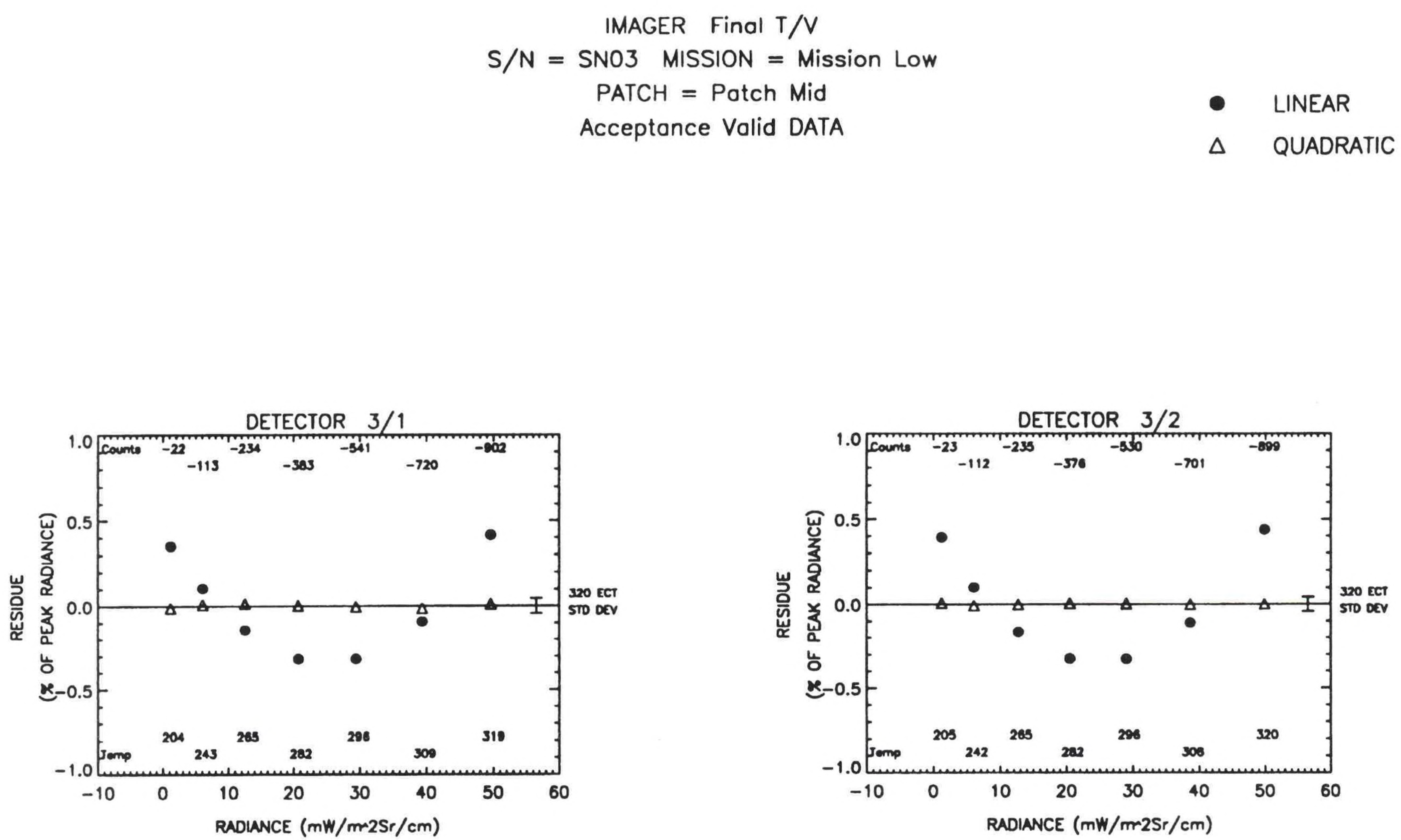

Figure A2-6. Residues of linear and quadratic fits versus radiance, channel 3.

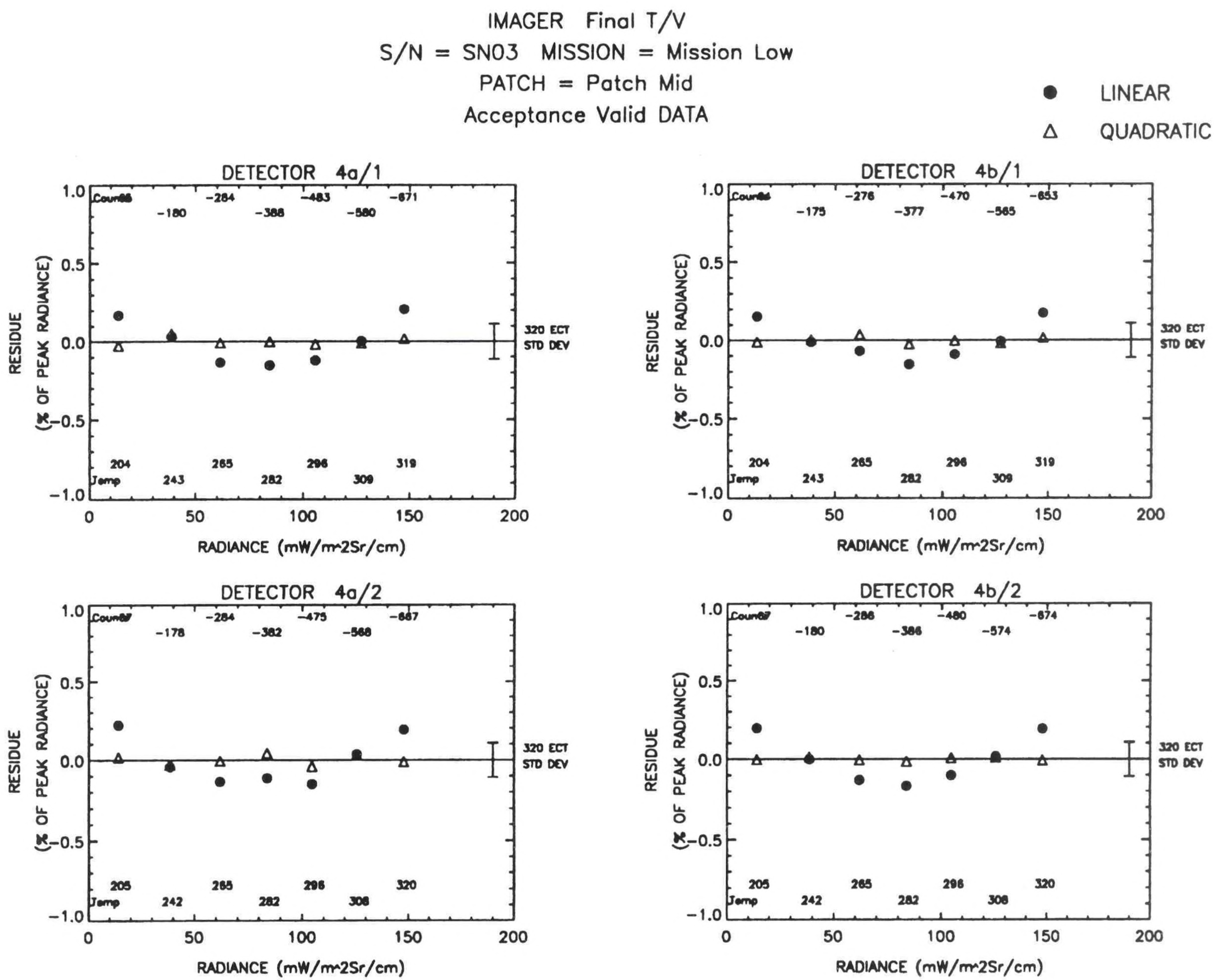

Figure A2-7. Residues of linear and quadratic fits versus radiance, channel 4.

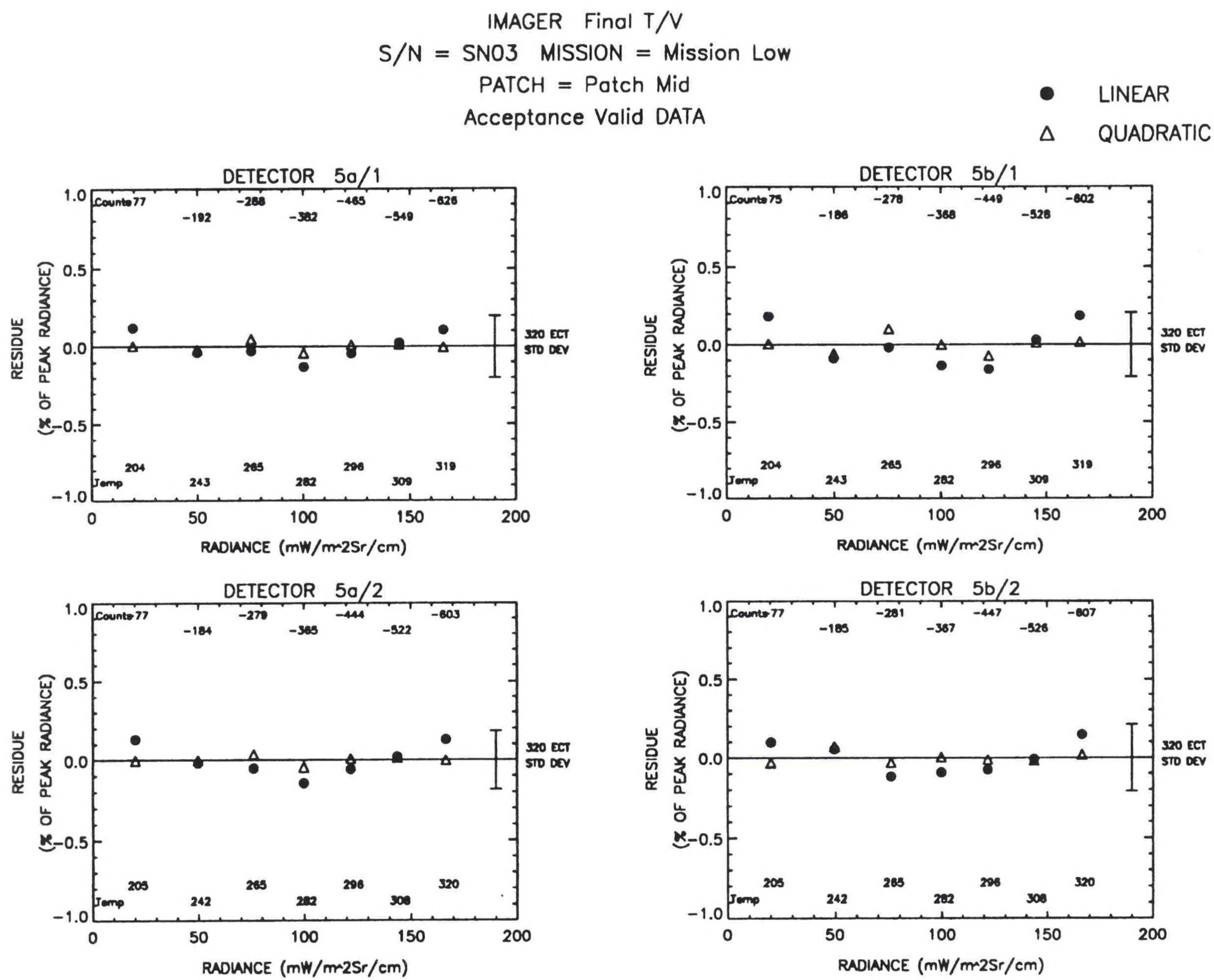

Figure A2-8. Residues of linear and quadratic fits versus radiance, channel 5.

TABLE A2-1

Noise and Residue Statistics

IMAGER
S/N = SN03

Final T/V
MISSION = Mission Low
PATCH = Patch Mid

Acceptance Valid Data

CH/SIDE	NEDT(K) MEAS/TEMP	NEDT(K) SPEC/TSPEC	PEAK LIN RES %	SPEC %	RMS LIN RES %	PEAK LIN RES N (mW/m^2Sr/cm)	PEAK QUAD RES %	RMS QUAD RES %	PEAK QUAD RES N (mW/m^2Sr/cm)
2a/1	0.1661/296.6	1.40/300.0	0.1526	1.7	0.0981	0.0031	0.0254	0.0142	0.0005
2b/1	0.1748/296.6	1.40/300.0	0.1589	1.7	0.1120	0.0032	0.0075	0.0073	0.0002
3/1	0.1055/243.1	1.00/230.0	0.4148	1.7	0.2771	0.2063	0.0124	0.0102	0.0062
4a/1	0.1057/296.6	0.35/300.0	0.2068	1.7	0.1357	0.3052	0.0509	0.0245	0.0752
4b/1	0.1005/296.6	0.35/300.0	0.1749	1.7	0.1137	0.2582	0.0369	0.0198	0.0545
5a/1	0.2086/296.6	0.50/300.0	0.1301	1.7	0.0825	0.2160	0.0466	0.0258	0.0773
5b/1	0.1950/296.6	0.50/300.0	0.1868	1.7	0.1312	0.3102	0.1005	0.0524	0.1669
2a/2	0.1660/296.1	1.40/300.0	0.1660	1.7	0.1290	0.0034	0.0288	0.0256	0.0006
2b/2	0.1841/296.1	1.40/300.0	0.1529	1.7	0.1146	0.0031	0.0384	0.0234	0.0008
3/2	0.1005/243.0	1.00/230.0	0.4367	1.7	0.2949	0.2169	0.0072	0.0049	0.0036
4a/2	0.1010/296.1	0.35/300.0	0.2180	1.7	0.1415	0.3215	0.0422	0.0282	0.0622
4b/2	0.0999/296.1	0.35/300.0	0.1944	1.7	0.1363	0.2868	0.0125	0.0098	0.0185
5a/2	0.1891/296.1	0.50/300.0	0.1456	1.7	0.0938	0.2418	0.0361	0.0227	0.0600
5b/2	0.2131/296.1	0.50/300.0	0.1464	1.7	0.0944	0.2432	0.0713	0.0337	0.1183

TABLE A2-2

Linear and Quadratic Fit Coefficients

IMAGER — Final T/V
S/N = SN03 — MISSION = Mission Low
PATCH = Patch Mid
Acceptance Valid Data

RAD = GAMM1 + M1 * C

CH/SIDE	GAMMA1			M1		
2a/1	-2.7988e-03	+/-	1.2640e-03	-2.6576e-03	+/-	3.3858e-06
2b/1	-2.7487e-03	+/-	1.4402e-03	-2.9376e-03	+/-	4.2712e-06
3/1	-2.3321e-01	+/-	1.0571e-01	-5.5014e-02	+/-	2.0608e-04
4a/1	-1.1964e+00	+/-	1.9106e-01	-2.2090e-01	+/-	4.4495e-04
4b/1	-1.2156e+00	+/-	1.6001e-01	-2.2703e-01	+/-	3.8301e-04
5a/1	-1.5281e+00	+/-	1.3878e-01	-2.6695e-01	+/-	3.3767e-04
5b/1	-1.8072e+00	+/-	2.2140e-01	-2.7788e-01	+/-	5.5911e-04
2a/2	-3.1741e-03	+/-	1.6442e-03	-2.7058e-03	+/-	4.5271e-06
2b/2	-2.5098e-03	+/-	1.4574e-03	-2.8945e-03	+/-	4.3021e-06
3/2	-2.5634e-01	+/-	1.1240e-01	-5.5508e-02	+/-	2.2211e-04
4a/2	-1.2765e+00	+/-	1.9967e-01	-2.2293e-01	+/-	4.7084e-04
4b/2	-1.2430e+00	+/-	1.9238e-01	-2.2077e-01	+/-	4.4913e-04
5a/2	-1.7181e+00	+/-	1.5862e-01	-2.7828e-01	+/-	4.0253e-04
5b/2	-1.5903e+00	+/-	1.5947e-01	-2.7617e-01	+/-	4.0206e-04

RAD = GAMMA2 + M2 * C + R * C^2

CH/SIDE	GAMMA2			M2			R		
2a/1	-8.7146e-04	+/-	2.4779e-04	-2.6315e-03	+/-	1.9822e-06	3.5740e-08	+/-	2.6075e-09
2b/1	-5.3637e-04	+/-	1.2714e-04	-2.9044e-03	+/-	1.1265e-06	5.0367e-08	+/-	1.6412e-09
3/1	-1.5686e-02	+/-	5.8872e-03	-5.3318e-02	+/-	3.2218e-05	1.8597e-06	+/-	3.4097e-08
4a/1	-6.6032e-01	+/-	6.2604e-02	-2.1677e-01	+/-	3.8939e-04	5.5705e-06	+/-	5.1205e-07

TABLE A2-2 (Continued)

Linear and Quadratic Fit Coefficients

4b/1	-7.6517e-01	+/-	5.0665e-02	-2.2348e-01	+/-	3.2372e-04	4.9359e-06	+/-	4.3731e-07
5a/1	-1.1155e+00	+/-	8.3581e-02	-2.6378e-01	+/-	5.3560e-04	4.4763e-06	+/-	7.3788e-07
5b/1	-1.1695e+00	+/-	1.7060e-01	-2.7280e-01	+/-	1.1347e-03	7.4471e-06	+/-	1.6232e-06
2a/2	-6.6740e-04	+/-	4.4506e-04	-2.6718e-03	+/-	3.5890e-06	4.7019e-08	+/-	4.7675e-09
2b/2	-2.9320e-04	+/-	4.0506e-04	-2.8623e-03	+/-	3.5035e-06	4.7842e-08	+/-	4.9886e-09
3/2	-2.4405e-02	+/-	2.8644e-03	-5.3712e-02	+/-	1.5611e-05	1.9791e-06	+/-	1.6577e-08
4a/2	-7.1525e-01	+/-	7.2292e-02	-2.1862e-01	+/-	4.4995e-04	5.8594e-06	+/-	5.9520e-07
4b/2	-6.9244e-01	+/-	2.5241e-02	-2.1659e-01	+/-	1.5557e-04	5.6350e-06	+/-	2.0375e-07
5a/2	-1.2314e+00	+/-	7.4227e-02	-2.7443e-01	+/-	4.9095e-04	5.6313e-06	+/-	7.0124e-07
5b/2	-1.1198e+00	+/-	1.1026e-01	-2.7247e-01	+/-	7.2507e-04	5.3808e-06	+/-	1.0291e-06

TABLE A2-3

IR Scan Run Numbers and Telemetry

IMAGER
S/N = SN03
Final T/V
MISSION = Mission Low
PATCH = Patch Mid
Acceptance Valid Data

RUN NO.	DATE:TIME	ELEC SIDE	ECT (K)	BASEPLATE (C)	NARROW PATCH (K)	SPACE TARGET (K)	COOLER RADIATOR (K)	COOLER HOUSING (K)	AFT OPTICS (C)	PATCH CONTROL (V)
522	13-MAR-1993 : 03:56:15.00	1	319.888	9.417	101.089	81.300	152.116	171.764	11.900	17.978
523	13-MAR-1993 : 07:30:00.00	1	309.153	9.402	101.077	81.700	152.260	171.741	11.900	17.967
524	13-MAR-1993 : 09:50:37.00	1	296.579	9.388	101.077	81.450	152.260	171.764	11.900	17.957
525	13-MAR-1993 : 14:26:15.00	1	282.739	9.289	101.089	81.450	152.280	171.764	11.800	17.831
526	13-MAR-1993 : 17:48:45.00	1	265.165	9.155	101.077	81.250	152.342	171.653	11.700	17.884
527	13-MAR-1993 : 20:31:52.00	1	243.140	9.083	101.083	81.350	152.404	171.631	11.700	17.884
528	14-MAR-1993 : 00:56:15.00	1	204.379	8.824	101.083	81.300	152.260	171.389	11.400	17.852
529	14-MAR-1993 : 02:31:52.00	2	205.509	8.713	101.034	81.350	152.486	171.499	11.400	18.145
530	14-MAR-1993 : 06:39:22.00	2	242.992	8.598	101.022	81.450	152.445	171.477	11.300	18.176
531	14-MAR-1993 : 09:05:37.00	2	265.639	8.705	101.016	81.450	152.568	171.367	11.400	18.207
532	14-MAR-1993 : 11:43:07.00	2	282.420	8.784	101.071	81.500	152.465	171.146	11.500	17.915
533	14-MAR-1993 : 14:26:15.00	2	296.084	8.934	101.046	81.400	152.507	171.213	11.600	18.134
534	14-MAR-1993 : 16:30:00.00	2	308.376	9.047	101.028	81.700	152.486	171.345	11.700	17.998
535	14-MAR-1993 : 20:37:30.00	2	320.210	9.191	101.065	81.550	152.465	171.455	11.900	18.040

APPENDIX A3. IMAGER IR SCAN REPORT

GOES SN03 IMAGER

MISSION TEMPERATURE – NOMINAL

PATCH TEMPERATURE – LOW

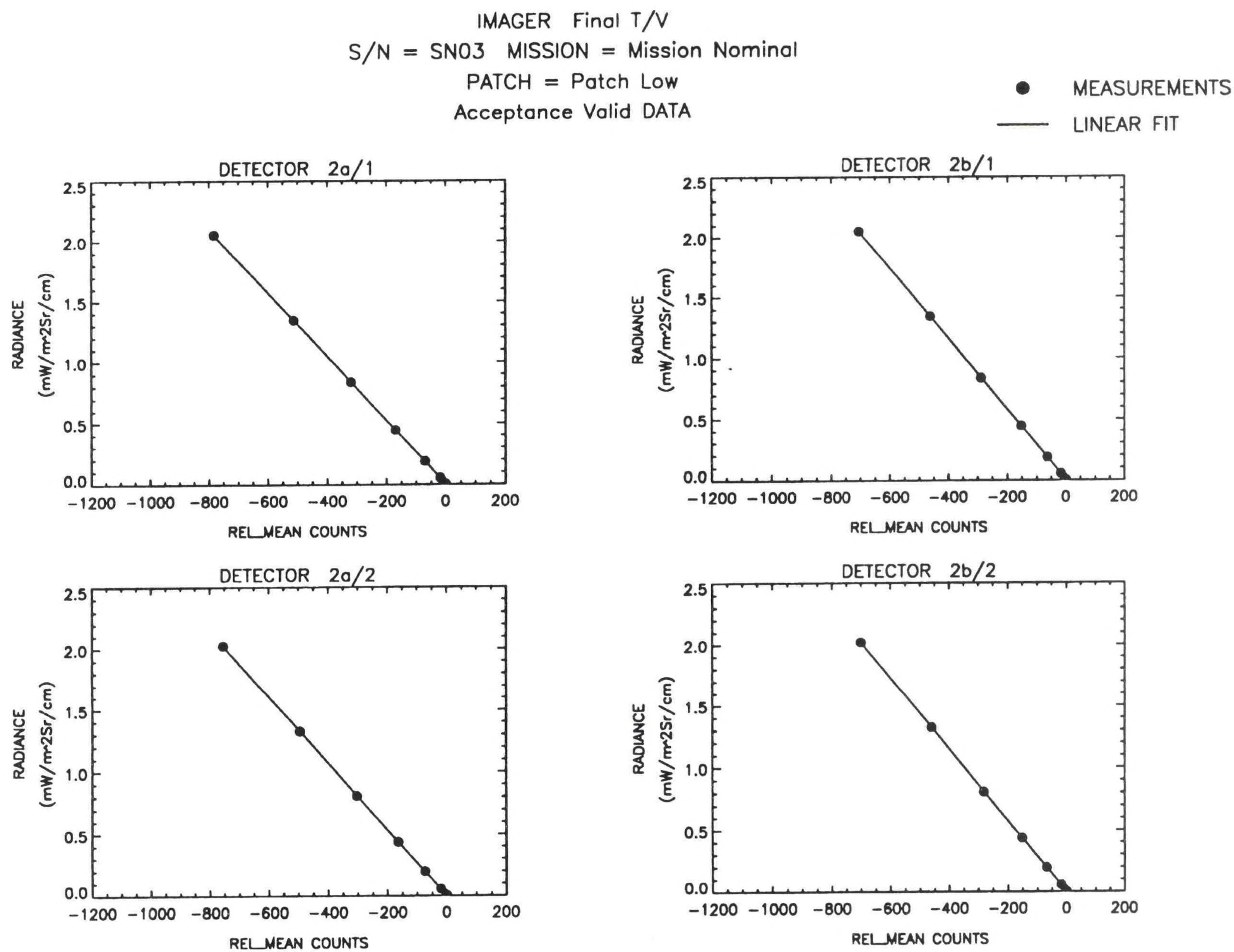

Figure A3-1. Radiance versus relative mean counts, channel 2.

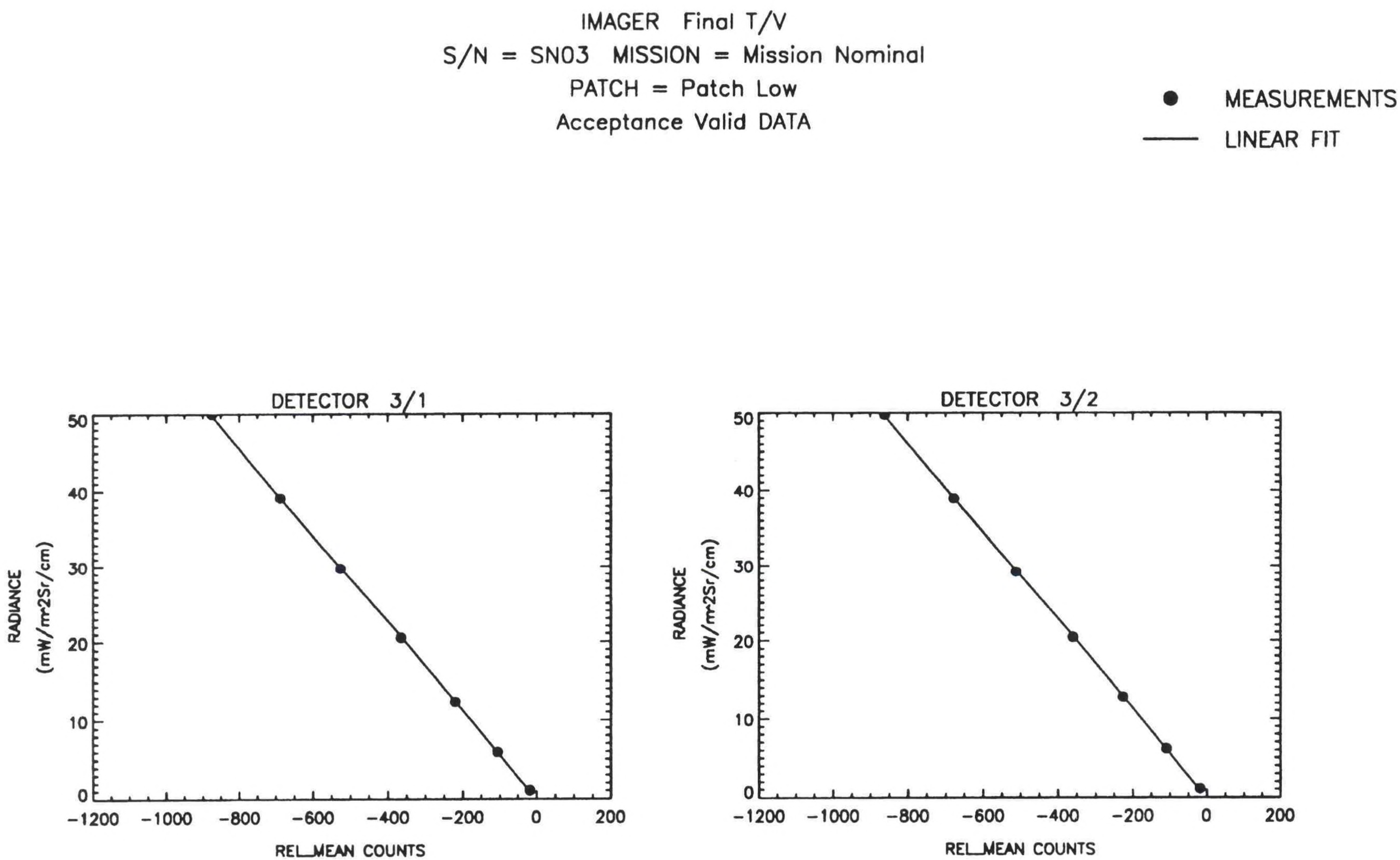

Figure A3-2. Radiance versus relative mean counts, channel 3.

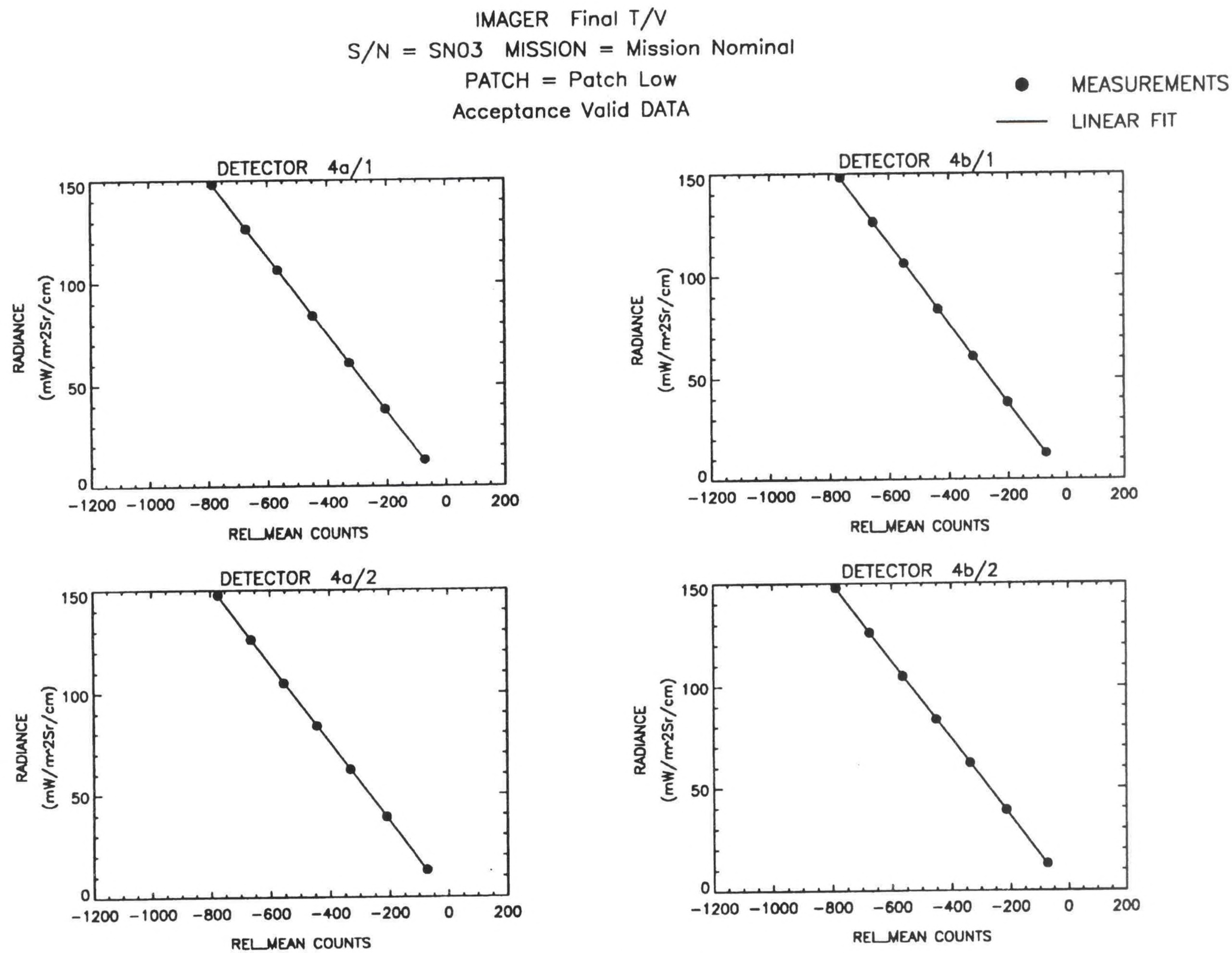

Figure A3-3. Radiance versus relative mean counts, channel 4.

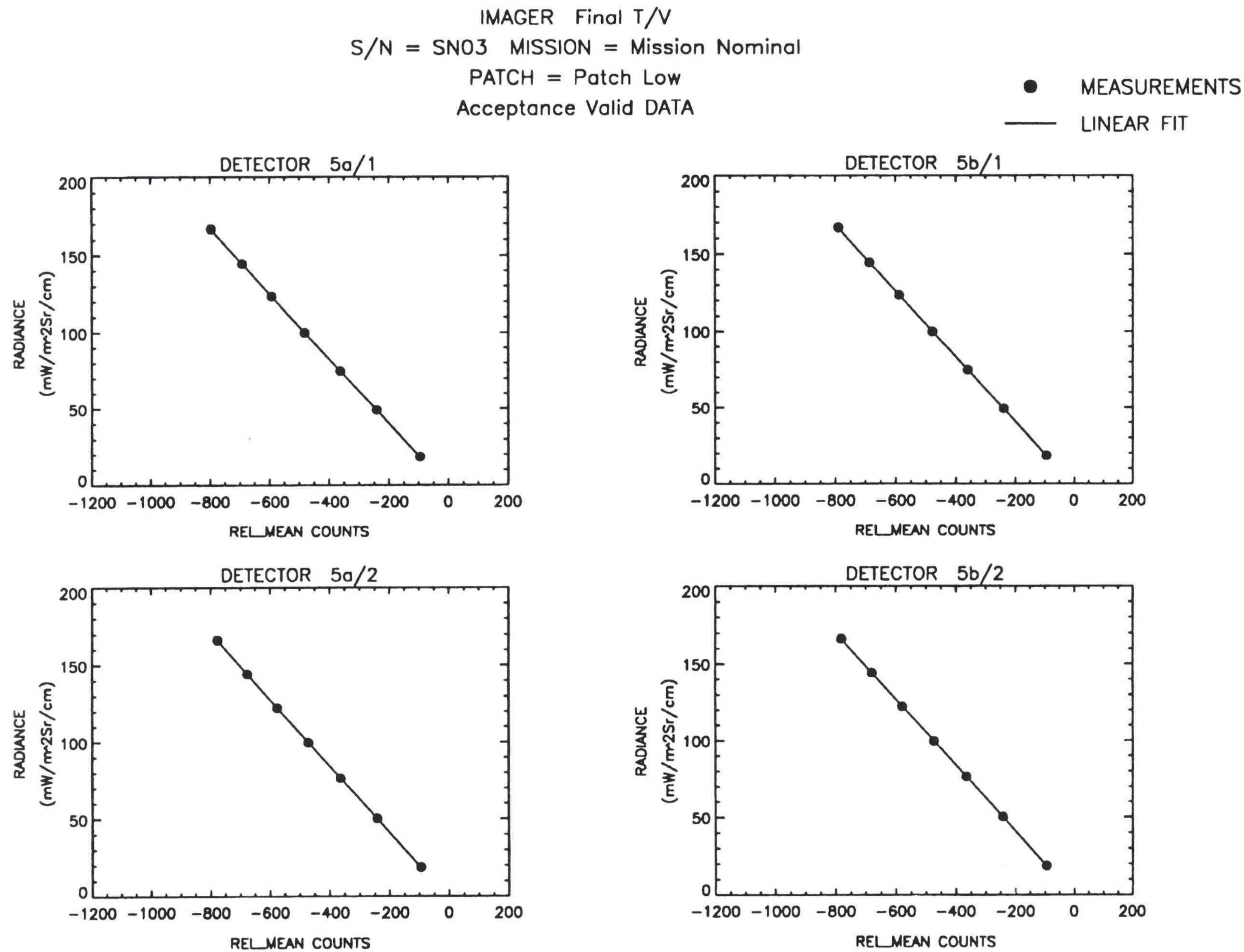

Figure A3-4. Radiance versus relative mean counts, channel 5.

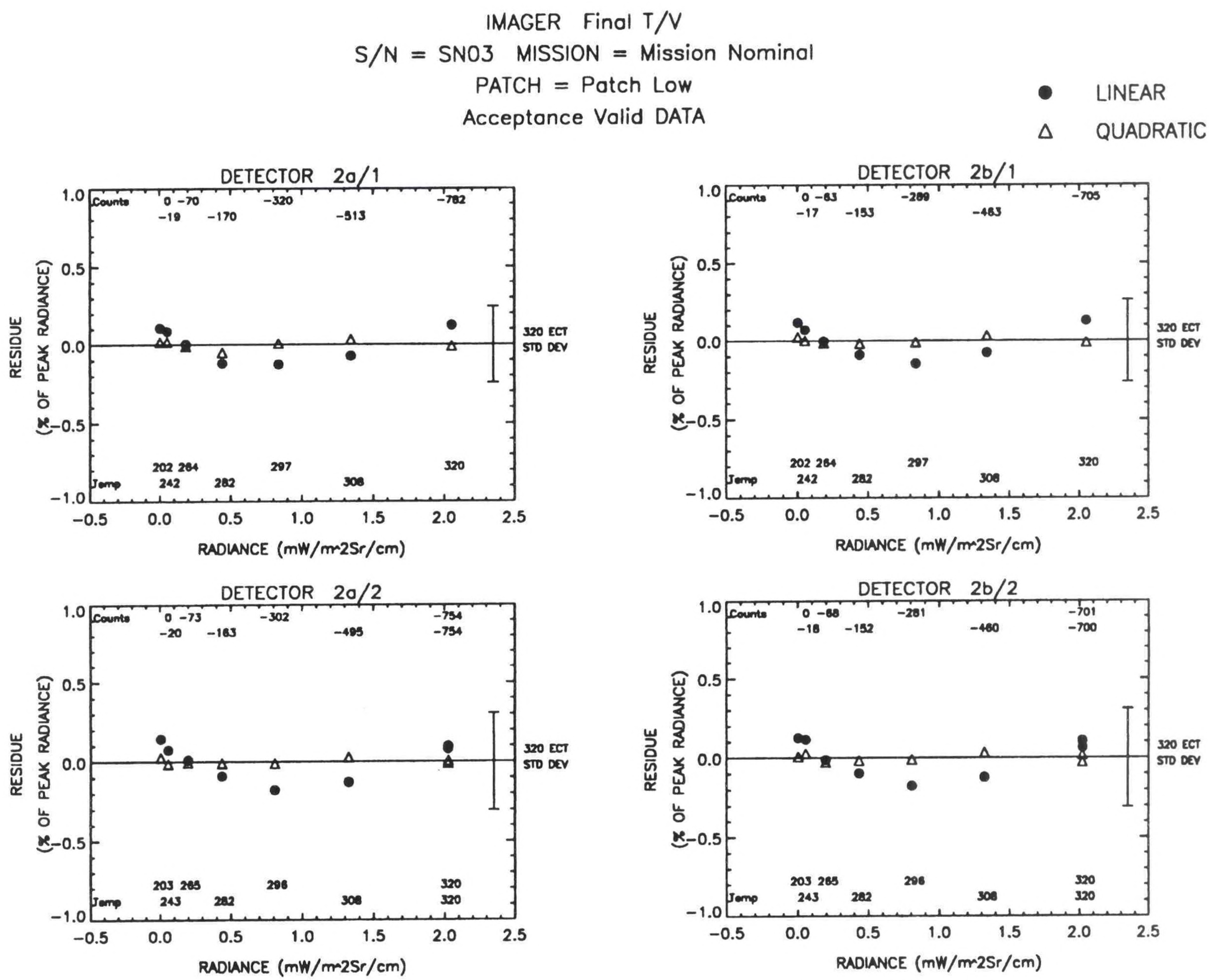

Figure A3-5. Residues of linear and quadratic fits versus radiance, channel 2.

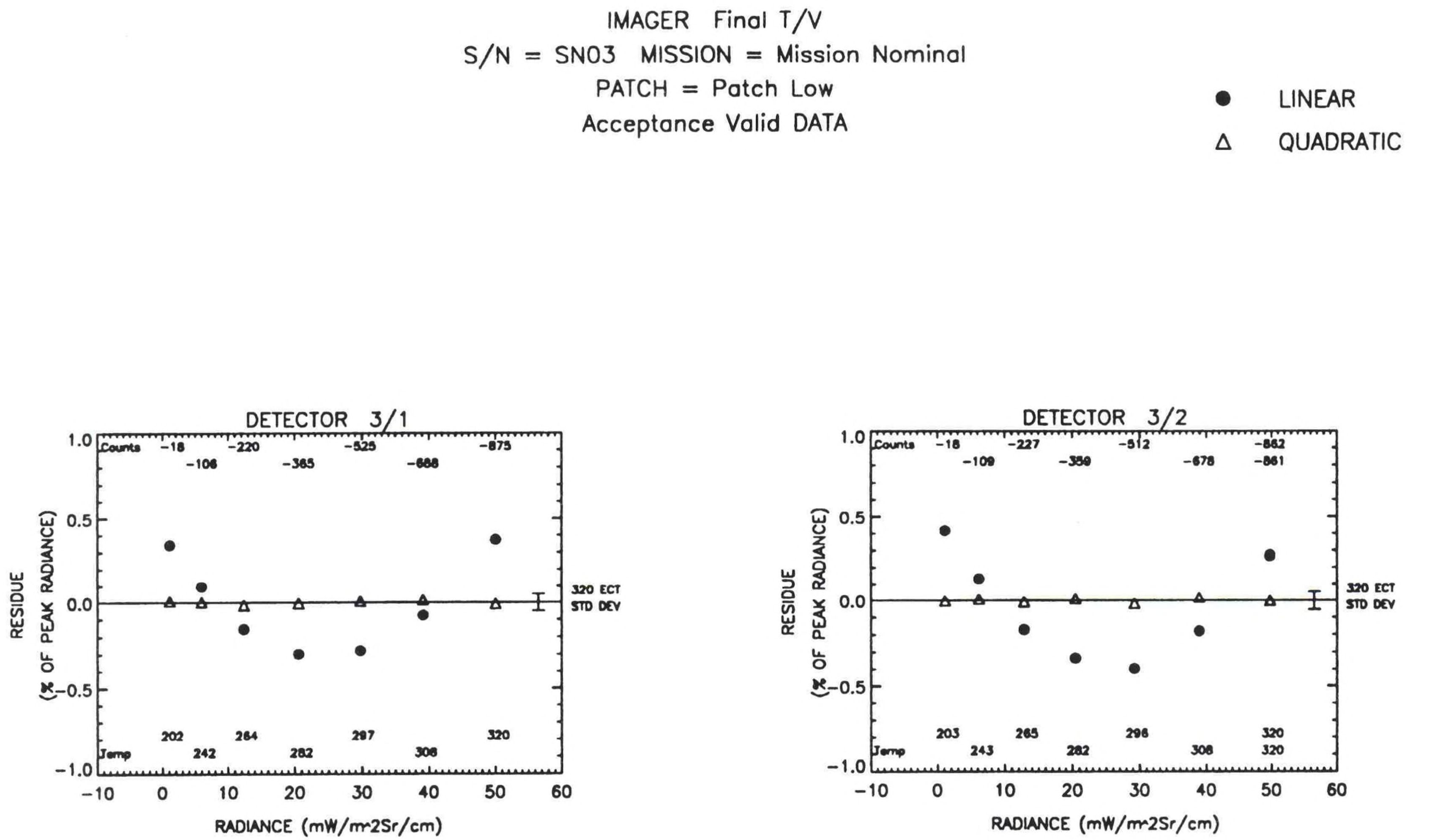

Figure A3-6. Residues of linear and quadratic fits versus radiance, channel 3.

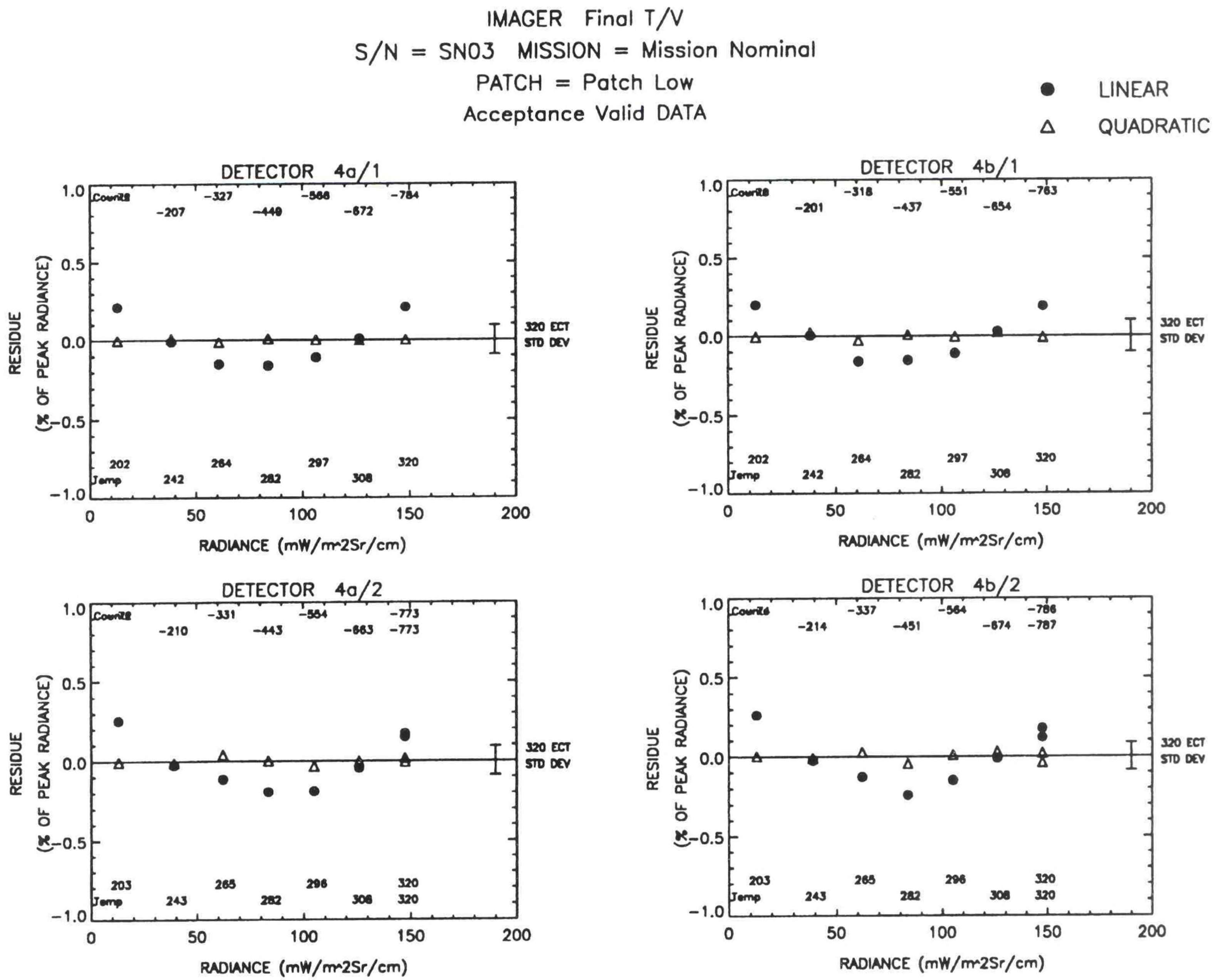

Figure A3-7. Residues of linear and quadratic fits versus radiance, channel 4.

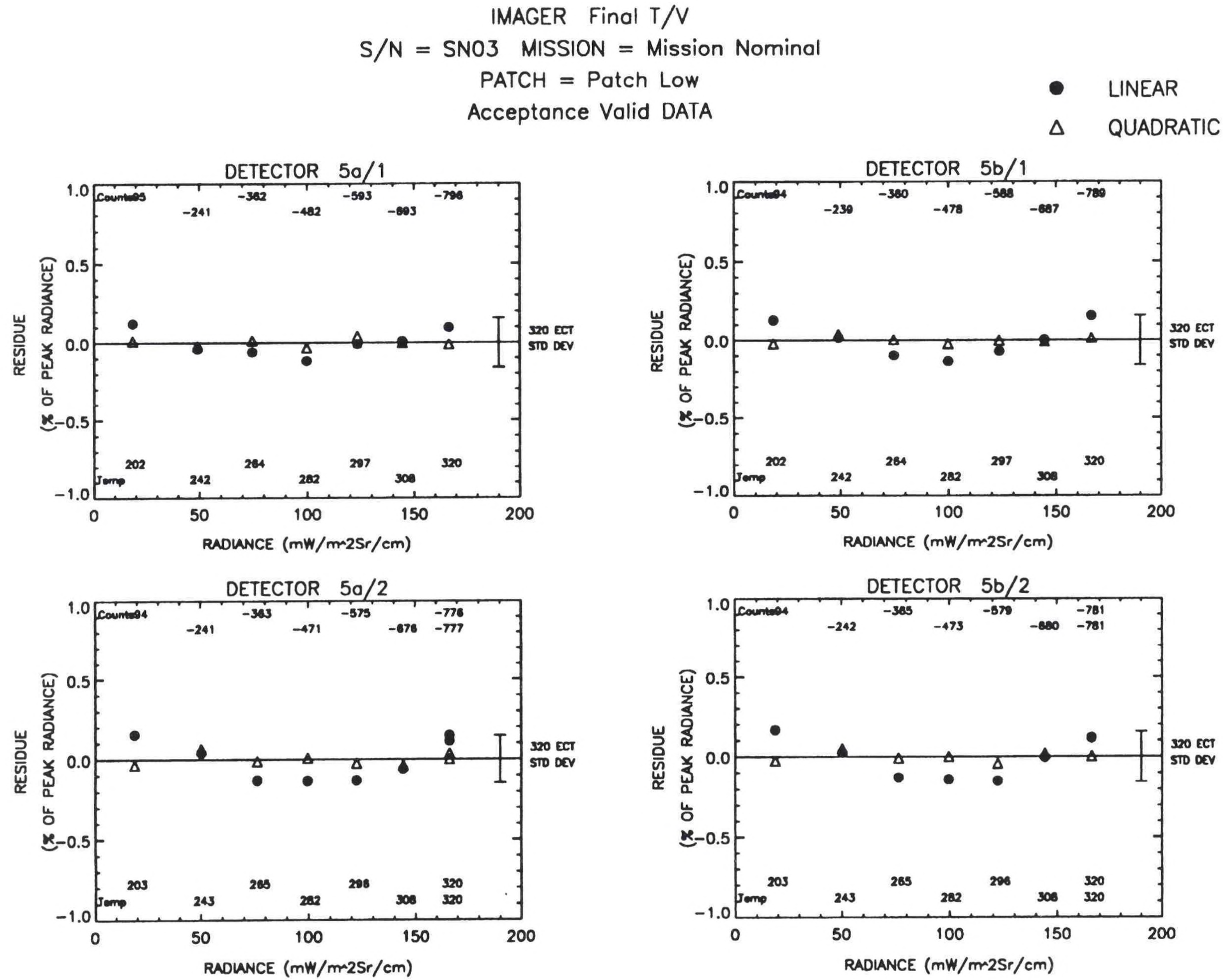

Figure A3-8. Residues of linear and quadratic fits versus radiance, channel 5.

TABLE A3-1

Noise and Residue Statistics

IMAGER
S/N = SN03

Final T/V
MISSION = Mission Nominal
PATCH = Patch Low

Acceptance Valid Data

CH/SIDE	NEDT(K) MEAS/TEMP	NEDT(K) SPEC/TSPEC	PEAK LIN RES %	SPEC %	RMS LIN RES %	PEAK LIN RES N (mW/m^2Sr/cm)	PEAK QUAD RES %	RMS QUAD RES %	PEAK QUAD RES N (mW/m^2Sr/cm)
2a/1	0.1607/297.0	1.40/300.0	0.1269	1.7	0.1002	0.0026	0.0327	0.0254	0.0007
2b/1	0.1719/297.0	1.40/300.0	0.1466	1.7	0.1005	0.0030	0.0318	0.0188	0.0006
3/1	0.1176/242.5	1.00/230.0	0.3726	1.7	0.2572	0.1853	0.0129	0.0097	0.0064
4a/1	0.0864/297.0	0.35/300.0	0.2127	1.7	0.1460	0.3140	0.0085	0.0068	0.0125
4b/1	0.0917/297.0	0.35/300.0	0.2000	1.7	0.1401	0.2952	0.0222	0.0164	0.0328
5a/1	0.1545/297.0	0.50/300.0	0.1236	1.7	0.0792	0.2052	0.0420	0.0233	0.0697
5b/1	0.1556/297.0	0.50/300.0	0.1569	1.7	0.1030	0.2605	0.0397	0.0200	0.0659
2a/2	0.1704/296.3	1.40/300.0	0.1785	1.7	0.1107	0.0036	0.0256	0.0157	0.0005
2b/2	0.1711/296.3	1.40/300.0	0.1758	1.7	0.1116	0.0035	0.0324	0.0227	0.0007
3/2	0.0900/243.5	1.00/230.0	0.4161	1.7	0.2889	0.2067	0.0155	0.0104	0.0077
4a/2	0.0814/296.3	0.35/300.0	0.2527	1.7	0.1603	0.3725	0.0388	0.0198	0.0571
4b/2	0.0820/296.3	0.35/300.0	0.2621	1.7	0.1626	0.3866	0.0308	0.0267	0.0454
5a/2	0.1327/296.3	0.50/300.0	0.1540	1.7	0.1199	0.2557	0.0645	0.0332	0.1071
5b/2	0.1616/296.3	0.50/300.0	0.1657	1.7	0.1195	0.2751	0.0501	0.0258	0.0832

TABLE A3-2

Linear and Quadratic Fit Coefficients

IMAGER — Final T/V
S/N = SN03 — MISSION = Mission Nominal
PATCH = Patch Low
Acceptance Valid Data

RAD = GAMM1 + M1 * C

CH/SIDE	GAMMA1			M1		
2a/1	-1.5915e-03	+/-	1.2852e-03	-2.6230e-03	+/-	3.3777e-06
2b/1	-1.7351e-03	+/-	1.2869e-03	-2.9044e-03	+/-	3.7508e-06
3/1	-1.7655e-01	+/-	9.7381e-02	-5.7127e-02	+/-	1.9700e-04
4a/1	-1.3626e+00	+/-	2.0401e-01	-1.9029e-01	+/-	4.0852e-04
4b/1	-1.2967e+00	+/-	1.9552e-01	-1.9529e-01	+/-	4.0216e-04
5a/1	-1.8807e+00	+/-	1.3219e-01	-2.1120e-01	+/-	2.5375e-04
5b/1	-1.8405e+00	+/-	1.7211e-01	-2.1308e-01	+/-	3.3320e-04
2a/2	-1.8584e-03	+/-	1.3544e-03	-2.6850e-03	+/-	3.1204e-06
2b/2	-2.1173e-03	+/-	1.3629e-03	-2.8851e-03	+/-	3.3791e-06
3/2	-2.1825e-01	+/-	1.0447e-01	-5.7792e-02	+/-	1.9064e-04
4a/2	-1.4710e+00	+/-	2.1273e-01	-1.9232e-01	+/-	3.9654e-04
4b/2	-1.4513e+00	+/-	2.1588e-01	-1.8916e-01	+/-	3.9564e-04
5a/2	-2.0813e+00	+/-	1.9041e-01	-2.1629e-01	+/-	3.4625e-04
5b/2	-1.8757e+00	+/-	1.8940e-01	-2.1473e-01	+/-	3.4248e-04

RAD = GAMMA2 + M2 * C + R * C^2

CH/SIDE	GAMMA2			M2			R		
2a/1	2.8284e-04	+/-	4.3876e-04	-2.5980e-03	+/-	3.4129e-06	3.3462e-08	+/-	4.3790e-09
2b/1	1.7192e-04	+/-	3.2552e-04	-2.8762e-03	+/-	2.8082e-06	4.1853e-08	+/-	3.9956e-09
3/1	1.9229e-02	+/-	5.5091e-03	-5.5524e-02	+/-	3.1273e-05	1.8222e-06	+/-	3.4296e-08
4a/1	-7.9271e-01	+/-	1.6934e-02	-1.8648e-01	+/-	9.0768e-05	4.4261e-06	+/-	1.0273e-07

TABLE A3-2 (Continued)

Linear and Quadratic Fit Coefficients

4b/1	-7.5443e-01	+/-	4.0833e-02	-1.9157e-01	+/-	2.2484e-04	4.4473e-06	+/-	2.6139e-07
5a/1	-1.4922e+00	+/-	7.4074e-02	-2.0883e-01	+/-	3.7528e-04	2.6468e-06	+/-	4.0821e-07
5b/1	-1.3213e+00	+/-	6.3519e-02	-2.0988e-01	+/-	3.2491e-04	3.6054e-06	+/-	3.5671e-07
2a/2	5.2276e-04	+/-	2.6018e-04	-2.6540e-03	+/-	2.0524e-06	4.0269e-08	+/-	2.5830e-09
2b/2	2.5445e-04	+/-	3.7596e-04	-2.8518e-03	+/-	3.1908e-06	4.6413e-08	+/-	4.3211e-09
3/2	2.4854e-02	+/-	5.6740e-03	-5.5901e-02	+/-	3.1324e-05	2.0480e-06	+/-	3.2933e-08
4a/2	-8.0408e-01	+/-	4.6878e-02	-1.8803e-01	+/-	2.4405e-04	4.8044e-06	+/-	2.6686e-07
4b/2	-7.7954e-01	+/-	6.3246e-02	-1.8491e-01	+/-	3.2365e-04	4.6790e-06	+/-	3.4796e-07
5a/2	-1.4475e+00	+/-	1.0003e-01	-2.1251e-01	+/-	4.9879e-04	4.1269e-06	+/-	5.3177e-07
5b/2	-1.2384e+00	+/-	7.7453e-02	-2.1094e-01	+/-	3.8425e-04	4.1134e-06	+/-	4.0750e-07

TABLE A3-3

IR Scan Run Numbers and Telemetry

IMAGER
S/N = SN03

Final T/V
MISSION = Mission Nominal
PATCH = Patch Low

Acceptance Valid Data

RUN NO.	DATE:TIME	ELEC SIDE	ECT (K)	BASEPLATE (C)	NARROW PATCH (K)	SPACE TARGET (K)	COOLER RADIATOR (K)	COOLER HOUSING (K)	AFT OPTICS (C)	PATCH CONTROL (V)
650	25-MAR-1993 : 19:58:07.00	1	320.283	19.894	94.248	81.850	152.465	235.745	22.600	14.658
652	25-MAR-1993 : 22:24:22.00	1	308.853	20.026	94.248	82.050	152.095	236.280	22.800	14.512
653	26-MAR-1993 : 01:13:07.00	1	297.033	19.999	94.248	81.900	152.465	236.816	22.900	14.344
654	26-MAR-1993 : 04:58:07.00	1	282.450	19.929	94.248	81.950	152.465	237.004	22.700	14.188
655	26-MAR-1993 : 09:33:45.00	1	264.621	19.814	94.248	81.800	152.260	237.085	22.700	14.459
656	26-MAR-1993 : 13:01:52.00	1	242.491	19.734	94.248	81.500	152.465	236.816	22.600	14.323
657	26-MAR-1993 : 18:45:00.00	1	202.630	19.625	94.248	81.500	152.260	236.548	22.500	14.616
658	26-MAR-1993 : 19:58:07.00	2	203.013	19.486	94.236	81.600	152.465	236.521	22.500	14.512
659	27-MAR-1993 : 00:00:00.00	2	243.521	19.487	94.248	82.000	152.260	236.521	22.600	14.699
660	27-MAR-1993 : 03:00:00.00	2	265.889	19.508	94.236	82.000	152.301	236.468	22.600	14.334
661	27-MAR-1993 : 05:26:15.00	2	282.296	19.624	94.218	82.300	152.589	236.441	22.600	14.626
662	27-MAR-1993 : 09:11:15.00	2	296.341	19.734	94.236	82.000	152.465	236.763	22.800	14.365
663	27-MAR-1993 : 13:41:15.00	2	308.670	19.890	94.213	82.250	152.465	236.655	22.900	14.574
664	27-MAR-1993 : 18:33:45.00	2	320.079	19.732	94.206	81.800	152.383	236.897	22.900	14.679
665	27-MAR-1993 : 18:45:00.00	2	320.061	19.742	94.248	82.000	152.342	236.870	22.900	14.574

APPENDIX A4. IMAGER IR SCAN REPORT

GOES SN03 IMAGER

MISSION TEMPERATURE — NOMINAL

PATCH TEMPERATURE — MID

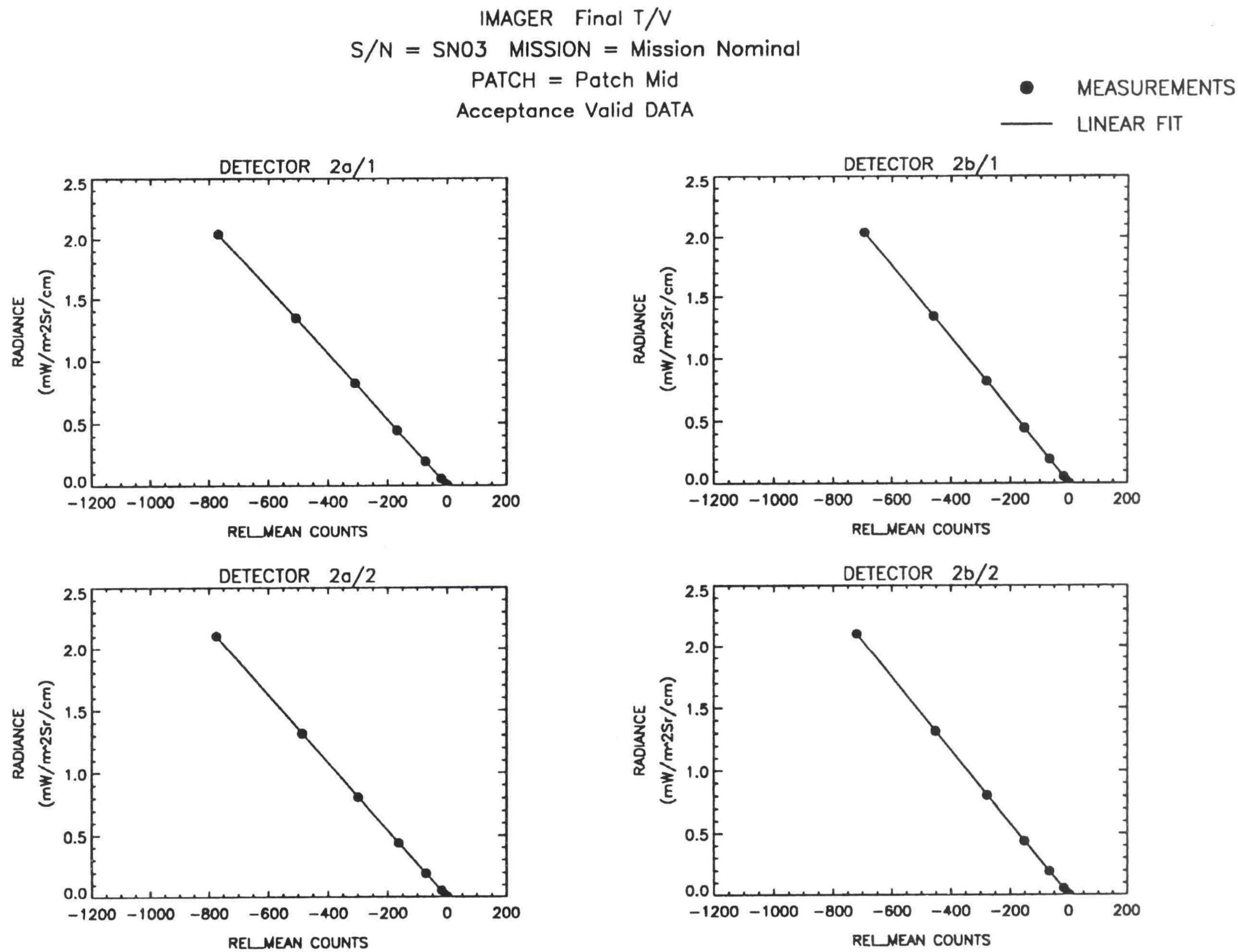

Figure A4-1. Radiance versus relative mean counts, channel 2.

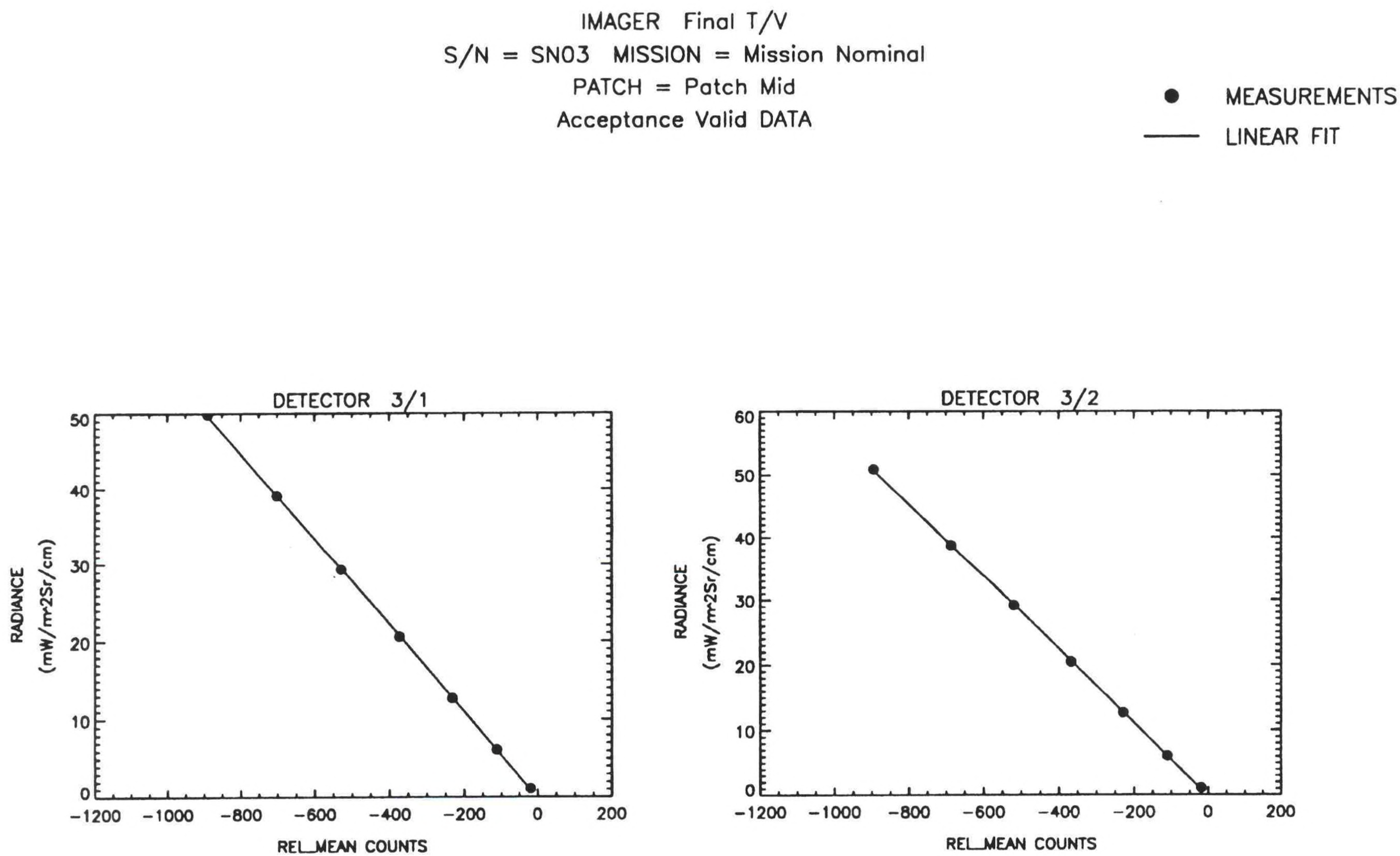

Figure A4-2. Radiance versus relative mean counts, channel 3.

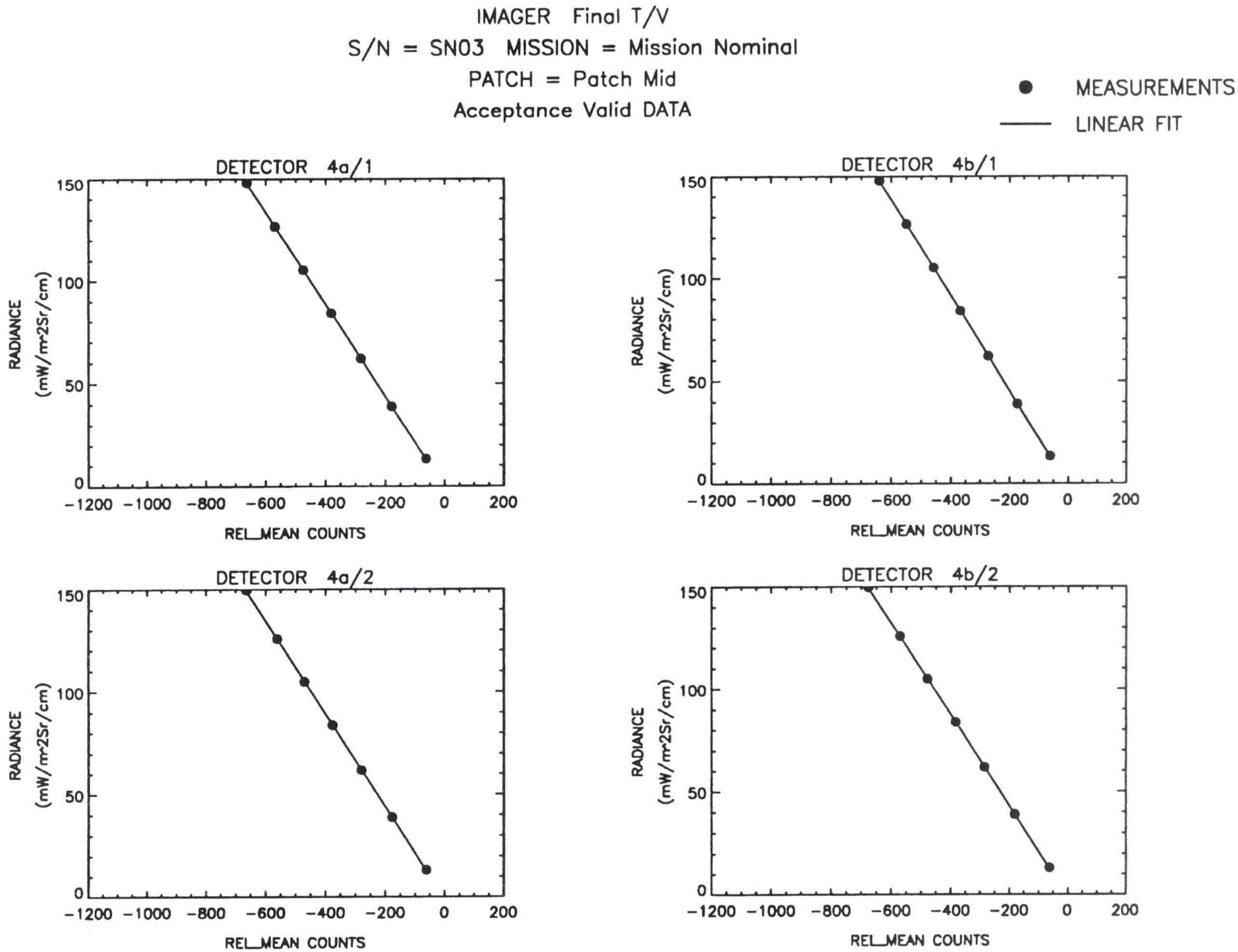

Figure A4-3. Radiance versus relative mean counts, channel 4.

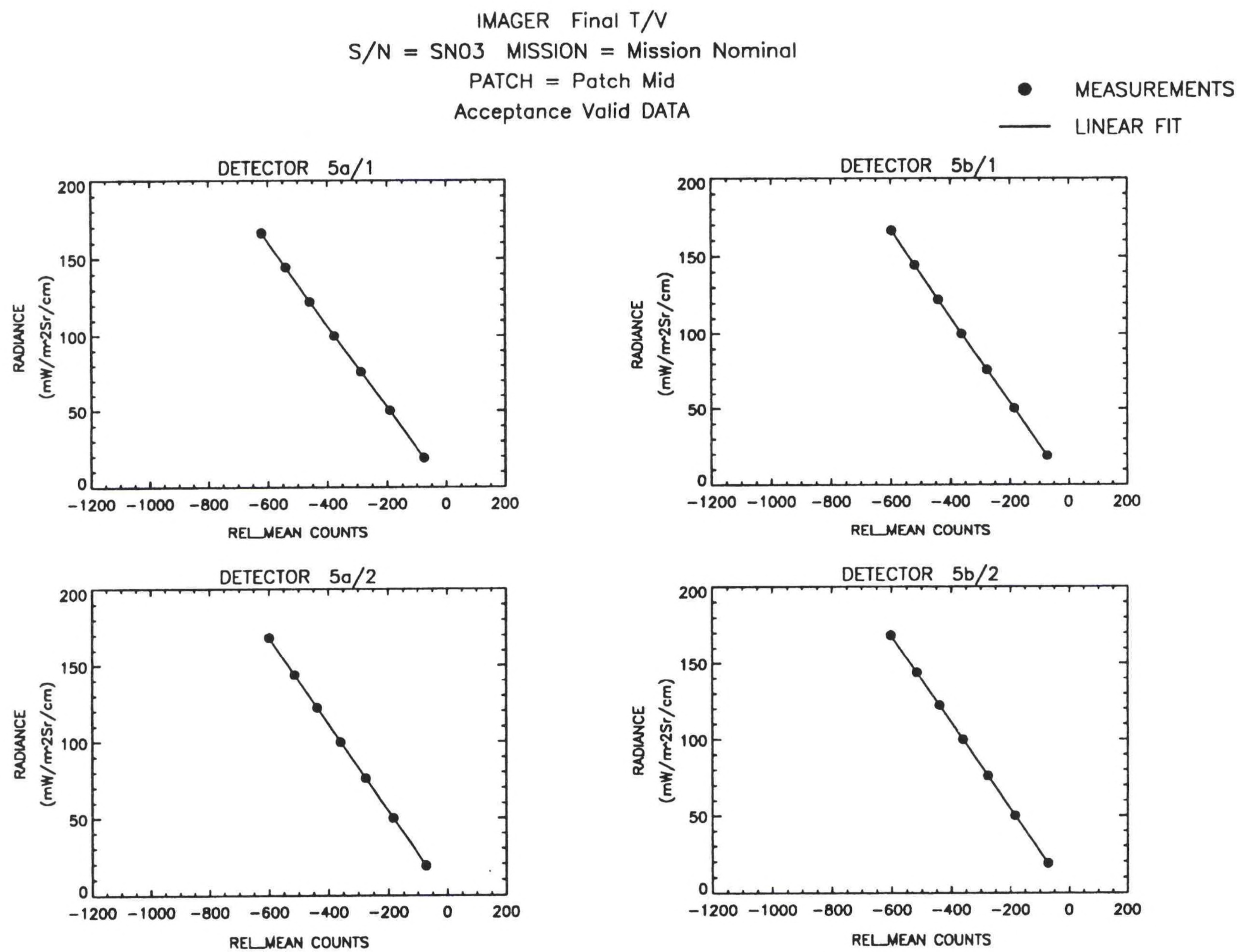

Figure A4-4. Radiance versus relative mean counts, channel 5.

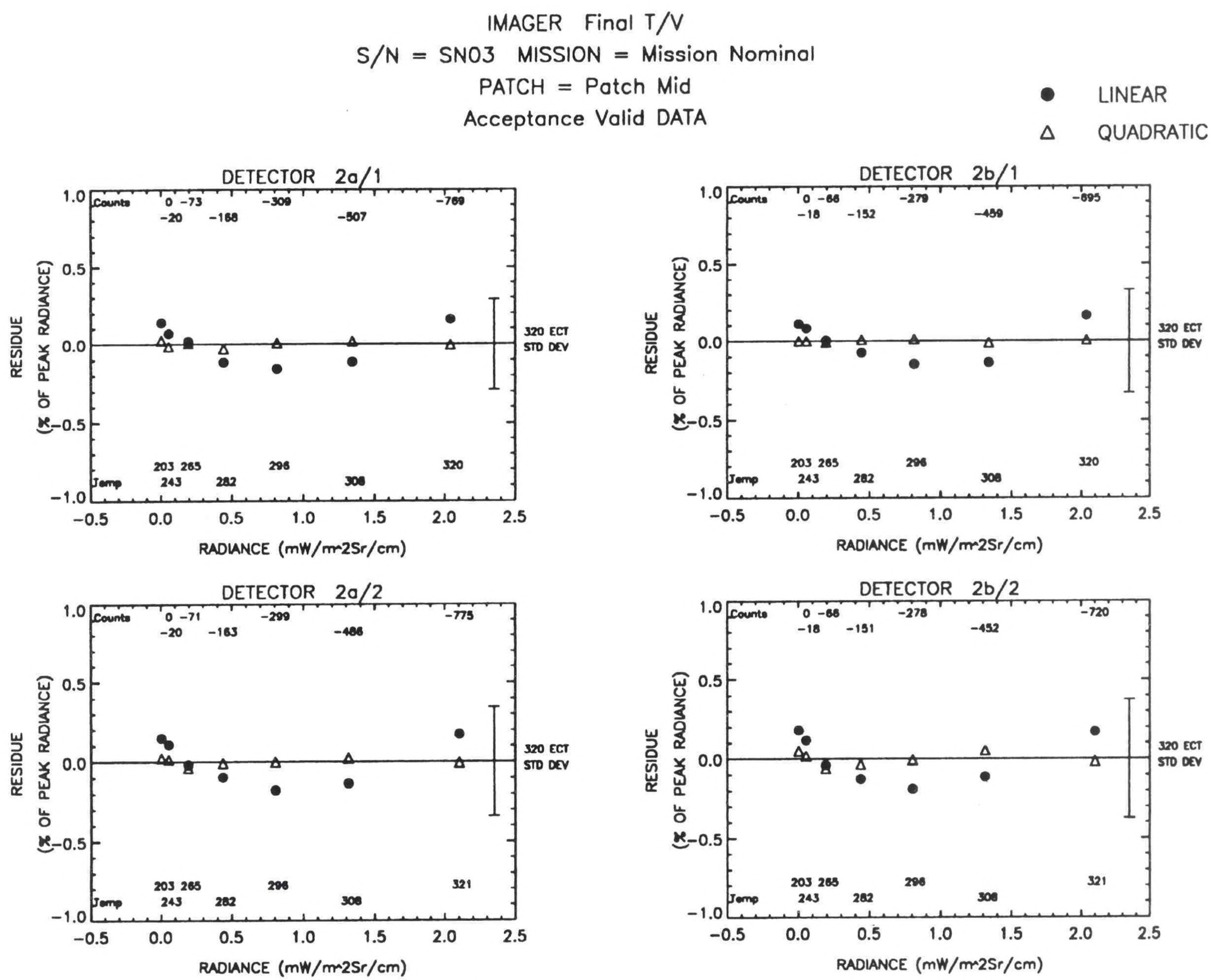

Figure A4-5. Residues of linear and quadratic fits versus radiance, channel 2.

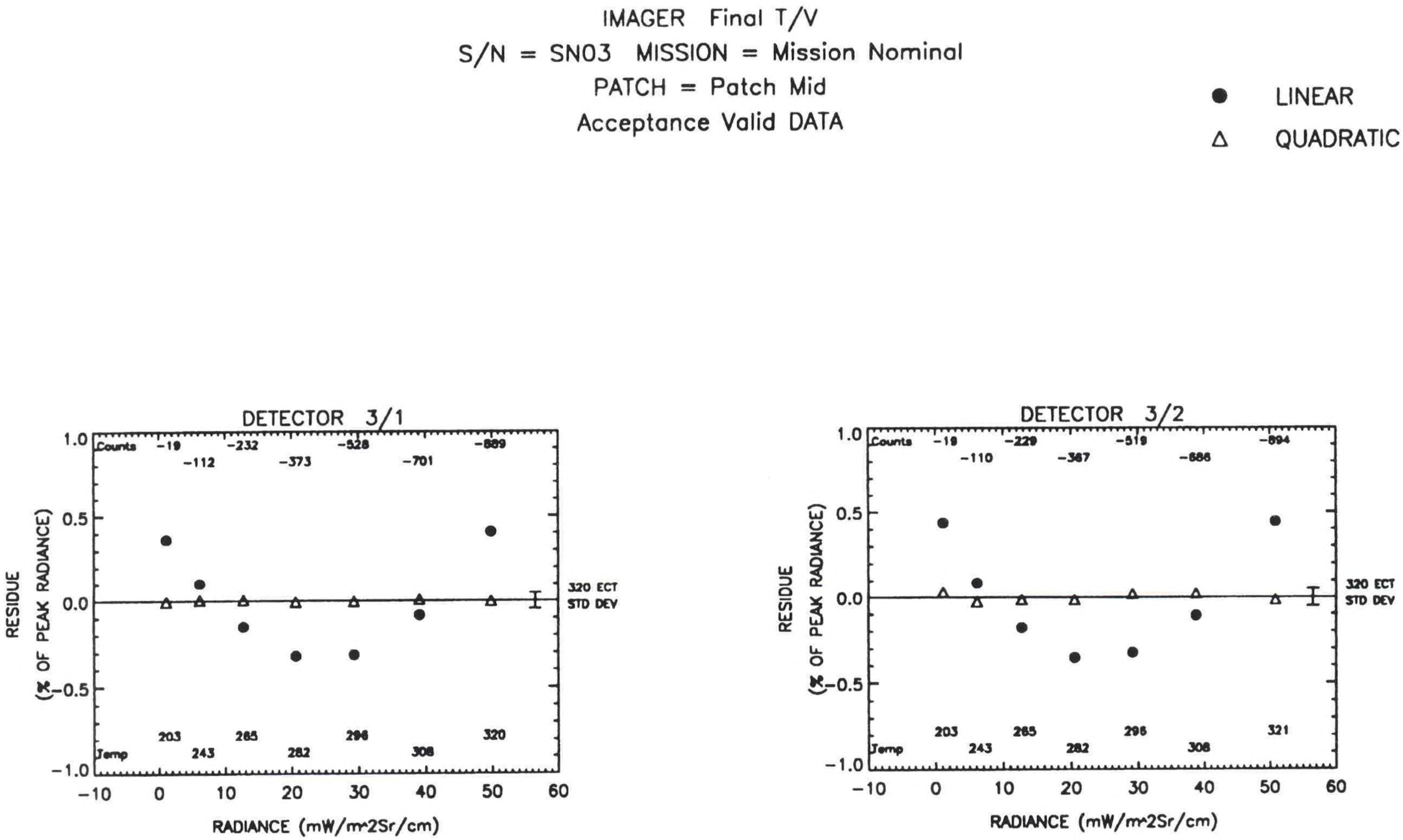

Figure A4-6. Residues of linear and quadratic fits versus radiance, channel 3.

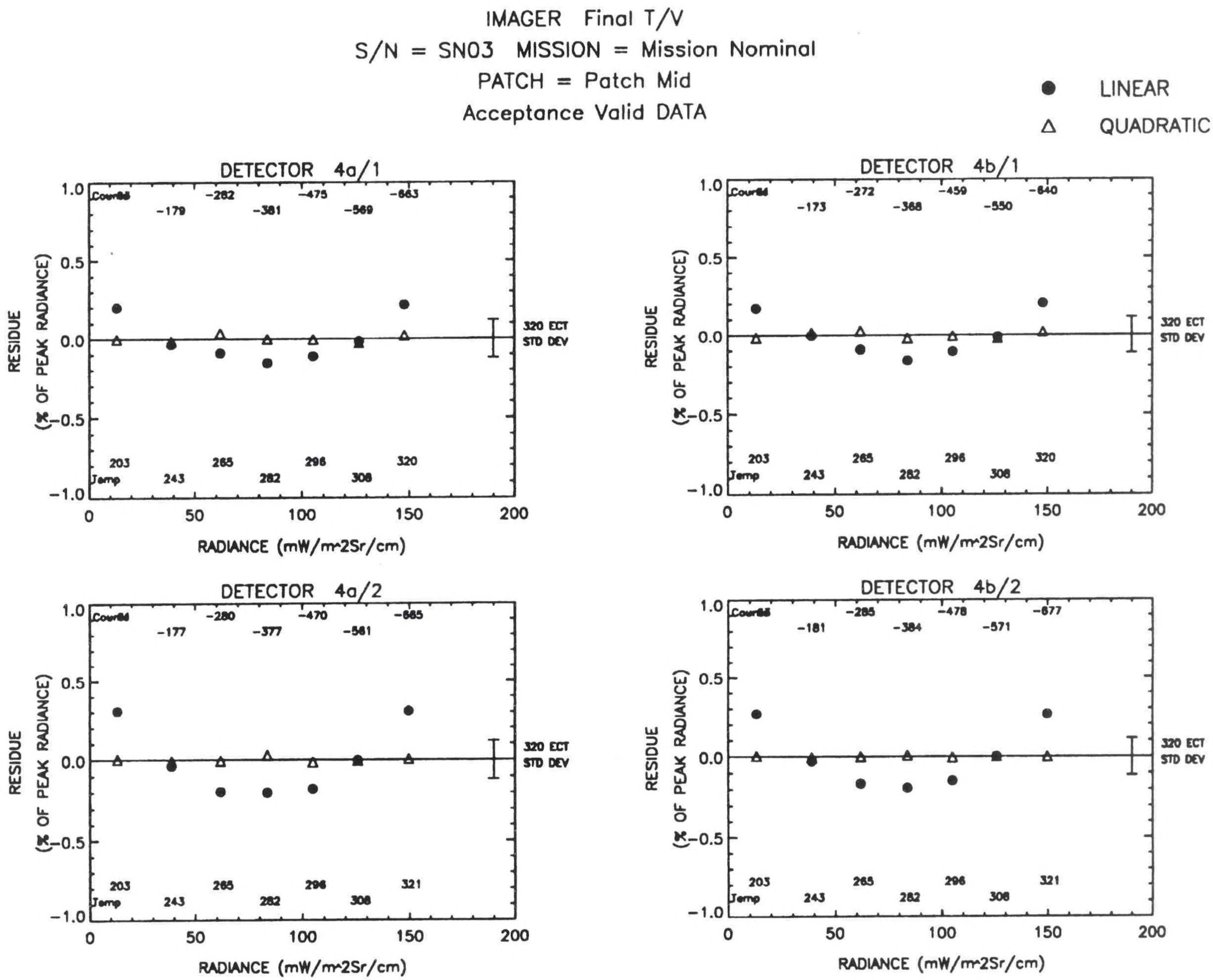

Figure A4-7. Residues of linear and quadratic fits versus radiance, channel 4.

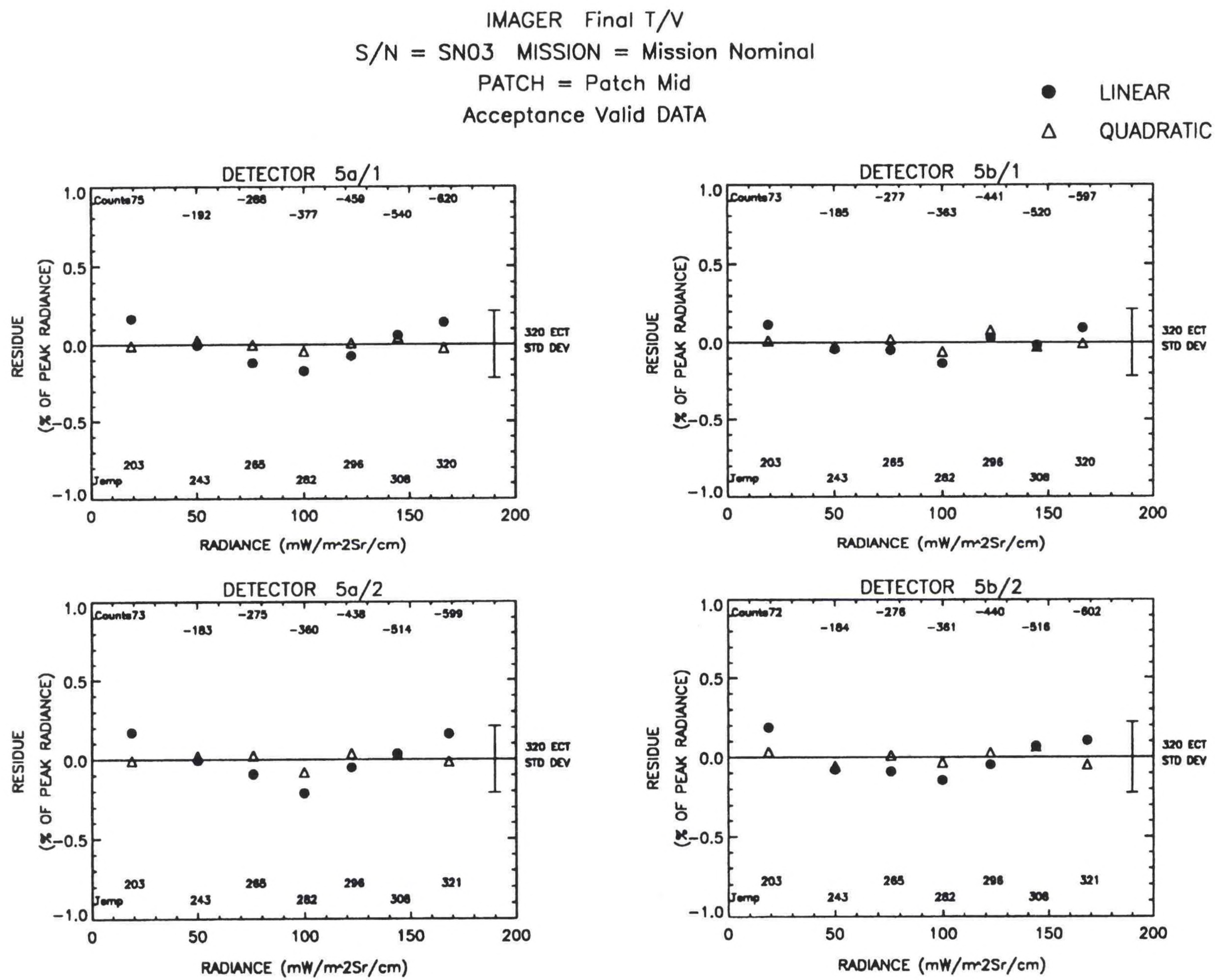

Figure A4-8. Residues of linear and quadratic fits versus radiance, channel 5.

TABLE A4-1

Noise and Residue Statistics

IMAGER
S/N = SN03

Final T/V
MISSION = Mission Nominal
PATCH = Patch Mid

Acceptance Valid Data

CH/SIDE	NEDT(K) MEAS/TEMP	NEDT(K) SPEC/TSPEC	PEAK LIN RES %	SPEC %	RMS LIN RES %	PEAK LIN RES N (mW/m^2Sr/cm)	PEAK QUAD RES %	RMS QUAD RES %	PEAK QUAD RES N (mW/m^2Sr/cm)
2a/1	0.1812/296.4	1.40/300.0	0.1589	1.7	0.1196	0.0032	0.0249	0.0175	0.0005
2b/1	0.1963/296.4	1.40/300.0	0.1622	1.7	0.1136	0.0033	0.0091	0.0075	0.0002
3/1	0.0973/243.4	1.00/230.0	0.4065	1.7	0.2777	0.2021	0.0073	0.0054	0.0036
4a/1	0.1207/296.4	0.35/300.0	0.2152	1.7	0.1376	0.3176	0.0366	0.0204	0.0540
4b/1	0.1247/296.4	0.35/300.0	0.2018	1.7	0.1288	0.2979	0.0280	0.0193	0.0413
5a/1	0.2104/296.4	0.50/300.0	0.1715	1.7	0.1197	0.2847	0.0437	0.0272	0.0726
5b/1	0.2185/296.4	0.50/300.0	0.1344	1.7	0.0808	0.2232	0.0803	0.0408	0.1334
2a/2	0.1856/296.3	1.40/300.0	0.1771	1.7	0.1324	0.0036	0.0221	0.0194	0.0004
2b/2	0.2171/296.3	1.40/300.0	0.1890	1.7	0.1421	0.0038	0.0511	0.0383	0.0010
3/2	0.1088/243.3	1.00/230.0	0.4430	1.7	0.3091	0.2200	0.0312	0.0221	0.0155
4a/2	0.0989/296.3	0.35/300.0	0.3072	1.7	0.2064	0.4530	0.0278	0.0131	0.0410
4b/2	0.1004/296.3	0.35/300.0	0.2670	1.7	0.1798	0.3938	0.0079	0.0043	0.0117
5a/2	0.1885/296.3	0.50/300.0	0.2127	1.7	0.1268	0.3532	0.0361	0.0378	0.0599
5b/2	0.2280/296.3	0.50/300.0	0.1874	1.7	0.1127	0.3112	0.0639	0.0421	0.1060

TABLE A4-2

Linear and Quadratic Fit Coefficients

IMAGER
S/N = SN03

Final T/V
MISSION = Mission Nominal
PATCH = Patch Mid

Acceptance Valid Data

RAD = GAMM1 + M1 * C

CH/SIDE	GAMMA1			M1		
2a/1	-1.6170e-03	+/-	1.5365e-03	-2.6512e-03	+/-	4.1065e-06
2b/1	-2.0629e-03	+/-	1.4581e-03	-2.9286e-03	+/-	4.3101e-06
3/1	-1.8950e-01	+/-	1.0579e-01	-5.6015e-02	+/-	2.1037e-04
4a/1	-1.2920e+00	+/-	1.9381e-01	-2.2445e-01	+/-	4.5840e-04
4b/1	-1.3550e+00	+/-	1.8141e-01	-2.3234e-01	+/-	4.4401e-04
5a/1	-1.7950e+00	+/-	2.0160e-01	-2.7039e-01	+/-	4.9595e-04
5b/1	-1.9726e+00	+/-	1.3633e-01	-2.8149e-01	+/-	3.4840e-04
2a/2	-2.0843e-03	+/-	1.6770e-03	-2.7123e-03	+/-	4.5292e-06
2b/2	-2.0816e-03	+/-	1.7975e-03	-2.9124e-03	+/-	5.2216e-06
3/2	-2.2180e-01	+/-	1.1701e-01	-5.6821e-02	+/-	2.3451e-04
4a/2	-1.3479e+00	+/-	2.8898e-01	-2.2636e-01	+/-	6.8786e-04
4b/2	-1.3942e+00	+/-	2.5208e-01	-2.2255e-01	+/-	5.8933e-04
5a/2	-2.0812e+00	+/-	2.1313e-01	-2.8382e-01	+/-	5.4758e-04
5b/2	-1.9032e+00	+/-	1.8910e-01	-2.8211e-01	+/-	4.8362e-04

RAD = GAMMA2 + M2 * C + R * C^2

CH/SIDE	GAMMA2			M2			R		
2a/1	7.2643e-04	+/-	3.0543e-04	-2.6199e-03	+/-	2.4151e-06	4.2476e-08	+/-	3.1427e-09
2b/1	1.8715e-04	+/-	1.3025e-04	-2.8953e-03	+/-	1.1394e-06	4.9788e-08	+/-	1.6396e-09
3/1	2.6294e-02	+/-	3.1079e-03	-5.4308e-02	+/-	1.7187e-05	1.9028e-06	+/-	1.8471e-08
4a/1	-7.5286e-01	+/-	5.1526e-02	-2.2024e-01	+/-	3.2366e-04	5.7716e-06	+/-	4.3179e-07

TABLE A4-2 (Continued)

Linear and Quadratic Fit Coefficients

4b/1	-8.4909e-01	+/-	4.8836e-02	-2.2826e-01	+/-	3.1735e-04	5.7905e-06	+/-	4.3796e-07
5a/1	-1.1906e+00	+/-	8.7290e-02	-2.6569e-01	+/-	5.6331e-04	6.7158e-06	+/-	7.8479e-07
5b/1	-1.6077e+00	+/-	1.3165e-01	-2.7855e-01	+/-	8.8097e-04	4.3515e-06	+/-	1.2733e-06
2a/2	4.8600e-04	+/-	3.3391e-04	-2.6783e-03	+/-	2.6234e-06	4.5642e-08	+/-	3.3774e-09
2b/2	5.9735e-04	+/-	6.5787e-04	-2.8743e-03	+/-	5.5569e-06	5.5067e-08	+/-	7.6950e-09
3/2	1.5018e-02	+/-	1.2646e-02	-5.4961e-02	+/-	6.9349e-05	2.0680e-06	+/-	7.4210e-08
4a/2	-5.4755e-01	+/-	3.2603e-02	-2.2010e-01	+/-	2.0429e-04	8.5995e-06	+/-	2.7278e-07
4b/2	-6.9246e-01	+/-	1.0744e-02	-2.1717e-01	+/-	6.6075e-05	7.2540e-06	+/-	8.6596e-08
5a/2	-1.4568e+00	+/-	1.2069e-01	-2.7880e-01	+/-	8.0580e-04	7.4566e-06	+/-	1.1650e-06
5b/2	-1.3672e+00	+/-	1.3370e-01	-2.7781e-01	+/-	8.8831e-04	6.3497e-06	+/-	1.2783e-06

TABLE A4-3

IR Scan Run Numbers and Telemetry

IMAGER
S/N = SN03

Final T/V
MISSION = Mission Nominal
PATCH = Patch Mid

Acceptance Valid Data

RUN NO.	DATE:TIME	ELEC SIDE	ECT (K)	BASEPLATE (C)	NARROW PATCH (K)	SPACE TARGET (K)	COOLER RADIATOR (K)	COOLER HOUSING (K)	AFT OPTICS (C)	PATCH CONTROL (V)
670	28-MAR-1993 : 02:37:30.00	1	320.117	19.181	101.065	81.850	152.465	237.192	22.200	21.099
671	28-MAR-1993 : 05:43:07.00	1	308.818	19.048	101.065	81.850	152.260	237.299	22.200	21.099
672	28-MAR-1993 : 07:52:30.00	1	296.410	19.066	101.059	82.050	152.383	237.219	22.200	21.141
673	28-MAR-1993 : 10:35:37.00	1	282.515	19.371	101.046	81.850	152.260	237.085	22.300	21.412
674	28-MAR-1993 : 14:03:45.00	1	265.610	19.079	101.059	81.900	152.260	237.085	23.100	21.193
675	28-MAR-1993 : 16:01:52.00	1	243.445	18.638	101.065	81.800	152.260	237.085	22.200	21.569
676	28-MAR-1993 : 21:00:00.00	1	203.503	18.142	101.071	81.650	152.260	236.816	20.900	20.984
677	28-MAR-1993 : 21:50:37.00	2	203.424	18.054	101.016	81.900	152.465	236.843	20.900	21.506
678	29-MAR-1993 : 01:18:45.00	2	243.338	17.994	101.016	81.850	152.301	236.843	20.900	21.381
679	29-MAR-1993 : 03:45:00.00	2	265.607	17.853	101.016	82.200	152.465	236.843	20.900	21.151
680	29-MAR-1993 : 09:28:07.00	2	282.406	20.341	101.016	81.950	152.424	236.870	22.700	21.141
681	29-MAR-1993 : 14:03:45.00	2	296.281	20.262	101.016	81.750	152.465	237.299	23.300	21.350
682	29-MAR-1993 : 16:18:45.00	2	308.487	20.212	101.016	82.050	152.465	237.165	23.200	21.297
683	29-MAR-1993 : 19:07:30.00	2	321.141	20.260	101.016	81.900	152.465	237.326	23.200	20.995

APPENDIX A5. IMAGER IR SCAN REPORT

GOES SN03 IMAGER

MISSION TEMPERATURE – NOMINAL

PATCH TEMPERATURE – HIGH

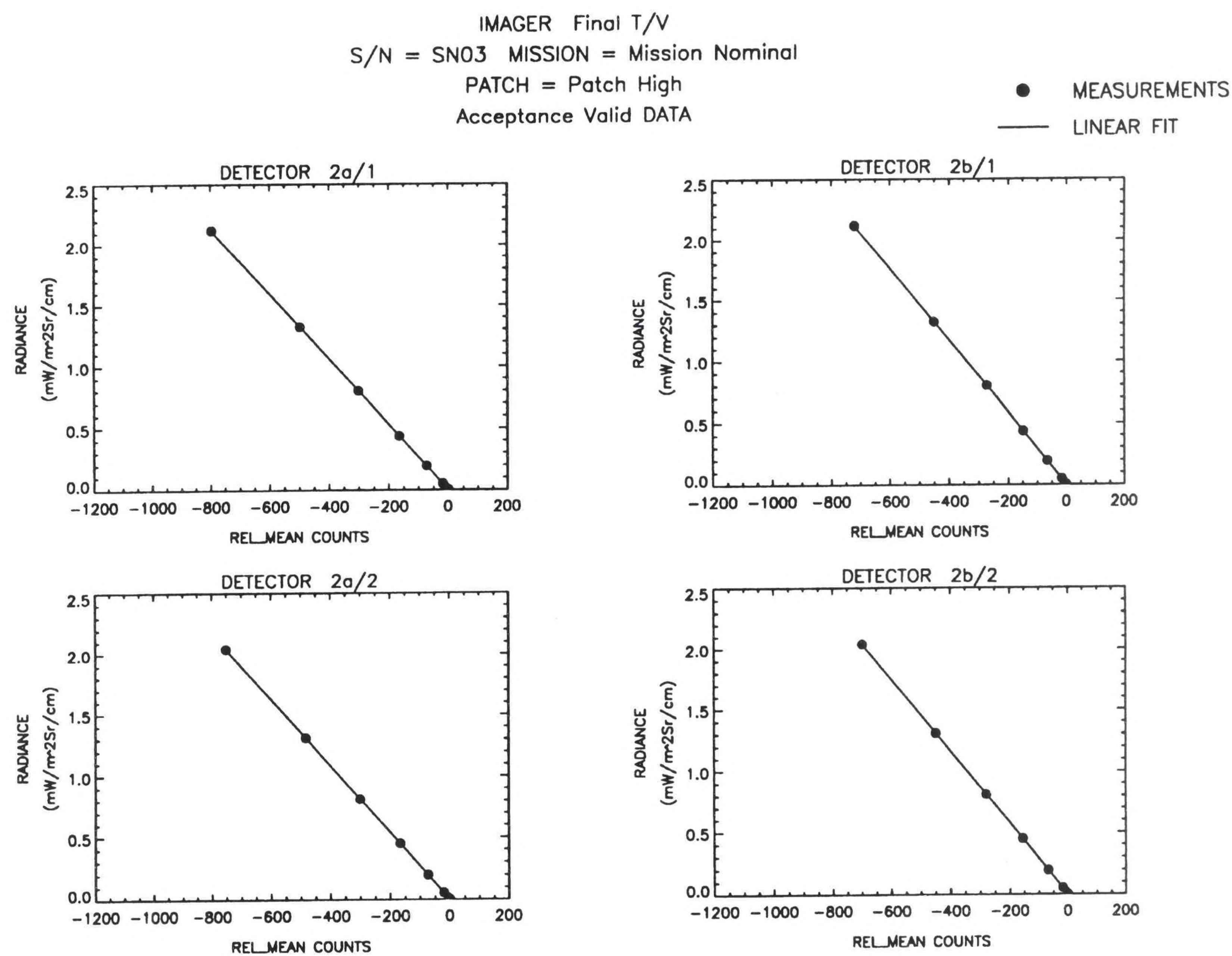

Figure A5-1. Radiance versus relative mean counts, channel 2.

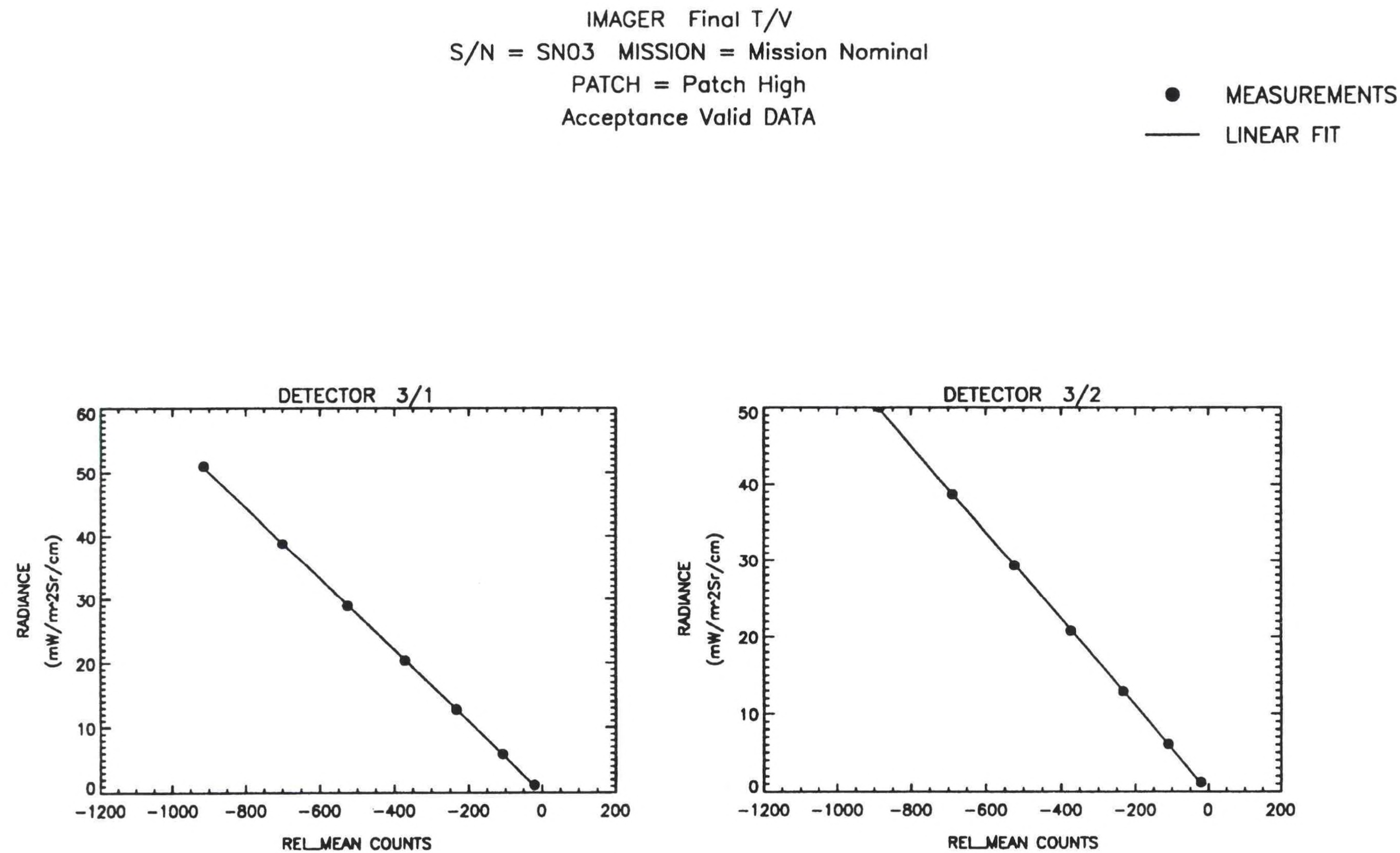

Figure A5-2. Radiance versus relative mean counts, channel 3.

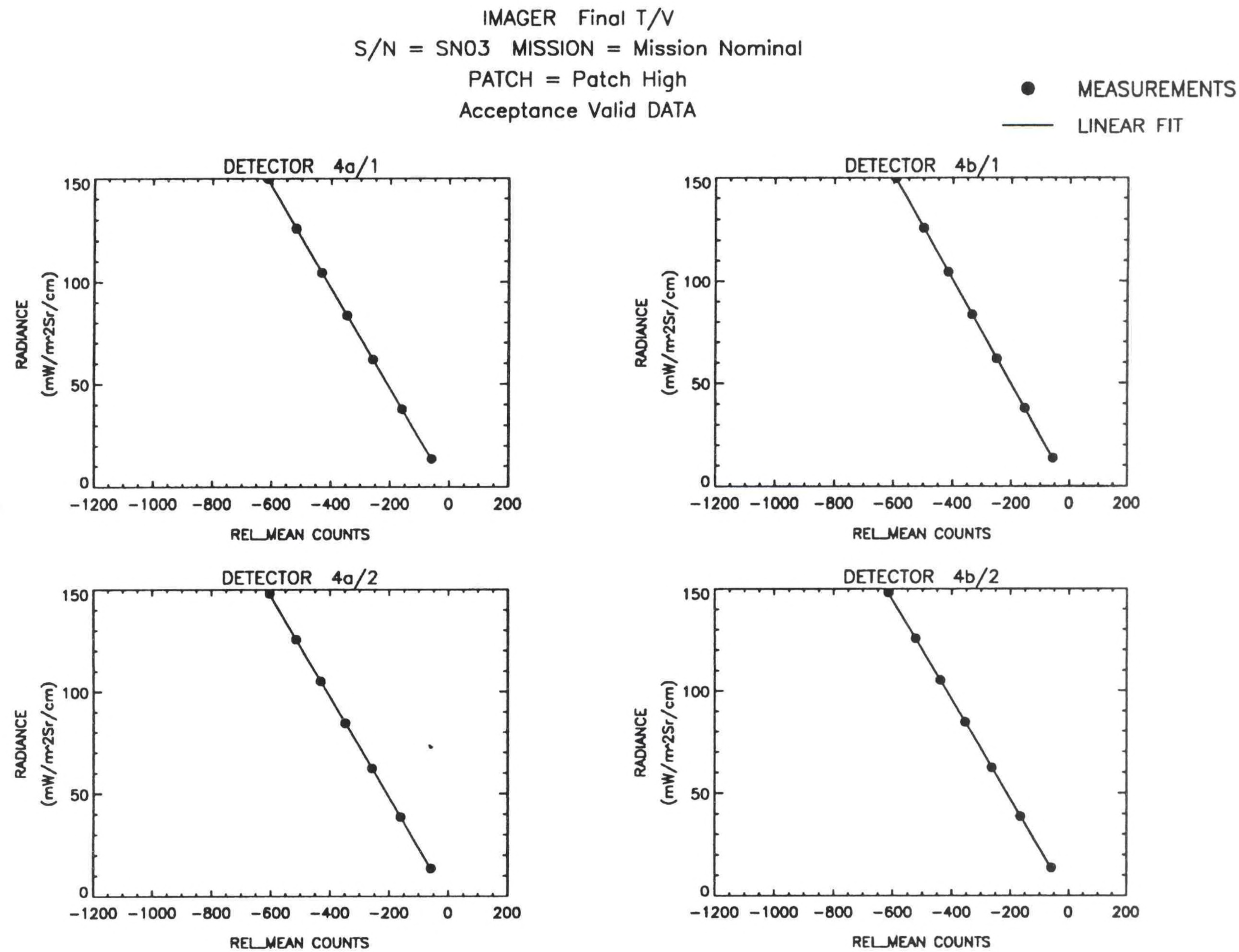

Figure A5-3. Radiance versus relative mean counts, channel 4.

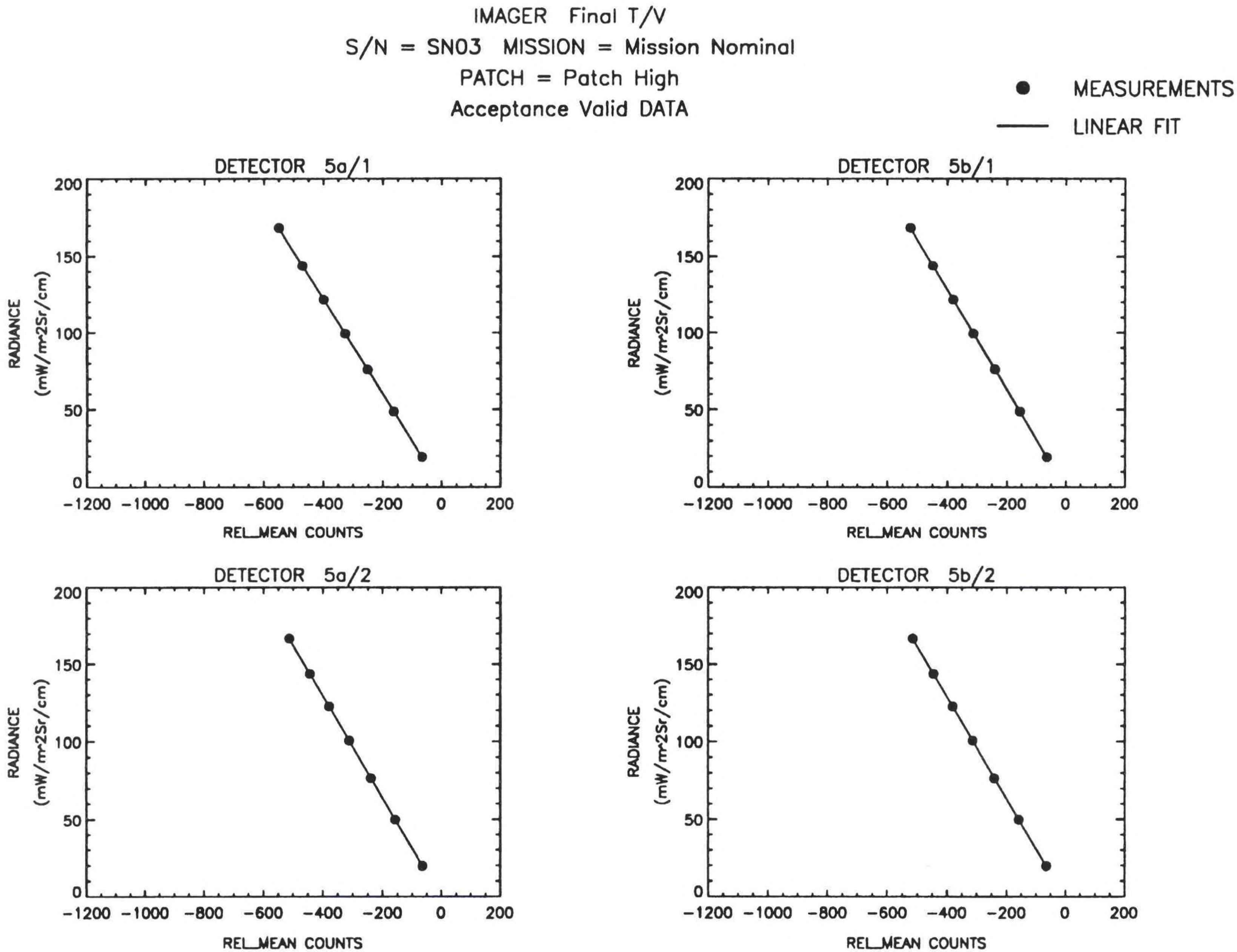

Figure A5-4. Radiance versus relative mean counts, channel 5.

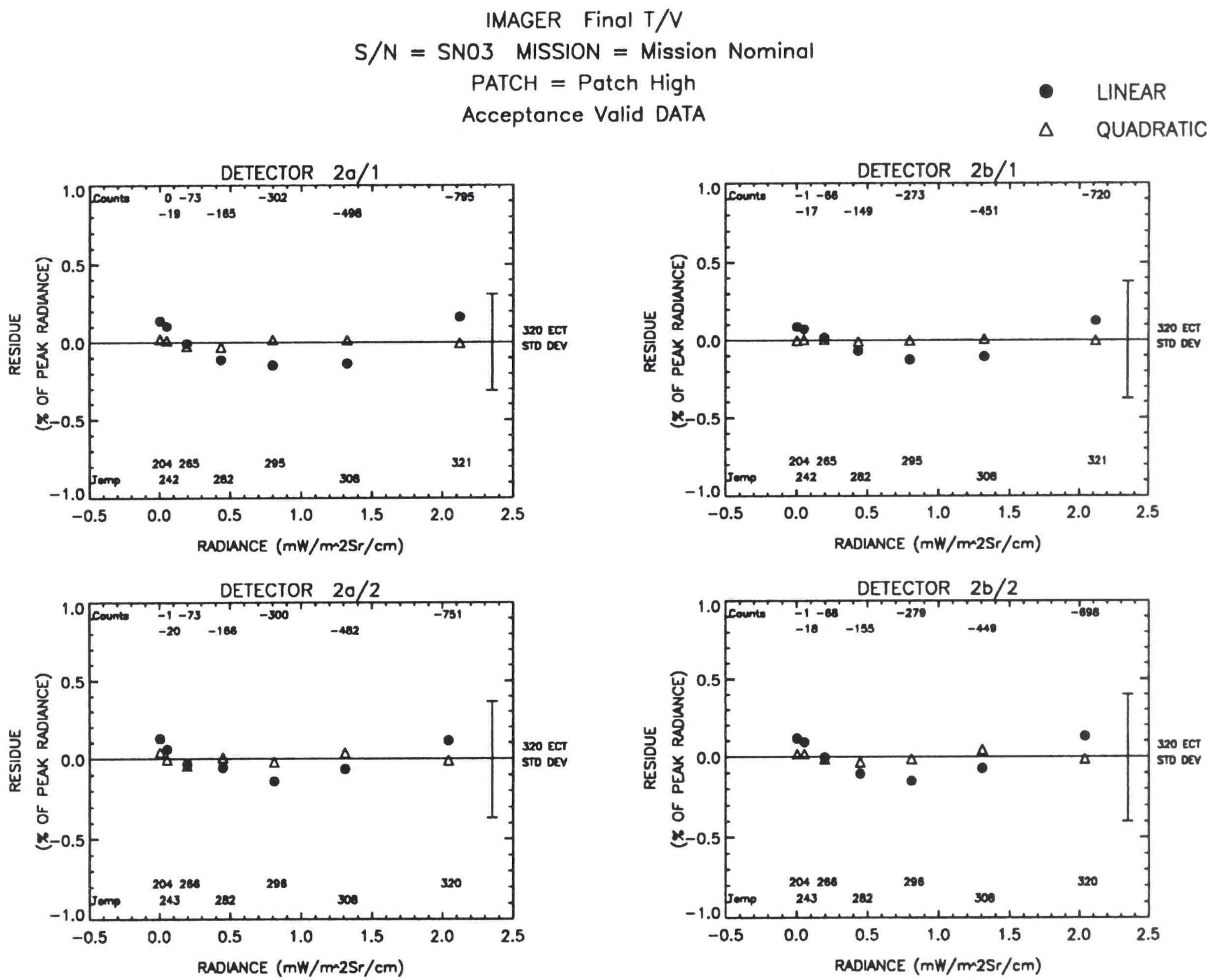

Figure A5-5. Residues of linear and quadratic fits versus radiance, channel 2.

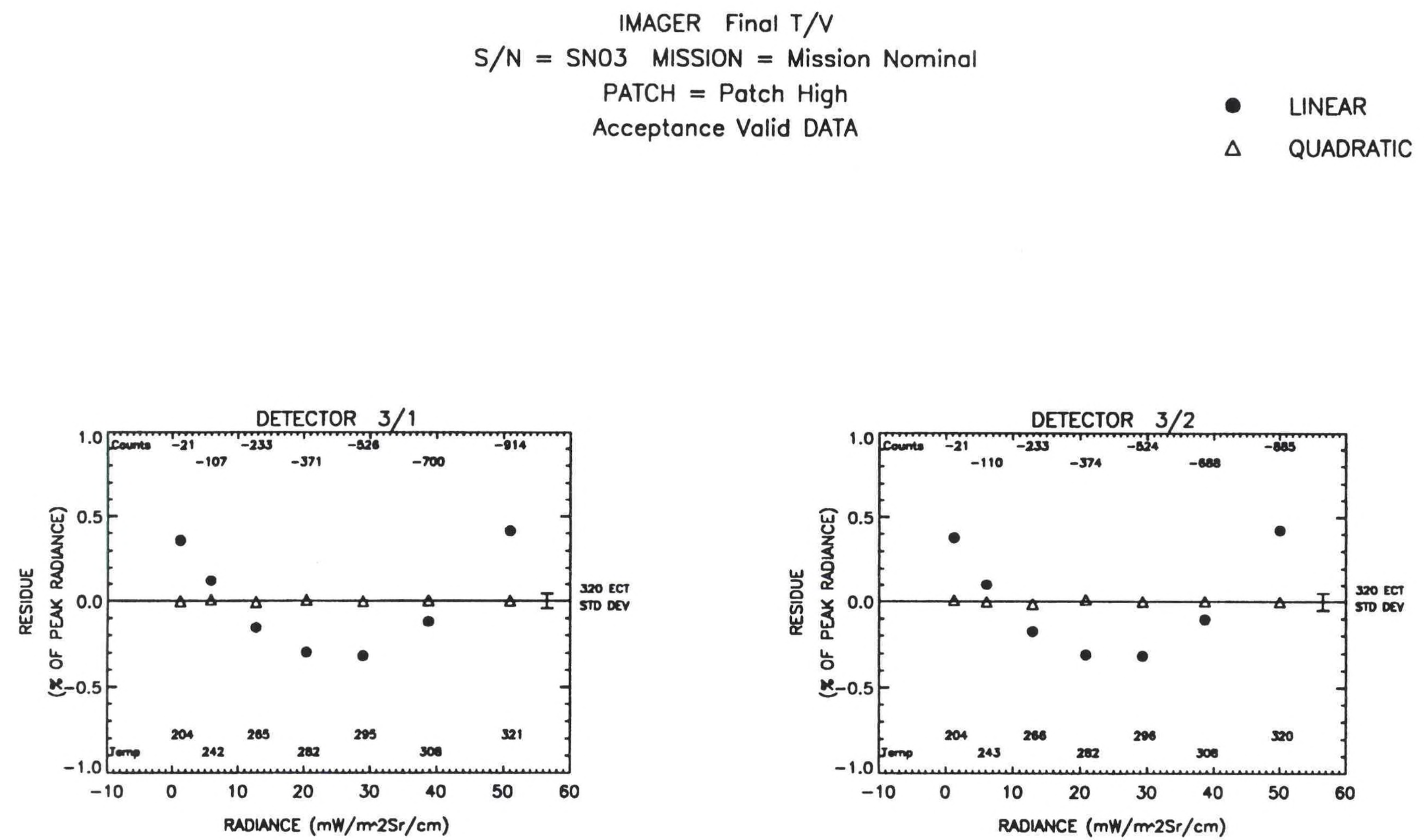

Figure A5-6. Residues of linear and quadratic fits versus radiance, channel 3.

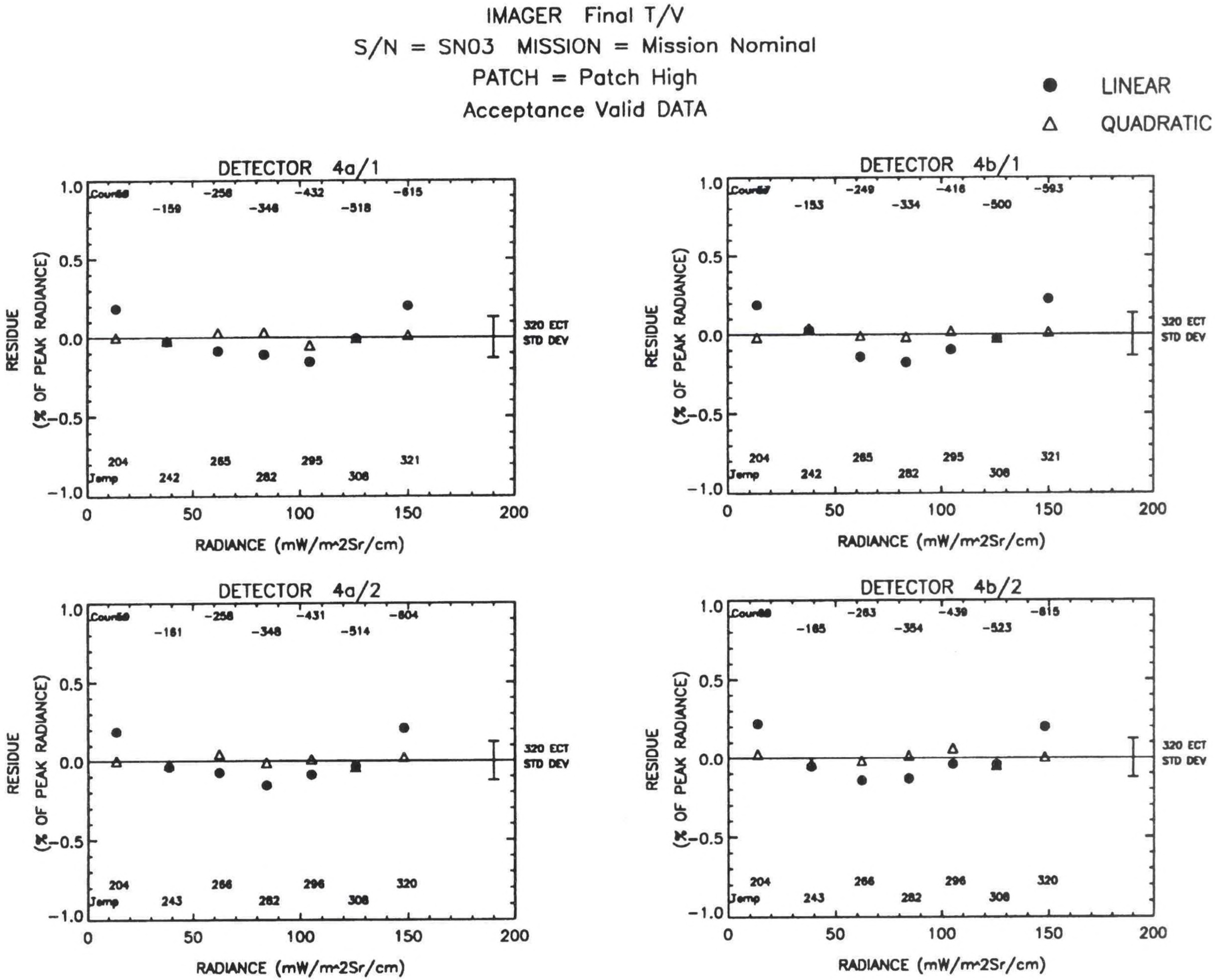

Figure A5-7. Residues of linear and quadratic fits versus radiance, channel 4.

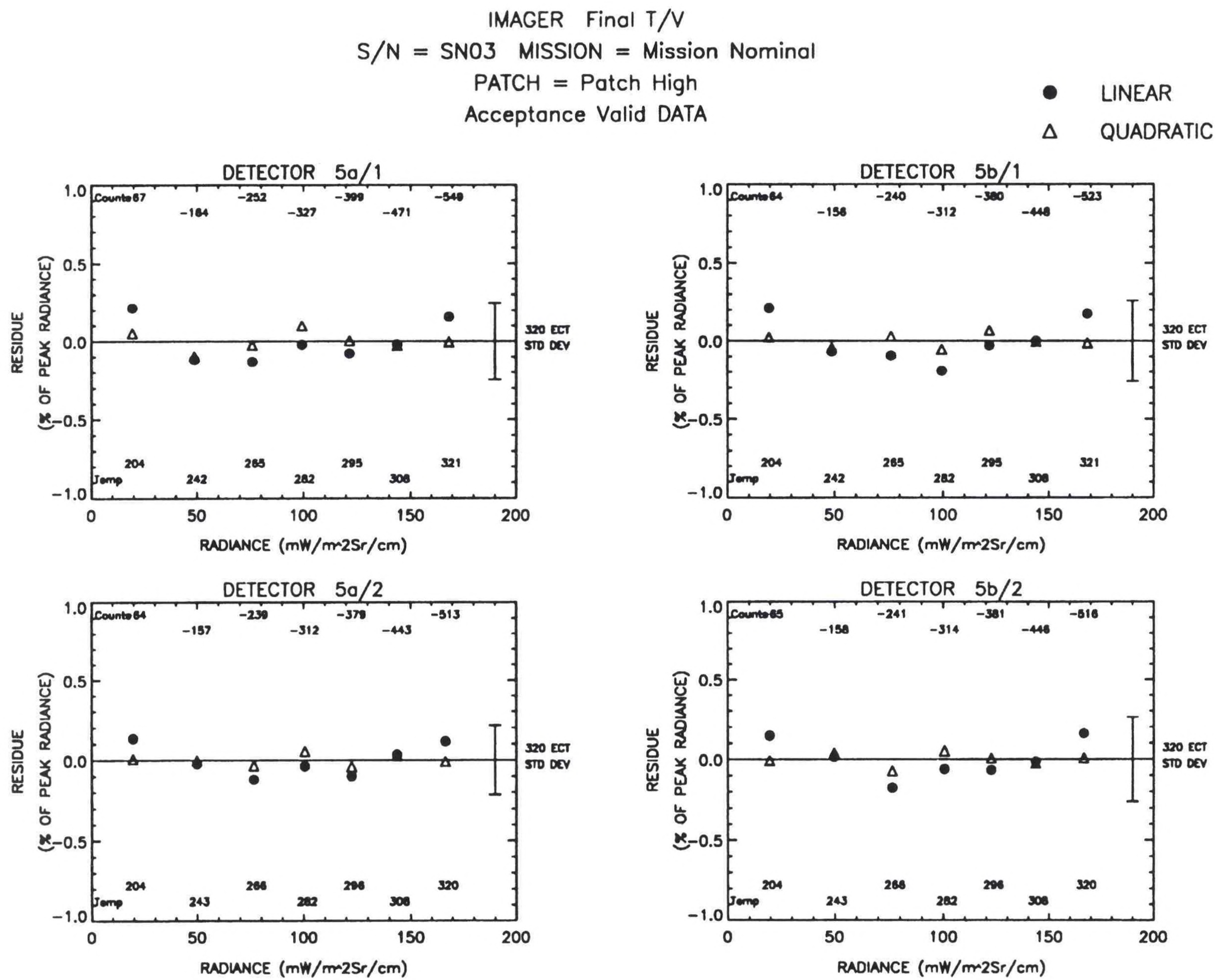

Figure A5-8. Residues of linear and quadratic fits versus radiance, channel 5.

TABLE A5-1

Noise and Residue Statistics

IMAGER
S/N = SN03

Final T/V
MISSION = Mission Nominal
PATCH = Patch High

Acceptance Valid Data

CH/SIDE	NEDT(K) MEAS/TEMP	NEDT(K) SPEC/TSPEC	PEAK LIN RES %	SPEC %	RMS LIN RES %	PEAK LIN RES N (mW/m^2Sr/cm)	PEAK QUAD RES %	RMS QUAD RES %	PEAK QUAD RES N (mW/m^2Sr/cm)
2a/1	0.2016/295.9	1.40/300.0	0.1628	1.7	0.1249	0.0033	0.0202	0.0192	0.0004
2b/1	0.2418/295.9	1.40/300.0	0.1252	1.7	0.0927	0.0025	0.0066	0.0049	0.0001
3/1	0.1130/242.1	1.00/230.0	0.4139	1.7	0.2785	0.2058	0.0059	0.0045	0.0029
4a/1	0.1153/295.9	0.35/300.0	0.2029	1.7	0.1310	0.2995	0.0331	0.0272	0.0489
4b/1	0.1190/295.9	0.35/300.0	0.2256	1.7	0.1463	0.3330	0.0399	0.0225	0.0588
5a/1	0.2369/295.9	0.50/300.0	0.2147	1.7	0.1252	0.3565	0.0989	0.0581	0.1642
5b/1	0.2254/295.9	0.50/300.0	0.2113	1.7	0.1350	0.3510	0.0665	0.0393	0.1105
2a/2	0.1970/296.5	1.40/300.0	0.1407	1.7	0.0927	0.0028	0.0400	0.0280	0.0008
2b/2	0.2306/296.5	1.40/300.0	0.1518	1.7	0.1051	0.0031	0.0437	0.0243	0.0009
3/2	0.0987/243.1	1.00/230.0	0.4218	1.7	0.2843	0.2095	0.0111	0.0073	0.0055
4a/2	0.1134/296.5	0.35/300.0	0.2084	1.7	0.1305	0.3072	0.0441	0.0264	0.0650
4b/2	0.1136/296.5	0.35/300.0	0.2188	1.7	0.1376	0.3227	0.0614	0.0355	0.0905
5a/2	0.2200/296.5	0.50/300.0	0.1332	1.7	0.0913	0.2212	0.0555	0.0308	0.0922
5b/2	0.2525/296.5	0.50/300.0	0.1766	1.7	0.1110	0.2932	0.0528	0.0385	0.0876

TABLE A5-2

Linear and Quadratic Fit Coefficients

IMAGER
S/N = SN03

Final T/V
MISSION = Mission Nominal
PATCH = Patch High

Acceptance Valid Data

RAD = GAMM1 + M1 * C

CH/SIDE	GAMMA1			M1		
2a/1	-2.2626e-03	+/-	1.5884e-03	-2.6646e-03	+/-	4.1899e-06
2b/1	-2.4546e-03	+/-	1.1774e-03	-2.9383e-03	+/-	3.4300e-06
3/1	-1.9986e-01	+/-	1.0513e-01	-5.5691e-02	+/-	2.0673e-04
4a/1	-1.2691e+00	+/-	1.8309e-01	-2.4524e-01	+/-	4.7275e-04
4b/1	-1.3088e+00	+/-	2.0445e-01	-2.5431e-01	+/-	5.4738e-04
5a/1	-1.7308e+00	+/-	2.0926e-01	-3.0902e-01	+/-	5.8833e-04
5b/1	-1.7143e+00	+/-	2.2592e-01	-3.2461e-01	+/-	6.6684e-04
2a/2	-2.8348e-03	+/-	1.1845e-03	-2.7201e-03	+/-	3.2645e-06
2b/2	-2.4226e-03	+/-	1.3401e-03	-2.9182e-03	+/-	3.9700e-06
3/2	-2.0216e-01	+/-	1.0842e-01	-5.6435e-02	+/-	2.1735e-04
4a/2	-1.2568e+00	+/-	1.8412e-01	-2.4669e-01	+/-	4.7914e-04
4b/2	-1.2860e+00	+/-	1.9424e-01	-2.4248e-01	+/-	4.9640e-04
5a/2	-1.8427e+00	+/-	1.5452e-01	-3.2803e-01	+/-	4.6052e-04
5b/2	-1.8572e+00	+/-	1.8785e-01	-3.2613e-01	+/-	5.5655e-04

RAD = GAMMA2 + M2 * C + R * C^2

CH/SIDE	GAMMA2			M2			R		
2a/1	1.7037e-04	+/-	3.3191e-04	-2.6331e-03	+/-	2.5508e-06	4.1153e-08	+/-	3.1985e-09
2b/1	-6.2535e-04	+/-	8.4739e-05	-2.9122e-03	+/-	7.1918e-07	3.7613e-08	+/-	9.9512e-10
3/1	1.3272e-02	+/-	2.5543e-03	-5.4047e-02	+/-	1.3746e-05	1.7879e-06	+/-	1.4394e-08
4a/1	-7.6501e-01	+/-	6.8307e-02	-2.4099e-01	+/-	4.6364e-04	6.3022e-06	+/-	6.6869e-07

TABLE A5-2 (Continued)

Linear and Quadratic Fit Coefficients

4b/1	-7.4036e-01	+/-	5.6605e-02	-2.4935e-01	+/-	3.9847e-04	7.6450e-06	+/-	5.9606e-07
5a/1	-1.1597e+00	+/-	1.8504e-01	-3.0400e-01	+/-	1.3516e-03	8.1312e-06	+/-	2.1326e-06
5b/1	-1.0483e+00	+/-	1.2526e-01	-3.1845e-01	+/-	9.6111e-04	1.0465e-05	+/-	1.5929e-06
2a/2	-1.0782e-03	+/-	4.8795e-04	-2.6965e-03	+/-	3.9118e-06	3.2770e-08	+/-	5.1989e-09
2b/2	-4.0073e-04	+/-	4.2171e-04	-2.8889e-03	+/-	3.6350e-06	4.3705e-08	+/-	5.1950e-09
3/2	1.8000e-02	+/-	4.2145e-03	-5.4692e-02	+/-	2.3286e-05	1.9548e-06	+/-	2.5163e-08
4a/2	-7.4708e-01	+/-	6.7125e-02	-2.4234e-01	+/-	4.6253e-04	6.5636e-06	+/-	6.7794e-07
4b/2	-7.5592e-01	+/-	9.0307e-02	-2.3803e-01	+/-	6.1076e-04	6.5815e-06	+/-	8.7914e-07
5a/2	-1.3892e+00	+/-	9.9875e-02	-3.2379e-01	+/-	7.7811e-04	7.3231e-06	+/-	1.3105e-06
5b/2	-1.3081e+00	+/-	1.2481e-01	-3.2102e-01	+/-	9.6712e-04	8.7715e-06	+/-	1.6198e-06

TABLE A5-3

IR Scan Run Numbers and Telemetry

IMAGER
S/N = SN03

Final T/V
MISSION = Mission Nominal
PATCH = Patch High

Acceptance Valid Data

RUN NO.	DATE:TIME	ELEC SIDE	ECT (K)	BASEPLATE (C)	NARROW PATCH (K)	SPACE TARGET (K)	COOLER RADIATOR (K)	COOLER HOUSING (K)	AFT OPTICS (C)	PATCH CONTROL (V)
690	30-MAR-1993 : 06:39:22.00	1	321.187	19.274	103.992	81.900	152.260	237.353	21.800	23.886
691	30-MAR-1993 : 10:24:22.00	1	308.454	19.513	103.986	81.800	152.445	237.273	22.100	23.949
692	30-MAR-1993 : 12:33:45.00	1	295.943	19.435	103.998	82.000	152.116	237.085	22.200	23.803
693	30-MAR-1993 : 15:22:30.00	1	282.146	19.325	104.011	81.550	152.260	237.085	22.200	23.782
694	30-MAR-1993 : 19:41:15.00	1	265.614	19.332	103.968	81.900	152.465	236.816	21.900	24.116
695	31-MAR-1993 : 01:13:07.00	1	242.118	19.035	103.992	81.800	152.260	236.816	21.800	23.928
697	31-MAR-1993 : 08:37:30.00	1	204.350	19.292	103.998	81.450	152.465	236.816	21.900	24.116
698	31-MAR-1993 : 09:33:45.00	2	204.646	19.447	103.955	81.800	152.465	237.004	22.300	24.043
699	31-MAR-1993 : 14:09:22.00	2	243.113	18.850	103.968	81.600	152.424	237.085	22.300	23.980
700	31-MAR-1993 : 16:52:30.00	2	266.032	18.936	103.968	81.650	152.465	236.897	22.000	24.137
701	31-MAR-1993 : 20:20:37.00	2	282.936	19.066	103.968	81.600	152.465	236.951	21.900	24.043
702	31-MAR-1993 : 23:31:52.00	2	296.452	19.050	103.949	81.950	152.260	236.843	22.000	24.106
703	01-APR-1993 : 01:41:15.00	2	308.359	19.113	103.961	81.400	152.465	237.058	22.100	24.085
704	01-APR-1993 : 06:50:37.00	2	320.323	19.183	103.968	82.050	152.424	237.219	22.100	24.085

APPENDIX A6. IMAGER IR SCAN REPORT

GOES SN03 IMAGER

MISSION TEMPERATURE – HIGH

PATCH TEMPERATURE – LOW

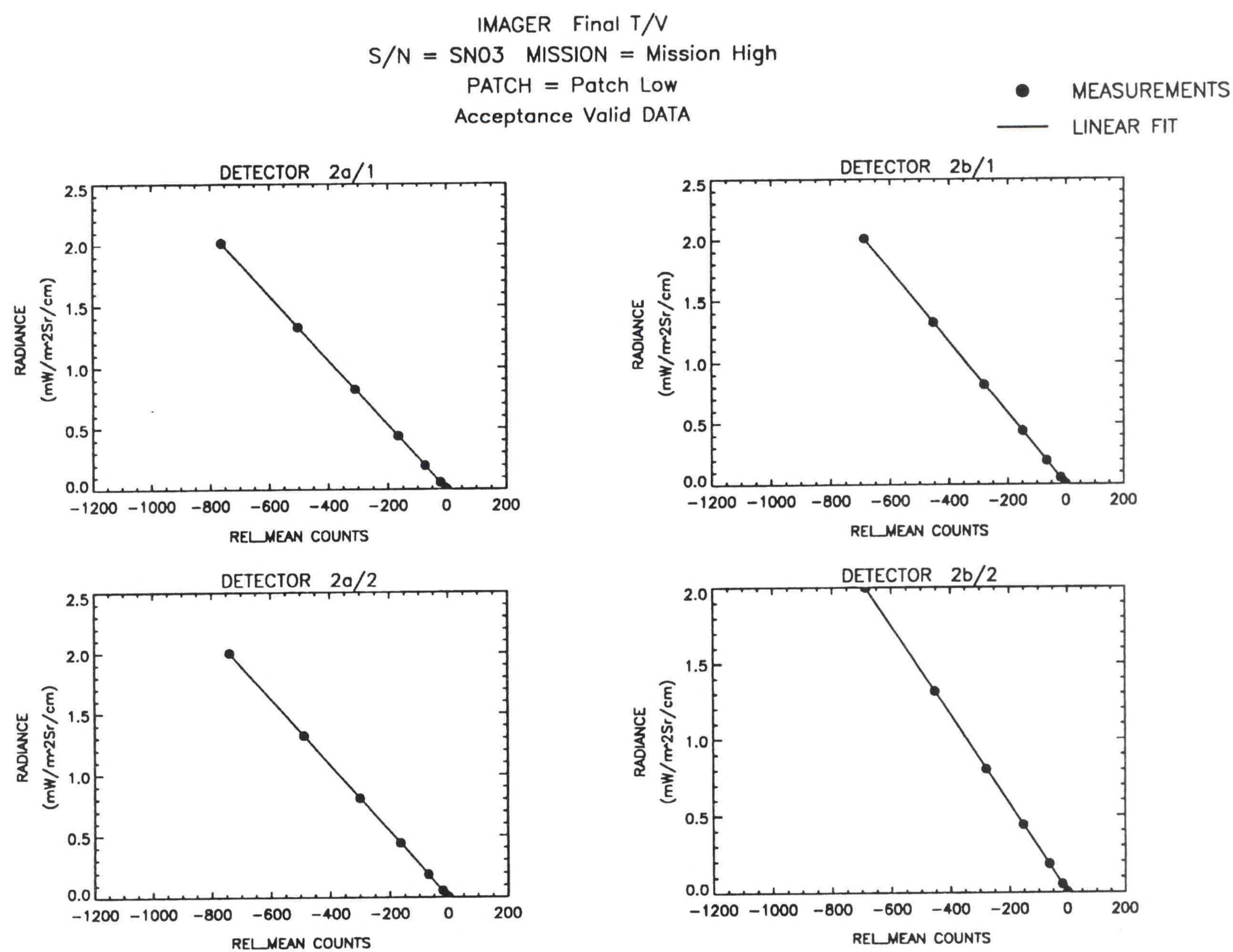

Figure A6-1. Radiance versus relative mean counts, channel 2.

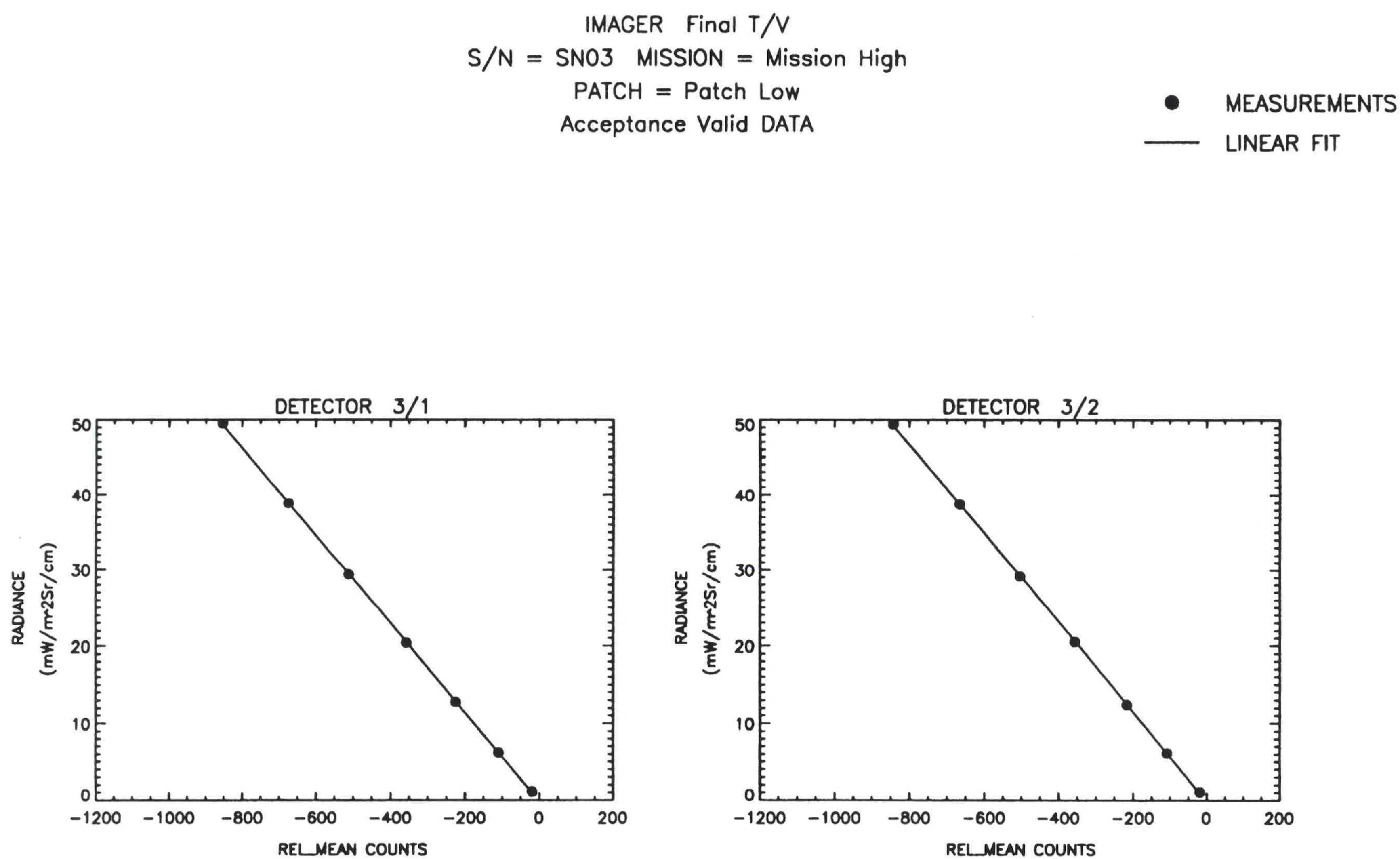

Figure A6-2. Radiance versus relative mean counts, channel 3.

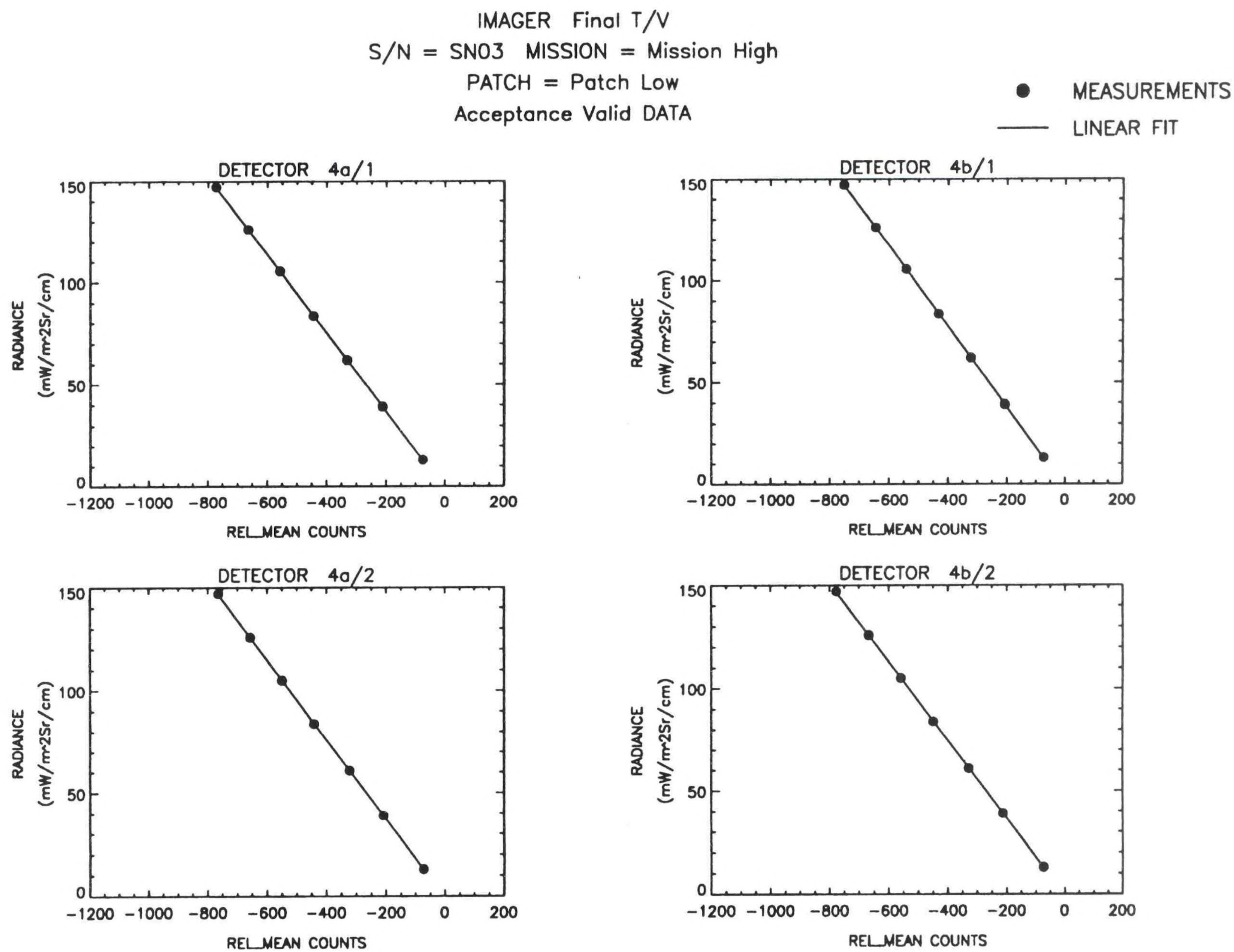

Figure A6-3. Radiance versus relative mean counts, channel 4.

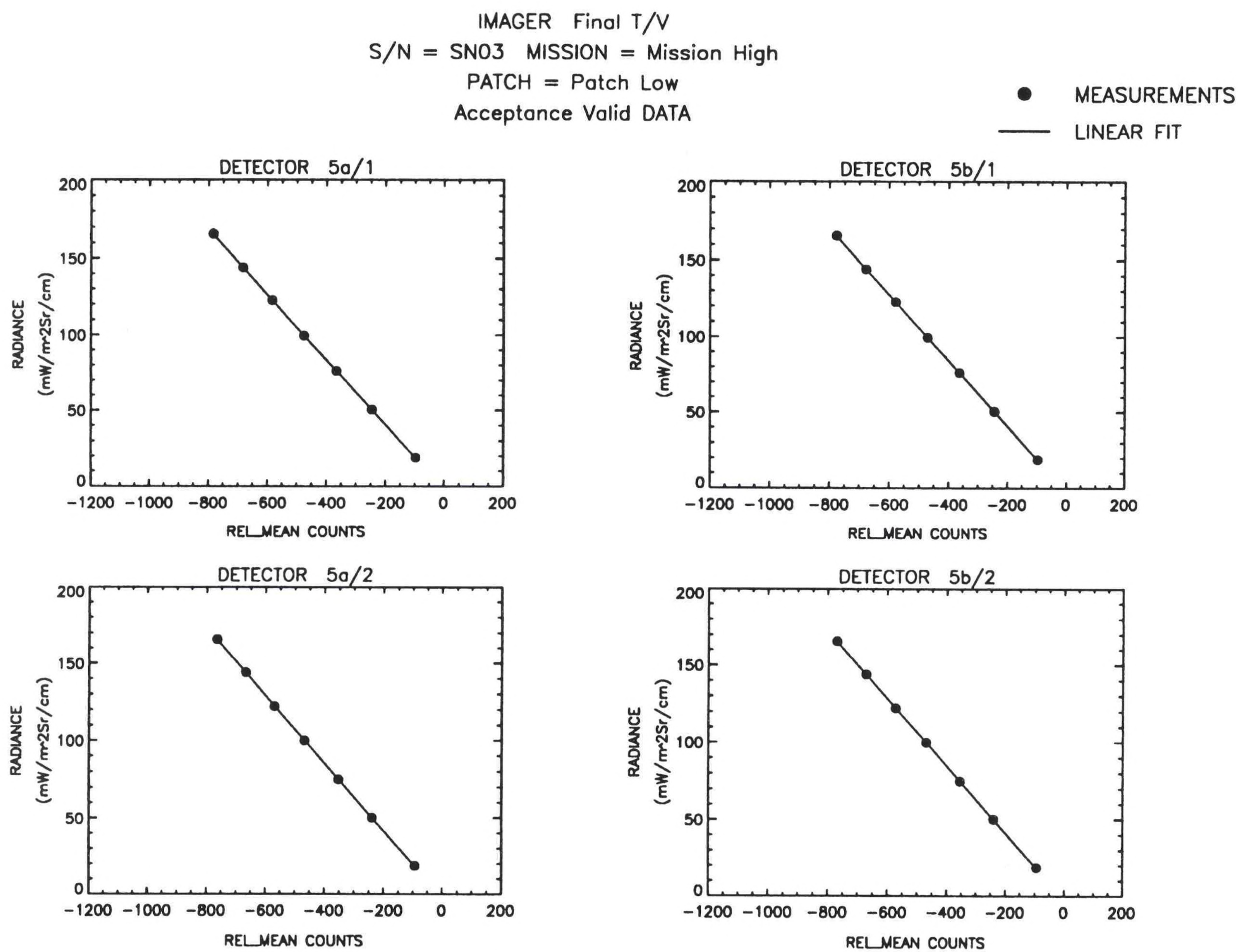

Figure A6-4. Radiance versus relative mean counts, channel 5.

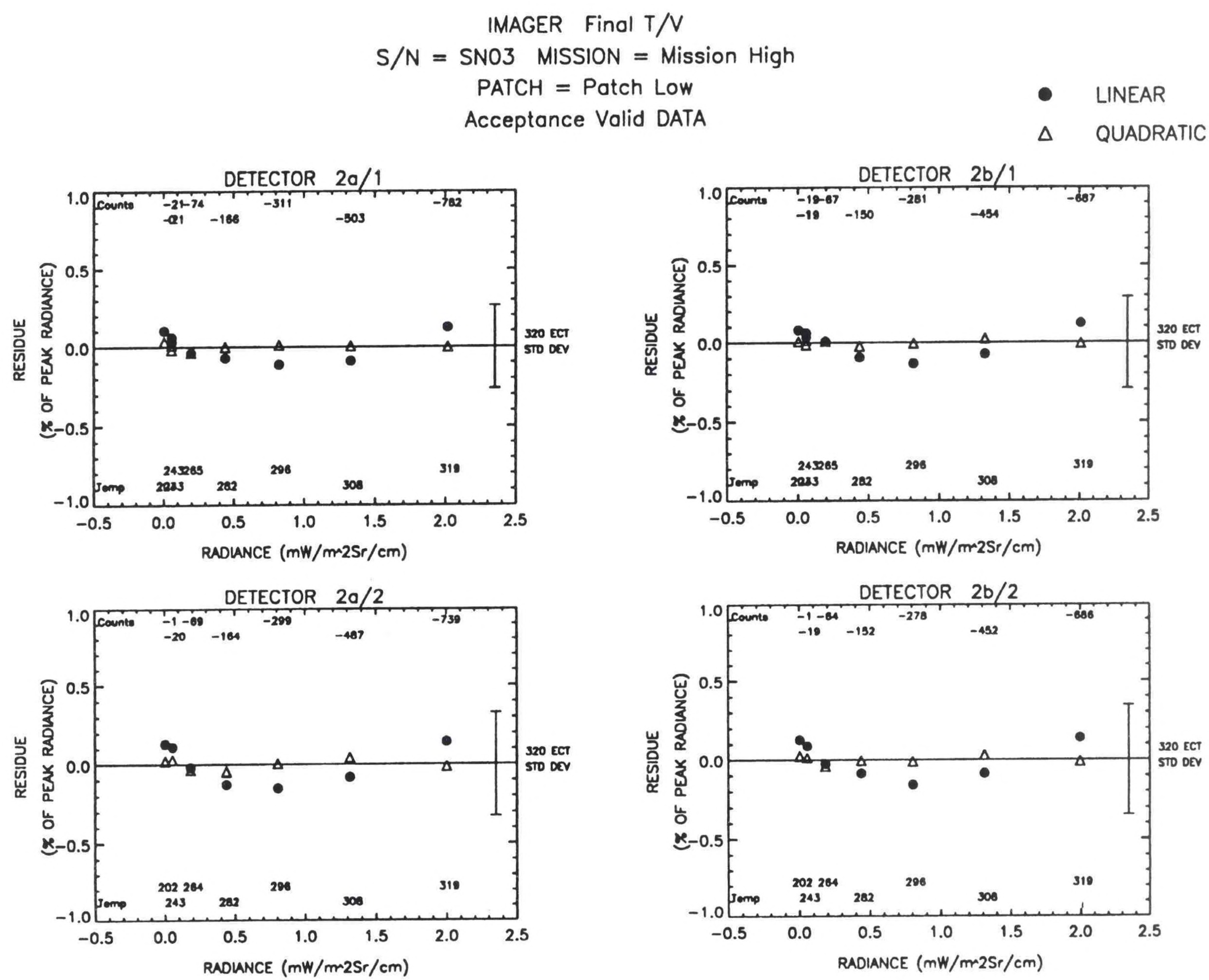

Figure A6-5. Residues of linear and quadratic fits versus radiance, channel 2.

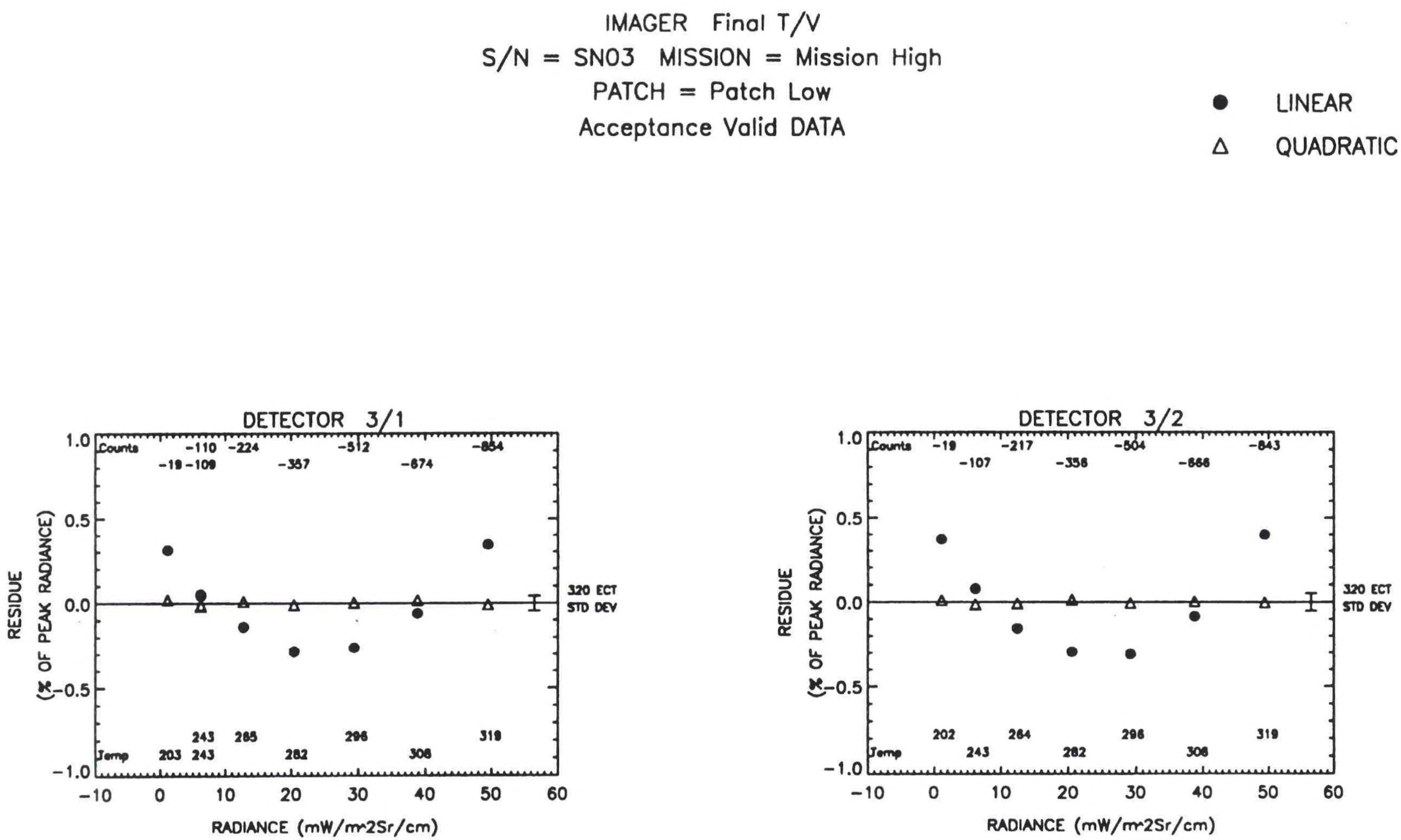

Figure A6-6. Residues of linear and quadratic fits versus radiance, channel 3.

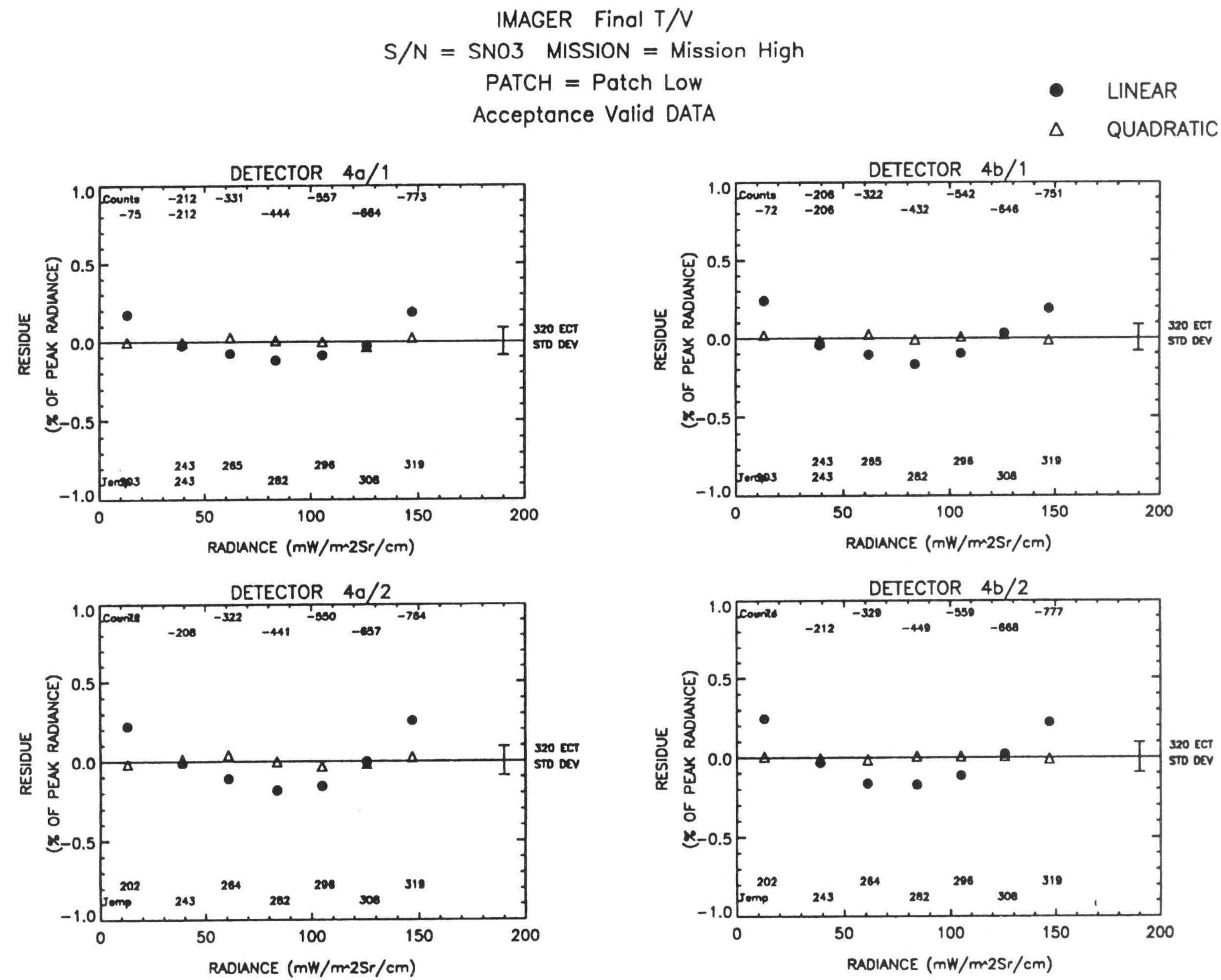

Figure A6-7. Residues of linear and quadratic fits versus radiance, channel 4.

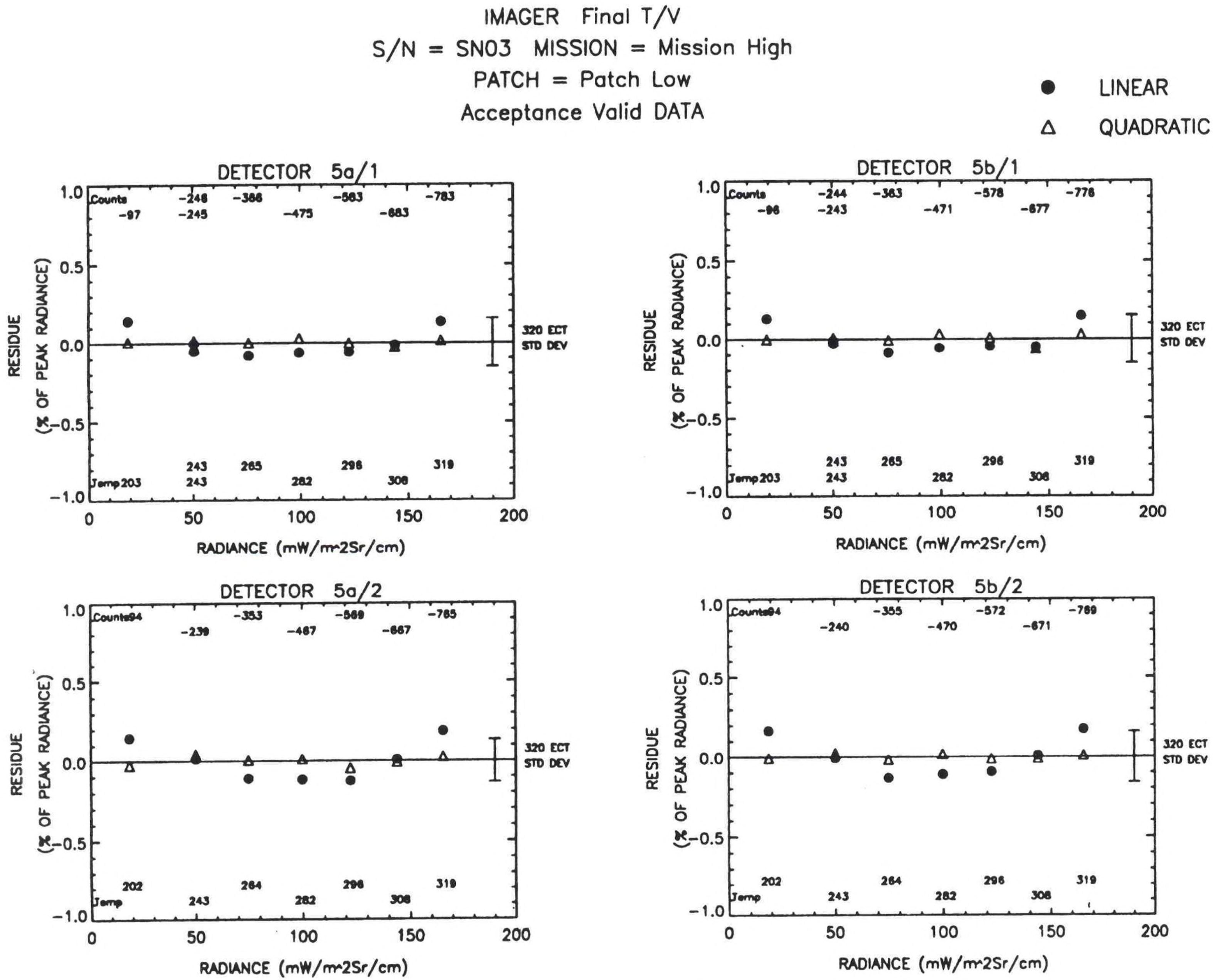

Figure A6-8. Residues of linear and quadratic fits versus radiance, channel 5.

TABLE A6-1

Noise and Residue Statistics

IMAGER — Final T/V
S/N = SN03 — MISSION = Mission High
PATCH = Patch Low
Acceptance Valid Data

CH/SIDE	NEDT(K) MEAS/TEMP	NEDT(K) SPEC/TSPEC	PEAK LIN RES %	SPEC %	RMS LIN RES %	PEAK LIN RES N (mW/m^2Sr/cm)	PEAK QUAD RES %	RMS QUAD RES %	PEAK QUAD RES N (mW/m^2Sr/cm)
2a/1	0.1835/296.5	1.40/300.0	0.1228	1.7	0.0848	0.0025	0.0320	0.0190	0.0006
2b/1	0.1870/296.5	1.40/300.0	0.1338	1.7	0.0856	0.0027	0.0224	0.0144	0.0005
3/1	0.1132/243.6	1.00/230.0	0.3427	1.7	0.2217	0.1704	0.0187	0.0128	0.0093
4a/1	0.0840/296.5	0.35/300.0	0.1879	1.7	0.1098	0.2773	0.0274	0.0191	0.0404
4b/1	0.0845/296.5	0.35/300.0	0.2391	1.7	0.1361	0.3528	0.0239	0.0183	0.0353
5a/1	0.1429/296.5	0.50/300.0	0.1417	1.7	0.0831	0.2353	0.0283	0.0199	0.0470
5b/1	0.1597/296.5	0.50/300.0	0.1492	1.7	0.0834	0.2478	0.0321	0.0277	0.0534
2a/2	0.1823/296.3	1.40/300.0	0.1525	1.7	0.1176	0.0031	0.0409	0.0306	0.0008
2b/2	0.1875/296.3	1.40/300.0	0.1579	1.7	0.1094	0.0032	0.0302	0.0224	0.0006
3/2	0.1237/243.4	1.00/230.0	0.3981	1.7	0.2716	0.1977	0.0141	0.0094	0.0070
4a/2	0.0838/296.3	0.35/300.0	0.2558	1.7	0.1633	0.3771	0.0374	0.0239	0.0552
4b/2	0.0872/296.3	0.35/300.0	0.2465	1.7	0.1621	0.3637	0.0078	0.0088	0.0115
5a/2	0.1422/296.3	0.50/300.0	0.1892	1.7	0.1196	0.3141	0.0440	0.0280	0.0731
5b/2	0.1614/296.3	0.50/300.0	0.1763	1.7	0.1186	0.2927	0.0237	0.0154	0.0393

TABLE A6-2

Linear and Quadratic Fit Coefficients

IMAGER
S/N = SN03

Final T/V
MISSION = Mission High
PATCH = Patch Low

Acceptance Valid Data

RAD = GAMM1 + M1 * C

CH/SIDE	GAMMA1			M1		
2a/1	-1.8612e-03	+/-	9.4810e-04	-2.6430e-03	+/-	2.7276e-06
2b/1	-2.3880e-03	+/-	9.5553e-04	-2.9268e-03	+/-	3.0478e-06
3/1	-2.0562e-01	+/-	7.3133e-02	-5.7957e-02	+/-	1.6103e-04
4a/1	-1.5775e+00	+/-	1.3596e-01	-1.9200e-01	+/-	2.9031e-04
4b/1	-1.5893e+00	+/-	1.6835e-01	-1.9742e-01	+/-	3.6968e-04
5a/1	-2.1990e+00	+/-	1.2365e-01	-2.1376e-01	+/-	2.5277e-04
5b/1	-2.1790e+00	+/-	1.2409e-01	-2.1583e-01	+/-	2.5599e-04
2a/2	-2.6751e-03	+/-	1.5022e-03	-2.7076e-03	+/-	4.1740e-06
2b/2	-2.9468e-03	+/-	1.3964e-03	-2.9123e-03	+/-	4.1799e-06
3/2	-2.3422e-01	+/-	1.0339e-01	-5.8587e-02	+/-	2.1649e-04
4a/2	-1.5744e+00	+/-	2.2990e-01	-1.9384e-01	+/-	4.7107e-04
4b/2	-1.6191e+00	+/-	2.2843e-01	-1.9073e-01	+/-	4.6008e-04
5a/2	-2.2723e+00	+/-	2.0191e-01	-2.1895e-01	+/-	4.0211e-04
5b/2	-2.2358e+00	+/-	2.0014e-01	-2.1755e-01	+/-	3.9616e-04

RAD = GAMMA2 + M2 * C + R * C^2

CH/SIDE	GAMMA2			M2			R		
2a/1	-4.1516e-04	+/-	2.7677e-04	-2.6205e-03	+/-	2.4172e-06	3.1468e-08	+/-	3.2433e-09
2b/1	-9.1027e-04	+/-	2.0932e-04	-2.9013e-03	+/-	2.0261e-06	3.9446e-08	+/-	3.0136e-09
3/1	-3.1338e-02	+/-	6.4576e-03	-5.6459e-02	+/-	4.0054e-05	1.7546e-06	+/-	4.5374e-08
4a/1	-1.1045e+00	+/-	4.5499e-02	-1.8890e-01	+/-	2.5105e-04	3.6208e-06	+/-	2.8624e-07

TABLE A6-2 (Continued)

Linear and Quadratic Fit Coefficients

4b/1	-1.0019e+00	+/-	4.3522e-02	-1.9346e-01	+/-	2.4697e-04	4.7626e-06	+/-	2.8971e-07
5a/1	-1.7331e+00	+/-	6.0624e-02	-2.1097e-01	+/-	3.1363e-04	3.1230e-06	+/-	3.4367e-07
5b/1	-1.7249e+00	+/-	8.4724e-02	-2.1309e-01	+/-	4.4237e-04	3.1002e-06	+/-	4.8920e-07
2a/2	-4.4606e-04	+/-	5.2993e-04	-2.6765e-03	+/-	4.3531e-06	4.3812e-08	+/-	5.8994e-09
2b/2	-8.4144e-04	+/-	3.8735e-04	-2.8808e-03	+/-	3.4281e-06	4.7947e-08	+/-	5.0036e-09
3/2	-2.2967e-02	+/-	5.4495e-03	-5.6824e-02	+/-	3.1818e-05	2.0715e-06	+/-	3.6058e-08
4a/2	-9.3322e-01	+/-	6.0647e-02	-1.8950e-01	+/-	3.3084e-04	5.1667e-06	+/-	3.8288e-07
4b/2	-9.7631e-01	+/-	2.2392e-02	-1.8646e-01	+/-	1.1997e-04	5.0000e-06	+/-	1.3645e-07
5a/2	-1.6627e+00	+/-	9.0550e-02	-2.1512e-01	+/-	4.7369e-04	4.4338e-06	+/-	5.3452e-07
5b/2	-1.6209e+00	+/-	4.9527e-02	-2.1371e-01	+/-	2.5747e-04	4.4217e-06	+/-	2.8879e-07

TABLE A6-3

IR Scan Run Numbers and Telemetry

IMAGER Final T/V
S/N = SN03 MISSION = Mission High
PATCH = Patch Low
Acceptance Valid Data

RUN NO.	DATE:TIME	ELEC SIDE	ECT (K)	BASEPLATE (C)	NARROW PATCH (K)	SPACE TARGET (K)	COOLER RADIATOR (K)	COOLER HOUSING (K)	AFT OPTICS (C)	PATCH CONTROL (V)
787	13-APR-1993 : 20:15:00.00	1	319.764	27.247	94.254	81.650	152.280	240.348	30.000	12.998
788	14-APR-1993 : 00:45:00.00	1	308.548	27.235	94.260	81.500	152.342	241.053	30.000	13.029
789	14-APR-1993 : 02:37:30.00	1	296.511	27.180	94.266	81.700	152.424	241.189	30.000	13.154
790	14-APR-1993 : 04:30:00.00	1	282.188	27.073	94.248	81.750	152.239	241.135	29.900	13.175
791	14-APR-1993 : 09:39:22.00	1	265.664	27.028	94.248	81.800	152.424	241.026	29.800	13.029
792	14-APR-1993 : 16:13:07.00	1	243.620	26.999	94.248	81.650	152.260	241.135	29.900	13.102
793	14-APR-1993 : 16:41:15.00	1	243.702	27.010	94.248	81.800	152.465	241.135	29.900	12.998
794	14-APR-1993 : 20:43:07.00	1	203.401	26.950	94.254	81.350	152.260	241.162	29.900	12.862
795	14-APR-1993 : 21:50:37.00	2	202.854	26.795	94.230	81.150	152.342	241.325	29.800	13.300
796	15-APR-1993 : 02:37:30.00	2	243.423	26.874	94.242	81.600	152.465	241.135	29.900	13.415
797	15-APR-1993 : 05:03:45.00	2	264.781	26.919	94.242	81.650	152.465	241.135	30.000	13.311
798	15-APR-1993 : 07:18:45.00	2	282.477	26.955	94.248	81.700	152.465	240.945	30.100	13.373
799	15-APR-1993 : 11:48:45.00	2	296.288	27.068	94.248	81.400	152.465	240.972	30.200	13.144
800	15-APR-1993 : 13:52:30.00	2	308.506	27.157	94.248	82.150	152.465	241.135	30.300	13.269
801	15-APR-1993 : 18:39:22.00	2	319.748	27.218	94.248	81.600	152.465	241.406	30.300	13.217

APPENDIX A7. IMAGER IR SCAN REPORT

GOES SN03 IMAGER

MISSION TEMPERATURE – HIGH

PATCH TEMPERATURE – MID

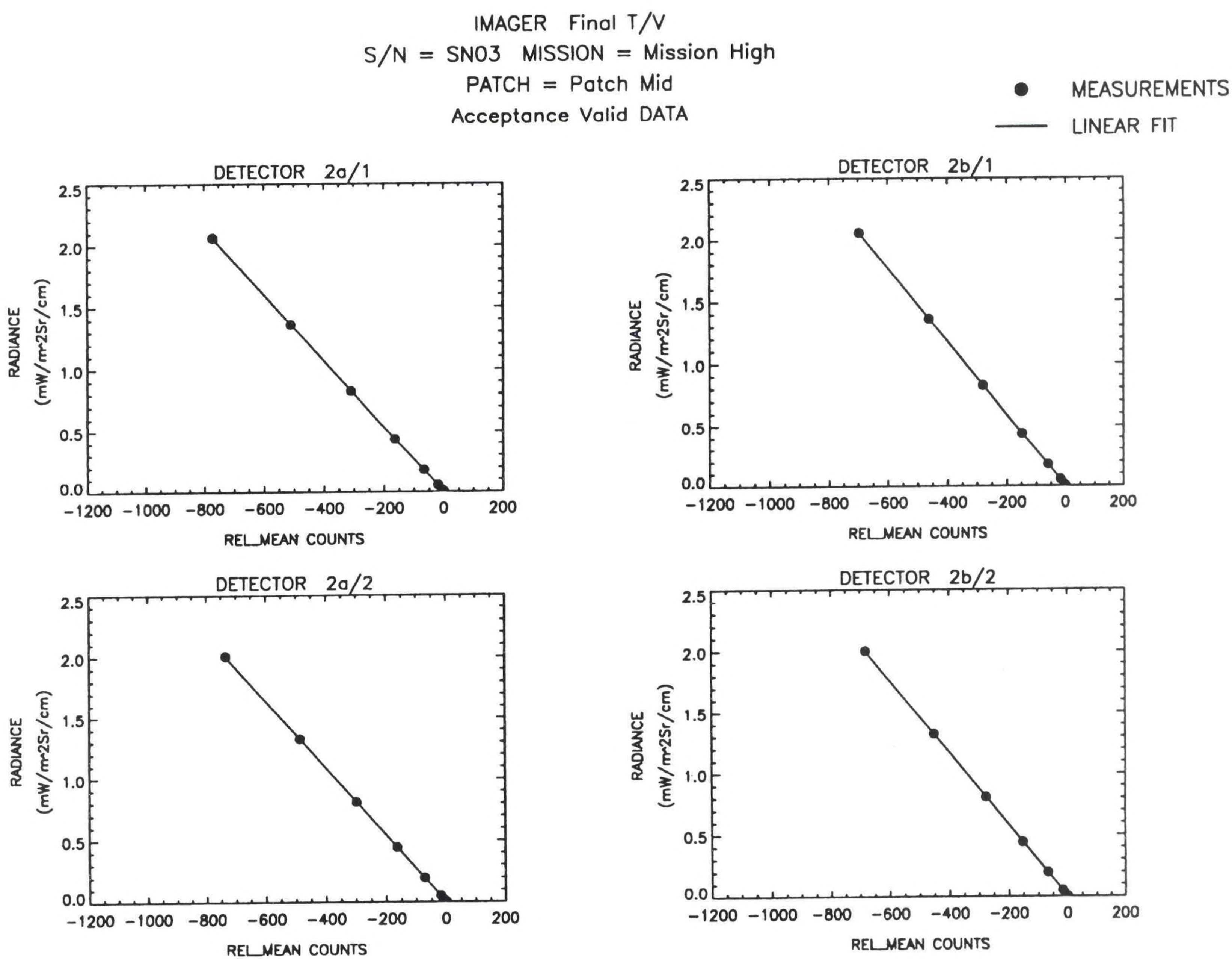

Figure A7-1. Radiance versus relative mean counts, channel 2.

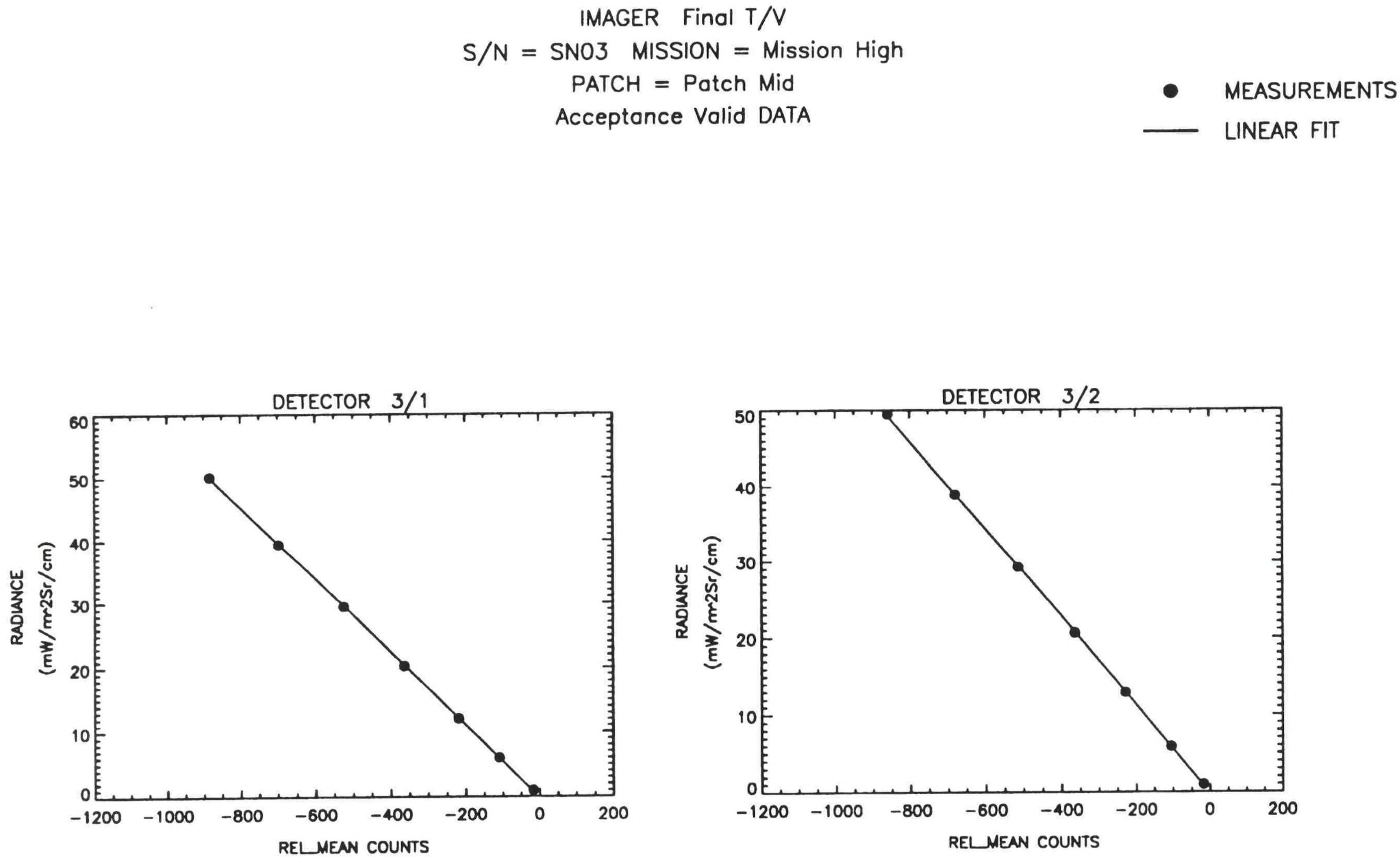

Figure A7-2. Radiance versus relative mean counts, channel 3.

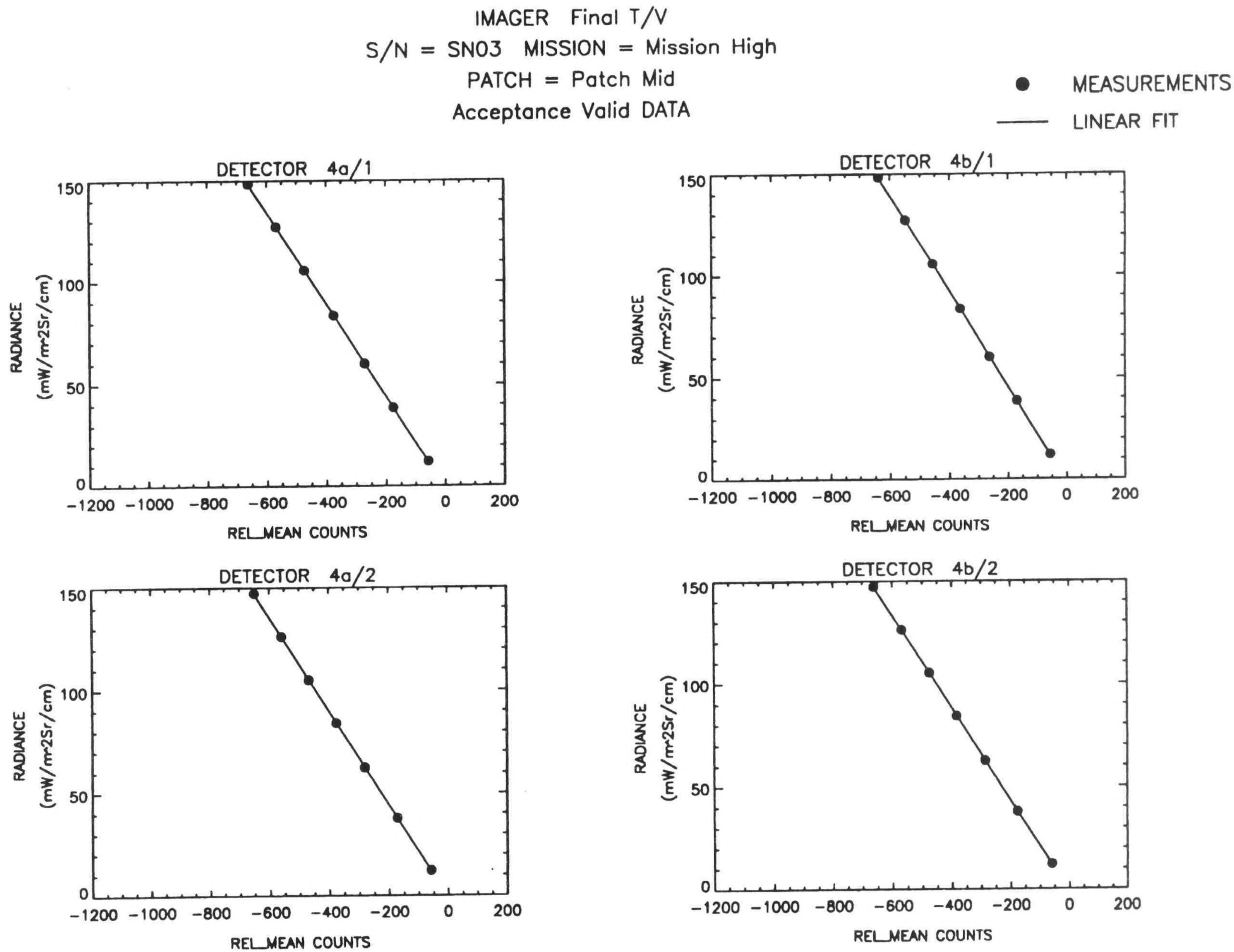

Figure A7-3. Radiance versus relative mean counts, channel 4.

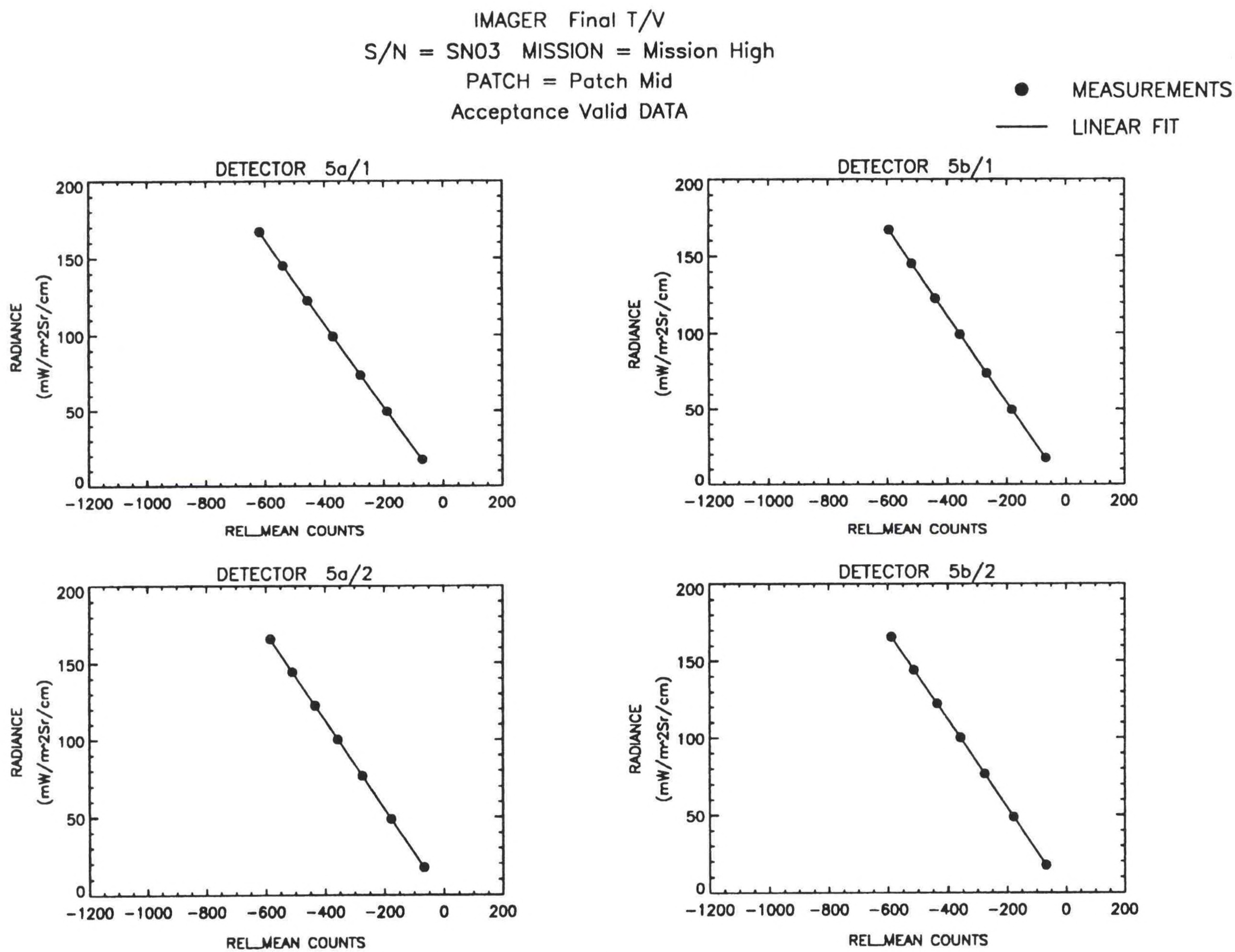

Figure A7-4. Radiance versus relative mean counts, channel 5.

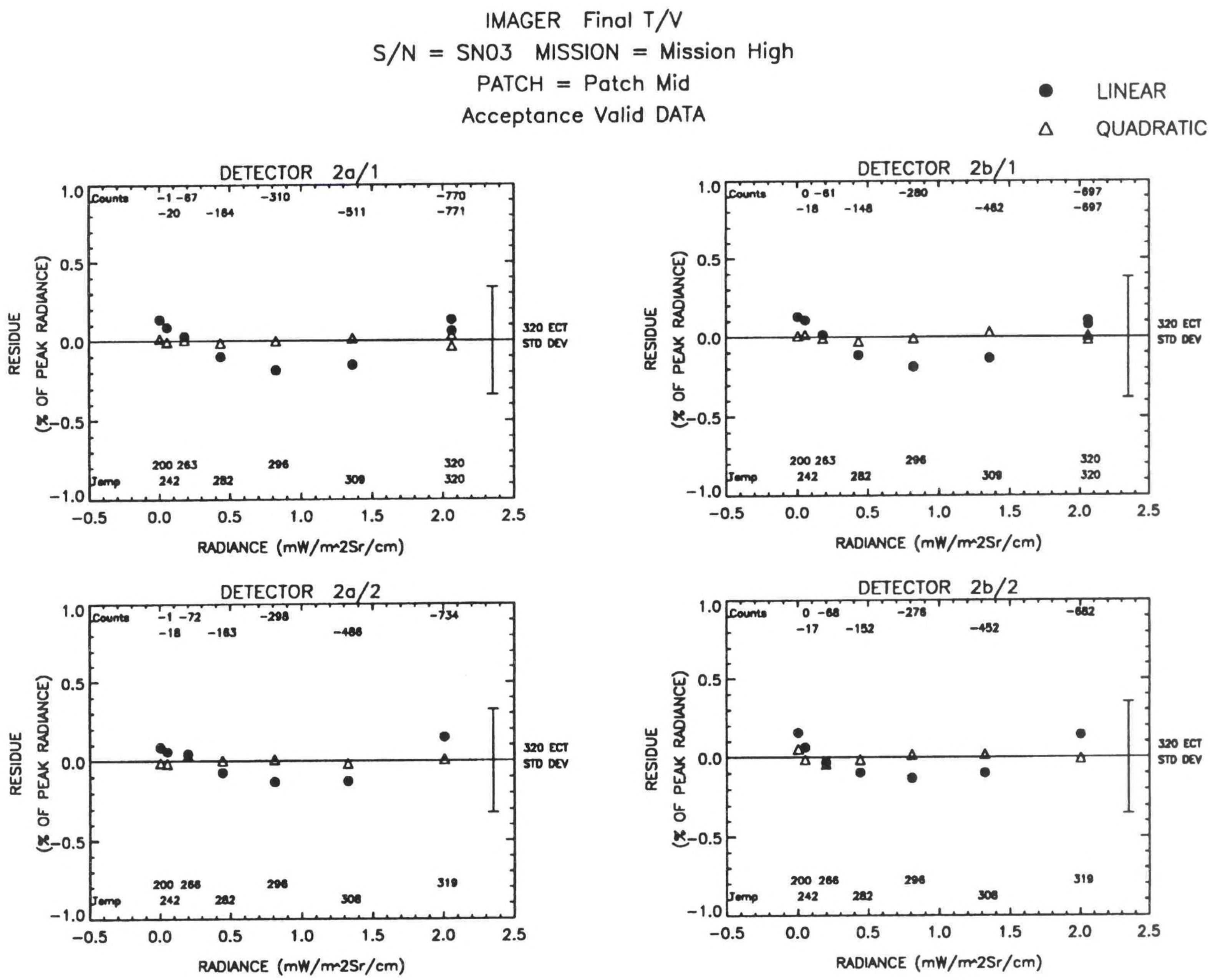

Figure A7-5. Residues of linear and quadratic fits versus radiance, channel 2.

IMAGER Final T/V
S/N = SN03 MISSION = Mission High
PATCH = Patch Mid
Acceptance Valid DATA

● LINEAR
Δ QUADRATIC

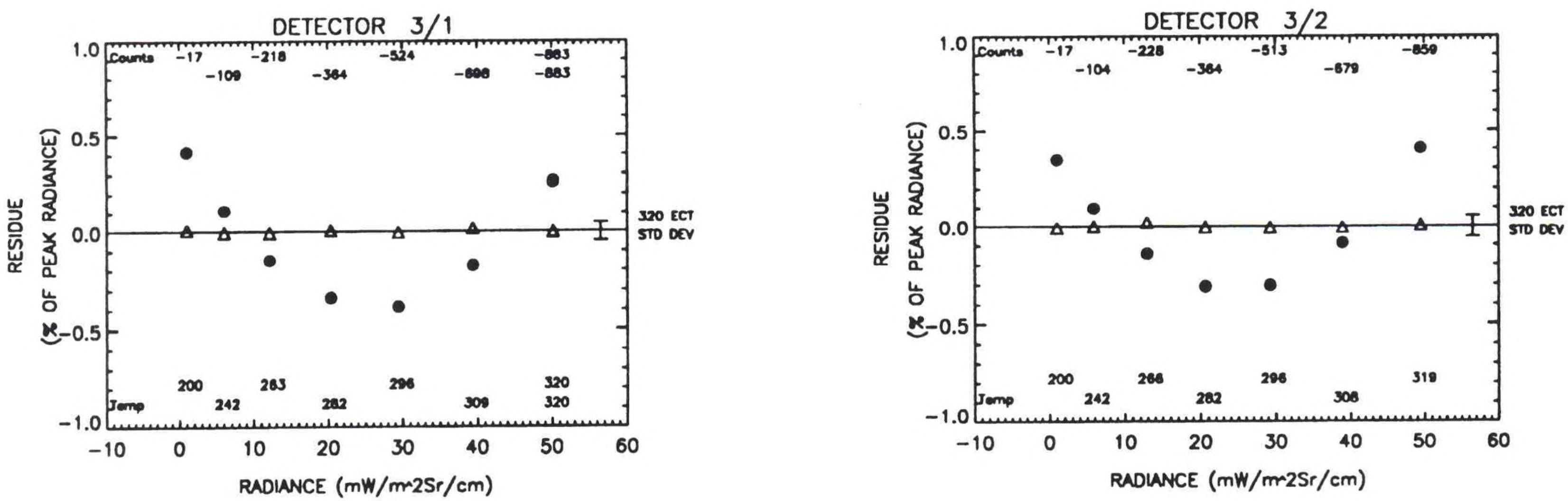

Figure A7-6. Residues of linear and quadratic fits versus radiance, channel 3.

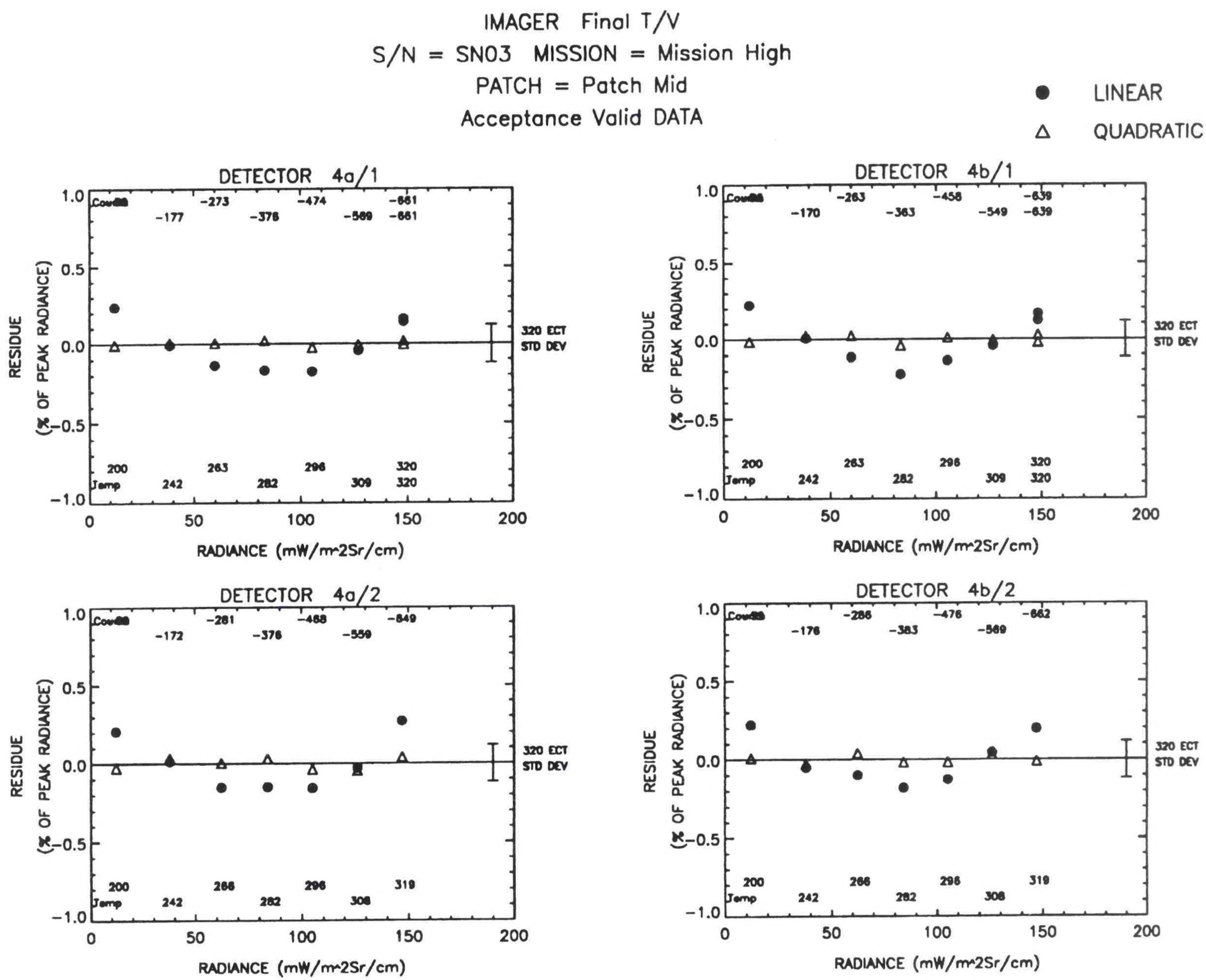

Figure A7-7. Residues of linear and quadratic fits versus radiance, channel 4.

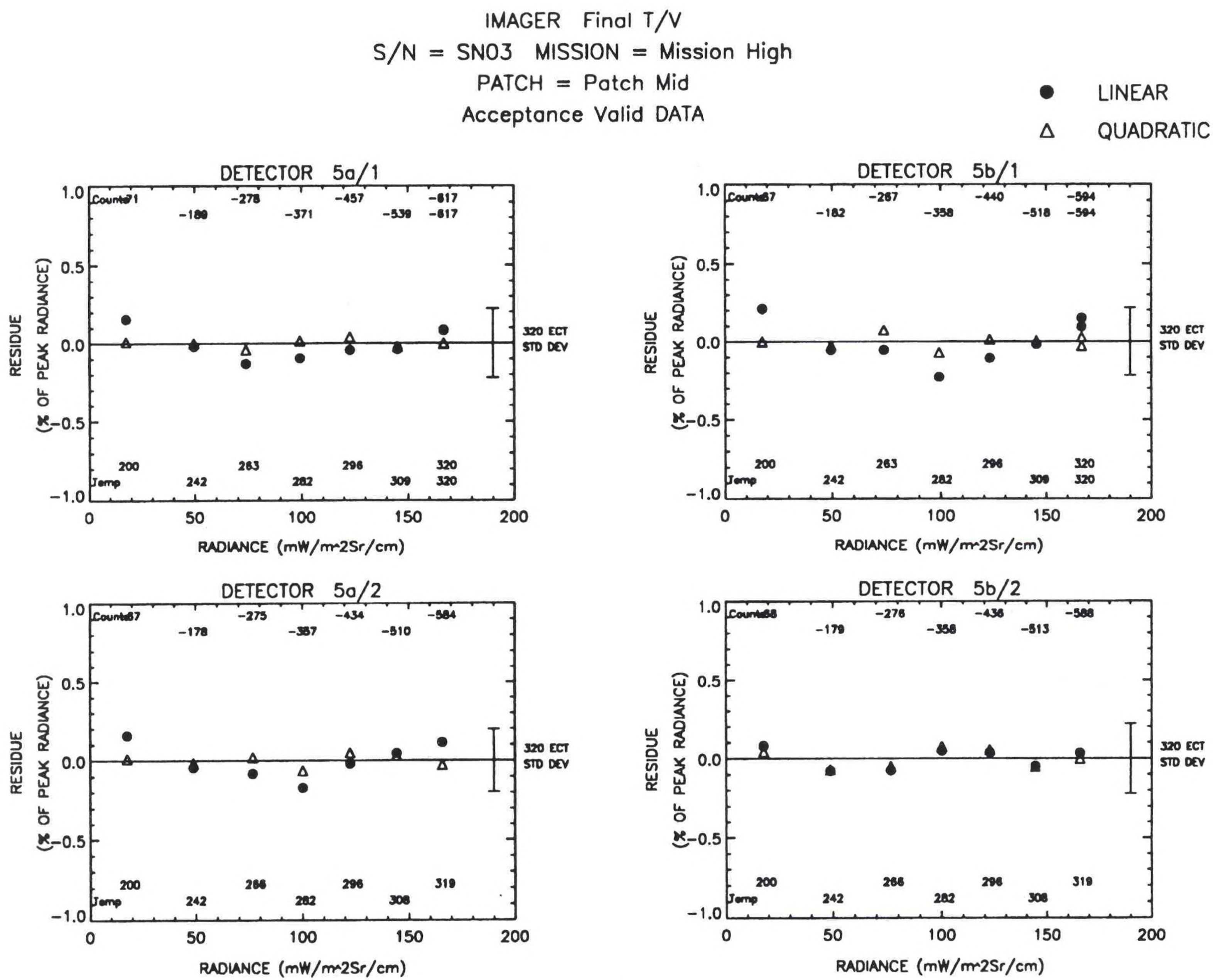

Figure A7-8. Residues of linear and quadratic fits versus radiance, channel 5.

TABLE A7-1

Noise and Residue Statistics

IMAGER Final T/V
S/N = SN03 MISSION = Mission High
PATCH = Patch Mid
Acceptance Valid Data

CH/SIDE	NEDT (K) MEAS/TEMP	NEDT (K) SPEC/TSPEC	PEAK LIN RES %	SPEC %	RMS LIN RES %	PEAK LIN RES N (mW/m^2Sr/cm)	PEAK QUAD RES %	RMS QUAD RES %	PEAK QUAD RES N (mW/m^2Sr/cm)
2a/1	0.1948/296.6	1.40/300.0	0.1860	1.7	0.1206	0.0038	0.0338	0.0202	0.0007
2b/1	0.2218/296.6	1.40/300.0	0.1878	1.7	0.1185	0.0038	0.0306	0.0179	0.0006
3/1	0.1088/242.8	1.00/230.0	0.4150	1.7	0.2826	0.2063	0.0137	0.0075	0.0068
4a/1	0.1067/296.6	0.35/300.0	0.2368	1.7	0.1506	0.3496	0.0187	0.0136	0.0276
4b/1	0.1086/296.6	0.35/300.0	0.2224	1.7	0.1468	0.3283	0.0260	0.0225	0.0383
5a/1	0.2109/296.6	0.50/300.0	0.1555	1.7	0.0920	0.2581	0.0407	0.0228	0.0676
5b/1	0.2115/296.6	0.50/300.0	0.2266	1.7	0.1342	0.3764	0.0747	0.0399	0.1241
2a/2	0.2044/296.4	1.40/300.0	0.1486	1.7	0.1024	0.0030	0.0343	0.0172	0.0007
2b/2	0.2232/296.4	1.40/300.0	0.1562	1.7	0.1108	0.0031	0.0525	0.0284	0.0011
3/2	0.1299/242.2	1.00/230.0	0.4035	1.7	0.2700	0.2004	0.0209	0.0096	0.0104
4a/2	0.1116/296.4	0.35/300.0	0.2693	1.7	0.1635	0.3970	0.0399	0.0336	0.0588
4b/2	0.1071/296.4	0.35/300.0	0.2198	1.7	0.1463	0.3243	0.0395	0.0245	0.0583
5a/2	0.1953/296.4	0.50/300.0	0.1708	1.7	0.1054	0.2837	0.0473	0.0350	0.0785
5b/2	0.2259/296.4	0.50/300.0	0.0792	1.7	0.0594	0.1315	0.0749	0.0540	0.1244

TABLE A7-2

Linear and Quadratic Fit Coefficients

IMAGER — Final T/V
S/N = SN03 — MISSION = Mission High
PATCH = Patch Mid
Acceptance Valid Data

RAD = GAMM1 + M1 * C

CH/SIDE	GAMMA1			M1		
2a/1	-3.5116e-03	+/-	1.4799e-03	-2.6756e-03	+/-	3.3310e-06
2b/1	-3.2807e-03	+/-	1.4510e-03	-2.9536e-03	+/-	3.6113e-06
3/1	-2.5573e-01	+/-	1.0142e-01	-5.6905e-02	+/-	1.8083e-04
4a/1	-1.6087e+00	+/-	1.9758e-01	-2.2637e-01	+/-	4.3168e-04
4b/1	-1.6262e+00	+/-	1.9262e-01	-2.3436e-01	+/-	4.3573e-04
5a/1	-2.2049e+00	+/-	1.4386e-01	-2.7339e-01	+/-	3.3011e-04
5b/1	-2.1455e+00	+/-	2.1000e-01	-2.8412e-01	+/-	5.0068e-04
2a/2	-2.5020e-03	+/-	1.3103e-03	-2.7326e-03	+/-	3.6586e-06
2b/2	-2.7439e-03	+/-	1.4157e-03	-2.9377e-03	+/-	4.2564e-06
3/2	-2.2695e-01	+/-	1.0274e-01	-5.7630e-02	+/-	2.1096e-04
4a/2	-1.5208e+00	+/-	2.2886e-01	-2.2806e-01	+/-	5.5074e-04
4b/2	-1.5637e+00	+/-	2.0513e-01	-2.2408e-01	+/-	4.8451e-04
5a/2	-2.1027e+00	+/-	1.7656e-01	-2.8656e-01	+/-	4.5994e-04
5b/2	-2.0232e+00	+/-	9.9526e-02	-2.8472e-01	+/-	2.5776e-04

RAD = GAMMA2 + M2 * C + R * C^2

CH/SIDE	GAMMA2			M2			R		
2a/1	-9.7041e-04	+/-	3.3371e-04	-2.6424e-03	+/-	2.6018e-06	4.2211e-08	+/-	3.2120e-09
2b/1	-7.8579e-04	+/-	2.9504e-04	-2.9175e-03	+/-	2.5434e-06	5.0714e-08	+/-	3.4721e-09
3/1	-2.1796e-02	+/-	4.0707e-03	-5.5093e-02	+/-	2.2259e-05	1.9210e-06	+/-	2.2919e-08
4a/1	-9.9420e-01	+/-	3.1670e-02	-2.2168e-01	+/-	1.9499e-04	6.1725e-06	+/-	2.5029e-07

TABLE A7-2 (Continued)

Linear and Quadratic Fit Coefficients

4b/1	-1.0314e+00	+/-	5.2480e-02	-2.2966e-01	+/-	3.3453e-04	6.4012e-06	+/-	4.4454e-07
5a/1	-1.7298e+00	+/-	6.6949e-02	-2.6977e-01	+/-	4.2439e-04	4.9951e-06	+/-	5.7162e-07
5b/1	-1.4640e+00	+/-	1.1693e-01	-2.7870e-01	+/-	7.7092e-04	7.7575e-06	+/-	1.0799e-06
2a/2	-5.0794e-04	+/-	2.9951e-04	-2.7047e-03	+/-	2.4716e-06	3.9485e-08	+/-	3.3694e-09
2b/2	-6.3352e-04	+/-	4.9265e-04	-2.9060e-03	+/-	4.3734e-06	4.8432e-08	+/-	6.4191e-09
3/2	-2.1655e-02	+/-	5.4734e-03	-5.5931e-02	+/-	3.1330e-05	1.9668e-06	+/-	3.4952e-08
4a/2	-9.1122e-01	+/-	8.2745e-02	-2.2312e-01	+/-	5.3354e-04	6.9622e-06	+/-	7.3017e-07
4b/2	-1.0132e+00	+/-	6.0517e-02	-2.1971e-01	+/-	3.8257e-04	6.0464e-06	+/-	5.1362e-07
5a/2	-1.6059e+00	+/-	1.0945e-01	-2.8239e-01	+/-	7.5422e-04	6.3602e-06	+/-	1.1211e-06
5b/2	-1.8990e+00	+/-	1.6884e-01	-2.8368e-01	+/-	1.1549e-03	1.5646e-06	+/-	1.7041e-06

TABLE A7-3

IR Scan Run Numbers and Telemetry

IMAGER Final T/V
S/N = SN03 MISSION = Mission High
PATCH = Patch Mid
Acceptance Valid Data

RUN NO.	DATE:TIME	ELEC SIDE	ECT (K)	BASEPLATE (C)	NARROW PATCH (K)	SPACE TARGET (K)	COOLER RADIATOR (K)	COOLER HOUSING (K)	AFT OPTICS (C)	PATCH CONTROL (V)
805	16-APR-1993 : 00:33:45.00	2	319.827	27.246	101.010	82.050	152.301	241.379	30.300	20.556
806	16-APR-1993 : 03:45:00.00	2	308.676	27.299	101.016	81.500	152.589	241.406	30.400	20.587
807	16-APR-1993 : 06:33:45.00	2	296.393	27.281	101.016	81.850	152.589	241.189	30.400	20.556
808	16-APR-1993 : 09:05:37.00	2	282.650	27.194	101.016	81.600	152.465	241.162	30.300	20.514
809	16-APR-1993 : 13:41:15.00	2	266.083	27.076	101.022	81.800	152.589	241.081	30.300	20.483
810	16-APR-1993 : 18:16:52.00	2	242.151	26.913	101.022	81.600	152.465	241.135	30.200	20.661
811	16-APR-1993 : 22:41:15.00	2	200.960	26.786	101.016	81.650	152.465	241.135	30.000	20.692
812	16-APR-1993 : 23:20:37.00	1	200.747	26.882	101.053	81.500	152.218	241.026	29.900	20.608
813	17-APR-1993 : 04:13:07.00	1	242.843	26.769	101.071	82.250	152.198	240.945	29.700	20.577
814	17-APR-1993 : 07:13:07.00	1	263.946	26.746	101.046	82.000	152.260	240.809	29.700	20.514
815	17-APR-1993 : 10:18:45.00	1	282.051	26.798	101.065	81.900	152.301	240.809	29.700	20.452
816	17-APR-1993 : 13:18:45.00	1	296.613	26.841	101.053	82.600	152.260	240.375	29.700	20.452
817	17-APR-1993 : 18:22:30.00	1	309.182	27.083	101.071	81.800	152.260	240.050	29.900	20.702
818	17-APR-1993 : 22:18:45.00	1	320.386	26.958	101.059	82.250	152.465	240.023	30.000	20.587
819	17-APR-1993 : 22:30:00.00	1	320.406	26.969	101.077	81.650	152.239	240.077	30.100	20.723

Unclassified

Unclassified